Development of an in-vitro Bioprinted Esophago-Gastric Cancer Platform for Therapy Evaluation and Immuno-Oncology Discovery

By

Salvador Flores Torres

Department of Bioengineering

McGill University, Montreal

January 2023

A thesis submitted to McGill University in partial fulfilment of the requirements of the degree of Doctor in Philosophy

Dedicated to those patients who fought,

to those patients who are fighting,

and to those who will fight cancer.

Table of contents

Abstracts:

English

Malignant tumor tissues exhibit inter- and intra-tumoral heterogeneities, aberrant development, dynamic stromal composition, diverse tissue phenotypes, and cell populations growing within localized mechanical stresses in hypoxic conditions. Efforts in developing in-vitro cancer models and discovery platforms are on the rise as these miniaturized disease replicas can emulate the therapeutic response of parental tumors as well as some of its important pathophysiological features. Extrusion bioprinting allows the fabrication of physiologically relevant architectures in-vitro. Here, we use this fabrication technique to develop an in-vitro platform that enables the expansion of patient-derived gastro-esophageal cancer cells. We incorporate biocompatible hydrogels that support cell encapsulation and extrusion without affecting cell viability. The biomaterials that comprise our cancer discovery platform were selected based on their compatibility with advanced analytical techniques and assays such as fluorescent microscopy, histology, and flow cytometry. Our extruded platforms support patient-derived cancer cell growth and development while promoting optimal cell viability. The biochemistry of our platform enabled us to document cancer harvest cancer spheroids at any point during development, evaluate quantitively their growth progress, and either reintroduce them into fresh new biomaterial or conduct tumor profiling experiments such as viability assessments with user-defined tumor formats. Furthermore, these engineered constructs containing patient-derived cancer cells were challenged with anticancer drugs. Our drug testing results show that our in-vitro tumor platform built with patient-derived cancer cells exhibited a comparable chemoresistance against the standard-of-care chemotherapy given to the patient in the clinic. Then, we designed a bioprintable co-

culture platform that allowed the interaction between patient-derived cancer cells and patient-derived lymphocytes (T-cells) in two adjacent regions. This engineered platform demonstrates the advantage of extrusion bioprinting when fabricating tumor models where precise geometric control is needed to deposit selected cell types into physiologically relevant configuration. Here, we use our multicellular cancer system (t-cell – cancer cell) to study T-cell activity and activation in the presence of cancer cells. Overall, this work yielded a set of defined cancer discovery tools that allow the evaluation of tumor tissue behavior within an engineered in-vitro platform.

Titre de la thèse: Développement d'une plateforme de cancer œsophago-gastrique bioprinté in-vitro pour l'évaluation des thérapies et la découverte de l'immuno-oncologie

French:

Les tissus tumoraux malins présentent des hétérogénéités inter- et intra-tumorales, un développement aberrant, une composition stromale dynamique, divers phénotypes tissulaires et des cellules qui se développent dans des conditions de stress mécanique localisé et d'hypoxie. Les efforts pour développer des modèles de cancer *in vitro* et des plateformes de recherche sont en hausse, car ces répliques miniaturisées de la maladie peuvent émuler la réponse thérapeutique des tumeurs parentales ainsi que certaines de ses caractéristiques physiopathologiques importantes. La bio-impression par extrusion permet la fabrication d'architectures physiologiquement pertinentes *in vitro*. Nous utilisons ici cette technique pour développer une plateforme *in vitro* qui permet le développement de cellules cancéreuses gastro-œsophagiennes dérivées de patients. Nous incorporons des hydrogels biocompatibles qui permettent l'encapsulation et l'extrusion des cellules sans affecter leur viabilité. Les biomatériaux qui composent notre plateforme de recherche ont été sélectionnés en fonction de leur compatibilité avec des tests et techniques analytiques tels que la microscopie à fluorescence, l'histologie et la cytométrie de flux. Nos plateformes extrudées favorisent la croissance et le développement des cellules cancéreuses dérivées de patients tout en favorisant une viabilité cellulaire optimale. La biochimie de notre plateforme nous a permis de documenter le prélèvement de sphéroïdes cancéreux à n'importe quel moment du développement, d'évaluer quantitativement leur progression de croissance, et soit de les réintroduire dans un nouveau biomatériau frais, soit de mener des expériences de profilage tumoral telles que des évaluations de viabilité avec des formats de tumeurs définis par l'utilisateur. En outre,

ces constructions contenant des cellules cancéreuses issues de patients ont été testées avec des médicaments anticancéreux. Les résultats de nos tests montrent que notre plateforme tumorale *in vitro* construite avec des cellules cancéreuses provenant de patients présente une chimiorésistance comparable à celle de la chimiothérapie standard administrée aux patients en clinique. Ensuite, nous avons conçu une plateforme de co-culture bio-imprimable qui permet l'interaction entre les cellules cancéreuses et les lymphocytes (cellules T) provenant respectivement de patients dans deux régions adjacentes. Cette plateforme démontre l'avantage de la bio-impression par extrusion lors de la fabrication de modèles tumoraux où un contrôle géométrique précis est nécessaire pour déposer des types cellulaires différents dans une configuration physiologiquement pertinente. Nous utilisons, ici, notre système multicellulaire cancéreux (cellule t - cellule cancéreuse) pour étudier l'activité et l'activation des cellules T en présence de cellules cancéreuses. Globalement, ce travail a permis de créer un ensemble d'outils de recherche du cancer qui permettent d'évaluer le comportement des tissus tumoraux au sein d'une plateforme *in vitro*.

Acknowledgements

First and foremost, I would like to thank those patients who decided to donate precious tissue samples. Without these crucial acts of bravery, the work being performed to improve cancer research and discovery would not be possible. Not a single cell was tested without purpose.

Next, I thank Jacqueline, my wife and life partner. She provided constant and unconditional support to this project. There are no words to describe what you have done to help me.

Special thanks to Matt Kinsella for the dedicated years to my project. He helped me become the inquisitive scientist I am today. Thank you for listening to my crazy ideas which became reality.

I want to thank Veena, my co-supervisor. It is hard to describe the amount of support you provided throughout the years. Thanks for the many collaborations you made possible for this project to become reality. Thanks for sharing your insights.

I want to thank Nick Bertos for his valuable philosophical discussions behind this project. Thanks for listening, sharing, and encouraging rational thoughts.

Additionally, I thank the members of my Ph.D. committee, Satya Prakash, Jianyu Lei, and Maryam Tabrizian. I appreciated your insights, suggestions, and willingness to guide my project.

I thank all my family for providing unconditional support. Thanks for loving and cheering me. Thanks for believing in me and helped me to preserve my essence.

Also, I thank all my friends and colleagues. Tao Jiang, Gil Munguia, Omar Peza, Joyce Jang, Sanjima Pal, Lucas Pardo, Lucy Kurtz, Nikos Dimitriou, Guangyu Bao, Michelle Tran, Xavier Elisseeff, this experience would not have been the same without you.

I thank all the collaborators including Hellen Kuasne, Anne Marie, Morag Park, Denis Flipo, Greg Bonnamour, Xavier Elisseeff, Audrey Ferlatte, Cleber Silveira Moraes, Kelly Sears, Lorenzo Ferri, Pina Sorrini, Julie Berube, and Sanjima Pal.

Finally, I want to thank all the funding sources that made my project possible. FRQNT (Fonds de recherche du Québec), McGill University, NSERC (Natural Sciences and Engineering Research Council of Canada), and the CIHR (Canadian Institutes of Health Research).

Contributions to Original Knowledge

Research article 1: Alginate–gelatin–Matrigel hydrogels enable the development and multigenerational passaging of patient-derived 3D bioprinted cancer spheroid models.

In this article, I prove my first hypothesis which states that controlling the composition of a bioactive hydrogel formulated with sodium alginate, gelatin, and Matrigel used to bioprint models will allow the rapid and gentle dissociation of spheroids. The isolated spheroids were then reintroduced into new hydrogels and passaged, or generations of, models from both patient gastric cells, and immortalized cell lines were shown to re-assemble into phenotypically stable patient spheroids over three passaging attempts.

The composite hydrogel was designed to be quickly de-crosslinked to isolate spheroids using the chelation of calcium ions. Matrigel, being an ECM-derived gel, provides a laminin-rich solubilized basement membrane that was used to incorporate a bioactive extracellular matrix that provides a tumor microenvironment-like niche for spheroid development. Specific consideration of the material properties was given to ensure that encapsulation of patient-derived esophagogastric cancer cells was capable without phenotypic changes.

Using rheology, I characterized the viscoelastic properties of the hydrogel to define its mechanical properties and formulate it according to the ranges required for viable cell encapsulation and extrusion bioprinting. Models created with my proposed formulation promoted spheroid development and reorganization of encapsulated patient esophagogastric cancer epithelial cells for three consecutive cycles of culture in the hydrogel for 21 days. During the 21 days, characteristics including growth rates, were

observed and fit into an exponential growth model. This quantitation allowed the spheroids to evaluate the response to standard-of-care doses of therapeutics and normalize inter-sample variability when cells are obtained from populations of patients.

The spheroids dissociated from the hydrogel can be further dissociated by trypsinizing to acquire single epithelial cells. This method allows spheroids undergoing proliferation and growth to be monitored using standard cell culture analysis. Creating generations of spheroids in a relevant matrix promotes cell-cell and cell-matrix interactions that can be observed as the environment varies depending on the experimental question. Overall, this dissociation method allows for patient-derived cancer cell spheroid expansion in bioactive printable hydrogels for up to three successive rounds of iterative printing over a total period of 84 days.

This model and method are relevant contributions that provide the capability of maturing and expanding spheroids over multiple generations. Each generation of single isolated cells from the previous generation's spheroid was provided a new bioactive hydrogel. Moreover, the material was the first demonstration of a mechanically tunable Matrigel with stiffness and shear thinning properties to be extrusion bioprinted. These properties provide tissue-relevant variables such as 3D architecture and a bioactive ECM, which promotes cellular interaction with their environment. I proved that this cell culturing method facilitates cancer cell expansion and allows the fabrication of multiple comparable cell-laden constructs suitable for drug testing experiments and downstream cellular analyses.

One of the current challenges in the field is the generation of miniaturized cancer models that are feasible to implement in drug screening and precision medicine applications

within a time frame that is clinically relevant for the patient. This model can be grown directly from biopsied or resected patient tissue samples. Using the geometric mean as an indicator for tumor surface area can provide direct feedback from different therapeutic combinations within three weeks. The platform integrates biomaterial engineering, bioprinting, and biological techniques to address the lack of a clinically relevant model for drug efficacy studies to drive personalized screening platforms using patient-derived tissues directly sourced from tumor sites.

Research article 2: Bioprinted Multi-Component Hydrogel Co-Culture Tumor-Immune Model for Assessing and Simulating Tumor-Infiltrated Lymphocyte Migration and Functional Activation.

In this article I proved the last aim of my hypothesis which explores the use of the previously developed model to measure and observe the migration cytotoxic tumor infiltrating lymphocytes through the physical barrier presented by the bioactive gel towards patient derived cancer organoids. To do this I designed a concentric co-culture model that mimics features of the geographical distribution of tumors and the immune system commonly found in solid *in-vivo* tumors. Esophagogastric cancer cells were grown in the interior of the model with 400-micron filaments extruded into a disc with a radius of 2400 microns and a single layer representing a tumor parenchyma-like region. The surrounding layers of the gel on the periphery containing TILs extruded to create a final disc model with an outer diameter of 4400 microns. The peripheral location of the TILs was inspired by histopathological observations that TILs in the stromal tissues migrate in immune active tumors from similar distances while experiencing similar biophysical barriers of the matrix.

Time-lapse and time series observations of the models during 15 days of culture provided quantifiable measurements of migration of the TILs towards the organoids. The chronological stages of degranulation and formation of the immunological synapse are measurable using quantitative microscopy. The results of these, and flow cytometry, experiments provided values used in a parameterized mathematical model that simulates migration mechanisms.

To perform the simulations a derivate of the FKPP equation that incorporates a cytotoxicity death term was developed. The outcome of the simulation provided insight that can be used to decouple passive from active cell migration mechanisms.

Traditional pre-clinical models fall short when used for immunotherapy since most models rely on immunocompromised animals. I demonstrated that is possible to reverse engineer and study crucial aspects of the immune response against cancer by implementing a bioprinted construct containing tumor cells and TILs within two adjacent zones. Importantly, I considered a clinically relevant time scale of 6-8 weeks from the initial diagnostic biopsy, to evaluate the motility and functional activity of TILs. I was able to see that cancer cells were not able to proliferate throughout the 15 days of development, demonstrating that migratory immune cells exerted an immunoregulatory effect.

Additionally, quantitation of TIL degranulation and protein secretion patterns suggest that cytotoxic activity in the presence of cancer cells took place. Behaviour that is not present in the TIL monoculture. This technology has the potential to be useful in personalized medicine as it provides results in a timeframe that is relevant for the patient. It can provide additional information to the oncology team to strategize cancer immune therapy depending on how patient TILs responded in experimental setting. This platform also has the potential to be used for novel immunotherapy treatments that do not have a traditional pre-clinical model available.

Finally, I had the opportunity to translate my insights and thoughts into a review article focused on how extrusion bioprinting has enabled the study of malignant neoplastic disease. Here I address the need for complex heterogeneous cancer models that recapitulate the complexity not only of the parenchymal component but also the stromal

compartments. I specifically contextualize tumor recapitulation using extrusion bioprinting, demonstrating the advantages of the technique and the potential to accelerate the field of cancer research. Furthermore, the most important message of this work is presented in the opportunity section where I detail the problems that are yet to be addressed and I provide an overview of the future research avenues and how to address these by implementing extrusion bioprinting.

The contributions and collaborative effort of co-authors are listed below.

Contribution of the Authors

Article type: Review Paper (DOI: 10.1021/acsbiomaterials.2c00998)

Constructing 3D in vitro Models of Heterocellular Solid Tumors and Stromal Tissues Using Extrusion-Based Bioprinting

Salvador Flores-Torres [a], Tao Jiang [d], Jacqueline Kort-Mascort [a], Yun Yang [d], Omar Peza-Chavez [a], Sanjima Pal [b], Alisia Mainolfi [a], Lucas Pardo [a], Lorenzo Ferri [b,c], Nicholas Bertos [b,c], Veena Sangwan[b] *, Joseph M. Kinsella [a,*]

Author contributions:

SFT consolidated the ideas within this manuscript, conducted the overall review of the methods, prepared the figures, wrote the first draft of the manuscript, and edited the manuscript throughout the review process.

TJ complemented the printability section of the manuscript including literature review and figure preparation and reviewed the manuscript.

JKM planned and created the tables within the manuscript, reviewed the literature for the extracellular matrix components section, and reviewed the manuscript.

YY complemented the printability section of the manuscript including literature review and figure preparation in the first draft.

OPC reviewed the literature regarding to extracellular matrix features and wrote the first draft of the corresponding section.

SP complemented all sections corresponding to cancer bioprinting within the manuscript, conducted literature review, and reviewed the manuscript.

AM helped preparing the first draft, conducted literature review, and suggested relevant literature for each section.

LAP helped preparing the first draft, conducted literature review, and reviewed the literature regarding the extracellular matrix.

LF complemented the manuscript with relevant literature, provided his clinical expertise, and reviewed the final version of manuscript.

NB complemented the manuscript with relevant literature regarding, provided insightful ideas, and reviewed the final version of manuscript.

VS guided the overall scope of the manuscript, supervised this work from start to finish, provided insightful ideas, and reviewed the manuscript first and final drafts.

JMK guided the overall scope of the manuscript, supervised this work throughout its creation, and edited the final version of the manuscript.

Article type: Research Paper (DOI: 10.1088/1758-5090/abdb87)

Alginate-gelatin-Matrigel hydrogels enable the development and multigenerational passaging of patient-derived 3D bioprinted cancer spheroid models

Salvador Flores-Torres [a], Omar Peza-Chavez [a], Hellen Kuasne [e], Jose G. Munguia-Lopez [a,b], Jacqueline Kort-Mascort [a], Lorenzo Ferri [d,g], Tao Jiang [c], Charles V. Rajadurai [e,f], Morag Park [e,f,g,h,i], Veena Sangwan [d*], Joseph M. Kinsella [a,*]

SFT designed, planned, and executed bioprinting, imaging, cell culture, drug testing experiments, and genotyping experiments, acquired, processed data, and wrote the first draft of the manuscript, and edited the manuscript afterwards.

OPC executed bioprinting, 3D cell culture, cell viability experiments, acquired and processed data.

HK developed the GP-118 and other organoids from PDXs established in the lab of MP.

JGML executed cell culture and assay experiments, acquired and processed data.

JKM contributed to image analysis and statistical data results.

TJ assisted in characterizing biomaterial printability.

LF provided patient samples and clinical expertise for the study.

CVR provided cell lines and expertise in 3D cell biology techniques.

MP provided cell lines and expertise in 3D cell biology techniques.

VS co-supervised this work, contributed to the experimental design and data processing.

JMK supervised this work, designed, and planned experimental methods.

Article type: Research paper (ready to submit)

Assessing tumor-infiltrated lymphocyte migration and activation within bioprinted co-culture tumor model.

Salvador Flores-Torres [a], Nikolaos M. Dimitriou [a], Lucas Antonio Pardo [a], Jacqueline Kort-Mascort [a], Sanjima Pal [d], Hellen Kuasne [f], Omar Peza-Chavez [a], Julie Berube [d], Nicholas Bertos [e], Lorenzo Ferri [d,g], Georgios D. Mitsis [a], Morag Park [f,g,h,i,j], Veena Sangwan [d,*], Joseph M. Kinsella [a,*].

Author contributions:

SFT designed, planned, troubleshooted, and executed bioprinting, imaging, flow cytometry, acquired data, processed data, interpreted data, wrote the first draft of the manuscript, and edited the manuscript.

ND wrote the and optimized code to describe experimental data, conducted calibration tests, and fine tunned the algorithm.

LAP executed cell culture, bioprinting, acquired data, and processed data, and edited the manuscript.

JKM assisted in experimental planning and troubleshooting, performed cell culture and statistical analysis.

SP planned the flow cytometry experiments, digested patient-derived samples to isolate T-cells, sub-cultured these for experimental purposes, and provided her expertise and aided in experimental design.

HK developed the GP-118 and other organoids from PDXs established in the lab of MP.

NB digested patient-derived samples to isolate T-cells, sub-cultured these for experimental purposes, and provided her expertise and aided in experimental design.

JB digested patient-derived samples to isolate T-cells, sub-cultured these for experimental purposes, and provided her expertise and aided in experimental design.

LF provided patient samples and clinical expertise for the study.

MP provided cell lines and expertise in 3D cell biology techniques.

VS co-supervised this work, contributed to the experimental design and data processing.

JMK supervised this work, designed, and planned experimental methods.

List of Figures and Tables

Literature Review

Figures in section 2.1 to 2.4

Tables in section 6.1 to 6.4

Review article

Figures in section 2.5

Tables in section 6.5

Research article No.1

Figure in section 3.1

Figures in section 7.1.1 to 7.1.9

Figures in section 7.1.10

Tables in section 7.1.10

Research article No.2

Figures in section 3.3

Tables in section 7.3

List of Abbreviations

2D: Two-dimensional

3D: Three-dimensional

5-FU: 5-Fluorouracil

AAfB: Aspiration-assisted freeform bioprinting

ADMSC: Adipocyte-derived mesenchymal stem/stromal cells

AFM: Atomic force microscopy

APC: Allophycocyanin

AR: Androgen receptor

ATC: Adoptive T-cell

AxGyMz: Alginate (%), Gelatin (%), Matrigel (%)

Breg: regulatory B cell

CAA: Cancer-associated adipocyte

CAF: Cancer-associated fibroblast

CAL: Computed axial lithography

CAR: Chimeric antigen receptor

CTLA4: cytotoxic T-lymphocyte antigen-4

DBB: Droplet-based bioprinting

DC: Dendritic cell

DCF: Docetaxel, Cisplatin, 5-Fluorouracil

dECM: Decellularized extracellular matrix

DLP: Digital light processing

DMD: digital micromirror device

DMEM: Dulbecco's modified eagle medium

DMSO: Dimethyl sulfoxide

DNA: Deoxyribonucleic Acid

D-PBS: Dulbecco's phosphate-buffered saline

EBB: Extrusion-based bioprinting

ECM: Extracellular matrix

EDTA: Ethylenediaminetetraacetic acid

EGA: Esophagogastric adenocarcinoma

EGF: Epidermal growth factor

EHS: Engelbreth-Holm-Swarm

EMT: Epithelial-mesenchymal transition

ER: Estrogen receptor

FACS: Flow cytometry staining

FasL: Fas ligand

FDA: Food and Drug Administration

FITC: Fluorescein isothiocyanate

FKPP: Fisher Kolmogorov Pishkunov Petrov

FLOT: Docetaxel, Oxaliplatin, 5-Fluorouracil

FRESH: Freeform reversible embedding of suspended hydrogels

GelMa: Gelatin methacrylate

GF: Growth factor

GFP: Green fluorescent protein

GM: Geometric mean

GR: Growth rate

GvHD: Graft versus host disease

H&E: Eosin and hematoxylin

HA: Hyaluronic acid

HER2: human epidermal growth factor receptor 2

HIF-1α: Hypoxia-inducible factor 1-alpha

Hu-PBL: Human peripheral blood leucocyte

HUVEC: Human vascular endothelial cell

i.e.: id est

IC: Inhibition concentrations

IFP: Interstitial fluid pressure

IL: Interleukin

ISRES: Improved Stochastic Ranking Evolution Strategy

LAB: Laser-assisted bioprinting

LAMP1: Lysosome-associated membrane protein 1

LC/MS/MS: Liquid chromatography tandem mass spectrometry

LEC: Lymphatic endothelial cell

LIFT: laser-induced forward transfer

MHMCMC: Metropolis Hastings Markov chain Monte Carlo

MHCI: Major histocompatibility complex I

MHCII: Major histocompatibility complex I

MH-MCMC:

MMP: Matrix metalloproteinase

MSC: Mesenchymal stem cell

MVN: Multivariate normal distribution

NOD: Nonobese diabetic

NRMSE: Normalized root mean squared error

P53: Transformation-related protein 53

PD1: Programmed dead protein 1

PDE: Partial Differential Equation

PDL1: Programmed dead protein ligand -1

PDOs: Patient-derived organoids

PDX: Patient-derived xenograft

PEGDA: Poly(ethylene glycol) diacrylate

PFA: Paraformaldehyde

PMBC: Peripheral blood monocyte

PR: Progesterone receptor

PSC: Pancreatic stellate cell

RGD: Arginine-glycine-aspartic acid

ROI: Region of interest

SCID: Severe combined immunodeficiency

SD: Standard deviation

SLA: Stereolithography

SSE: Sum of the squared error

STR: Short tandem repeat

SWIFT: Sacrificial writing into functional tissue

TACS: Tumor-associated collagen signatures

TAM: Tumor-associated macrophage

TAN: Tumor-associated neutrophil

TCR: T-cell receptor

TGF-β: Transforming growth factor β

TIL: Tumor-infiltrated lymphocyte

TIME: Tumor immune microenvironment

TME: Tumor microenvironment

TMF: Triggered-micropore-forming

TMZ: Temozolomide

UV: Ultraviolet

VBP: Volumetric bioprinting

VEGFA: Vascular endothelial growth factor A

VEGF-C: Vascular endothelial growth factor C

VEGF-D: Vascular endothelial growth factor D

1. Introduction

The global estimated number of cases for all cancers combined is expected to reach approximately 28.4 million new cases in 2040. This is almost a 47% increase from the number of cases observed in 2020 (19.3 million)[1]. It is recognized that cancer prevention is the most sustainable way into the future and mitigation strategies have been implemented however, the global incidence for cancer continues to increase at a rapid pace[2]. This phenomenon is attributed to the multiple risk factors for cancer such as smoking, alcohol consumption, air pollution, diet patterns, obesity, sunlight exposure, etc[3]. Naturally, some malignancies are more aggressive and harder to resolve by current treatment options as reflected by the annual number of deaths per cancer type. Examples of these include lung cancer, pancreatic cancer, stomach cancer, liver cancer, esophageal cancer, and gastric cancer. Malignancies of the esophageal duct and the stomach rank in 7th and 5th place in terms of incidence and 6th and 4th in mortality worldwide (respectively). With combined estimates reaching nearly 1.3M new cases and almost 900K deaths[1], esophagogastric adenocarcinomas (EGA) or gastroesophageal cancers are an important public health concern. Malignancies of the esophagus and the stomach are categorized as squamous cell carcinoma, esophagogastric junction adenocarcinoma, and distal adenocarcinomas. Worldwide, the overall 5-year survival rate of esophagogastric malignancies is around 20%[4,5] and it is highly dependent on the demographic group, stage of cancer, and treatment regime[6].

Since gastroesophageal cancers are not associated with specific symptoms or an effective screening modality, patients are often diagnosed with advanced disease and there are few therapeutic options for them. Ferri *et al.* (2012)[7] was the first group to demonstrate the

efficacy of neoadjuvant Docetaxel for gastroesophageal malignancies, helping to establish four cycles of Docetaxel-based triplet chemotherapy pre- and post-surgery (DCF (Docetaxel/Cisplatin/5-FU) or FLOT (Docetaxel/Oxaliplatin/5-FU)) as the standard of care[8]. This treatment, the most effective approach to date, has an initial response rate of >60%[8]. However, in addition to the ~40% of patients with innately resistant tumors who receive several months of futile and toxic treatment prior to curative-intent surgery, recurrence due to acquired resistance arises in 50% of initial responders, resulting in a sustained response rate of ~30%, and a 5-year survival below 20%[9]. Therapies targeting genomic changes in tumor epithelial cells have largely failed, challenged by not only the enormous diversity of genetic and non-genetic alterations and intra-tumoral (cellular) heterogeneity[10,11] but also interactions between the neoplastic cells and the tumor microenvironment. Alternate strategies are therefore urgently needed to complement traditional systemic chemotherapy for tumors that develop resistance throughout the course of treatment or spawn innately resistant. Moreover, there is an increasing need for predictive non-invasive tumor surrogates of response to increase the effectiveness and appropriateness of treatments[12].

The main objective of this project is to develop an *in-vitro* co-culture platform to interrogate the biological interactions between patient-derived gastroesophageal cancer cells and tumor-infiltrated lymphocytes. Additional requirements for this platform are mainly compatibility with current analytical assays and methodologies such as, confocal microscopy, flow cytometry, antibody labeling, and automated handling techniques. In the future, this project is expected to stem towards enabling T-cell selection strategies for adoptive T-cell therapy**. I hypothesize that e*xtrusion bioprinting (EB) of***

alginate-gelatin-Matrigel-based biomaterial scaffolds will enable the study of tumor-infiltrating lymphocyte (TIL) directional motility and activation towards gastric cancer cells. To validate my hypothesis, I will use a reconstructed 3D cell culture model consisting of patient-derived tumor epithelial cells and cytotoxic tumor infiltrating lymphocytes deposited into specific initial locations, with controlled cell density, and a mechanically and bioactive tunable matrix material comprised of Matrigel, alginate, and gelatin. The proposed bioprinted co-cultures will be used to assess the utility of therapeutics against gastroesophageal cancer within a clinically relevant timeframe. I will conduct the studies along the following aims:

Aim 1: Characterize the rheological performance of alginate-gelatin-Matrigel (AxGyMz) hydrogels, evaluate the effect of the matrix constituents on cell culture, and document the chemosensitivity of cancer spheroids.

The rationale behind selecting alginate, gelatin, and Matrigel comes from the need to build a volumetric construct to host cells while providing biomechanical inputs that stimulate their behavior. I had the opportunity to participate in developing bioprintable material libraries based on alginate and gelatin. In this previous investigation[13], hydrogels comprised of distinct concentrations alginate and gelatin were used to encapsulate cancer cells that served as biomechanical inputs. This material tunability enabled us to identify two biomaterial candidates that provided the best environments for cancer cells to reorganize into multicellular spheroids. Over the course of 21 days, we observed different growth patterns and morphologies.

Aim 2: Evaluate 3D cell culture passaging by chelating calcium ions from calcium-alginate and document post-printing cancer spheroid development.

The rationale for conducting this aim is the need to have a compatible cell culture platform with current analytical techniques. My line of thought was to take advantage of the susceptibility of calcium ions to be chelated from alginate chains. This is often depicted as one of the limitations of alginate-based cell systems. I investigated calcium-alginate decrosslinking by chelating calcium ions from the alginate chain with citrate ions in the presence of sodium ions. Within the critical achievements of this work, I sought to recover the cellular content within the bioprinted constructs. This would allow me to evaluate the status of the cells and maintain the cancer cell culture for long periods of time. As we will see in chapter 2, alginate decalcification was achieved by exposing the crosslinked constructs to citrate ions.

Aim 3: Evaluate tumor-infiltrated lymphocytes motility, and activation in bioprinted co-culture constructs.

The intention behind working with tumor infiltrated lymphocytes (TILs) is the increasing need for *in-vitro* platforms that address the challenges behind the selection of T-cell subpopulations in adoptive T-cell therapy. I foresaw the possibility of including TILs within a compartmentalized co-culture system alongside cancer cells. Using extrusion-based bioprinting, tumor cells and TILs could be strategically deposited in two-distinct adjacent regions. These regions would allow the study of the interactions between T-cells and cancer cells in a controlled environment. Chapter 3 will present the results of this aim.

The results of these 3 are presented after the introductory section and chapter 1. First, I introduce a literature review to discuss the strategies to create *in-vitro* cancer models. Then, the advantages of bioprinting as the enabling technique in cancer research will be

presented and the technical aspect behind the extrusion-based bioprinting method will be reviewed. In addition, chapter 1 complements this introduction by presenting the review article titled "*Constructing 3D in vitro Models of Heterocellular Solid Tumors and Stromal Tissues Using Extrusion-Based Bioprinting*" where I present state-of-the-art behind bioprinting the tumor microenvironment. Subsequently, the second chapter will introduce my first scientific article where I present an innovative method centered around a bioprintable biomaterial formulation that facilitates the generation of multicellular tumor spheres using patient-derived esophagogastric adenocarcinoma cells. Finally, the third chapter introduces the second research manuscript where the above-mentioned biomaterials and tumor replicas are used to create a bioprintable co-culture system that helps in characterizing the behavior of patient-derived tumor-infiltrated lymphocytes in the presence of malignant cancer cells. Each of the following chapters offers a complementary literature review and successive logical connection with the main goal of this work.

2. Literature Review

Cancer is a group of progressive diseases characterized by an uncontrolled proliferation of malignant cells that often endow their adjacent stroma with pro-tumoral functions[14]. In early 2000, Hanahan and Weinberg proposed a framework to rationalize the complexity of tumor pathogenesis[15]. In their publication, "*The Hallmarks of Cancer*", the authors summarized decades of cancer research in six main characteristics that all cancerous cells possess: self-sufficiency in growth signals, insensitivity to growth suppressor signals, apoptotic resistance, tissue invasion and metastasis, limitless proliferation potential, and angiogenesis[15]. Later in 2011, the same authors complemented his original work with two new hallmarks and two enabling characteristics[16]. In this update, authors acknowledge that tumor biology can no longer be centered around the cancerous cells, but it must also consider the presence and contributions of the surrounding microenvironment where a heterogeneous population of cells reside. At that time, the emerging hallmarks of cancer biology recognized the altered metabolism of cancer cells and their ability to avoid the immune system.

Additionally, genomic instability in cancer cells and tumor-promoting inflammation by the immune system were listed as cancer-enabling characteristics. Then, almost eleven years after, in 2022, Hanahan updated the Hallmarks of Cancer by introducing cancer cell phenotypic plasticity and cellular proliferative arrest (senescence) as emerging hallmarks and non-mutational epigenetic reprogramming and polymorphic microbiomes are described as cancer-enabling characteristics[17]. These pieces of elegant literature are evidence of the ongoing effort behind understanding neoplastic disease coupled with a colossal interest in mitigating the increasing burden of cancer worldwide.

Patient prognosis is strongly guided by the immune's system ability to recognize and eradicate cancer cells where an iterative cancer-immunity cycle is required to achieve complete removal of tumor cells[18]. The immune system treats a tumor as an emerging pathogen and responds to it by mounting an immune response that aims to produce T-cells equipped with tumor recognition and killing molecular machinery[19]. The sub-lineage, functional state, and abundance of immune cells within and around the tumor have been directly linked with disease progression in cancer patients[20-24]. More specifically, the prognostic significance of tumor-infiltrated lymphocytes (TILs) has been extensively documented for most cancers, including triple-negative breast cancers[25-27], colorectal[28-30] and gastric cancers[31,32], lung cancers[33,34], head and neck squamous cell carcinomas[35], prostate cancer[36], cervical[37] and ovarian cancers[38], and skin melanomas[39].

The complex interactions between a malignant neoplasm and the immune system often culminate in tumor eradication or immune evasion by the tumor[40]. As the tumor progresses into a clinically detectable malignant mass, the complex interactions between cancer cells and the immune system often transition into an anergic state where T-cells become hyporesponsive and tolerate tumor growth[41]. Thus, cancer progression is often undisturbed.

The human body's tumoricidal response consists of identifying cancer cell antigens using dendritic cells to prime and activate T-cells destined to infiltrate the tumor, eradicate malignant cells, and continue the cancer-immunity cycle[18]. The immune response against a tumor is characterized by the complex interactions between the immune system and the tumor microenvironment that involve the secretion of cytokines and upregulation of membranal proteins[42]. These processes are elegantly described in detail by Chen and

Mellman[18]. Briefly, oncogenesis and tumor development produce cancer antigens. Ideally, these antigens are picked up by dendritic cells (DCs) for processing and presentation. Then, DCs prime and activate T-cells by presenting antigens on MHCI and MHCII (major histocompatibility complex) molecules. The primed and activated T-cells (effector cells) journey to and infiltrate the tumor. The effector cells will specifically recognize, bind, and kill cancer cells using their T-cell receptor (TCR) and cognate antigen bound to MCHI. Finally, eradicating cancer cells culminates with more tumor-associated antigens that will only aid in increasing the immune response against the tumor mass. However, the TIME is regularly an immunosuppressed biosystem that provides sanctuary to cancer cells[43]. Solid tumors often develop immunosuppressive strategies that challenge the immune system's ability to eradicate malignant cells[44]. Cancer cells can evade immune surveillance by exploiting T-cell tolerance[45], disrupting antigen presentation pathways[46-48], and activating co-inhibitory signals[49]. If effector T-cells reach the tumor, an immunosuppressive environment will challenge effector cells through cytokine stimulation and protein binding[44,50]. Some of the immune evasion mechanisms that tumors develop to avoid eradication are the overexpression of membrane proteins. Some examples of these proteins are the programmed dead protein ligand - 1 (PDL1), Fas ligands (FasL) to bind to Fas on the membrane of effector cells and trigger their apoptosis, and CTLA4 binding site that promotes T-cell anergy[51].

Genomic profiling has been performed on tumors to identify somatic DNA alterations, assuming that these genomic biomarkers would guide the selection of targeted therapies[52,53]. However, in esophagogastric tumors, targeted therapies other than HER2 inhibitors have failed[54]. The Food and Drug Administration (FDA) has approved

immunotherapy (Pembrolizumab (PD-1 inhibitor)) for metastatic tumors, regardless of tumor type[55]. However, response rates to checkpoint inhibition in gastroesophageal cancers in the metastatic setting have generally been unsatisfactory[56], suggesting a limited understanding of the tumor immune microenvironment for a good response to immunotherapy. Recent studies have identified tumor-specific genetic alterations driving vulnerabilities that can be exploited to target the tumor with combination therapeutics[57]. Importantly, these studies revealed multiple oncogenic alterations in the same tumor, which may be a potential cause of treatment failure and the development of resistance. In addition, the presence of an immunosuppressive environment represents a challenge for effector cells[58]. Thus, it is crucial for pre-clinical models to recapitulate the above-mentioned characteristics.

Current approaches to study the interactions between human cancers and the immune system rely on the use of immunosuppressed mouse models[59,60]. Even though these murine models can support the co-engraftment of human tumors and human immune cells[61,62], significant challenges limit their successful application. Aside from their overall immunological vulnerability, immunocompromised organisms often develop graft-versus-host disease (GvHD). This life-threatening condition compromises the integrity of the organism and significantly limits the experimental outcomes[63]. Significant differences between murine models and the human species have been framed as the reasons behind the poor performance of anticancer treatments in clinical trials[64-66]. Moreover, the precise real-time prediction power of small animals engrafted with human tumors is difficult to align with the clinical decisions behind treating a patient[67].

An attractive alternative to small animal models is the use of patient-derived organoids. These multicellular biological structures present a better opportunity to provide predictive data within a time frame clinically relevant to the patient[68-70]. As I will explain in the following section, cancer organoids can recapitulate essential features of the parental tumor, such as chemosensitivity[71], morphological features[72,73], and genetic diversity[74]. These *in-vitro* elucidations have become extremely important in guiding the future of cancer immunology research and precision medicine[75].

2.1. Miniaturized models of neoplastic disease: 2D vs. 3D cell cultures

Even though two-dimensional (2D) *in-vitro* cancer cell monocultures and small animal models have proven useful and are still used in cancer research, the significant number of limitations has motivated researchers to superior *in-vitro* platforms that accurately recapitulate the features of parental tumors[76,77]. More recently, emerging cancer models have been instrumental in fundamental biological discoveries and therapeutic success. Three-dimensional (3D) cancer cell culture strategies have become part of the essential cancer discovery toolbox. Unlike in 2D monoculture, cancer cells in 3D environments reorganize into multicellular organoids and can recapitulate some of the features of human tumors, such as nutrient gradients and drug resistance[78]. The most representative *in-vitro* elucidation of a parental tumor can be achieved through patient-derived cancer organoids (PDOs). PDOs have been proposed as a reliable alternative to pre-clinical animal models as they preserve critical features of the original tumor, such as chemosensitiviy[79,80]. These similarities between the elucidation and the parental tumor are instrumental in cancer research as researchers can use miniaturized tumor versions to predict patient outcomes and strategize alternative therapies. Such is the importance of PDOs that these have been proposed as a platform to test the efficacy of immunotherapy[75]. Traditional methods implemented to create *in-vitro* multicellular cancer spheroids include centrifugation-induced spheroids[81], hanging drop[82], constant rotation within microgravity bioreactors[83,84], magnetic levitation[85], microfluidic devices[86,87], cell-laden hydrogels[88], and 3D bioprinting[89-91]. Together, these techniques are pipelines cancer researchers follow to establish reliable models of neoplastic disease. Despite their reorganization into tumor-like structures in suspension conditions, cancer cells *in-vivo* are in constant biomolecular and biomechanical exchange with their

adjacent stroma. Thus, an appropriate extracellular matrix (ECM) analog not only populated with a correct number and type of cells but also with the relevant mechanical features is required to increase the physiological relevance of *in-vitro* cancer models. Hydrogels are popular biomaterials used in 3D culture to simulate ECM, and their most attractive characteristics include biomechanical tunability, bioactivity, biodegradability, biocompatibility, and their ability to store large amounts of water[92]. Advanced 3D *in-vitro* cancer cell culture platforms and disease models not only include relevant cell populations, but also consider crucial architectural features present in tumors. Manual casting of hydrogels has been a successful approach to induce 3D cancer spheres nevertheless, complex tumor elucidations require certain degree of control that is unfeasible to recreate by hand. Automated material handling techniques such as 3D bioprinting are an attractive solution to this problem. As a biofabrication technique, bioprinting holds unexploited potential to accelerate cancer research because it enables the use of multiple cell types and user-defined biomaterials without loosing control over the initial conditions of the 3D cell culture models. It has been demonstrated that bioprinted cancer cell-laden constructs can be used as miniaturized disease models where complex biological conditions and pathological features of the TME can be studied[93-103]. The following section introduces the bioprinting modalities alongside their advantages and limitations. Moreover, the technical aspects of extrusion bioprinting and reviewed.

2.2. Three-Dimensional Bioprinting

Fundamentally, through diverse mechanisms and computer software, bioprinting approaches implement cell-laden biomaterials to aid the creation of *in-vitro* cell constructs. So far, there is no single technique that enables the production of all tissue scales. Each specific bioprinting strategy offers specific advantages and holds significant limitations that will be discussed hereafter.

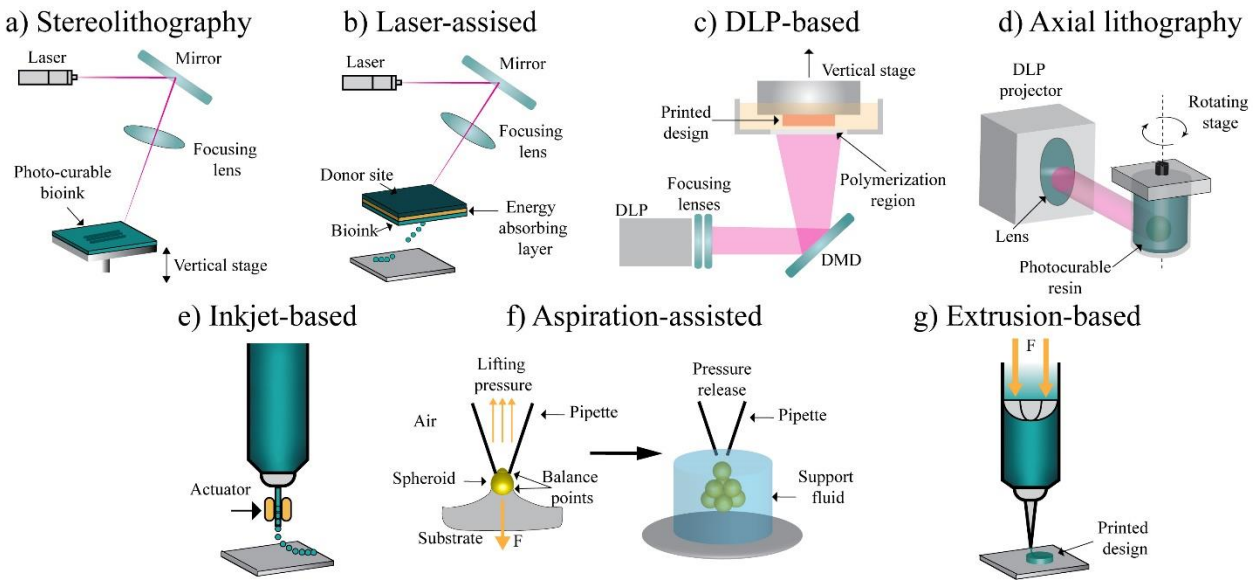

Figure 1. Schematic representation of current bioprinting techniques. a) Stereolithography printers use a laser to induce photopolymerization of materials into layer-by-layer assemblies. b) Laser-assisted printers focus a pulsed incident laser beam onto an energy-absorbing material, causing a vapor bubble to be generated, and propels a bioink droplet onto a surface. c) DLP-based printers photopolymerize single planes of photoreactive monomers, creating polymerized layers. The printed design is then accumulated as the stage moves upwards, polymerizing materials at each plane based on projected light patterns. d) Volumetric printing or axial lithography. Axial lithography or volumetric printing produces structures using a light source to photo-simulate a rotating

container with photocurable resin. e) Inkjet printers utilize and actuator to generate small drops of bioink sequentially. f) Aspiration-assisted printers utilize aspiration forces to handle multicellular spheres and allocate them within support fluids at defined positions. g) Extrusion printers conduct the continuous deposition of soft materials by applying a controlled pneumatic pressure or a mechanical force. The desired structures are vertically accumulated.

2.2.1. Stereolithography (SLA)

Stereolithography (SLA) relies on a controlled illumination beam to selectively crosslink photocurable biocompatible polymers or photo-activated proteins (**Figure 1.a**). The SLA bioprinting strategy provides access to complex architectures other bioprinting techniques struggle with (i.e., hollow vessels and free-standing arches). Also, laser and beam based bioprinting modalities offer shear-free material deposition, an important advantage over extrusion-based methods. Challenges associated with this technique are: (1) bioink design must consider a photo-sensitive element, (2) photo-crosslinking processes can reduce and compromise cell viability, and (3) the SLA technique is unable to incorporate multiple cell types and materials[104]. Nevertheless, some groups have proposed manual rinsing steps of the crosslinked geometry before resubmerging into different liquid bioinks and photo-curing new structures[105-107].

2.2.2. Laser-assisted bioprinting (LAB)

LAB relies on the principles of laser-induced forward transfer (LIFT). LAB techniques involve a 'donor' layer of material responsive to laser stimulation. This donor layer is comprised of an overlying metallic energy-absorbing layer and an underlying layer of suspended bioink solution. A laser pulse is applied to a small area of the absorbing donor layer material, causing it to vaporize and form a small pressure bubble at its interface with

the bioink layer. Then, the high-pressure bubble propels the bioink onto the collecting substrate, which is subsequently crosslinked (**Figure 1.b**). The resolution of LAB is set by laser fluence, surface tension, wettability, the air gap distance between donor and substrate, and the thickness and viscosity of the biological layer[108]. LAB facilitates non-contact between the dispenser and the bioink, thereby reducing mechanical stress on the cells. Laser printing mitigates many of the challenges of inkjet printing as it is amendable to a wide range of bioink viscosities (1-300 mPa·s) and higher cell densities of up to 10^8 cells/mL. LAB offers microscale resolution of single cells per droplet using a laser pulse repetition rate of 5 kHz, with speeds up to 1,600 mm/s[109]. However, providing high structural resolution requires rapid gelation kinetics, which results in a low overall flow rate and speaks to the time constraints inherent to LAB. Additional limitations include the potentially unknown effects of laser exposure on cells, high cost, complexity, and difficulty accurately targeting and positioning cells (due to the nature of the donor coating mechanism)[110].

2.2.3. Digital light processing (DLP)-based bioprinting

DLP-based technology is a type of SLA that uses a mirror to focus a beam. DLP-based bioprinting uses a projector to project light onto a photosensitive prepolymer bath. The designed structure is generated on a vertical stage that moves on the *z-axis* at a constant speed. During printing, light is controlled by a digital micromirror device (DMD). The desired 3D structures are built by coordinating the movement of the stage position in the *Z*-axis as the resin is photocured (**Figure 1.c**). Printing speeds vary from 25 to 1000 mm/s[111], and submicron resolutions are possible[112].

2.2.4. Volumetric bioprinting (VBP) or computed axial lithography (CAL)

Volumetric printing, also known as computed axial lithography (CAL), is a printing method that entered the additive manufacturing paradigm in recent years. Volumetric printing uses multiple light sources that emit patterned light from angled directions, unlike the layer-by-layer forming mechanism employed in all other printing methods. The energy of each single light source alone is insufficient to cure the photo-sensitive material. However, the contribution of the light sources from multiple directions causes a point in space to reach the curing threshold[113]. A further developed VBP method features a single light (**Figure 1.d**) source casting a laser onto a rotating resin container to simulate the effects of multiple light sources[114-116]. Volumetric printing significantly increases printing speed since objects are built volume by volume rather than layer by layer. For example, the fabrication time of a human auricle model (0.15 cm^3) using VBP takes only 22.7 seconds, while using extrusion printing and DLP-based printing methods take 263.9 s and 686 s, repectively[114]. VBP has been successfully used in building porous bone and liver-like metabolic models where living cells are embedded, showing promising cell viability and functionality[114,117]. This printing method can potentially be employed to rapidly build complex cancer models within seconds.

2.2.5. Inkjet/Droplet-based bioprinting (DBB)

Inkjet bioprinting, or DBB (**Figure 1.e**), uses different energy sources such as sound, temperature, and electricity to elicit volumetric changes within the nozzle, thereby generating controlled-size droplets in a high-throughput fashion [104,118]. Inkjet printers are advantageous for their low cost, given their close resemblance to commercial printers, rapid printing speeds, high cell viability, and ability to avoid contamination through

contactless printing[118] [104]. However, current inkjet printer heads are based on microelectromechanical system devices that prevent them from working with highly viscous bioinks. As such, the fidelity of inkjet printing is limited to materials with less than 15mPa·s viscosities and less than $1x10^6$ cells/mL [104]. More so, settling effects, whereby cells begin to settle within the cartridge, can introduce undesired defects in the constructs. This challenge can be mitigated by agitation to reduce cellular aggregation, settling, and nozzle clogging [104,119].

2.2.6. Aspiration-assisted freeform bioprinting (AAfB)

Additive manufacturing through aspiration maneuvers harnesses the power of aspiration forces to position biologics precisely. This technique is commonly used to embed cell spheroids in yield-stress gels. Pre-fabricated cell spheroids are picked up from a reservoir, lifted from their culture dish, quickly transported to the bioprinting stage and introduced into a yield-stress gel exhibiting Herschel-Bulkey properties[120] (**Figure 1.g**). A delicate balance between the suction force and the drag force experienced by the cellular aggregate must be evaluated to achieve an appropriate aspiration force while circumventing complete aspiration of the spheroid, breakage, piercing, or significant loss of cell viability[121,122]. The AAfB technique stands out from others as it utilizes cell aggregates as building blocks. In combination with functionalized yield-stress gels, strategic positioning of cellular aggregates has been demonstrated to be vital for experimental outcomes[123].

2.2.7. Extrusion-based bioprinting (EBB)

Extrusion bioprinting is the most used bioprinting modality due to its simple mechanical setup. Generally, cartridges filled with bioinks cells are mounted onto a computer-controlled XYZ stage. Using either pneumatic pressure or mechanical force, the robotic

stage will additively stack bioink in the Z direction, with each deposited layer serving as the base for the next[104] (**Figure 1.h**). Materials with viscosities ranging from 30mPa·s to $6x10^7$ mPa·s are compatible with EBB[110]. Usually, EBB-compatible materials can be described as non-Newtonian fluids: their viscosity depends on the shear rate they experience. A substantial amount of research must be dedicated to bioink design to meet the biomechanical requirements of an "ideal bioink" (discussed in the following sections). Briefly, during extrusion, the bioink should experience shear-thinning and thixotropic behavior to prevent clogging of the extrusion microneedles, protect cells from the shear stress that builds during material ejection, and assume a stable structure at rest. After extrusion, as the bioink exits the nozzle and shear forces are no longer present, the biomaterial must regain most of its original mechanical properties to hold its weight against gravity (avoid spreading). For those bioinks with unfavorable properties for post-shear reconstitution, freeform reversible embedding of suspended hydrogels (FRESH) 3D bioprinting represents an alternative for their use. By introducing a support bath with a yield-stress behavior that allows the insertion and movement of a nozzle, low viscosity, "ultrasoft" bioinks can be embedded within a material (Bingham plastic or Herschel-Bulkley fluid) that resolidifies and locks the deposited filament as the nozzle travels the printing path[124]. Biological structures and cell-laden environments have been successfully constructed using support baths[125-127].

Despite the advantages of EBB, high extrusion pressures impose high mechanical stresses that significantly impact cell viability. This challenge can be mitigated with larger nozzle diameters and smaller extrusion pressures; however, resolution and speed are major trade-offs[128]. Moreover, optimizing diverse biomaterials with appropriate viscosity,

melting temperature, modulus, gelation, crosslinking, and post-deposition secondary characteristics is necessary to maintain post-extrusion high structural fidelity and cell viability.

In the following two sections, we will focus on the specifics of 3D bioprinting through extrusion mechanisms since it favors the automated handling of multiple materials and multiple cell types at high cell densities to create heterogenous models. The ideal features of an extrudable material will be discussed. Then, we will review the importance of material printability and the different printability evaluation strategies.

2.3. Designing the ideal bioink for extrusion-based printing

Biomaterial design for EBB is a challenging task. Broadly, 'bioinks' are composites of biomaterials and living cells that are fundamental to the bioprinting process. Hydrogels, often used as material constituents of bioinks, possess high water content and are particularly attractive for their ability to incorporate and sustain bioactive compounds in a 3D extracellular-matrix-emulating environment. These networks, comprised of crosslinked hydrophilic polymer chains, can be natural or synthetic and precisely engineered via mechanical and biochemical tunability. Importantly, biochemical and mechanical hydrogel properties must also be optimized depending on the selected biofabrication method. Specifically, we can define different performance criteria to which bioinks must adhere before, during, and after extrusion, as well as throughout 3D cell culture timeline (**Figure 2**). Although most features can be engineered into a hydrogel bioink, specific requirements pertaining to bioadhesion, bioactivity, degradation, transport, and mechanics are paramount. More so, bioinks must be subject to rigorous design criteria given that their fabrication is limited to the opposing constraints of the

'Biofabrication Window'. Briefly, bioinks must simultaneously show high structural fidelity, appropriate rheology, and biocompatibility to ensure printability and favorable cell behavior. Figure 2 details the phases of bioink performance in extrusion bioprinting.

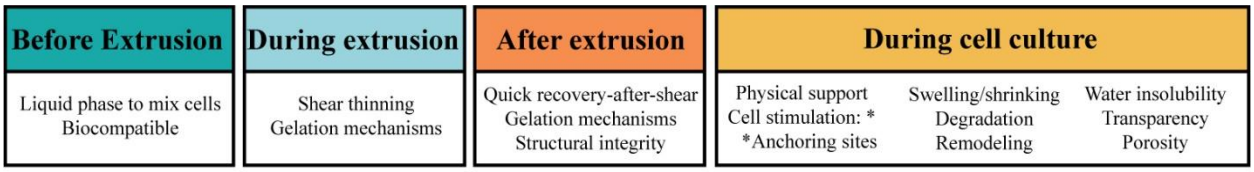

Figure 2. Bioink performance requirements.

(1) Before , the bioink must be in an induced liquid phase (G" > G') or exhibit properties of a "weak gel" to favor endogenous cell encapsulation in a biocompatible environment. The most common way of achieving the sol phase of a bioink material is by choosing a material composition that will undergo reversible internal configuration changes at specific temperatures (i.e., alginate-gelatin blends)[13]. (2) During extrusion, the bioink must exemplify shear thinning behavior to avoid high extrusion pressures that decrease cell viability[129-131]. The reduction of apparent viscosity results from the disruption of weak intramolecular interactions as the material is forced to flow through a nozzle[104]. In other words, macroscopic flow results from internal structural changes such as fiber alignment, droplet elongation, and overall structural orientation in the direction of the flow. Aligned fibers will be subjected to less friction amongst themselves, allowing the material to flow without the same resistance that would be seen if fibers were to be in a random configuration[132]. Physical and/or chemical gelation mechanisms during extrusion determine the bioprinting window, as these influence the viscosity of the bioink[133]. Gelation time sweeps reveal the time points at which cells should ideally be incorporated[134]. More so, the bioink sol-gel transition will occur within a specific time

window, before and after which the viscosity of the material continually changes with time and imposed shear. According to the gelation kinetics, a defined time window exists in which optimal printing conditions are achieved by balancing the interplay between the material's dynamic mechanical behavior and extrusion variables such as pressure[134]. (3) After extrusion, the bioink must be able to recover its structural integrity upon removing stress, reflecting its physical self-healing behavior; in other words, a rapid regain of yield stress[104]. The hydrogel must undergo additional gelation or crosslinking, critical to shape preservation in aqueous cell culture conditions[135]. Crosslinking can be physical, chemical, or a combination of the two[135]. Physical crosslinking mechanisms rely on non-chemical interactions that induce the entanglement of polymer chains via ionic interactions, hydrogen bridges, or hydrophobic interactions[135]. For example, alginate gels undergo rapid gelation when immersed in calcium chloride solutions. Calcium ions (Ca^{2+}) in alginate will interact with the negatively charged carboxylic acid groups within alginate chains[136]. Differently, chemical crosslinking methods connect gel precursor molecules via covalent bonds. Chemical crosslinking can involve exposure to radiation, temperature, or reaction of complementary chemical groups via Michael addition reactions, click chemistry, or enzymatic reactions[135]. For instance, gelatin methacrylate (GelMa) will photopolymerize into a hydrogel under the effects of specific wavelengths (i.e., UV light)[137].

Regarding sustaining cell culture post-printing (4), the hydrogel must adhere to additional criteria such as providing physical support, favoring cell adhesion, swelling, shrinking, degradation, porosity, etc. These criteria all refer to creating and maintaining a hospitable environment for cell propagation and development. Cell attachment sites are

crucial for *in-vitro* cell development and differentiation. Biopolymers such as collagen[138] can be incorporated within the bioink composite to enhance bioactivity. Alternatively, bioinert polymers can be modified with adhesion peptides. For example, cells do not interact with alginate polysaccharides. However, these polymers can be modified with cell adhesion motifs (RGD)[139,140].

One should note that it is not strictly necessary for a material to exhibit the abovementioned properties under the same steps. As long as there is a way (i.e., temperature changes, pH, or vibration) to change the material properties to meet the requirements for each stage, the material can be printable and sustain cell populations.

In the following tables, **Table 1** and **Table 2**, I provide detail of the variables relevant to EBB. These variables directly influence material printability and have an impact on cellular integrity. **Table 1** summarizes those parameters relevant to the extruding action, construct deposition, and their impacts on cell integrity. Similarly, **Table 2** describes the physical attributes of an ideal bioink and their impact on cellular integrity. Together, these tables offer an overall view of those parameters and attributes present during bioprinting through extrusion mechanisms. Regarding the flow properties of a bioink, these physical attributes can be evaluated by studying their rheological behavior[104,141,142].

Table 1. Biomaterial deposition parameters and their impacts on material printability and cellular integrity

Parameter	Material printability	Cellular integrity	Refs
Deposition speed	Printing speed is related to extrusion flow rate. Optimal speeds must be determined through shape fidelity and printability experiments.	---	143,144
Extrusion pressure	Ideal extrusion pressure will enable desired filament deposition and induce shear thinning phenomena (reduced viscosity). However, excessive pressure can result in poor printability, unstable extrusion, and material jetting.	Excessive pressures compromise cell viability.	129-131
Nozzle size	Nozzle sizes determine filament dimensions. Smaller nozzle sizes produce filaments with higher resolutions. However, these required higher pressures to extrude.	Shear stress increases as nozzle size decreases, hence affecting bioactivity	129,145
Model height	Gravitational force will limit model from reaching certain height.	Depending on model geometry, cell viability may decrease because of limited oxygen and nutrient availability.	104,146
Extrusion time window	The extrusion window will define working conditions at distinct time points. This time window defines the suitable mechanical conditions for high printability and shape fidelity of scaffolds.	---	147
Ambient humidity	Reduces hydrogel dehydration, and changes in polymer network density.	Dehydration can reduce cell viability.	148
Cartridge temperature	Some bioinks exhibit desirable flow properties at specific temperatures. Generally, the higher the temperature, the lower the viscosity of the material.	Long exposures to non-physiological temperatures can reduce cell viability.	148
Bed temperature	Differences between cartridge temperature and bed temperature are required to induce thermal gelation in those biomaterials with temperature-dependent mechanics to increasing its printability and shape fidelity. Some bioinks require constant temperature conditions.	Thermal shocks may be detrimental to cell culture.	149,150

Table 2 Bioink physical attributes and their impact in material printability and cellular integrity

Attribute	Material printability	Cellular integrity	Refs
Shear thinning	Shear thinning materials aligns material components as these exit the nozzle, reducing apparent viscosity, extruding pressure, and shear forces.	Shear thinning bioinks favor cell viability.	151
Loss tangent (δ)	Loss tangent values are correlated to extrusion uniformity and structural integrity of extruded scaffolds.	---	152
Structural recovery after shear conditions	Fast structural recovery upon flow enables the material to (partially or fully) recover its mechanical properties and retain the desired shape after printing.	---	142
Yield stress	Counters construct deformation from gravity and surface tension effects. Materials will low yield stress will tend to collapse during continuous layering.	---	153,154
Viscosity (η)	Highly viscous materials require more pressure to exit the nozzle. High viscosity post-extrusion can be beneficial to promote geometry fidelity by allowing the construct to retain its shape.	Highly viscous bioinks have an impact on cell viability as these require high pressures to flow.	128
Molecular weight of fiber constituents	As the molecular weight of fiber polymers increases, the onset of non-Newtonian shear thinning behavior will occur at lower shear rates. However, higher molecular weights tend to possess higher viscosities which would require elevated extruding pressures.	The pressure needed to extrude polymers with high molecular weight may result in reduced viability.	128,155
Bioink polymer density	Dense polymeric networks generally exhibit high viscosity that translates into higher extruding pressure. Also, denser networks are susceptible to higher degrees of crosslinking which will have a direct impact on overall mechanics and matrix pore size.	Dense polymer networks hinder nutrient diffusion and matter exchange in 3D matrices. Cell proliferation and spreading is often restricted when cells are encapsulated in dense polymer networks. Denser polymer networks will require higher extruding pressures; thus, cell viability could be compromised.	156
Crosslinking and gelation mechanisms	Physical gelation kinetics defines the boundaries of the bioprinting window. Also, gelation mechanisms are necessary to preserve freshly printed construct shape and long-term structural integrity under cell culture environments.	Some crosslinking mechanisms expose cells to ionizing radiation (UV) or concentrated ionic solutions.	135,147
Swelling, shrinking and degradation	Swelling, shrinking, and degradation rates induce geometrical inaccuracies in the extruded construct over time.	Controlled degradation aids *in-vitro* cell development through environmental remodeling.	157-160
Cell density	Certain densities of encapsulated cells are known to modify intrinsic flow properties of a biomaterial. Rheological characterization must be considered when encapsulating large cell numbers.	In post-printing conditions, increased dense cell populations within the construct may suffer from nutrient unavailability at the center of the bioprinted construct resulting in necrosis and altered biological behavior.	161

2.4. Printability

A critical aspect of bioprinting via extrusion is the concept of printability. In order to achieve complex and precise *in-vitro* models using extrusion-based bioprinting (EBB), the printability and shape fidelity of materials must be optimized. Many interpretations have been proposed to define the printability of a bioink. Gregorya and colleagues defined it as: "*The ability of a material when subjected to a certain set of printing conditions… to be printed in a way which results in printing outcomes which are desirable for a given application*"[162]. Yu's group defined it as printing accuracy and standardization in the printing process, including selecting printing materials and hard brush parameters[163]. In our view, printability needs to be explained from two angles.

2.4.1. Shape fidelity

An essential method of evaluating bioprinting quality is to measure the geometric differences between the designed and the printed structure. Based on this concept, several qualitative and quantitative assessments have been reported.

Ribeiro *et al.* (2017)[164] designed shape fidelity experiments based on Therriault *et al.*,(2004)[165]. A lattice mesh was designed, and the differences between the designed and printed structure were compared via simple visual and qualitative observation. The thickness change in the Z-axis direction and the change in the shape of the square hole in the X-Y plane were studied. In addition, a quantitative collapse evaluation model was proposed. The printed hydrogel filaments were taken from columns with different distances to cross these columns in turn, and the deflection angle θ of the wires at the columns was measured and compared with the predicted value θ_0:

$$\boldsymbol{\theta_0 = sin^{-1}(\frac{\rho g l}{\sigma_{yield}})} \qquad \text{(Equation 1)}$$

Where ρ is the density of the printed hydrogel, g is the acceleration of gravity, l is the span of the filament, and σ_{yield} is the yield stress of the hydrogel.

To complement Ribeiro's qualitative observation, Naghieh, S. *et al.* (2021)[166] introduced the irregularity index to specify the accuracy of the printed scaffold considering its original design considering its volumetric arrangement in X, Y, or Z directions. Therefore:

$$\textbf{Irregularity} = \frac{|\textbf{Experimental length}_{\text{X,Y,Z}}|}{\textbf{Design length}_{\text{X,Y,Z}}} \times \mathbf{100}\% \qquad \text{(Equation 2)}$$

Where $\text{Experimental length}_{\text{X,Y,Z}}$ is the printed size of the scaffold, $\text{Design length}_{\text{X,Y,Z}}$ is the designed size of X, Y, or Z direction, and the Irregularity represents the overall size of the printing structure. In addition, the diameter of the printed filament is used as an evaluation object to propose an index for strand printability:

$$\boldsymbol{D_s} = \sqrt{\frac{4Q}{\pi V}} \qquad \text{(Equation 3)}$$

$$\textbf{Strand printability} = \frac{D_e}{D_s} \times \mathbf{100} \qquad \text{(Equation 4)}$$

Where V, Q, and D_s represent needle speed, bio-ink flow rate and ideal chain diameter respectively; D_e represents the average diameter of the filament in the experiment.

Moreover, Ouyang *et al.,* (2016)[167] proposed the printability function Pr of bio-ink based on the square hole formed from intersected filaments.

$$\boldsymbol{Pr} = \frac{L^2}{16A} \qquad \text{(Equation 5)}$$

Where L is the perimeter of the printed closed structure and A is its enclosed area. Ideally Pr =1 means the intersected filament formed a perfect square, indicating high shape fidelity.

Furthermore, Lin, Z. *et al.,* (2021)[168] proposed a 10-point roughness evaluation method based on the 10-point roughness measurement method used in mechanical engineering. The random quantity was taken as the width of 10 positions of the printed thin line, the mean value (W_{SD}) and standard deviation (W_m) were calculated, and the function R_N was defined:

$$\boldsymbol{R_N} = \frac{\boldsymbol{W_{SD}}}{\boldsymbol{W_m}} \tag{6}$$

A smaller value of R_N translates into smoother filaments and indicates a better printing quality.

2.4.2. Shear stress at the nozzle

Another avenue to evaluate bioprintability is to assess the shear stress at the nozzle, as excessive shear stress can damage cell membranes[131]. Blaeser, A. *et al.* (2016)[169] proposed a bioprinted system where a simple fluid dynamics model was used to accurately predict and control the shear stress at the nozzle by adjusting the extrusion pressure, hydrogel viscosity, and nozzle diameter. In addition, Nair, K. *et al.,* (2009)[170] proposed empirical models based on percentages of living cells, injured cells, and dead cells that were used to understand the limit of pressure and nozzle diameter that could be employed in extrusion bioprinting. A quantitative model correlating process parameters to the maximum shear force was also deduced. Combining the two can effectively predict the maximum shear stress caused during printing.

Distler, T. *et al.* (2020)[171] fabricated hydrogel scaffolds containing skeleton muscle cells using needles of different diameters and extrusion pressures and cultured and treated the cells in vitro for 14 days before assessing cell proliferation to evaluate the effect of shear force during bioprinting.

Further on, Lin, S. *et al.* (2022)[172] proposed a multi-dimensional micro-vibration assisted 3D printing method to reduce the viscosity and shear stress of the hydrogel material with the intent of improving cell viability. The simulation software ANSYS was employed to understand the viscosity distribution of the hydrogel inside the nozzle under different vibration modes, including uniaxial vibrations, radial vibrations, axial vibrations, multi-dimensional vibrations, double radial vibrations, axial plus radial vibrations, and vibration-free scenarios. 2D and 3D vibration effects on viscosity and shear stress were investigated, and a multi-dimensional vibration-assisted 3D printing platform was designed. It was found that this platform can effectively reduce the viscosity of hydrogels in use and subsequently reduce the shear stress, which casts light on alleviating damage on cells embedded in viscous hydrogels during bioprinting.

Materials with high printability are often preferred as these will increase sample reproducibility, aiding overall experimental success. Moreover, favorable material printability is vital since the goal of using EBB in the first place is to pattern a preprogrammed structure into a tangible body with almost no structural differences between the two. In the contrary, materials with poor printability can compromise cell viability and sample reproducibility.

2.5. Review Article: Constructing 3D in vitro Models of Heterocellular Solid Tumors and Stromal Tissues Using Extrusion-Based Bioprinting

Overall, we have reviewed the technical aspects of extrusion bioprinting and the attributes and performance requirements for a biomaterial to function as a bioink. I have presented the current global cancer statistics and focused on gastroesophageal malignancies. I chose to highlight extrusion bioprinting as the biofabrication technique due to its flexibility, compatibility, and unexploited potential in cancer research. The following section aims to put solid tumors in context and justify the implementation of extrusion bioprinting as the enabling technique for disease modeling. By looking at solid tumors as discrete smalls organ-like systems, I demonstrate how bioprinting facilitates the generation of *in-vitro* mimics of the key features of neoplastic diseases and its potential to be unified into complex tumor models. I highlight the engineering maneuvers adopted by the scientific community to elucidate the tumoral microenvironment and its subsystems using extrusion bioprinting. In this work, I provide a biological overview of some most elucidated and relevant cancer subsystems as well as examples of their successful *in-vitro* reconstitution. Finally, the conclusion of this review provides insights on the opportunities and challenges for the future of cancer model biofabrication.

Article type: Review Paper

Status: Published - DOI: 10.1021/acsbiomaterials.2c00998

Title: Constructing 3D in vitro Models of Heterocellular Solid Tumors and Stromal Tissues Using Extrusion-Based Bioprinting

Salvador Flores-Torres [a], Tao Jiang [e], Jacqueline Kort-Mascort [a], Yun Yang [e], Omar Peza-Chavez [a], Sanjima Pal [b], Alisia Mainolfi [a], Lucas Pardo [a], Lorenzo Ferri [b,c], Nicholas Bertos [d], Veena Sangwan[b] *, Joseph M. Kinsella [a,*]

[a] Department of Bioengineering, McGill University, Montreal, Quebec, Canada.

[b] Department of Surgery, McGill University, Montreal, Quebec, Canada.

[c] Department of Medicine, McGill University, Montreal, Quebec, Canada.

[d] Research Institute of the McGill University Health Centre (RI-MUHC)

[e] Department of Intelligent Machinery and Instrument, College of Intelligence Science and Technology, National University of Defense Technology Changsha, Hunan, 410073, China.

* Corresponding author.

Keywords: Extrusion bioprinting, tumor microenvironment, miniaturized tumor subsystems.

2.5.1. Abstract

Malignant tumor tissues exhibit inter- and intra-tumoral heterogeneities, aberrant development, dynamic stromal composition, diverse tissue phenotypes, and cell populations growing within localized mechanical stresses in hypoxic conditions. Experimental tumor models employing engineered systems that isolate and study these complex variables using *in-vitro* techniques are under development as complementary methods to preclinical *in vivo* models. Here, advances in extrusion bioprinting as an enabling technology to recreate the three-dimensional tumor milieu and its complex heterogeneous characteristics are reviewed. Extrusion bioprinting allows for the deposition of multiple materials, or selected cell types and concentrations, into models based upon physiological features of the tumor. This affords the creation of complex samples with representative extracellular or stromal compositions that replicate the biology of patient tissue. Biomaterial engineering of printable materials that replicate specific features of the tumor microenvironment offer experimental reproducibility, throughput, and physiological relevance compared to animal models. In this review, we describe the potential of extrusion-based bioprinting to recreate the tumor microenvironment within *in-vitro* models.

2.5.2. Introduction

Human solid tumor heterogeneity

Tumors are complex entities that remodel their surroundings as selective pressures originate from disease progression. The tumor milieu is a highly dynamic biological system that relies upon multiple feedback loops instructing cell physiology towards malignancy[1]. Human tumors are classified depending on their tissue of origin. Carcinomas originate from the epithelial cells of an organ; lymphomas originate in the lymphoid tissues; sarcomas spawn in connective tissue, muscle, bone, or blood vessels; and myelomas are cancers of the plasma cells[2]. Several of the most common forms of cancer are classified as carcinomas. Examples of these are (by incidence): breast cancer, lung cancer, prostate cancer, non-melanoma of the skin, colon cancer, stomach cancer, liver cancer, rectal cancer, cervix cancer, esophageal cancer, thyroid cancer, bladder cancer, and the list continues[3]. In this review, we consider the anatomy of human carcinomas to present the current state-of-the-art.

The tumor microenvironment (TME) of a solid tumor (**Figure. 1**) comprises a heterogeneous mass of cells[4] residing, sensing, and maintaining biomolecular dialogue within a complex entanglement of proteins known as the extracellular matrix (ECM)[5]. In addition to providing architectural support and cell-anchoring sites, healthy interstitial ECM plays a significant role in homeostasis[5-7]. Corruption, unnatural modifications, and mutations of the genetic material of a cell are recognized as critical factors in cancer initiation[8] that progresses into remodeling of the extracellular matrix (ECM) tissue[9]. Furthermore, malignant cells are known to dysregulate ECM by altering its composition and architecture through diverse mechanisms such as fiber deposition[7], stromal cell

recruitment[10], and proteolytic activity[11]. Tumor progression is the result of an ever-changing microenvironment that further influences cellular genomic instability, promoting cancer initiation, development, tumor immune evasion, drug resistance, and metastasis[1]. Despite extensive and rigorous research, tumor heterogeneity stands out as the major challenge when modeling cancer *in-vitro*.

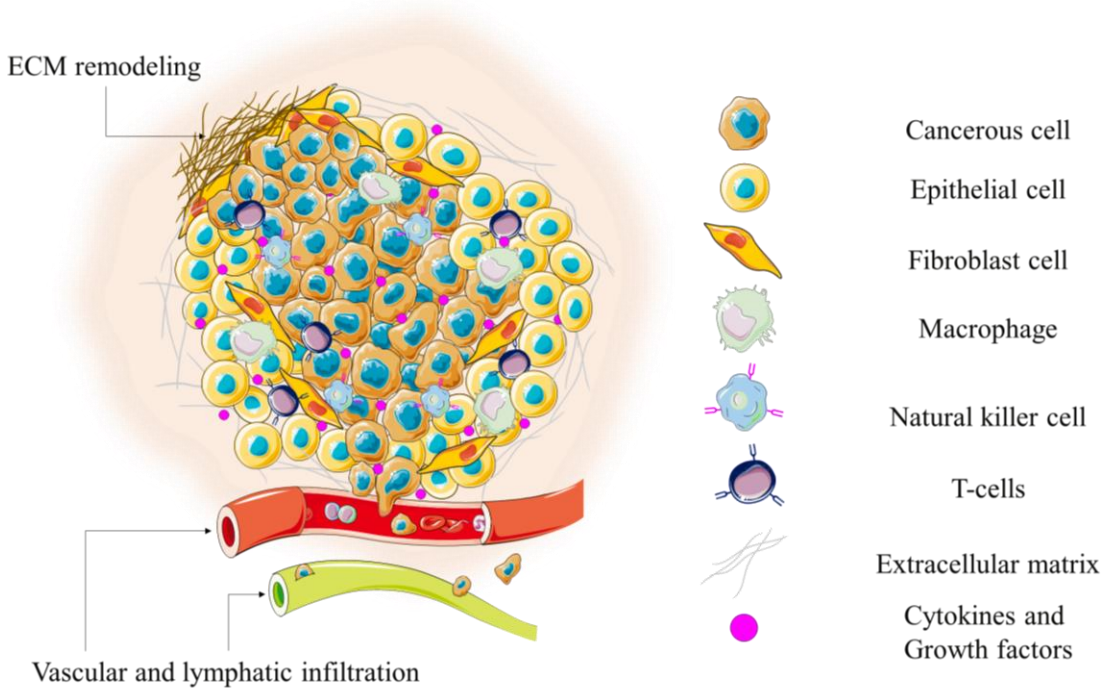

Figure 1. Illustration of the cellular and molecular heterogeneity of a solid tumor.

Co-evolution of cancer cells and their microenvironment is the result of dynamic, reciprocal events and cell plasticity. Cellular plasticity endows cells with the ability to adopt different molecular and phenotypic identities[12].

Bissell and Radisky (2001)[13] proposed that tumors can be considered small functional organs and their substructures can be individually targeted. However, the bidirectional interactions amongst diverse malignant cells and their microenvironment create a

complex tumor biosystem. The concept of tumors as organs was later reviewed by Egeblad *et al.*in (2011)[14]. Tumor subcomponents can be seen as: the epithelial tumor mass (parenchyma), vascular tissue, lymphatic vessels, regions of remodeled and healthy ECM, stromal cells, immune cells, and in some cases metastatic tumor nests[14]. Although reductionist in vitro approaches have enabled mechanistic insights into basic cancer biology, it is increasingly understood that interactions within the tumor milieu are critical to understand cancer biology and further develop the advanced therapies. Therefore, in vitro cancer models that integrate and replicate the complex tumor subcomponents and their bidirectional interactions are needed.

Current challenges in the field

Two-dimensional (2D) cancer models have been instrumental to our basic understanding of cancer biology but possess fundamental biological limitations that interfere with the study of malignancies. For instance, murine models can easily support the development of primary tumor xenografts, but a reliable murine model that reflects the physiology and architecture of stage-specific cancers is not available[15]. Animal models enable insight into *in vivo* cancer biology but due to genomic, immunologic, and species-specific biological differences when compared to humans, animal models remain poor predictors of clinical efficacy of modern treatment protocols[16,17]. More recently, patient-derived cancer organoids (PDOs) have been proposed as a reliable alternative to pre-clinical animal models as they preserve critical features of the patient's tumor[18,19]. Several techniques have been used to create models of the parenchymal component of a tumor including centrifugation-induced spheroids[20], hanging drop[21], constant rotation within microgravity bioreactors[22,23], magnetic levitation[24], microfluidic devices[25,26], cell-laden

hydrogels[27], and 3D bioprinting[28-30]. Although some of these techniques are useful to create multicellular aggregates in suspension, cancer cells *in vivo* are intimately associated with stromal components and ECM.

To elucidate the TME, an ECM analog should be provided to host relevant combinations of cancer and stromal cells. The biochemistry and mechanics of the ECM play essential roles in dormancy[31] and malignancy progression[32]. The tumor milieu is often elucidated using cell-laden hydrogels. Even though manual deposition of hydrogels has been a successful technique to start 3D tissue cultures, the lack of architectural control in sample manufacturing results in poor reproducibility and low sample quality for experimental purposes. Nevertheless, pairing advanced material handling techniques such as 3D bioprinting with oncological research has enabled the creation of superior heterogeneous *in-vitro* cancer models that recapitulate complex biological conditions, mechanisms, and physiological features of the TME[33-43]. As a biofabrication technique, bioprinting enables the creation of complex cell-laden scaffolds while maintaining a high degree of volumetric control, high efficiency, low cost, and sample reproducibility. Moreover, bioprinting has demonstrated its potential to significantly accelerate cancer research as it facilitates the inclusion of user defined biomaterial inks (bioinks) laden with selected cell types to build multi-material multi-cell 3D constructs.

2.5.3. Bioprinting the tumor microenvironment

As previously predicted, the 21st century is seeing the vast implementation of cell and organ printers as biomedical research tools[44]. Fundamentally, through diverse mechanisms and computer software, bioprinting techniques make use of cells and biomaterials to create volumetric cell-laden constructs. However, no single technique favors the production of all scales of tissues (yet). Three-dimensional bioprinting has demonstrated its utility in the field by allowing the fabrication of architectural features that are not possible to create with traditional techniques. Bioprinting has been used to elucidate the elements of malignant neoplastic diseases by incorporating tumoral components within biomaterial constructs[45-49]. The two main components of human tumors are considered to be the tumor parenchyma and its adjacent stromal region[50]. The stroma is comprised of vascular and lymphatic structures, ECM, and cells such as fibroblasts, immune cells, healthy epithelial cells, and other types of cells depending on the tissue in question, while the tumor parenchyma is the cancerous epithelial compartment of a tumor (**Figure 2.**).

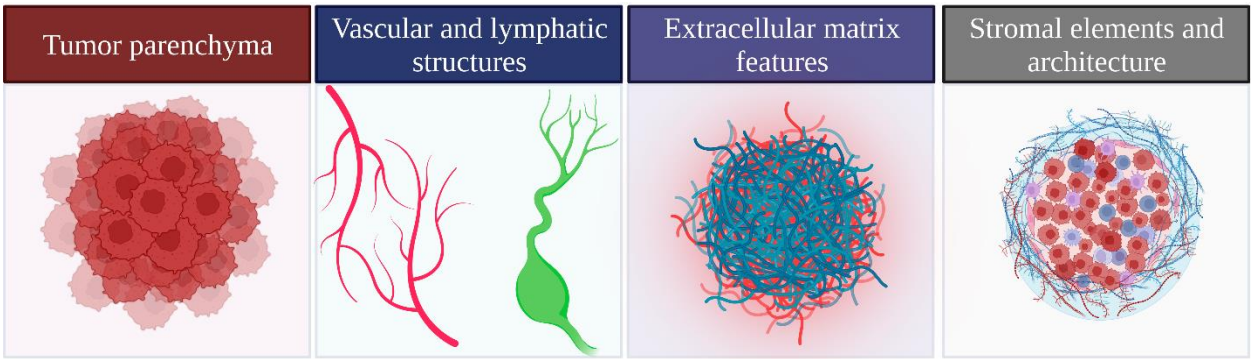

Figure 2. Cellular and structural elements of malignant neoplastic carcinomas.

In this review, we will highlight the use of extrusion-based bioprinting (EBB) as the fabrication technique of tumor heterogeneous *in-vitro* cancer models. Extrusion

bioprinting is the most frequently used bioprinting modality due to its simple mechanical and upgradeable setup, compatibility with laboratory workflows, and training requirements. The fundamental factor that enables the creation of heterocellular bioprinted constructs through EBB is its compatibility with a great variety of viscous biomaterials (30mPa·s to $6x10^7$mPa·s)[51]. The biological activity of printable materials can be adjusted by including ECM-derived biomolecules (**Figure 3.A**). These modifications can include relevant ECM biomolecules from the native tumoral microenvironment. Additional features from the tumor milieu can be incorporated through the mechanical modification of its constituents in the form of ECM crosslinking agents, porosity profiles and polymer density (**Figure 3.B**). Moreover, complex structures such as vascular vessels by the creation of hollow channels within volumetric constructs (**Figure 3.C**). Control upon biomaterial deposition and construct shape fidelity are achieved by conducting printability tests where the properties of the biofilament are documented and tuned to meet geometrical requirements (**Figure 3.D**). Favorable material printability will enable patterning of a preprogrammed structure into a tangible body with almost no structural differences between the digital and real versions. In the contrary, materials with poor printability can compromise cell viability and sample reproducibility. To keep this review in line with the efforts behind bioprinting the elements of neoplastic diseases, we invite the reader to read the following pieces of literature where the engineering aspects of extrusion bioprinting and material printability are reviewed[52-56].

The following section will offer an individual isolated view of the tumor milieu subsystems present in Figure. 2., the strategies to elucidate these components using extrusion

bioprinting maneuvers, their experimental importance, and the challenges that remain to be addressed.

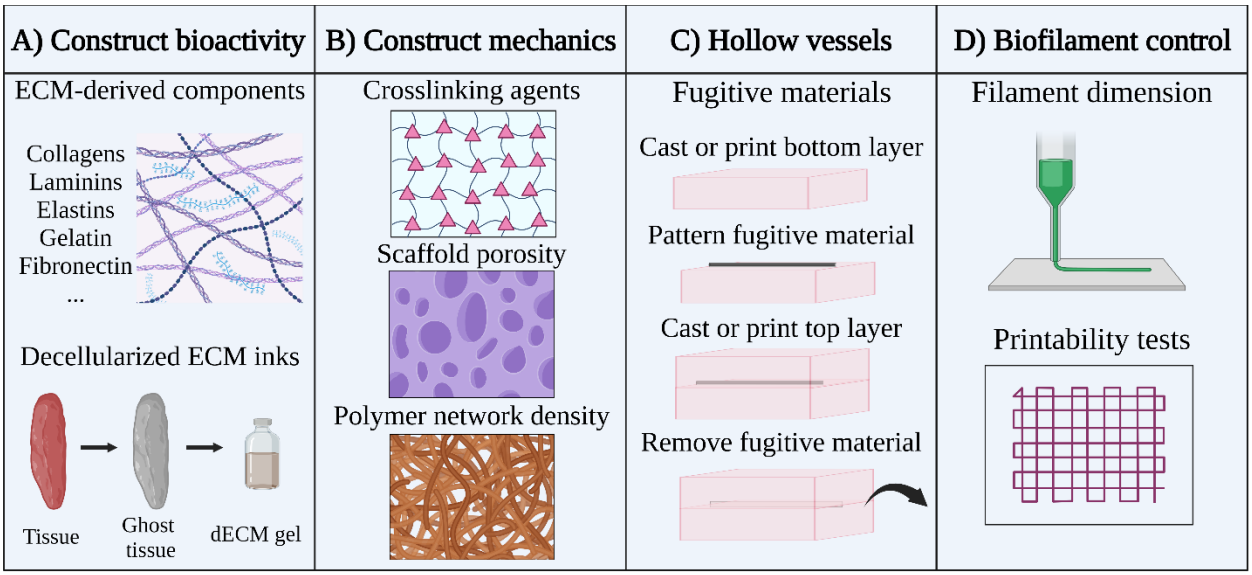

Figure 3. Factors that aid in the fabrication of successful extrusion-based bioprinted constructs. Bioink modifications: A) Construct bioactivity and B) Construct mechanics. Fabrication enablers: C) Hollow vessel bioprinting with fugitive materials and D) biofilament control promote construct fidelity and architecture.

Bioprinting tumor spheres

Cells in our body are continuously exposed to damage and stress from diverse sources such as UV radiation from sunlight and substances that cause oxidative stress from our diets. Insults to the genetic material of cells can result in carcinogenesis and uncontrolled cellular division. Over 50% of human cancers carry a mutation in the genetic sequence for p53[57]; a gene that regulates the cell cycle and suppresses tumor growth by sending rogue cells through the apoptosis cascade. The tumor parenchyma (**Figure 2.**) is one of the main targets for anticancer therapy and it is often recapitulated *in-vitro* by encapsulating

immortalized or patient-derived epithelial cancer cells in bioactive soft materials that will enable their division and reorganization into spheroid-like structures. These miniaturized tumor mimics are used extensively in cancer research and have been proposed as prognostic markers since patient-derived parenchymal material retains disease-specific features[58] and mimic the therapy response of parental tumors[59].

Printable cell-friendly materials have been used to encapsulate and pattern tumor cells from different cancer types. Bioprinting cancer cell-laden environments improves sample quality and reproducibility since an automated machine is controlling the amount of material that is coming out of a nozzle. This feature has enabled researchers to use bioprinted samples in drug testing experiments. For instance, Johnson *et at.,* (2022)[60] developed a high throughput bioprinted platform to interrogate colorectal cancer spheroids with chemotherapy and radiation. Their methodology exemplifies how extrusion bioprinting is a feasible technique to fabricate numerous identical samples for the purpose of therapy evaluation with low cell number requirements. Zhao *et al.,* (2014)[35] used extrusion based bioprinting (EBB) to fabricate a cervical cancer model using HeLa cells. In their bioprinted constructs, authors observed increased proliferation rates, decreased drug sensitivity, and increased MMP secretion compared to 2D monolayers. Hong S. and Song M.J. (2022)[61] evaluated drug sensitivity of isolated breast cancer stem cells (derived from the MCF-7 breast cancer cell line) in bioprinted scaffolds (**Figure 4.A.1**). Flores-Torres, S. *et al.,* (2021)[62] bioprinted patient-derived gastric cancer cells (**Figure 4.A.2**). In their investigation, authors challenged cancer spheres with chemotherapy drugs and observed resistance patterns to the same treatment regime given to the patient. Moreover, 3D bioprinted cancer cultures differed from their

monolayer counterparts as the former exhibit different cell proliferation rates, morphologies, and chemosensitivity. Wan, X, *et al.,* (2018)[63] bioprinted a glioma tumor model using glioma stem cells (**Figure 4.A.3**). Authors observed significant differences in vascular endothelial growth factor A (VEGFA) in 3D cultures compared with 2D cell culture conditions. Interestingly, they also found an upregulation of HIF-1α, which regulates vascularization of in the TME[64]. Other cancer types recapitulated *in-vitro* as spheroids inside bioprinted matrices include breast cancer[65], melanoma[66], colorectal cancer[67], lung cancer[68], glioma[69], glioblastoma[63], neuroblastoma[70], and cervical cancer[71].

A key factor in tumor sphere elucidation for drug testing purposes is maintaining spheroid size uniformity. *In-vitro* tumoral size is correlated with metabolic heterogeneity and drug responsiveness[72]. Underlying factors such as initial cell density have an important impact on the size of cancer spheres. One of the main challenges in developing drug testing platforms is inducing and maintaining uniform spheroid size across every sample. Tumor spheroid cultures develop proliferative and metabolic gradients in response to oxygen and nutrient availability. Once a critical size is reached, usually around 400-600 μm, spheroids develop central necrosis and a proliferation gradient; cells in the inner zones of the tumor spheres become quiescent and necrotic while the outermost cell layers are in a proliferative state[73]. Moreover, the dimensions and scale are not only descriptive and for the epithelial region of the tumor. Nutrient and metabolic waste removal routes must be available to all the components of the tumor model to promote uniformity. The next section will present how vascular vessels can be included within an in vitro model to provide cells with vital nutrients.

Overall, the epithelial compartment of malignancy is recognized as one of the main drivers of cancer progression. The cancerous epithelium relies on the complex interactions with its adjacent stroma as these two elements co-evolve as the disease progresses. In the following subsections, we describe the tumor-associated stromal elements, their relevance, and how these have been engineered as bioprinted *in-vitro* models.

Engineering vasculature in tumor models

The vascular network of mammalian organisms conveys nutrients and oxygen to cells and organs and removes metabolic waste products. Oxygen diffusion is one of the limiting factors for *in-vitro* engineered tissues. Oxygen diffusion limit in cell-rich tissues is limited to ~200 μm[74]. An efficient and healthy vascular network is regulated by metabolic demand and angiogenic and anti-angiogenic molecular factors secreted by tissues[75]. To achieve growth beyond the size allowed by the existing oxygen and nutrient diffusion, tumors benefit from adjacent vascular formations and overexpress angiogenic factors which promote the rapid formation of aberrant vasculature characterized as immature and hyperpermeable[76]. Recruited vascular formations are comprised of a poorly defined, discontinuous endothelial cell lining with abnormalities in its basement membrane. Tumor angiogenesis serves as a prognostic indicator for a wide variety of tumors[77]. Vessels can emerge from sprouting, intussusception, or by the incorporation of endothelial precursors from the bone marrow. The molecular and cellular mechanisms behind these processes are reviewed elsewhere[76,78-80].

Paradoxically, solid tumor angiogenesis enables tumor growth while eventually reducing its access to antineoplastic drugs[81,82]. Early-stage (V <1 mm^3) tumors are usually well

perfused[83]. As the malignancy grows, it usually compresses the blood supply rather than outgrowing it[84], resulting in increased interstitial pressure from leaky blood vessels, and central necrosis[83].

To elucidate *in-vitro* vascularized tumor systems, sacrificial or fugitive materials are utilized to create hollow channels using extrusion-based bioprinting and mold casting techniques. These channels are later populated with endothelial cells. Implementation of sacrificial bioprinting relies on gel-to-sol phase transitions of biomaterials. Similar to the "lost-wax" technique, fugitive materials shape the positive mold of the vascular vessel and are removed by inducing their liquid phase or by extracting them with mechanical force (**Figure 3.C**). To create a hollow vessel, fugitive materials undergo a successive series of steps: (1) the fugitive bioink is printed in its solid-like stable phase and serves as the "positive mold" for the future vascular conduct; next (2) a different hydrogel, serving as an ECM substitute, is extruded or cast on top and around the sacrificial biofilament; (3) the non-sacrificial fraction of the system is commonly crosslinked; (4) the fugitive material is evacuated through gel-to-sol phase changes, mechanical extraction, or dissolution. Modifications to this brief protocol include: (1) inclusion of stromal and endothelial cells in the non-sacrificial ECM analog and (2) endothelialization of the vascular conducts with the infusion of high densities of endothelial cells. Examples of suitable biomaterials for sacrificial bioprinting maneuvers are detailed in **Table 1**.

Table 1. Examples of commonly used biomaterials for sacrificial bioprinting maneuvers.

Fugitive materials	Physical attributes	Removal process	Refs
Pluronic F127	Liquid phase at T ~ 4 C° and a gel phase at T ~ 37 C°	Thermal melting	85-87
Gelatin	Sol-to-gel transition at T ~35 C° and a gel-to-sol transition at T ~24 C°	Thermal melting	88
Agarose	Gels at T<35 C° and melts at high, incompatible temperatures T ~ 85 C°. The gelling temperature depends on the agarose concentration.	Mechanical extraction	89,90
Sugar inks or carbohydrate glass	Soluble in water.	Dissolution	91-93
Carbopol	Keeps its gel phase over a wide range of temperatures and it is soluble in water.	Dissolution	94

One should note that hollow vessel printing relies on highly printable materials. We invite the reader to visit the pieces of literature that detail how to conduct material printability assessments (**Figure 3.D**). Here we provide a few examples[41,53,95-100].

Several groups have created vascularized tissues. For instance, Kolesky *et al.* (2016)[101] reported engineered large (>1cm) vascularized multicellular tissue models. In their work, authors utilize Pluronic F-127 as the fugitive ink and positive mold for blood vessels. They allowed human vascular endothelial cell (HUVEC) attachment under zero-flow conditions before commencing any active perfusion of the whole network. Skylar-Scott *et al.* (2019)[88] introduced the term *sacrificial writing into functional tissue* (SWIFT). This maneuver involves embedding a fugitive material into a dense functional tissue. By using 5% (w/v) gelatin as a fugitive material, authors incorporated channels within highly dense cellular environments (~10^8 cells/ml). Taking advantage of its gel-to-sol transitions,

gelatin was evacuated from the final construct by raising the temperature to 37 C°. Within their results, they demonstrate that vascular channels are vital for cells to reside and function in dense artificial tissues.

Several groups have bioprinted vascular structures within tumor systems. Lee *et al.,* (2015)[102] patterned gelatin as a fugitive material to create a mold for vascular vessels and seeded fluorescently labeled HUVECs inside the patterned channels. Gelatin was initially cast to create the mold for the vessel and removed by inducing its liquid phase. The result was a hollow vessel. Then, patient-derived glioma stem cells were manually injected near the channel and confocal microscopy was used to follow model progression and cell migration towards the vascular channel (**Figure 4.B**). Neufeld *et al.* (2021)[103] used Pluronic F127 as fugitive material to create a vascular lumen within a bioprinted chip. The lumen was primed with fibronectin and vascular cells were incubated before any perfusion. Authors demonstrated the use of their tumor vascularized model as a preclinical tool after including patient-derived cells and challenging the glioblastoma tumors with temozolomide (TMZ), a chemotherapeutic agent used to treat specific types of brain cancer. Moreover, Ozturk *et al.* (2020)[104] reported the use of sacrificial bioprinting to create a vascularized glioblastoma model. Using gelatin as a fugitive material, authors included two linear vascular channels around the tumor site. Authors explored the drug response of mature tissues by preculturing these prior to any perfusion of chemotherapy drugs. Authors observed distinct responses to TMZ between different patient-derived cells in their 3D models compared to 2D monolayer conditions of the same cells. These unique experimental formats differ from traditional 2D monolayer drug

experiments as the patterned architectures provide a relevant administration route for drugs compared to simple diffusion.

Furthermore, vascular vessel sprouting has been investigated in 3D bioprinted models. Lee *et al.* (2014)[105] studied angiogenic sprouting in a bioprinted HUVEC-fibroblast microvascular bed with adjacent vascular channels. As tissue samples matured with time, angiogenic vascular vessel sprouting occurred and characteristic thin filopodia protrusions formed at the sprout tips. In bioprinted cancer models, sprouting behavior has been observed when tumors are near engineered vascular vessels[106]. Angiogenic sprouting emulation *in-vitro* is important when designing and testing antiangiogenic treatments. Both vascularized and vascular sprouting in vitro models offer relevant experimental modalities, where the effects of therapy can be evaluated in both the endothelial and tumor system without the need to sacrifice a small animal. Model traceability is a unique feature offered by *in-vitro* models. Compared to small animal models whose tumor burden develops away from detailed observation, bioprinted vascular models are an attractive and feasible approach to thoroughly study the effects of therapeutic regimes on vascularized tumor models.

Blocking tumor angiogenesis *in vivo* has a profound impact on tumor development[107]. Vascularized tumor models are a clear opportunity to recapitulate distinct angiogenic states of a tumor. Compared to animal models whose malignancy develops under the skin and away from real-time detailed cell imaging over the course of months, bioprinted vascularized models enable researchers to overcome this limitation and document real-time effects of potential therapies without the need to terminate an experiment. Vascularization is key for increasing the dimension and complexity of lab-made tumor

models. For instance, elucidating vessels is a fundamental step towards *in-vitro* metastatic models. Furthermore, circulation of nutrients through vasculature plays an essential role in human pathologies. Engineering functional microvascular architectures that mimic the aberrant tumor vasculature, not only in form, but also in function, remains a challenge for the field. As mentioned above, bioprinting is a feasible technique to pattern functional vascular vessels near the tumor parenchyma that respond to environmental stimuli. Human-on-a-chip approaches have demonstrated their versatility by adapting the microfluidic systems to host a tumoral microenvironment[108-111]. Tumor-on-a-chip microfluidic devices that enable real-time imaging of specimens and provide fine control over simulated conditions such as nutrient, cell-cell interactions, reproducibility, and oxygen gradients[112]. Integration of extrusion bioprinting with microfluidic devices can improve spaciotemporal control of relevant variables and compartments within an *in-vitro* cancer model[37].

Engineering cancer lymphatics

Although often overlooked, it is important to account for lymphatic architecture in tumor models. For some human tumors such as those often found in breast tissue, current treatment regimens include the surgical removal of cancer-positive and sentinel lymph nodes[113]. When it comes to *in vivo* cancer progression, solid tumors and their stroma induce the growth of new lymphatic vessels from pre-existing lymphatic structures by secreting growth factors such as VEGF-C and VEGF-D[114-116]. These growth factors promote lymphatic vessel enlargement and increased flow rates that enable tumor cell entry[117,118]. Aside from their involvement in cancer progression, lymphatic vessels also provide the preferential recycling route for most administered antitumor drugs[119]. Early

approaches to study the lymphatic system have included incorporating lymphatic endothelial cells (LECs) into 3D matrices to build lymphatic capillaries[120,121]. This has since progressed into 3D LEC cultures in hydrogel-based matrices. As many other cells, LECs in 3D conditions are susceptible to microenvironmental cues provided by the gels they are set into[122,123].

The strategy to generate lymphatic networks is similar to the one used for vascularized networks. Fugitive or sacrificial materials are often selected to create "positive molds" for lymphatic channels. Examples of these materials are provided in **Table 1**. Sacrificial bioprinting techniques have enabled lymphatic vessels to be elucidated. Liu *et al.* (2021)[124] successfully seeded human lymphatic endothelial cells (LECs) into microchannels made using agarose as a fugitive material (**Table 1.**) extruded into a gelatin methacrylate (GelMA) hydrogel matrix. With time, LECs were able to successfully spread and proliferate over the entire channel area (**Figure 4.C**). This *in-vitro* model was used to study the interplay between LECs and breast cancer cells in a 3D microenvironment, thereby recapitulating the dynamism that exists between lymphangiogenesis and tumor progression. Specifically, increasing VEGF-C treatment increased LEC sprouting in the peritumoral environment while simultaneously attracting breast tumor cells to the vicinity of the LECs where they showed enhanced spreading. Alternatively, Cao *et al.* (2019)[125] captured both vasculature and lymphatics in a single tumor-on-a-chip system. Their model featured bioprinted perfusable blood vessels, a single-outlet lymphatic vessel, and tumor cells seeded between the hybrid microcirculatory network. By tuning the GelMA, alginate, and poly(ethylene glycol) diacrylate (PEGDA) composition of the printed bioink, this study illustrates that blood

and lymphatic vessel permeability can be controlled to recapitulate different drug delivery and drainage scenarios to and from the TME.

Lymphatic structures are among the first tissues to be invaded by malignant cancer cells and this phenomenon is correlated with poor cancer prognosis[126,127]. Thus, lymphatic structures are attractive therapeutic targets[128,129]. Even though the mechanisms of tumor metastasis via the vascular system had received plenty of attention, most cancers will first invade and metastasize through the nearby lymphatic structures[130,131]. Although upregulation of genes and protein expression levels have been quantified in simple co-culture systems, an accurate reconstruction of the TME where LECs can respond to growth factors and migrate towards tumor cells is needed to elucidate initial stages of tumor invasion and metastasis.

Inclusion of immune components

In normalcy, the immune response is tasked with the eradication of cancerous lesions[132]. Nonetheless, malignancy progresses in most cancer patients. The tumor-immune microenvironment (TIME) is comprised of neutrophils, macrophages, natural killer cells, dendritic cells, T-cells, and B cells[133]. Solid tumors can benefit from the presence of certain immune cells to enhance tumor progression[134]. Neutrophils are amongst the first recruited immune cells to mount an immune response when a cancerous inflammation is detected. However, the TME mediates the pro-cancer (N2) and anti-cancer (N1) phenotypes in neutrophils[135]. Cancer-associated neutrophils (TANs) aid tumor progression through the release of proteolytic granule proteins (MMP9), which will promote tumor angiogenesis[136,137]. Moreover, interest has been placed behind tumor-associated macrophages (TAMs). TAMs have been described as tumor accomplices since

TAM tumor infiltration is associated with poor patient survival[138,139]. Macrophages have two polarization states: M1 and M2. Macrophages in the M1 polarization state promote anti-tumoral and pro-inflammatory activity by boosting the immune response against the tumor[140]. On the contrary, M2 macrophages boost tumor progression by producing immunosuppressive cytokines such as IL-10, Il-13 and TGF-β[140]. TAMs populations near the tumor often resemble the M2 subtype and are implicated in therapy resistance[141,142].

Grolman, J. *et al.,* (2015)[143] studied macrophage-cancer cell interactions in co-culture systems. Using a coaxial bioprinting system, authors patterned a "core" of macrophages surrounded by a "shell" of MDA-MB-231 breast adenocarcinoma cells in a peptide-conjugated alginate gel with improved cell adhesion (**Figure 4.D**). They used their platform as a tool to evaluate the effects of inhibitory drugs. Within the spatially organized constructs, macrophages migrated towards the cancer cell region and interacted with tumor cells in control samples but remained immobile under the effects of the migration inhibitory drugs Gefitinib, zoledronic acid, and a Rac1 inhibitor II.

Heinrich M. A *et al (2019)*[144] fabricated miniaturized brain models to study glioblastoma-macrophage interactions. Their model served as a tool to study macrophage recruitment and polarization in malignancy. Using GelMA, their model was created in a two-step bioprinting process: First (1), the brain mass containing macrophages was extruded first and (2) the glioblastoma cells were layered afterward. Glioblastoma cells acquired a migratory phenotype as they lost expression of vimentin, nestin, and e-cadherin. Also, macrophages exhibited preferential in migration towards glioblastoma cells when compared to migration towards acellular sites or themselves. Gene expression in the miniaturized brain systems was proven to be of clinical relevance as authors found high

expression of crucial genes previously reported to be upregulated in patients with poor prognosis. Compared to 2D culture, authors observed an increase in EMC-remodeling enzymes matrix metalloproteinases (MMP2 and MMP9) and and reported increased drug sensitivity of cancer cells after the interactions between cancer and macrophages were inhibited in 3D co-culture conditions.

Furthermore, bioprinted scaffolds have been used to expand T-cells. Jin, Z. *et al.,* (2021)[145] bioprinted human T-cells from healthy donors within 24 h of collection. Within the coaxial alginate-only fibers, authors observed significantly less T-cell exhaustion and CD4+ and CD8+ T-cell differentiation, while alginate-gelatin constructs instructed cells into a resting state. This work demonstrates how specific volumetric arrangements instruct embedded T-cells towards different fates.

Our knowledge of the anti-cancer immune response is still maturing. Many unknown processes are yet to be fully elucidated. For instance, what are the biological and mechanical microenvironmental features that prevent T-cells from infiltrating? How can we better target the tumor milieu and solidify an anti-tumoral immune response? How can we train or edit autologous immune cells to overcome these challenges and implant them back into that patient? These are among the important questions that could be addressed with an appropriate TIME *in-vitro* model.

Tumor extracellular matrix features: Matrix rigidity and biomolecular makeup

Tumor heterogeneity manifests biologically and mechanically. It is progressive and governed by intertwined feedback loops between cells and the ECM. *In vivo* cellular arrangements hold a remarkable complexity that is tightly linked to their physiological

functions. Several bodies of literature have evaluated *in-vitro* cell physiological processes as a function of their architectural organization and surroundings[146-149]. The consensus reveals that cellular composition, ECM architecture, and ECM molecular fingerprint are responsible for cell metabolism, division rates, genetic expression, proteomic makeup, and resistance to therapy. Tumors are known for their ability to remodel the surrounding microenvironment through ECM secretion, alteration, and degradation[150]. Accumulated tumor ECM is more abundant, stiffer, and denser than normal ECM, it acts as a barrier to therapy, and it shields cancer cells from the immune system[151-153].

Collagen is the most abundant ECM fibrous protein in the TME of carcinoma tumors and it is involved in cancer progression[154]. Its presence and spatial organization have been used as a prognostic value in the clinic[154], particularly in breast cancer[155]. Collagen heterogeneity and organization in breast cancer are described by the tumor-associated collagen signatures (TACS) system[156]. In detail, TACS1 refers to the collagen deposition around the tumor, TACS2 indicates the spherical arrangement of collagen around the tumor, and TACS3 describes collagen fibers that are perpendicularly aligned with the tumor boundary[157]. Clinical evidence reveals that TACS3 is positively correlated with a poor clinical outcome when present in breast cancer biopsies[158]. These collagen arrangements are imperative descriptors of tumor progression *in vivo*. Conducting extrusion of fibrous materials induces alignment of fibers after these exit the nozzle[159]. Fundamentally, fiber alignment in extrusion printing is the result of a shear-induced phenomenon known as shear-thinning. Macroscopic flow is the result of internal structural changes such as fiber alignment, droplet elongation, and overall structural orientation in the direction of the flow. Aligned fibers will be subjected to less friction

among themselves, allowing the material to flow without the same resistance than would be seen if fibers were to be in a random configuration[160]. Kim *et al.* (2020)[161] induced shear stress to a stromal-derived ECM bioink to produce optically transparent cornea analogs. Authors exerted precise control upon the level of ECM by tuning extrusion parameters such as nozzle size and pressure. Their results demonstrate that ECM fiber alignment plays important roles in cell viability, optical properties, and maturation of their *in-vitro* model. Moreover, Nerger *et al.* (2019)[162] demonstrated that 3D extrusion printing of collagen-Matrigel bioinks produced aligned ECM microstructures that influence cancer cell spheroid actin protrusion alignment in the direction of the collagen network.

The effects of mechanical ECM rigidity and density have been investigated *in-vitro* by seeding cells in biomaterials with different pore sizes, stiffness gradients, and biomolecule densities. For example. Bao G., *et al.,* (2020)[163] reported for the first time, a method designated as "triggered-micropore-forming (TMF)" bioprinting. Their results demonstrate the advantage of cell-sized pores within the bioprinted scaffolds. These pores supported mass transport across large bioprinted structures (6 mm/side cubes) and enabled high cell viability. The constructs promoted cancer cell proliferation, migration, and invasiveness, when compared to nonporous constructs, implying the role of mechanotransduction and its mediation through the viscoelastic properties of bioprinted scaffolds. Moreover, Monferrer E. *et al.,* (2020)[164] demonstrated that porous features decreased in size as bioink constituent concentration was increased. Also, authors documented pore size changes through time and inversely correlated cell density within cancer spheroids and matrix stiffness. The same group also investigated the effects of

ECM stiffness on neuroblastoma cell lines (SK-N-BE and SH-SY5Y cells) in co-culture with stromal glial cells (SW10 cells). Their results suggest that stiffness influences how stromal cells affect cancer cell proliferation[165]. The effects of ECM stiffness have been further investigated in other applications outside of the cancer field. Kuzucu *et al.,* (2021)[166] reported a platform where bioprinting with a gradient of stiffness and cell concentration was possible through the use of functionally graded biomaterials with carboxylated agarose. The platform paves the way towards mimicking tissue behavior where gradients play important roles. Freeman *et al.,* (2017)[167] used a tunable alginate bioink for controlled growth factor delivery in mesenchymal stem cell (MSC) cultures through alteration of the mechanical properties of the constructs. Spatial modulation of stiffness within the constructs had a noticeable effect on MSCs; stiffer regions promoted osteogenesis over adipogenesis. demonstrating a significant advancement in biomaterials with tunable mechanical properties and biomimetic architecture for *in-vitro* disease modeling.

The biological composition of the ECM modulates the behavior of cells within the TME[32]. Simple and defined ECM gels such as collagen 1 are commercially available ECM analogs that enable reproducible experimentation. However, these systems lack an important number of features from the native ECM. To circumvent this issue, researchers have developed tissue repurposing techniques that facilitate the implementation of ECM-based materials. To consider the use of ECM-derived materials from tissue sources, tissue must undergo a process referred to as decellularization[168,169]. Tissue decellularization is a process that depletes cells from tissue leaving behind a decellularized ECM (dECM)[168]. Using a combination of detergent washes, mechanical breakdown, and enzymatic

cleavage, ECM is purified from its previous host's cells and genetic material. A successful dECM is a non-immunogenic and bioactive tissue-specific soft biomaterial. Several decellularization processes have been reviewed elsewhere[168,170,171]. The dECM product is known to retain the inherent bioactivity of the native tissue and it allows further remodeling when new cells are seeded on/in it. However, due to its biological complexity and unsuitable mechanical properties[172,173], tissue-specific ECM materials require extensive biomechanical characterization and appropriate `reinforcement for EBB applications.

To create dECM hydrogels, the decellularized tissue is solubilized via enzymatic digestion[174,175]. The resulting dECM hydrogel loses some of the mechanical integrity of the issue of origin, thus it can be combined with other biomaterials to improve its stability. dECM hydrogels are thermosensitive, they show an increase in moduli at physiological temperature as a result of an entropy-driven process known as collagen kinetics[176]. Rheological characterization is required to reveal the viscoelastic properties and thermal dependencies of dECM hydrogels. For a comprehensive review on dECM hydrogels, we suggest the work published by Saldin *et al.,* (2017)[177]. In their review, authors describe how dECM hydrogels are formed; how these are characterized biochemically and mechanically. Moreover, they review their thermal dependencies and their viscoelastic tendencies.

The use of dECM hydrogels as bioinks in 3D cancer cell culture has been documented. Kort-Mascort *et al.,* (2021)[172] created a miniaturized disease model for head and neck cancer (**Figure 4.E.1**). Authors decellularized and characterized porcine tongue tissue using atomic force microscopy (AFM) and mass spectrometry (LC/MS/MS). They

achieved a dECM-based composite biomaterial comprised of alginate-gelatin-dECM with mechanical properties similar to those of a mouse tongue tumor from the same cancer cells. In their journey towards disease modeling, authors investigated tumor development and its tolerances to standard-of-care drugs. Chen Y., *et al.,* (2022)[178] (**Figure 4.E.2**) bioprinted a tumor model using an adipose dECM-based hydrogel. Authors reported lower nanoparticle uptake and reduced drug sensitivity in the 3D tumors compared to 2D conditions. Moreover, dECM hydrogels have been modified to produce extrudable bioinks with different mechanical properties. Skardal *et al.,* (2015)[179] reported a composite liver dECM material formulation where the incorporation of crosslinkers yielded tunable bioinks with a variety of shear stiffness properties and created *in-vitro* liver constructs with high cell viability. Jang *et al.,* (2016)[180] developed a vitamin B2-induced UVA-crosslinked decellularized heart tissue bioink for 3D bioprinting, offering precise control over the printed lines, and the crosslinking resulted in a dECM bioink 33 times stiffer than thermally crosslinked gels, achieving mechanical properties like that of native cardiac tissue.

Overall, structural aberrancies in the tumor milieu activate signaling pathways through mechanoreceptors on the cellular membrane[181]. High tumor ECM stiffness is common in different cancer types such as breast[182], liver[183], colorectal[184], and pancreatic[185] tumors. Cancer cells thrive in different stiffness settings[186] and even in anchoring-independent conditions[187]. Developments from the biomaterial community during the past 20 years have demonstrated that tumor biology can be elucidated across a wide range of extracellular matrix (ECM) analogs. Moreover, tissue ECM has been investigated as a therapeutic target (reviewed elsewhere)[188-190]. Clinical trials targeting collagen secretion

using fresolimumab, an anti-TGF-β monoclonal antibody are currently ongoing, (NCT01401062). Nevertheless, organ- and stage-specific cancer models are required for accurate *ex vivo* elucidations of neoplastic diseases. For example, different cancers exhibit different elasticities. Through AFM studies, breast cancer tissue exhibits characteristics peaks at 0.57 kPa and at 5.75kPa[182] while liver cancer reads lower peaks at 0.42 kPa for neoplastic tissue and 1.10 kPa for paraneoplastic tissue[191]. Similarly, necrotic glioblastoma tissue possesses an average Young's modulus of 1kPa while glioblastoma tumor cores averaged an elastic modulus of 10^3 kPa[192].

Stromal elements and stromal architectural relevance.

Cancer-associated cell migration and allocation around the tumor parenchyma have been research fields for the past decades. Precision therapies have been developed to target specific stromal cells and ECM components[188]. Tumor-specific microenvironments develop because of neoplastic cell development at different organs. For example, adipocytes in the breast TME promote neoplastic cell survival by (1) increasing drug distribution, (2) altering drug clearance, and (3) disrupting the drug-protein binding processes. For instance, obesity increases the volume over which antineoplastic drugs are distributed[193], thus reducing its efficacy towards cancerous cells[194]. Cancer-associated adipocytes (CAA) in breast cancers are cells that overexpress pro-inflammatory cytokines known as adipokines, matrixins (MMPs), and insulin growth factor[195,196]. Given their roles in cancer progression, CAA have been investigated as potential targets for precision therapies[197].

Wang Y., *et al.* (2018)[198] studied the effects of obesity in chemotherapy treatment by surrounding MDA-MB-231 breast cancer cells with adipocyte-derived mesenchymal

stem/stromal cells (ADMSC) in a bioprinted gel system. Authors simulated different degrees of obesity by increasing the adipocyte layer thickness as seen in **Figure 4.F.1**. They challenged the co-culture models with doxorubicin (a standard of care drug for breast cancer) and found an inverse correlation between drug sensitivity and ADMSC layer thickness. To prove that ADMSC not only dim the effect of doxorubicin by posing as a physical barrier, but also alter the drug response of cancer cells to the drug, authors explored genetic expression and found upregulation of multidrug resistance related genes (i.e., ABCC1. ABCB1, and ABCG1). Further experimentation proved that ADMSCs are the drivers of decreased drug sensitivity, as increasing the adipocyte layer thickness did not upregulate the multidrug resistance genes. Moreover, Langer *et al.,* (2019)[34], demonstrated the profound role of the stroma in determining tumorigenic phenotypes. Authors used an *in-vitro* 3D printed model that considered both tumor and stromal cells in a defined spatial architecture. Specifically, tissue containing a patient-derived xenograft-derived pancreatic cancer cell line surrounded by a stromal mixture of pancreatic stellate cells (PSCs) and human umbilical vein endothelial cells (HUVECs) (**Figure 4.F.2**). A distinct tumor-stromal border was visible with notable interaction between cancer and endothelial cells occurring in the stromal region. Authors observed increased cancer cell invasion and increased stromal cell density in response to TGF-β. Their study demonstrates that *in-vitro* TME elements respond to microenvironmental biomolecular signals. The study elucidates the dynamic reciprocity that exists between an expanding tumor microenvironment, its contribution to tumor progression, and therapeutic resistance. To elucidate the *in-vitro* migratory patterns of the TME, Jiang *et al., (2016)*[199] patterned triple negative breast cancer cells and fibroblast cells within a hydrogel matrix at precise initial locations relative to one another. Fibrotic cells migrated

through the acellular regions of the hydrogel and towards the tumor spheroids. Moreover, Meng F., *et al.* (2019)[106] demonstrated that *in-vitro* models are responsive to growth factors. Authors instructed tumor migration through the use of epidermal growth factor (EGF) within a bioprinted construct.

As described by Hanahan and Coussens (2012)[200], most of the hallmarks of cancer are the result of varying degrees of contributions from stromal cells. These cell populations are responsible for the distinct features of the microenvironment as the malignancy develops and progresses. Conditions such as tumor fibrosis, hypoxia, and vascularization are all orchestrated by cells present in the tumor milieu. A fundamental understanding of single and collective cell migration within the TME is paramount in targeted therapy development[201]. Specifically, studying the interplay between constituents of the TME and its migratory patterns necessitates precise control over position and patterning of different cell types, cell density, and the matrix biochemistry of stromal and tumor epithelia. These complex scenarios can be elucidated by using extrusion bioprinting as it enables spatial control and recapitulation of relevant architectural features.

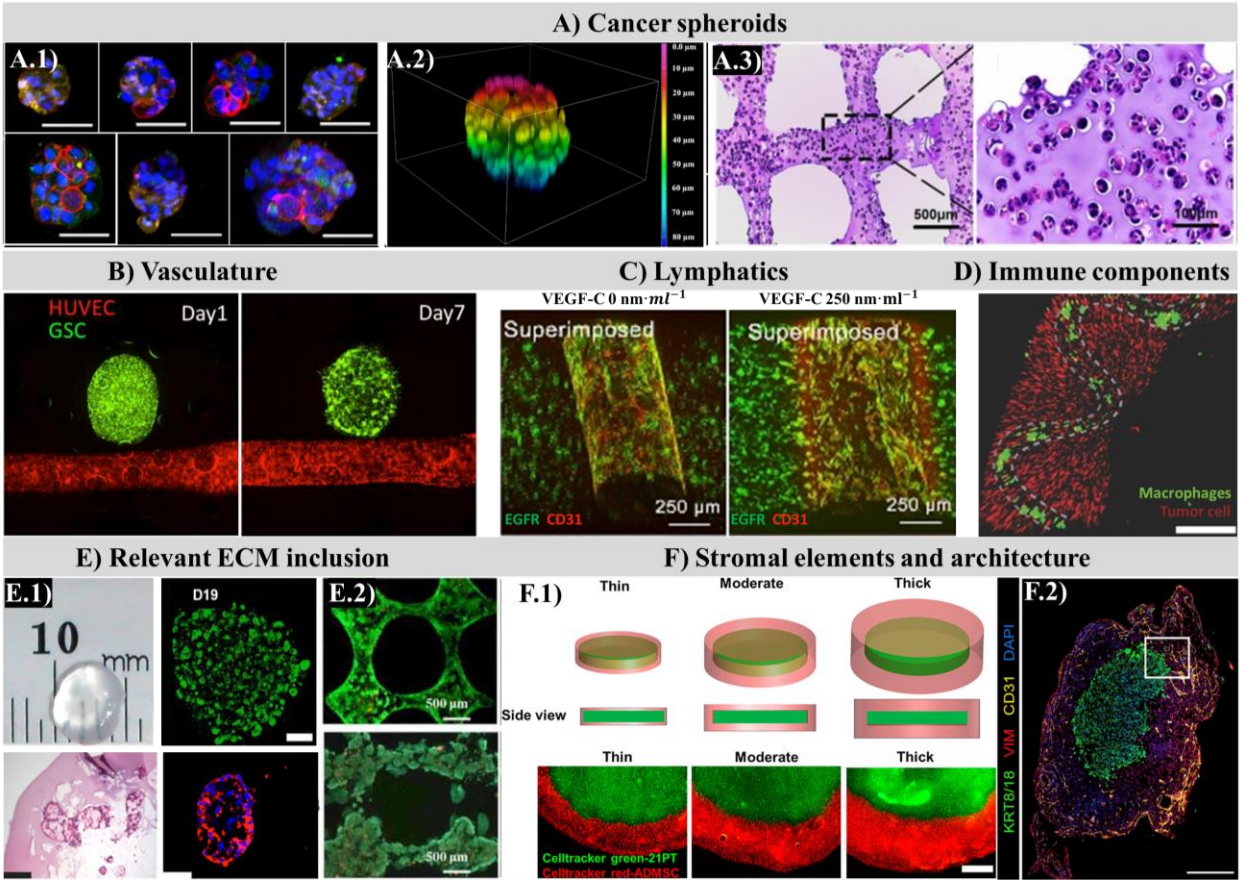

Figure 4. Bioprinted elements of the tumor microenvironment. A) Cancer spheroids developed inside bioprinted matrices. A.1) Drug-resistant breast cancer tumoroids (anti-GRP-79 in green, anti-ABCG2 in red, and nuclei in blue via Hoechst). Reproduced with permission from ref 61. Copyright 2022 Elsevier. A.2) Patient-derived gastric cancer spheroid. Reproduced with permission from ref 62. Copyright 2021 IOP Publishing. A.3) Glioma stem cell spheroids inside a grid-like matrix. Histological evaluation via H&E stains. Reproduced with permission from ref 63. Copyright 2018 Elsevier. B) Bioprinted vasculature architecture with a cancer sphere nearby. Reproduced with permission form ref 102. Copyright 2020 IEEE. C**)** Bioprinted lymphatic vessel structure, day 20 of co-incubation of lymphocyte endothelial cells (CD31, red) and MDA-MB-231 breast cancer cells (EGFR, green) cell culture. Reproduced with permission from ref 124. Copyright

2021 IEEE. D) Coaxially bioprinted macrophages (green) and tumor cells (red, MDA-MB-231). Day 0 of co-culture. Reproduced with permission from ref 143. Copyright 2015 John Wiley and Sons. E) Relevant ECM inclusion in cancer models as decellularized tissue-based bioinks. E.1) Miniaturized disease model for head and neck cancer bioprinted in porcine tongue decellularized ECM (dECM) reinforced with alginate and gelatin. Reproduced with permission from ref 172. Copyright 2021 American Chemical Society. E.2) 3D printed MCF-7 breast cancer cells in hybrid adipose dECM-GelMA (gelatin methacrylate) controls free of treatment day 7 (top panel) and day 14 (bottom panel) (live-dead assay, green and red respectively). Reproduced with permission from ref 178. Copyright 2022 IOP Publishing. F) Stromal elements and architecture. F.1) Bioprinted breast cancer cells (green) with adipocyte-derived mesenchymal stem/stromal cells (red) in a gel system. Reproduced with permission from ref 198. Copyright 2018 American Chemical Society. F.2) Bioprinted tissue containing patient-derived pancreatic tumor tissue surrounded by pancreatic stellate cancer cells and HUVECs. 7 days in cell culture conditions. Reproduced with permission from ref 34. Copyright 2019 Elsevier.

2.5.4. Conclusions

As reviewed in the previous sections, solid tumors (carcinomas) are characterized by a parenchymal region that interacts with a heterogeneous mass of stromal cells and ECM. Current efforts to recapitulate each one of the subcomponents of cancer seen in Figure. 4 have yielded new methods, tools, and *in-vitro* models to interrogate neoplastic diseases in a reproducible and feasible way. Nevertheless, many questions remain unanswered. Combining all these *in-vitro* elucidations into a more complex model where both the tumor parenchyma and its stroma are physiologically relevant mimics of the TME *in vivo* will pave the way into new therapies and fundamental knowledge. In the following section

we identify the areas of opportunity where extrusion bioprinting can be implemented to study some of these aspects of tumor biology.

2.5.5. Opportunities

In this section, we present a detailed summary of the challenges that are yet to be addressed in the field and how extrusion bioprinting could be implemented to enable new experimental setups. In **Figure 5.**, we present a graphical summary of the opportunity section.

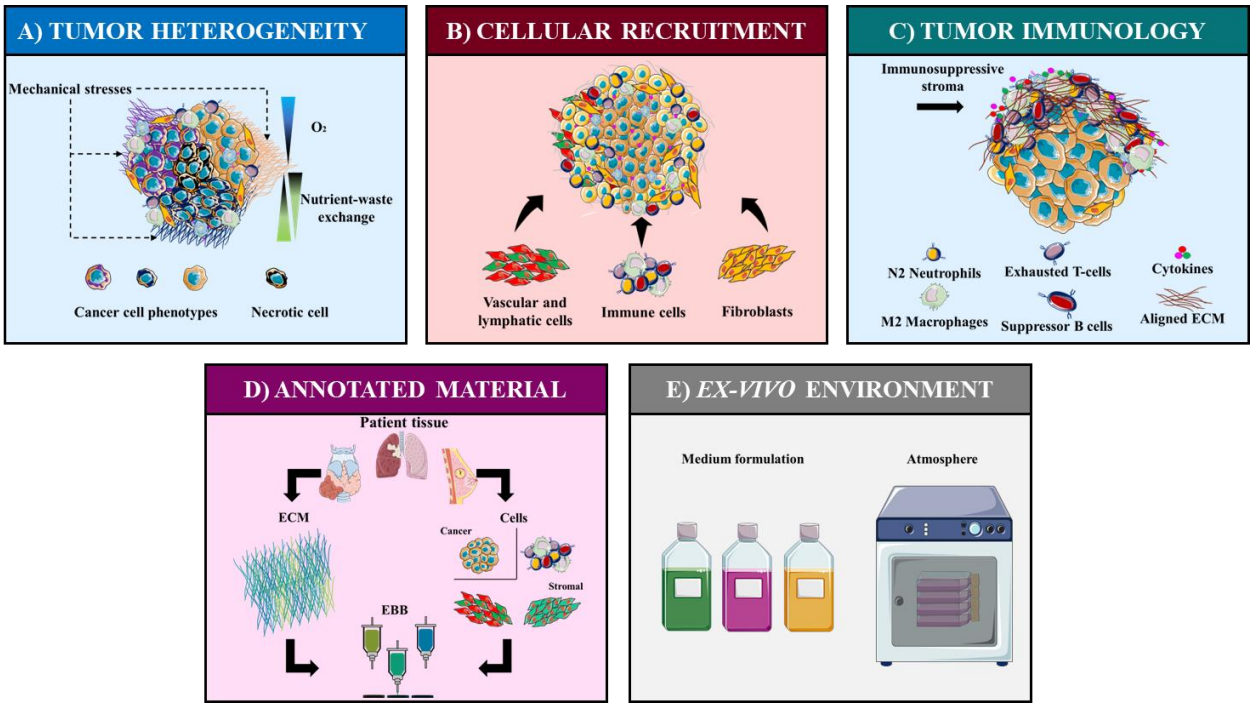

Figure 5. Graphical representation of current opportunities in the field of cancer bioengineering.

Tumor heterogeneity

Heterogeneity manifests as dynamic aberrations during tumor progression. Elucidating the heterogeneous nature of the TME remains a challenge for current *in-vitro* models. A biomaterial that can fully replicate the everchanging tumor milieu is yet to be developed. Every cancer type possesses a unique ECM fingerprint, thus disease- and stage-specific biomaterials are needed to recapitulate pathological features. Intrinsic tumor heterogeneity is present as genetic mutations and it is one of the major causes of therapeutic resistance[202]. Phenotypical cancer heterogeneity can be considered a somatic Darwinian evolution process. Those cancer cells with genetic traits that boost their survival are the ones that will pass on their acquired mutations, eventually becoming a highly malignant phenotype[203,204].

Tumor heterogeneity may also result from interactions between cancer cells and the surrounding stroma (**Figure 5.A**). Tumor-associated cells such as cancer-associated fibroblasts (CAFs), or tumor-associated macrophages (TAMs) are cells that infiltrate the TME, increase malignancy, and promote therapeutic resistance[205-207]. Moreover, tumoral architecture influences tumor heterogeneity. As cancer progresses, the increased tumor mass often experiences hypoxia and recruits vasculature to overcome size and oxygen diffusion limits[76]. The presence of hypoxic tumor regions drives proliferative heterogeneity; subpopulations of cancer cells within a hypoxic tumor exhibit different proliferation rates, dormancy, immunosuppression, chemoresistance, and altered metabolism[208-211]. This is a particular challenge for therapeutic strategies that rely on cancer cell division or cancer cell metabolism. Furthermore, mechanical heterogeneity and elevated mechanical stress are characteristic features of solid tumors[182,212].

Mechanical incongruities can be attributed to the intrinsic dynamic events within the TME such as increased tumoral mass, recruited cells, ECM secretion, and ECM remodeling.

Single-cell RNA sequencing has enabled the identification of genetic subvariants within cancer cell populations[213]. Atomic force microscopy (AFM) techniques have allowed us to obtain the mechanical signatures of tumoral microenvironments[182]. In combination with extrusion-based bioprinting and biomaterial engineering, human tumor genetic and mechanical heterogeneity can be recapitulated in the laboratory. Bioprinting maneuvers can integrate architectural features, cellular content, and user-defined biomaterials to engineer heterogeneous tumor models. In this sense, tumor heterogeneity can be better addressed *in-vitro* by adopting 3D bioprinting techniques in conjunction with physiologically relevant biomaterials and cells. Moreover, bioprinting offers the possibility of escalating model complexity without losing control over important parameters. Soon, *in-vitro* tumor models must consider heterogeneous cell populations that reflect stage- and site-specific cancers. We know that not only cancer epithelial cells are involved in malignancy progression, but it is also the surrounding stroma and the biomechanical state of the microenvironment that promote the cancerous onslaught.

Cellular recruitment in the tumor microenvironment

Tumor progression is highly dynamic. Neoplastic cells remain in constant contact and biomolecular dialogue with both the extracellular matrix and stromal components in their microenvironment. Distinction can be made between metastasis and migration. Cancer metastasis refers to an advanced stage of malignancy whereby cancer cells populate distant secondary sites forming new tumor nests[214]. Prior to metastasis, cancerous cells

recruit non-malignant cells to aid TME reshaping. Recruited cells migrate, move, and relocate on and in the tumor. Vascular cells, infiltrating immune cells, and CAFs are amongst the most common cells recruited towards the TME. For instance, cancer-associated fibroblasts (CAFs) enroll in tumor progression as they to contribute to the increase in stiffness of the tumor milieu[215,216], and macrophages are amongst the most important immune cells that contribute to cancer prognosis. Inhibition of TAM recruitment to the TME has been proven to decrease primary tumor progression, reduces metastasis, and improves CD8+ T-cell activity[217]. Elucidating cellular movements and migratory patterns in *in-vitro* models requires precise positioning of selected cell populations. Bioprinting enables control over the precise allocation of cells within defined biomaterial constructs. Optimized printable biomaterials grant us access to controlled experimental conditions where the volumetric arrangement is an observable and quantifiable variable that offers insights on migratory patterns and their dependencies on intercellular dialogue.

The tumor immune microenvironment (TIME)

Most solid tumors have been challenged with antineoplastic therapy in laboratory conditions. However, the interactions between effector T-cells and tumors in 3D volumetric environments, have not received the same attention. From the immune response perspective, tumors can be divided into two broad categories: immune-hot and immune-cold. These terms are used to refer to those tumors that are recognized (hot) and those that appear undetected (cold) by the immune system. Hot tumors have an abundance of tumor-infiltrated lymphocytes (TILs), and the immune system can mount an immune response. On the other hand, cold tumors can be further divided in two

subcategories: immune-excluded where T-cells are physically unable to reach the parenchyma, and immune-ignored where T-cells are unable to recognize the tumor formation as a foreign body and mount an appropriate immune reponse[218]. Most T-cells in the TME are in a dysfunctional state known as exhaustion. Exhausted T-cells express receptors for inhibitory molecules such as the programmed dead protein 1 (PD1)[219] that drives T-cells to apoptosis when bound to programmed dead ligand 1 (PD-L1) presented by the target cell[220]. Overcoming an existing anergic state has been one of the goals of immunotherapy strategies such as immune-checkpoint inhibitors and chimeric antigen receptor (CAR) modified T-cells [221,222]. Nonetheless, drawbacks of CAR-T cell therapy still include T-cell associated toxicities, T cell trafficking, tumor infiltration, and the presence of an immunosuppressive microenvironment[223].

Tumors are known to possess immunosuppressive mechanisms by which they oppose the body's natural ability to eradicate neoplastic malignancies[224]. The immunosuppressive strategies of tumor cells allow them to escape immune surveillance by exploiting T-cell tolerance[225], disrupting tumor antigen presentation cascades[226-228], and activating negative costimulatory signals[229]. For instance, regulatory B cells (Bregs) can produce immunoregulatory cytokines, however, Bregs can also supress those T-cells responsible for mounting an antitumoral response[230]. In addition, the physical characteristics of the stroma also influence the migration of T-cells towards the tumor core. For instance, solid tumors with abundant aligned ECM fibers can direct the migration and fate of infiltrated immune cells[231,232].

Furthermore, solid tumors tend to possess an immunosuppressive stroma[233] (**Figure 5.C**) and are commonly ignored by the immune system[234]. Even though we understand

some of the mechanisms through which a tumor finds sanctuary and evades immune surveillance, our understanding of how native and engineered T-cells are recruited towards the TME is still maturing. It is recognized that T-cells will undergo motility through mesenchymal-amoeboid plasticity balance[235]. Mesenchymal-like movements refer to adhesive spreading, whereas amoeboid-like describes low-adhesion conditions of movement[235]. We know that these mechanisms are regulated in response to the microenvironment[236]. Extrusion printing enables the creation of volumetric arrangements with defined spatial features. This is important when considering "cold" tumor models. In the end, the combination of the appropriate cancer cell type and density with an architecturally relevant adjacent stroma comprised of representative cellular populations can afford us a representative tumor model to study T-cell interactions with not only cancer cells, but also with a potentially immunosuppressive stroma. T-cell infiltration, allocation, and function are highly dependent on the spatio-temporal status of the tumor[134]. A TME model that elucidates T-cell infiltration into a known tumor system is yet to be developed. These models would provide the necessary tools to test immunotherapy strategies in known tumor models and will aid the search for druggable targets within the ECM to facilitate *in vivo* T-cell infiltration.

Clinically annotated cell and ECM material

Most of our *in-vitro* cancer models have been first fabricated and troubleshot using commercially available cells and biomaterials. Epithelial cancer cell lines are robust, easy to work with, and most of them grow in 3D constructs. However, these cells tend to accumulate mutations with every mitotic cycle, creating genetically distinguishable subclones at an accelerated pace. The problem with this type of genetic drift is that

emerging mutations may not reflect the result of cancer progression, instead, some of these could be attributed to aberrant cell culture conditions that are not representative of their native environment[237]. Nevertheless, cancer cell lines are a way to enable reproducibility of experimental methods around the world.

Patient-derived cancer cells, primary cancer cells, or clinically annotated cancer cells are by far the best type of biological material that could be used to elucidate malignancies *in-vitro* (**Figure 5.D**). However, accessibility to these resources is difficult and strict ethical regulations must be followed. Primary cells have been used to establish patient-derived organoids (PDOs) that recapitulate features from the original tumor[59,238]. Also, tumor-derived ECM has been decellularized and utilized to study macrophage polarization and differentiation[239].

Overall, annotated cell and ECM materials increase the relevance of bioprinted *in-vitro* models. However, robust cell expansion methodologies are required prior to bioprinting maneuvers. Moreover, patient-derived materials have the potential to retain distinctive clinical history including therapeutic response if the appropiate *ex vivo* conditions are provided. Bioprinted annotated cancer models are likely to become patient avatars in which identifying new treatment regimes will be possible, thus enabling precision medicine.

***Ex vivo* culture conditions**

Often overlooked, *ex vivo* cell culture conditions are important variables that dictate behavior and fate of cells in culture[240,241]. The most common way to maintain cells outside the body is to keep them submerged in cell medium within a reservoir and inside a special incubator where atmospheric conditions such as temperature, relative humidity, oxygen,

carbon dioxide levels, and pressure are monitored (**Figure 5.E**). Solid tumor biology describes a substantial number of environmental conditions such as oxygen availability, nutrient exchange, and metabolic state[242-244]. To emulate solid tumor biology in the laboratory, controlled environmental conditions are needed. For instance, certain tumor lineages benefit from environmental hypoxia to recruit vascular vessels, acquire therapeutic resistance, evade the immune system, switch their phenotype, and metastasize[208,245].

Solid tumor interstitial fluid pressure (IFP) has been framed as an obstacle in cancer therapy because it acts as a barrier that shields the tumor from therapeutic agents[246]. Elevated IFP is an microenvironmental abnormality that manifests when unmature blood vessels leak fluids in the tumor area. In the laboratory, several groups have reported important differences in cellular behavior after cells are maintained cultured under simulated high IFP[247,248]. One of the most important goals of a cytotoxic drug in the body is to reach a tumor from a blood vessel. The drug must first diffuse through a dense ECM network that is present in and around the solid tumor. This process can be hindered by having high IFP levels as it causes fluid to flow from the tumor instead of flowing into it[249,250]. Extrusion bioprinting can bridge these important environmental variables with relevant tissue architectures. Having a vascularized tumor model inside an incubator that provides fluid pressure balance can enable new alternatives to current paradoxical treatments that aim to reduce elevated IFP around the tumor by reducing angiogenesis in the tumor while at the same time decreasing the delivery of cytotoxic drugs[251].

Furthermore, standard cell culture medium formulations are oversimplified versions of the dynamic physiological cocktail of hormones, cytokines, nutrients, and metabolites

that are present in the tumor milieu. Some of the commercially available formulations were designed half a century ago and are disconnected from tissue physiology[252]. Originally, these were tailored to support continuous *ex vivo* cell division[252]. Replicating the *in vivo* metabolic environment of solid tumors is amongst the most important parameters to control and it remains a challenge not just for the bioengineering field. Throughout development, neoplastic lesions depend upon small signaling molecules such as cytokines and chemokines[253], growth factors (GFs)[254], and hormones. The aberrant expression of cytokines promotes cancer development, progression, and chemoresistance[255,256]. For instance, interleukin-6 promotes DNA repair after therapy induced damage[257,258]. Moreover, GFs play critical roles in all stages of malignancy[254]. For instance, the transforming growth factor-β boosts malignancy as it activates epithelial-mesenchymal transition (EMT)[259] through both SMAD-dependent and SMAD2-independent pathways[260]. Furthermore, certain types of cancers are known to overexpress hormone receptors and make use of these to initiate[261] and progress[262]. Some breast cancers are known to express the estrogen receptor (ER) and/or the progesterone receptor (PR) and make use of these to proliferate[263,264]. Clinically, these hormone-receptor positive cancers are treated with specialized receptor targeting drugs[265]. Another example of hormone sensitive cancers are some types of prostate cancer which are progesterone sensitive cancers that have altered androgen receptor (AR) signaling that promotes their proliferation and progression[266].

As an important way of *in-vitro* cell behavior, cell culture medium recipes and supplementation strategies cannot be overlooked when engineering disease models. The physiological relevance of an engineered disease model may be lost due to the absence of

critical growth factors or hormonal supplements. In the practical setting, signaling molecules are often deployed alongside the cell culture medium. It has been demonstrated that cell culture medium formulation dictates cell behavior in cancer organoids[267]. We must figure out the optimal way of administering relevant oxygen levels, pressure conditions, vitamins, GFs, hormones, and cytokines while considering their effectiveness in medium.

The progressiveness of science and technology: Innovation as a vulnerability.

The pace at which new scientific discoveries and technological developments are brought to light has increased over the past 50 years. Many inventions and new technologies come and go so fast that their true potential is not completely exploited. In regard to biofabrication of disease models, we presented a field that continues to mature and is still vulnerable to falling into a never-ending race for innovation devoid of true application and fundamental knowledge. We identify this issue as one of the main reasons why many biofabrication techniques have not been adopted in the clinic and thus, well-established, conventional 2D cell monolayer models, small animal models, and simple 3D gel casts continue to dominate the fields of preclinical research.

As the bioengineering and oncology fields coalesce, the implementation of automated tools such as bioprinting will enable clinical scientists to create new experimental conditions that will help navigate the current sea of questions regarding neoplastic diseases. Unifying the bioprinted sub-elements of neoplastic diseases into a more complex and physiologically relevant model is a step towards having humanized tumor mimics for basic discovery and therapy testing.

2.5.6. Acknowledgements

JMK thanks the National Science and Engineering Research Council (RGPIN-2020-5692) for funding. SFT thanks the FRQNT (291010) and the McGill Engineering Doctoral Award (90025) for the scholarships. JKM thanks the FRQNT (288490) and the McGill Engineering Doctoral Award (90025) for the scholarships. The authors acknowledge the use of Servier Medical Art as the graphical abstract and Figures 1 and 5 were partly generated using Servier Medical Art, provided by Servier, licensed under a Creative Commons Attribution 3.0 unported license. The authors acknowledge the use of Biorender.com to create Figures 2 and 3.

2.5.7. References:

1 Hanahan, D. & Robert. Hallmarks of Cancer: The Next Generation. *Cell* (2011). **144**, 646-674 https://doi.org:10.1016/j.cell.2011.02.013

2 Carbone, A. Cancer Classification at the Crossroads. *Cancers (Basel)* (2020). **12** https://doi.org:10.3390/cancers12040980

3 Sung, H., Ferlay, J., Siegel, R. L., Laversanne, M., Soerjomataram, I., Jemal, A. & Bray, F. Global Cancer Statistics 2020: GLOBOCAN Estimates of Incidence and Mortality Worldwide for 36 Cancers in 185 Countries. *CA: A Cancer Journal for Clinicians* (2021). **71**, 209-249 https://doi.org:10.3322/caac.21660

4 Balkwill, F. R., Capasso, M. & Hagemann, T. The tumor microenvironment at a glance. *Journal of Cell Science* (2012). **125**, 5591-5596 https://doi.org:10.1242/jcs.116392

5 Frantz, C., Stewart, K. M. & Weaver, V. M. The extracellular matrix at a glance. *Journal of Cell Science* (2010). **123**, 4195-4200 https://doi.org:10.1242/jcs.023820

6 Humphrey, J. D., Dufresne, E. R. & Schwartz, M. A. Mechanotransduction and extracellular matrix homeostasis. *Nature Reviews Molecular Cell Biology* (2014). **15**, 802-812 https://doi.org:10.1038/nrm3896

7 Cox, T. R. & Erler, J. T. Remodeling and homeostasis of the extracellular matrix: implications for fibrotic diseases and cancer. *Disease Models & Mechanisms* (2011). **4**, 165-178 https://doi.org:10.1242/dmm.004077

8 Alhmoud, J. F., Woolley, J. F., Al Moustafa, A. E. & Malki, M. I. DNA Damage/Repair Management in Cancers. *Cancers (Basel)* (2020). **12** https://doi.org:10.3390/cancers12041050

9 Winkler, J., Abisoye-Ogunniyan, A., Metcalf, K. J. & Werb, Z. Concepts of extracellular matrix remodelling in tumour progression and metastasis. *Nature Communications* (2020). **11** https://doi.org:10.1038/s41467-020-18794-x

10 Hill, B. S., Sarnella, A., D'Avino, G. & Zannetti, A. Recruitment of stromal cells into tumour microenvironment promote the metastatic spread of breast cancer. *Seminars in*

Cancer Biology (2020). **60**, 202-213 https://doi.org:https://doi.org/10.1016/j.semcancer.2019.07.028

11 Itoh, Y. & Nagase, H. Matrix metalloproteinases in cancer. *Essays in Biochemistry* (2002). **38**, 21-36 https://doi.org:10.1042/bse0380021

12 Yuan, S., Norgard, R. J. & Stanger, B. Z. Cellular Plasticity in Cancer. *Cancer Discovery* (2019). **9**, 837-851 https://doi.org:10.1158/2159-8290.cd-19-0015

13 Bissell, M. J. & Radisky, D. Putting tumours in context. *Nature Reviews Cancer* (2001). **1**, 46-54 https://doi.org:10.1038/35094059

14 Egeblad, M., Nakasone, E. S. & Werb, Z. Tumors as organs: complex tissues that interface with the entire organism. *Dev Cell* (2010). **18**, 884-901 https://doi.org:10.1016/j.devcel.2010.05.012

15 Gengenbacher, N., Singhal, M. & Augustin, H. G. Preclinical mouse solid tumour models: status quo, challenges and perspectives. *Nature Reviews Cancer* (2017). **17**, 751-765 https://doi.org:10.1038/nrc.2017.92

16 Mak Isabella Wy, I. W. Lost in translation: animal models and clinical trials in cancer treatment. *American Journal of Translational Research* (2014). **6**, 114-118

17 Van Norman, G. A. Limitations of Animal Studies for Predicting Toxicity in Clinical Trials: Is it Time to Rethink Our Current Approach? *JACC: Basic to Translational Science* (2019). **4**, 845-854 https://doi.org:https://doi.org/10.1016/j.jacbts.2019.10.008

18 Kim, J., Koo, B.-K. & Knoblich, J. A. Human organoids: model systems for human biology and medicine. *Nature Reviews Molecular Cell Biology* (2020). **21**, 571-584 https://doi.org:10.1038/s41580-020-0259-3

19 Tuveson, D. & Clevers, H. Cancer modeling meets human organoid technology. *Science* (2019). **364**, 952-955 https://doi.org:doi:10.1126/science.aaw6985

20 Ivascu, A. & Kubbies, M. Rapid Generation of Single-Tumor Spheroids for High-Throughput Cell Function and Toxicity Analysis. *Journal of Biomolecular Screening* (2006). **11**, 922-932 https://doi.org:10.1177/1087057106292763

21 Timmins, N. E. & Nielsen, L. K. Generation of multicellular tumor spheroids by the hanging-drop method. *Methods Mol Med* (2007). **140**, 141-151 https://doi.org:10.1007/978-1-59745-443-8_8

22 Ingram, M., Techy, G. B., Saroufeem, R., Yazan, O., Narayan, K. S., Goodwin, T. J. & Spaulding, G. F. Three-dimensional growth patterns of various human tumor cell lines in simulated microgravity of a NASA bioreactor. *In-vitro Cellular & Developmental Biology - Animal* (1997). **33**, 459-466 https://doi.org:10.1007/s11626-997-0064-8

23 Distefano, T., Chen, H. Y., Panebianco, C., Kaya, K. D., Brooks, M. J., Gieser, L., Morgan, N. Y., Pohida, T. & Swaroop, A. Accelerated and Improved Differentiation of Retinal Organoids from Pluripotent Stem Cells in Rotating-Wall Vessel Bioreactors. *Stem Cell Reports* (2018). **10**, 300-313 https://doi.org:10.1016/j.stemcr.2017.11.001

24 Souza, G. R., Molina, J. R., Raphael, R. M., Ozawa, M. G., Stark, D. J., Levin, C. S., Bronk, L. F., Ananta, J. S., Mandelin, J., Georgescu, M.-M., Bankson, J. A., Gelovani, J. G., Killian, T. C., Arap, W. & Pasqualini, R. Three-dimensional tissue culture based on magnetic cell levitation. *Nature Nanotechnology* (2010). **5**, 291-296 https://doi.org:10.1038/nnano.2010.23

25 Li, X., Valadez, A. V., Zuo, P. & Nie, Z. Microfluidic 3D cell culture: potential application for tissue-based bioassays. *Bioanalysis* (2012). **4**, 1509-1525 https://doi.org:10.4155/bio.12.133

26 Van Duinen, V., Trietsch, S. J., Joore, J., Vulto, P. & Hankemeier, T. Microfluidic 3D cell culture: from tools to tissue models. *Current Opinion in Biotechnology* (2015). **35**, 118-126 https://doi.org:10.1016/j.copbio.2015.05.002

27 Tibbitt, M. W. & Anseth, K. S. Hydrogels as extracellular matrix mimics for 3D cell culture. *Biotechnology and Bioengineering* (2009). **103**, 655-663 https://doi.org:10.1002/bit.22361

28 Deo, K. A., Singh, K. A., Peak, C. W., Alge, D. L. & Gaharwar, A. K. Bioprinting 101: Design, Fabrication, and Evaluation of Cell-Laden 3D Bioprinted Scaffolds. *Tissue Engineering Part A* (2020). **26**, 318-338 https://doi.org:10.1089/ten.tea.2019.0298

29 Knowlton, S., Onal, S., Yu, C. H., Zhao, J. J. & Tasoglu, S. Bioprinting for cancer research. *Trends in Biotechnology* (2015). **33**, 504-513 https://doi.org:10.1016/j.tibtech.2015.06.007

30 Zhuang, P., Chiang, Y. H., Fernanda, M. S. & He, M. Using Spheroids as Building Blocks Towards 3D Bioprinting of Tumor Microenvironment. *International journal of bioprinting* (2021). **7**, 444 https://doi.org:10.18063/ijb.v7i4.444

31 Barkan, D., Green, J. E. & Chambers, A. F. Extracellular matrix: A gatekeeper in the transition from dormancy to metastatic growth. *European Journal of Cancer* (2010). **46**, 1181-1188 https://doi.org:10.1016/j.ejca.2010.02.027

32 Pickup, M. W., Mouw, J. K. & Weaver, V. M. The extracellular matrix modulates the hallmarks of cancer. *EMBO reports* (2014). **15**, 1243-1253 https://doi.org:https://doi.org/10.15252/embr.201439246

33 Reid, J. A., Palmer, X.-L., Mollica, P. A., Northam, N., Sachs, P. C. & Bruno, R. D. A 3D bioprinter platform for mechanistic analysis of tumoroids and chimeric mammary organoids. *Scientific Reports* (2019). **9** https://doi.org:10.1038/s41598-019-43922-z

34 Langer, E. M., Allen-Petersen, B. L., King, S. M., Kendsersky, N. D., Turnidge, M. A., Kuziel, G. M., Riggers, R., Samatham, R., Amery, T. S., Jacques, S. L., Sheppard, B. C., Korkola, J. E., Muschler, J. L., Thibault, G., Chang, Y. H., Gray, J. W., Presnell, S. C., Nguyen, D. G. & Sears, R. C. Modeling Tumor Phenotypes In Vitro with Three-Dimensional Bioprinting. *Cell Reports* (2019). **26**, 608-623.e606 https://doi.org:10.1016/j.celrep.2018.12.090

35 Zhao, Y., Yao, R., Ouyang, L., Ding, H., Zhang, T., Zhang, K., Cheng, S. & Sun, W. Three-dimensional printing of Hela cells for cervical tumor model in vitro. *Biofabrication* (2014). **6**, 035001 https://doi.org:10.1088/1758-5082/6/3/035001

36 Swaminathan, S., Hamid, Q., Sun, W. & Clyne, A. M. Bioprinting of 3D breast epithelial spheroids for human cancer models. *Biofabrication* (2019). **11**, 025003 https://doi.org:10.1088/1758-5090/aafc49

37 Datta, P., Dey, M., Ataie, Z., Unutmaz, D. & Ozbolat, I. T. 3D bioprinting for reconstituting the cancer microenvironment. *npj Precision Oncology* (2020). **4** https://doi.org:10.1038/s41698-020-0121-2

38 Ma, X., Yu, C., Wang, P., Xu, W., Wan, X., Lai, C. S. E., Liu, J., Koroleva-Maharajh, A. & Chen, S. Rapid 3D bioprinting of decellularized extracellular matrix with regionally varied mechanical properties and biomimetic microarchitecture. *Biomaterials* (2018). **185**, 310-321 https://doi.org:10.1016/j.biomaterials.2018.09.026

39 Tang, M., Xie, Q., Gimple, R. C., Zhong, Z., Tam, T., Tian, J., Kidwell, R. L., Wu, Q., Prager, B. C., Qiu, Z., Yu, A., Zhu, Z., Mesci, P., Jing, H., Schimelman, J., Wang, P., Lee, D., Lorenzini, M. H., Dixit, D., Zhao, L., Bhargava, S., Miller, T. E., Wan, X., Tang, J., Sun, B., Cravatt, B. F., Muotri, A. R., Chen, S. & Rich, J. N. Three-dimensional bioprinted glioblastoma microenvironments model cellular dependencies and immune interactions. *Cell Research* (2020). **30**, 833-853 https://doi.org:10.1038/s41422-020-0338-1

40 Hakobyan, D., Médina, C., Dusserre, N., Stachowicz, M.-L., Handschin, C., Fricain, J.-C., Guillermet-Guibert, J. & Oliveira, H. Laser-assisted 3D bioprinting of exocrine pancreas spheroid models for cancer initiation study. *Biofabrication* (2020). **12**, 035001 https://doi.org:10.1088/1758-5090/ab7cb8

41 Mondal, A., Gebeyehu, A., Miranda, M., Bahadur, D., Patel, N., Ramakrishnan, S., Rishi, A. K. & Singh, M. Characterization and printability of Sodium alginate -Gelatin hydrogel for bioprinting NSCLC co-culture. *Scientific Reports* (2019). **9** https://doi.org:10.1038/s41598-019-55034-9

42 Xiang, Y., Miller, K., Guan, J., Kiratitanaporn, W., Tang, M. & Chen, S. 3D bioprinting of complex tissues in vitro: state-of-the-art and future perspectives. *Archives of Toxicology* (2022). https://doi.org:10.1007/s00204-021-03212-y

43 Shukla, P., Yeleswarapu, S., Heinrich, M. A., Prakash, J. & Pati, F. Mimicking tumor microenvironment by 3D bioprinting: 3D cancer modeling. *Biofabrication* (2022). **14**, 032002 https://doi.org:10.1088/1758-5090/ac6d11

44 Mironov, V., Boland, T., Trusk, T., Forgacs, G. & Markwald, R. R. Organ printing: computer-aided jet-based 3D tissue engineering. *Trends in Biotechnology* (2003). **21**, 157-161 https://doi.org:10.1016/s0167-7799(03)00033-7

45 Zhang, Y. S., Duchamp, M., Oklu, R., Ellisen, L. W., Langer, R. & Khademhosseini, A. Bioprinting the Cancer Microenvironment. *ACS Biomaterials Science & Engineering* (2016). **2**, 1710-1721 https://doi.org:10.1021/acsbiomaterials.6b00246

46 Bae, J., Han, S. & Park, S. Recent Advances in 3D Bioprinted Tumor Microenvironment. *BioChip Journal* (2020). **14**, 137-147 https://doi.org:10.1007/s13206-020-4201-8

47 Oztan, Y. C., Nawafleh, N., Zhou, Y., Liyanage, P. Y., Hettiarachchi, S. D., Seven, E. S., Leblanc, R. M., Ouhtit, A. & Celik, E. Recent advances on utilization of bioprinting for tumor modeling. *Bioprinting* (2020). **18**, e00079 https://doi.org:https://doi.org/10.1016/j.bprint.2020.e00079

48 Sánchez-Salazar, M. G., Álvarez, M. M. & Trujillo-de Santiago, G. Advances in 3D bioprinting for the biofabrication of tumor models. *Bioprinting* (2021). **21**, e00120 https://doi.org:https://doi.org/10.1016/j.bprint.2020.e00120

49 Tang, M., Rich, J. N. & Chen, S. Biomaterials and 3D Bioprinting Strategies to Model Glioblastoma and the Blood–Brain Barrier. *Advanced Materials* (2021). **33**, 2004776 https://doi.org:10.1002/adma.202004776

50 Bremnes, R. M., Dønnem, T., Al-Saad, S., Al-Shibli, K., Andersen, S., Sirera, R., Camps, C., Marinez, I. & Busund, L.-T. The Role of Tumor Stroma in Cancer Progression and Prognosis: Emphasis on Carcinoma-Associated Fibroblasts and Non-small Cell Lung Cancer. *Journal of Thoracic Oncology* (2011). **6**, 209-217 https://doi.org:10.1097/jto.0b013e3181f8a1bd

51 Murphy, S. V. & Atala, A. 3D bioprinting of tissues and organs. *Nature Biotechnology* (2014). **32**, 773-785 https://doi.org:10.1038/nbt.2958

52 Schwab, A., Levato, R., D'Este, M., Piluso, S., Eglin, D. & Malda, J. Printability and Shape Fidelity of Bioinks in 3D Bioprinting. *Chemical Reviews* (2020). **120**, 11028-11055 https://doi.org:10.1021/acs.chemrev.0c00084

53 Naghieh, S. & Chen, X. Printability–A key issue in extrusion-based bioprinting. *Journal of Pharmaceutical Analysis* (2021). **11**, 564-579 https://doi.org:https://doi.org/10.1016/j.jpha.2021.02.001

54 Ribeiro, A., Blokzijl, M. M., Levato, R., Visser, C. W., Castilho, M., Hennink, W. E., Vermonden, T. & Malda, J. Assessing bioink shape fidelity to aid material development in 3D bioprinting. *Biofabrication* (2017). **10**, 014102 https://doi.org:10.1088/1758-5090/aa90e2

55 Blaeser, A., Duarte Campos, D. F., Puster, U., Richtering, W., Stevens, M. M. & Fischer, H. Controlling Shear Stress in 3D Bioprinting is a Key Factor to Balance Printing Resolution and Stem Cell Integrity. *Advanced Healthcare Materials* (2016). **5**, 326-333 https://doi.org:https://doi.org/10.1002/adhm.201500677

56 Jiang, T., Munguia-Lopez, J. G., Flores-Torres, S., Kort-Mascort, J. & Kinsella, J. M. Extrusion bioprinting of soft materials: An emerging technique for biological model fabrication. *Applied Physics Reviews* (2019). **6**, 011310 https://doi.org:10.1063/1.5059393

57 Ozaki, T. & Nakagawara, A. Role of p53 in Cell Death and Human Cancers. *Cancers (Basel)* (2011). **3**, 994-1013 https://doi.org:10.3390/cancers3010994

58 Sylvia, Hwang, C.-I., Lindsey, Iok, Dannielle, Corbo, V., Jager, M., Ponz-Sarvise, M., Tiriac, H., Mona, Gracanin, A., Oni, T., Kenneth, Ruben, Huch, M., Keith, John, Michael, Öhlund, D., Handly-Santana, A., Christine, Ludwig, M., Elyada, E., Alagesan, B., Biffi, G., Georgi, Delcuze, B., Creighton, B., Wright, K., Park, Y., Folkert, I, Inne, Cuppen, E., Hao, Y., Jin, Y., Isaac, Iacobuzio-Donahue, C., Steven, Darryl, Hammell, M., David, Basturk, O., Ralph, George, Robert, Clevers, H. & David. Organoid Models of Human and Mouse Ductal Pancreatic Cancer. *Cell* (2015). **160**, 324-338 https://doi.org:10.1016/j.cell.2014.12.021

59 Driehuis, E., van Hoeck, A., Moore, K., Kolders, S., Francies, H. E., Gulersonmez, M. C., Stigter, E. C. A., Burgering, B., Geurts, V., Gracanin, A., Bounova, G., Morsink, F. H., Vries, R., Boj, S., van Es, J., Offerhaus, G. J. A., Kranenburg, O., Garnett, M. J., Wessels, L., Cuppen, E., Brosens, L. A. A. & Clevers, H. Pancreatic cancer organoids recapitulate disease and allow personalized drug screening. *Proc Natl Acad Sci U S A* (2019). **116**, 26580-26590 https://doi.org:10.1073/pnas.1911273116

60 Johnson, P. A., Menegatti, S., Chambers, A. C., Alibhai, D., Collard, T. J., Williams, A. C., Bayley, H. & Perriman, A. W. A rapid high throughput bioprinted colorectal cancer spheroid platform for in vitro drug- and radiation-response. *Biofabrication* (2022). **15**, 014103 https://doi.org:10.1088/1758-5090/ac999f

61 Hong, S. & Song, J. M. 3D bioprinted drug-resistant breast cancer spheroids for quantitative in situ evaluation of drug resistance. *Acta Biomaterialia* (2022). **138**, 228-239 https://doi.org:https://doi.org/10.1016/j.actbio.2021.10.031

62 Flores-Torres, S., Peza-Chavez, O., Kuasne, H., Munguia-Lopez, J. G., Kort-Mascort, J., Ferri, L., Jiang, T., Rajadurai, C. V., Park, M., Sangwan, V. & Kinsella, J. M. Alginate–gelatin–Matrigel hydrogels enable the development and multigenerational passaging of patient-derived 3D bioprinted cancer spheroid models. *Biofabrication* (2021). **13**, 025001 https://doi.org:10.1088/1758-5090/abdb87

63 Wang, X., Li, X., Dai, X., Zhang, X., Zhang, J., Xu, T. & Lan, Q. Bioprinting of glioma stem cells improves their endotheliogenic potential. *Colloids and Surfaces B: Biointerfaces* (2018). **171**, 629-637 https://doi.org:https://doi.org/10.1016/j.colsurfb.2018.08.006

64 Hashimoto, T. & Shibasaki, F. Hypoxia-Inducible Factor as an Angiogenic Master Switch. *Frontiers in Pediatrics* (2015). **3** https://doi.org:10.3389/fped.2015.00033

65 Swaminathan, S., Hamid, Q., Sun, W. & Clyne, A. M. Bioprinting of 3D breast epithelial spheroids for human cancer models. *Biofabrication* (2019). **11**, 025003-025003 https://doi.org:10.1088/1758-5090/aafc49

66 Schmidt, S. K., Schmid, R., Arkudas, A., Kengelbach-Weigand, A. & Bosserhoff, A. K. Tumor Cells Develop Defined Cellular Phenotypes After 3D-Bioprinting in Different Bioinks. *Cells* (2019). **8** https://doi.org:10.3390/cells8101295

67 Sbirkov, Y., Molander, D., Milet, C., Bodurov, I., Atanasov, B., Penkov, R., Belev, N., Forraz, N., McGuckin, C. & Sarafian, V. A Colorectal Cancer 3D Bioprinting Workflow as a Platform for Disease Modeling and Chemotherapeutic Screening. *Frontiers in Bioengineering and Biotechnology* (2021). **9** https://doi.org:10.3389/fbioe.2021.755563

68 Wang, X., Zhang, X., Dai, X., Wang, X., Li, X., Diao, J. & Xu, T. Tumor-like lung cancer model based on 3D bioprinting. *3 Biotech* (2018). **8**, 501-501 https://doi.org:10.1007/s13205-018-1519-1

69 Dai, X., Ma, C., Lan, Q. & Xu, T. 3D bioprinted glioma stem cells for brain tumor model and applications of drug susceptibility. *Biofabrication* (2016). **8**, 045005 https://doi.org:10.1088/1758-5090/8/4/045005

70 Duarte Campos, D. F., Bonnin Marquez, A., O'Seanain, C., Fischer, H., Blaeser, A., Vogt, M., Corallo, D. & Aveic, S. Exploring Cancer Cell Behavior In Vitro in Three-Dimensional Multicellular Bioprintable Collagen-Based Hydrogels. *Cancers* (2019). **11**, 180 https://doi.org:10.3390/cancers11020180

71 Othman, S. A., Soon, C. F., Ma, N. L., Tee, K. S., Lim, G. P., Morsin, M., Ahmad, M. K., Abdulmaged, A. I. & Cheong, S. C. Alginate-gelatin bioink for bioprinting of hela spheroids in alginate-gelatin hexagon shaped scaffolds. *Polymer Bulletin* (2021). **78**, 6115-6135 https://doi.org:10.1007/s00289-020-03421-y

72 Mehta, G., Hsiao, A. Y., Ingram, M., Luker, G. D. & Takayama, S. Opportunities and challenges for use of tumor spheroids as models to test drug delivery and efficacy. *Journal of Controlled Release* (2012). **164**, 192-204 https://doi.org:10.1016/j.jconrel.2012.04.045

73 Zanoni, M., Piccinini, F., Arienti, C., Zamagni, A., Santi, S., Polico, R., Bevilacqua, A. & Tesei, A. 3D tumor spheroid models for in vitro therapeutic screening: a systematic approach to enhance the biological relevance of data obtained. *Scientific Reports* (2016). **6**, 19103 https://doi.org:10.1038/srep19103

74 Helmlinger, G., Yuan, F., Dellian, M. & Jain, R. K. Interstitial pH and pO2 gradients in solid tumors in vivo: High-resolution measurements reveal a lack of correlation. *Nature Medicine* (1997). **3**, 177-182 https://doi.org:10.1038/nm0297-177

75 Shiojima, I. & Walsh, K. Role of Akt Signaling in Vascular Homeostasis and Angiogenesis. *Circulation Research* (2002). **90**, 1243-1250 https://doi.org:10.1161/01.res.0000022200.71892.9f

76 Carmeliet, P. & Jain, R. K. Angiogenesis in cancer and other diseases. *Nature* (2000). **407**, 249-257 https://doi.org:10.1038/35025220

77 Nishida, N., Yano, H., Nishida, T., Kamura, T. & Kojiro, M. Angiogenesis in cancer. *Vascular Health and Risk Management* (2006). **2**, 213-219 https://doi.org:10.2147/vhrm.2006.2.3.213

78 Carmeliet, P. Mechanisms of angiogenesis and arteriogenesis. *Nature Medicine* (2000). **6**, 389-395 https://doi.org:10.1038/74651

79 Bergers, G. & Benjamin, L. E. Tumorigenesis and the angiogenic switch. *Nature Reviews Cancer* (2003). **3**, 401-410 https://doi.org:10.1038/nrc1093

80 Katayama, Y., Uchino, J., Chihara, Y., Tamiya, N., Kaneko, Y., Yamada, T. & Takayama, K. Tumor Neovascularization and Developments in Therapeutics. *Cancers* (2019). **11**, 316 https://doi.org:10.3390/cancers11030316

81 Wu, M., Frieboes, H. B., McDougall, S. R., Chaplain, M. A. J., Cristini, V. & Lowengrub, J. The effect of interstitial pressure on tumor growth: Coupling with the blood and lymphatic vascular systems. *Journal of Theoretical Biology* (2013). **320**, 131-151 https://doi.org:10.1016/j.jtbi.2012.11.031

82 Cantelmo, A. R., Conradi, L.-C., Brajic, A., Goveia, J., Kalucka, J., Pircher, A., Chaturvedi, P., Hol, J., Thienpont, B., Teuwen, L.-A., Schoors, S., Boeckx, B., Vriens, J., Kuchnio, A., Veys, K., Cruys, B., Finotto, L., Treps, L., Stav-Noraas, T. E., Bifari, F., Stapor, P., Decimo, I., Kampen, K., De Bock, K., Haraldsen, G., Schoonjans, L., Rabelink, T., Eelen, G., Ghesquière, B., Rehman, J., Lambrechts, D., Malik, A. B., Dewerchin, M. & Carmeliet, P. Inhibition of the Glycolytic Activator PFKFB3 in Endothelium Induces

Tumor Vessel Normalization, Impairs Metastasis, and Improves Chemotherapy. *Cancer Cell* (2016). **30**, 968-985 https://doi.org:10.1016/j.ccell.2016.10.006

83 Folkman, J. Clinical Applications of Research on Angiogenesis. *New England Journal of Medicine* (1995). **333**, 1757-1763 https://doi.org:10.1056/nejm199512283332608

84 Tumor Angiogenesis: A Possible Control Point in Tumor Growth. *Annals of Internal Medicine* (1975). **82**, 96-100 https://doi.org:10.7326/0003-4819-82-1-96

85 Xu, Y., Hu, Y., Liu, C., Yao, H., Liu, B. & Mi, S. A Novel Strategy for Creating Tissue-Engineered Biomimetic Blood Vessels Using 3D Bioprinting Technology. *Materials* (2018). **11**, 1581 https://doi.org:10.3390/ma11091581

86 Kolesky, D. B., Truby, R. L., Gladman, A. S., Busbee, T. A., Homan, K. A. & Lewis, J. A. 3D Bioprinting of Vascularized, Heterogeneous Cell-Laden Tissue Constructs. *Advanced Materials* (2014). **26**, 3124-3130 https://doi.org:10.1002/adma.201305506

87 Gioffredi, E., Boffito, M., Calzone, S., Giannitelli, S. M., Rainer, A., Trombetta, M., Mozetic, P. & Chiono, V. Pluronic F127 Hydrogel Characterization and Biofabrication in Cellularized Constructs for Tissue Engineering Applications. *Procedia CIRP* (2016). **49**, 125-132 https://doi.org:10.1016/j.procir.2015.11.001

88 Skylar-Scott, M. A., Uzel, S. G. M., Nam, L. L., Ahrens, J. H., Truby, R. L., Damaraju, S. & Lewis, J. A. Biomanufacturing of organ-specific tissues with high cellular density and embedded vascular channels. *Science Advances* (2019). **5**, eaaw2459 https://doi.org:10.1126/sciadv.aaw2459

89 Massa, S., Sakr, M. A., Seo, J., Bandaru, P., Arneri, A., Bersini, S., Zare-Eelanjegh, E., Jalilian, E., Cha, B.-H., Antona, S., Enrico, A., Gao, Y., Hassan, S., Acevedo, J. P., Dokmeci, M. R., Zhang, Y. S., Khademhosseini, A. & Shin, S. R. Bioprinted 3D vascularized tissue model for drug toxicity analysis. *Biomicrofluidics* (2017). **11**, 044109 https://doi.org:10.1063/1.4994708

90 Zhang, Y., Yu, W., Lv, G., Zhu, J., Wang, W., Ma, X. & Liu, X. The Artificial Organ (Elsevier, 2011) 99-114 https://doi.org:10.1016/b978-0-08-088504-9.00219-1.

91 Miller, J. S., Stevens, K. R., Yang, M. T., Baker, B. M., Nguyen, D.-H. T., Cohen, D. M., Toro, E., Chen, A. A., Galie, P. A., Yu, X., Chaturvedi, R., Bhatia, S. N. & Chen, C. S. Rapid casting of patterned vascular networks for perfusable engineered three-dimensional tissues. *Nature Materials* (2012). **11**, 768-774 https://doi.org:10.1038/nmat3357

92 Gauvin-Rossignol, G., Legros, P., Ruel, J., Fortin, M.-A. & Bégin-Drolet, A. Sugar glass fugitive ink loaded with calcium chloride for the rapid casting of alginate scaffold designs. *Heliyon* (2018). **4** https://doi.org:https://doi.org/10.1016/j.heliyon.2018.e00680

93 Gelber, M. K., Hurst, G., Comi, T. J. & Bhargava, R. Model-guided design and characterization of a high-precision 3D printing process for carbohydrate glass. *Additive Manufacturing* (2018). **22**, 38-50 https://doi.org:https://doi.org/10.1016/j.addma.2018.04.026

94 Ozbolat, V., Dey, M., Ayan, B. & Ozbolat, I. T. Extrusion-based printing of sacrificial Carbopol ink for fabrication of microfluidic devices. *Biofabrication* (2019). **11**, 034101 https://doi.org:10.1088/1758-5090/ab10ae

95 Gao, T., Gillispie, G. J., Copus, J. S., Pr, A. K., Seol, Y. J., Atala, A., Yoo, J. J. & Lee, S. J. Optimization of gelatin-alginate composite bioink printability using rheological parameters: a systematic approach. *Biofabrication* (2018). **10**, 034106 https://doi.org:10.1088/1758-5090/aacdc7

96 Paxton, N., Smolan, W., Böck, T., Melchels, F., Groll, J. & Jungst, T. Proposal to assess printability of bioinks for extrusion-based bioprinting and evaluation of rheological properties governing bioprintability. *Biofabrication* (2017). **9**, 044107 https://doi.org:10.1088/1758-5090/aa8dd8

97 Ouyang, L., Yao, R., Zhao, Y. & Sun, W. Effect of bioink properties on printability and cell viability for 3D bioplotting of embryonic stem cells. *Biofabrication* (2016). **8**, 035020 https://doi.org:10.1088/1758-5090/8/3/035020

98 Mouser, V. H. M., Melchels, F. P. W., Visser, J., Dhert, W. J. A., Gawlitta, D. & Malda, J. Yield stress determines bioprintability of hydrogels based on gelatin-

methacryloyl and gellan gum for cartilage bioprinting. *Biofabrication* (2016). **8**, 035003 https://doi.org:10.1088/1758-5090/8/3/035003

99 He, Y., Yang, F., Zhao, H., Gao, Q., Xia, B. & Fu, J. Research on the printability of hydrogels in 3D bioprinting. *Scientific Reports* (2016). **6**, 29977 https://doi.org:10.1038/srep29977

100 Kyle, S., Jessop, Z. M., Al-Sabah, A. & Whitaker, I. S. 'Printability' of Candidate Biomaterials for Extrusion Based 3D Printing: State-of-the-Art. *Advanced Healthcare Materials* (2017). **6**, 1700264 https://doi.org:10.1002/adhm.201700264

101 Kolesky, D. B., Homan, K. A., Skylar-Scott, M. A. & Lewis, J. A. Three-dimensional bioprinting of thick vascularized tissues. *Proceedings of the National Academy of Sciences* (2016). **113**, 3179-3184 https://doi.org:doi:10.1073/pnas.1521342113

102 Lee, V. K., Guohao, D., Hongyan, Z. & Seung-Schik, Y. Generation of 3-D glioblastoma-vascular niche using 3-D bioprinting. (2015). https://doi.org:10.1109/nebec.2015.7117111

103 Neufeld, L., Yeini, E., Reisman, N., Shtilerman, Y., Ben-Shushan, D., Pozzi, S., Madi, A., Tiram, G., Eldar-Boock, A., Ferber, S., Grossman, R., Ram, Z. & Satchi-Fainaro, R. Microengineered perfusable 3D-bioprinted glioblastoma model for in vivo mimicry of tumor microenvironment. *Sci Adv* (2021). **7** https://doi.org:10.1126/sciadv.abi9119

104 Ozturk, M. S., Lee, V. K., Zou, H., Friedel, R. H., Intes, X. & Dai, G. High-resolution tomographic analysis of in vitro 3D glioblastoma tumor model under long-term drug treatment. *Science Advances* (2020). **6**, eaay7513 https://doi.org:doi:10.1126/sciadv.aay7513

105 Lee, V. K., Lanzi, A. M., Ngo, H., Yoo, S.-S., Vincent, P. A. & Dai, G. Generation of Multi-scale Vascular Network System Within 3D Hydrogel Using 3D Bio-printing Technology. *Cellular and Molecular Bioengineering* (2014). **7**, 460-472 https://doi.org:10.1007/s12195-014-0340-0

106 Meng, F., Meyer, C. M., Joung, D., Vallera, D. A., McAlpine, M. C. & Panoskaltsis-Mortari, A. 3D Bioprinted In Vitro Metastatic Models via Reconstruction of Tumor

Microenvironments. *Advanced Materials* (2019). **31**, 1806899 https://doi.org:10.1002/adma.201806899

107 Zirlik, K. & Duyster, J. Anti-Angiogenics: Current Situation and Future Perspectives. *Oncology Research and Treatment* (2018). **41**, 166-171 https://doi.org:10.1159/000488087

108 Liu, X., Fang, J., Huang, S., Wu, X., Xie, X., Wang, J., Liu, F., Zhang, M., Peng, Z. & Hu, N. Tumor-on-a-chip: from bioinspired design to biomedical application. *Microsystems & Nanoengineering* (2021). **7**, 50 https://doi.org:10.1038/s41378-021-00277-8

109 Trujillo-de Santiago, G., Flores-Garza, B. G., Tavares-Negrete, J. A., Lara-Mayorga, I. M., González-Gamboa, I., Zhang, Y. S., Rojas-Martínez, A., Ortiz-López, R. & Álvarez, M. M. The Tumor-on-Chip: Recent Advances in the Development of Microfluidic Systems to Recapitulate the Physiology of Solid Tumors. *Materials (Basel)* (2019). **12** https://doi.org:10.3390/ma12182945

110 Tsai, H.-F., Trubelja, A., Shen, A. Q. & Bao, G. Tumour-on-a-chip: microfluidic models of tumour morphology, growth and microenvironment. *Journal of The Royal Society Interface* (2017). **14**, 20170137 https://doi.org:10.1098/rsif.2017.0137

111 Carvalho, M. R., Barata, D., Teixeira, L. M., Giselbrecht, S., Reis, R. L., Oliveira, J. M., Truckenmüller, R. & Habibovic, P. Colorectal tumor-on-a-chip system: A 3D tool for precision onco-nanomedicine. *Science Advances* (2019). **5**, eaaw1317 https://doi.org:doi:10.1126/sciadv.aaw1317

112 Zou, H., Yue, W., Yu, W.-K., Liu, D., Fong, C.-C., Zhao, J. & Yang, M. Microfluidic Platform for Studying Chemotaxis of Adhesive Cells Revealed a Gradient-Dependent Migration and Acceleration of Cancer Stem Cells. *Analytical Chemistry* (2015). **87**, 7098-7108 https://doi.org:10.1021/acs.analchem.5b00873

113 Louis-Sylvestre, C., Clough, K., Asselain, B., Vilcoq, J. R., Salmon, R. J., Campana, F. & Fourquet, A. Axillary treatment in conservative management of operable breast cancer: dissection or radiotherapy? Results of a randomized study with 15 years of follow-

up. *Journal of clinical oncology* (2004). **22**, 97-101 https://doi.org:10.1200/JCO.2004.12.108

114 Schoppmann, S. F., Birner, P., Stöckl, J., Kalt, R., Ullrich, R., Caucig, C., Kriehuber, E., Nagy, K., Alitalo, K. & Kerjaschki, D. Tumor-associated macrophages express lymphatic endothelial growth factors and are related to peritumoral lymphangiogenesis. *Am J Pathol* (2002). **161**, 947-956 https://doi.org:10.1016/s0002-9440(10)64255-1

115 Kerjaschki, D. The crucial role of macrophages in lymphangiogenesis. *J Clin Invest* (2005). **115**, 2316-2319 https://doi.org:10.1172/jci26354

116 Riabov, V., Gudima, A., Wang, N., Mickley, A., Orekhov, A. & Kzhyshkowska, J. Role of tumor associated macrophages in tumor angiogenesis and lymphangiogenesis. *Front Physiol* (2014). **5**, 75 https://doi.org:10.3389/fphys.2014.00075

117 He, Y., Rajantie, I., Pajusola, K., Jeltsch, M., Holopainen, T., Yla-Herttuala, S., Harding, T., Jooss, K., Takahashi, T. & Alitalo, K. Vascular endothelial cell growth factor receptor 3-mediated activation of lymphatic endothelium is crucial for tumor cell entry and spread via lymphatic vessels. *Cancer Res* (2005). **65**, 4739-4746 https://doi.org:10.1158/0008-5472.Can-04-4576

118 Wirzenius, M., Tammela, T., Uutela, M., He, Y., Odorisio, T., Zambruno, G., Nagy, J. A., Dvorak, H. F., Ylä-Herttuala, S., Shibuya, M. & Alitalo, K. Distinct vascular endothelial growth factor signals for lymphatic vessel enlargement and sprouting. *The Journal of experimental medicine* (2007). **204**, 1431-1440 https://doi.org:10.1084/jem.20062642

119 Sato, T., Mori, S., Arai, Y. & Kodama, T. The Combination of Intralymphatic Chemotherapy with Ultrasound and Nano-/Microbubbles Is Efficient in the Treatment of Experimental Tumors in Mouse Lymph Nodes. *Ultrasound in Medicine & Biology* (2014). **40**, 1237-1249 https://doi.org:10.1016/j.ultrasmedbio.2013.12.012

120 Swartz, M. A. & Skobe, M. Lymphatic function, lymphangiogenesis, and cancer metastasis. *Microscopy Research and Technique* (2001). **55**, 92-99 https://doi.org:https://doi.org/10.1002/jemt.1160

121 Schneider, J., Pultar, M. & Holnthoner, W. Ex vivo engineering of blood and lymphatic microvascular networks. *Vascular biology (Bristol, England)* (2019). **1**, H17-H22 https://doi.org:10.1530/VB-19-0012

122 Helm, C.-L. E., Zisch, A. & Swartz, M. A. Engineered blood and lymphatic capillaries in 3-D VEGF-fibrin-collagen matrices with interstitial flow. *Biotechnology and Bioengineering* (2007). **96**, 167-176 https://doi.org:https://doi.org/10.1002/bit.21185

123 Knezevic, L., Schaupper, M., Mühleder, S., Schimek, K., Hasenberg, T., Marx, U., Priglinger, E., Redl, H. & Holnthoner, W. Engineering Blood and Lymphatic Microvascular Networks in Fibrin Matrices. *Frontiers in Bioengineering and Biotechnology* (2017). **5** https://doi.org:10.3389/fbioe.2017.00025

124 Liu, T., Liu, Q., Anaya, I., Huang, D., Kong, W., Mille, L. S. & Zhang, Y. S. Investigating lymphangiogenesis in a sacrificially bioprinted volumetric model of breast tumor tissue. *Methods* (2021). **190**, 72-79 https://doi.org:https://doi.org/10.1016/j.ymeth.2020.04.003

125 Cao, X., Ashfaq, R., Cheng, F., Maharjan, S., Li, J., Ying, G., Hassan, S., Xiao, H., Yue, K. & Zhang, Y. S. A Tumor-on-a-Chip System with Bioprinted Blood and Lymphatic Vessel Pair. *Advanced functional materials* (2019). **29**, 1807173 https://doi.org:10.1002/adfm.201807173

126 Fisher, B., Bauer, M., Wickerham, D. L., Redmond, C. K., Fisher, E. R., Cruz, A. B., Foster, R., Gardner, B., Lerner, H., Margolese, R., Poisson, R., Shibata, H., Volk, H. & Other Nsabp, I. Relation of number of positive axillary nodes to the prognosis of patients with primary breast cancer. An NSABP update. *Cancer* (1983). **52**, 1551-1557 https://doi.org:https://doi.org/10.1002/1097-0142(19831101)52:9

127 Yang, J., Lu, Z., Li, L., Li, Y., Tan, Y., Zhang, D. & Wang, A. Relationship of lymphovascular invasion with lymph node metastasis and prognosis in superficial esophageal carcinoma: systematic review and meta-analysis. *BMC Cancer* (2020). **20**, 176 https://doi.org:s12885-020-6656-3

128 Alitalo, A. & Detmar, M. Interaction of tumor cells and lymphatic vessels in cancer progression. *Oncogene* (2012). **31**, 4499-4508 https://doi.org:10.1038/onc.2011.602

129 Xie, Y., Bagby, T. R., Cohen, M. S. & Forrest, M. L. Drug delivery to the lymphatic system: importance in future cancer diagnosis and therapies. *Expert Opinion on Drug Delivery* (2009). **6**, 785-792 https://doi.org:10.1517/17425240903085128

130 Padera, T. P., Meijer, E. F. J. & Munn, L. L. The Lymphatic System in Disease Processes and Cancer Progression. *Annual review of biomedical engineering* (2016). **18**, 125-158 https://doi.org:10.1146/annurev-bioeng-112315-031200

131 Karaman, S. & Detmar, M. Mechanisms of lymphatic metastasis. *The Journal of clinical investigation* (2014). **124**, 922-928 https://doi.org:10.1172/JCI71606

132 Dunn, G. P., Old, L. J. & Schreiber, R. D. The Three Es of Cancer Immunoediting. *Annual Review of Immunology* (2004). **22**, 329-360 https://doi.org:10.1146/annurev.immunol.22.012703.104803

133 Gonzalez, H., Hagerling, C. & Werb, Z. Roles of the immune system in cancer: from tumor initiation to metastatic progression. *Genes & development* (2018). **32**, 1267-1284 https://doi.org:10.1101/gad.314617.118

134 Gonzalez, H., Hagerling, C. & Werb, Z. Roles of the immune system in cancer: from tumor initiation to metastatic progression. *Genes & development* (2018). **32**, 1267-1284 https://doi.org:10.1101/gad.314617.118

135 Xiong, S., Dong, L. & Cheng, L. Neutrophils in cancer carcinogenesis and metastasis. *Journal of Hematology & Oncology* (2021). **14**, 173 https://doi.org:10.1186/s13045-021-01187-y

136 Kuang, D. M., Zhao, Q., Wu, Y., Peng, C., Wang, J., Xu, Z., Yin, X. Y. & Zheng, L. Peritumoral neutrophils link inflammatory response to disease progression by fostering angiogenesis in hepatocellular carcinoma. *J Hepatol* (2011). **54**, 948-955 https://doi.org:10.1016/j.jhep.2010.08.041

137 Ardi, V. C., Kupriyanova, T. A., Deryugina, E. I. & Quigley, J. P. Human neutrophils uniquely release TIMP-free MMP-9 to provide a potent catalytic stimulator of angiogenesis. *Proceedings of the National Academy of Sciences* (2007). **104**, 20262-20267 https://doi.org:doi:10.1073/pnas.0706438104

138 Hu, Y., He, M. Y., Zhu, L. F., Yang, C. C., Zhou, M. L., Wang, Q., Zhang, W., Zheng, Y. Y., Wang, D. M., Xu, Z. Q., Wu, Y. N. & Liu, L. K. Tumor-associated macrophages correlate with the clinicopathological features and poor outcomes via inducing epithelial to mesenchymal transition in oral squamous cell carcinoma. *J Exp Clin Cancer Res* (2016). **35**, 12 https://doi.org:10.1186/s13046-015-0281-z

139 Arima, K., Komohara, Y., Bu, L., Tsukamoto, M., Itoyama, R., Miyake, K., Uchihara, T., Ogata, Y., Nakagawa, S., Okabe, H., Imai, K., Hashimoto, D., Chikamoto, A., Yamashita, Y. I., Baba, H. & Ishimoto, T. Downregulation of 15-hydroxyprostaglandin dehydrogenase by interleukin-1β from activated macrophages leads to poor prognosis in pancreatic cancer. *Cancer Sci* (2018). **109**, 462-470 https://doi.org:10.1111/cas.13467

140 Chen, Y., Song, Y., Du, W., Gong, L., Chang, H. & Zou, Z. Tumor-associated macrophages: an accomplice in solid tumor progression. *Journal of Biomedical Science* (2019). **26**, 78 https://doi.org:10.1186/s12929-019-0568-z

141 Paulus, P., Stanley, E. R., Schäfer, R., Abraham, D. & Aharinejad, S. Colony-stimulating factor-1 antibody reverses chemoresistance in human MCF-7 breast cancer xenografts. *Cancer Res* (2006). **66**, 4349-4356 https://doi.org:10.1158/0008-5472.Can-05-3523

142 Shiao, S. L., Ruffell, B., DeNardo, D. G., Faddegon, B. A., Park, C. C. & Coussens, L. M. TH2-Polarized CD4(+) T Cells and Macrophages Limit Efficacy of Radiotherapy. *Cancer Immunol Res* (2015). **3**, 518-525 https://doi.org:10.1158/2326-6066.Cir-14-0232

143 Grolman, J. M., Zhang, D., Smith, A. M., Moore, J. S. & Kilian, K. A. Rapid 3D Extrusion of Synthetic Tumor Microenvironments. *Advanced Materials* (2015). **27**, 5512-5517 https://doi.org:10.1002/adma.201501729

144 Heinrich, M. A., Bansal, R., Lammers, T., Zhang, Y. S., Michel Schiffelers, R. & Prakash, J. 3D-Bioprinted Mini-Brain: A Glioblastoma Model to Study Cellular Interactions and Therapeutics. *Advanced Materials* (2019). **31**, 1806590 https://doi.org:10.1002/adma.201806590

145 Jin, Z., Li, X., Zhang, X., DeSousa, P., Xu, T. & Wu, A. Engineering the fate and function of human T-Cells via 3D bioprinting. *Biofabrication* (2021). **13**, 035016 https://doi.org:10.1088/1758-5090/abd56b

146 Baker, B. M. & Chen, C. S. Deconstructing the third dimension – how 3D culture microenvironments alter cellular cues. *Journal of Cell Science* (2012). **125**, 3015-3024 https://doi.org:10.1242/jcs.079509

147 Jensen, C. & Teng, Y. Is It Time to Start Transitioning From 2D to 3D Cell Culture? *Frontiers in Molecular Biosciences* (2020). **7** https://doi.org:10.3389/fmolb.2020.00033

148 Imamura, Y., Mukohara, T., Shimono, Y., Funakoshi, Y., Chayahara, N., Toyoda, M., Kiyota, N., Takao, S., Kono, S., Nakatsura, T. & Minami, H. Comparison of 2D- and 3D-culture models as drug-testing platforms in breast cancer. *Oncology Reports* (2015). **33**, 1837-1843 https://doi.org:10.3892/or.2015.3767

149 Harunaga, J. S. & Yamada, K. M. Cell-matrix adhesions in 3D. *Matrix Biology* (2011). **30**, 363-368 https://doi.org:https://doi.org/10.1016/j.matbio.2011.06.001

150 Winkler, J., Abisoye-Ogunniyan, A., Metcalf, K. J. & Werb, Z. Concepts of extracellular matrix remodelling in tumour progression and metastasis. *Nature Communications* (2020). **11**, 5120 https://doi.org:10.1038/s41467-020-18794-x

151 Henke, E., Nandigama, R. & Ergün, S. Extracellular Matrix in the Tumor Microenvironment and Its Impact on Cancer Therapy. *Frontiers in Molecular Biosciences* (2020). **6** https://doi.org:10.3389/fmolb.2019.00160

152 Salmon, H. & Donnadieu, E. Within tumors, interactions between T cells and tumor cells are impeded by the extracellular matrix. *Oncoimmunology* (2012). **1**, 992-994 https://doi.org:10.4161/onci.20239

153 Salmon, H., Franciszkiewicz, K., Damotte, D., Dieu-Nosjean, M.-C., Validire, P., Trautmann, A., Mami-Chouaib, F. & Donnadieu, E. Matrix architecture defines the preferential localization and migration of T cells into the stroma of human lung tumors.

The Journal of clinical investigation (2012). **122**, 899-910 https://doi.org:10.1172/JCI45817

154 Xu, S., Xu, H., Wang, W., Li, S., Li, H., Li, T., Zhang, W., Yu, X. & Liu, L. The role of collagen in cancer: from bench to bedside. *Journal of Translational Medicine* (2019). **17** https://doi.org:10.1186/s12967-019-2058-1

155 Xi, G., Guo, W., Kang, D., Ma, J., Fu, F., Qiu, L., Zheng, L., He, J., Fang, N., Chen, J., Li, J., Zhuo, S., Liao, X., Tu, H., Li, L., Zhang, Q., Wang, C., Boppart, S. A. & Chen, J. Large-scale tumor-associated collagen signatures identify high-risk breast cancer patients. *Theranostics* (2021). **11**, 3229-3243 https://doi.org:10.7150/thno.55921

156 Provenzano, P. P., Eliceiri, K. W., Campbell, J. M., Inman, D. R., White, J. G. & Keely, P. J. Collagen reorganization at the tumor-stromal interface facilitates local invasion. *BMC Medicine* (2006). **4**, 38 https://doi.org:10.1186/1741-7015-4-38

157 Brett, E. A., Sauter, M. A., Machens, H.-G. & Duscher, D. Tumor-associated collagen signatures: pushing tumor boundaries. *Cancer & Metabolism* (2020). **8** https://doi.org:10.1186/s40170-020-00221-w

158 Conklin, M. W., Eickhoff, J. C., Riching, K. M., Pehlke, C. A., Eliceiri, K. W., Provenzano, P. P., Friedl, A. & Keely, P. J. Aligned collagen is a prognostic signature for survival in human breast carcinoma. *Am J Pathol* (2011). **178**, 1221-1232 https://doi.org:10.1016/j.ajpath.2010.11.076

159 Griffanti, G., Rezabeigi, E., Li, J., Murshed, M. & Nazhat, S. N. Rapid Biofabrication of Printable Dense Collagen Bioinks of Tunable Properties. *Advanced functional materials* (2020). **30**, 1903874 https://doi.org:https://doi.org/10.1002/adfm.201903874

160 Wyss, H. M. Rheology of soft materials. *Fluids, colloids and soft materials: An introduction to soft matter physics* (2016). 149-164 https://doi.org:10.1002/9781119220510.ch9

161 Kim, H., Jang, J., Park, J., Lee, K. P., Lee, S., Lee, D. M., Kim, K. H., Kim, H. K. & Cho, D. W. Shear-induced alignment of collagen fibrils using 3D cell printing for corneal

stroma tissue engineering. *Biofabrication* (2019). **11**, 035017 https://doi.org:10.1088/1758-5090/ab1a8b

162 Nerger, B. A., Brun, P. T. & Nelson, C. M. Microextrusion printing cell-laden networks of type I collagen with patterned fiber alignment and geometry. *Soft Matter* (2019). **15**, 5728-5738 https://doi.org:10.1039/c8sm02605j

163 Bao, G., Jiang, T., Ravanbakhsh, H., Reyes, A., Ma, Z., Strong, M., Wang, H., Kinsella, J. M., Li, J. & Mongeau, L. Triggered micropore-forming bioprinting of porous viscoelastic hydrogels. *Materials Horizons* (2020). **7**, 2336-2347 https://doi.org:10.1039/d0mh00813c

164 Monferrer, E., Martín-Vañó, S., Carretero, A., García-Lizarribar, A., Burgos-Panadero, R., Navarro, S., Samitier, J. & Noguera, R. A three-dimensional bioprinted model to evaluate the effect of stiffness on neuroblastoma cell cluster dynamics and behavior. *Scientific Reports* (2020). **10** https://doi.org:10.1038/s41598-020-62986-w

165 Monferrer, E., Sanegre, S., Martín-Vañó, S., García-Lizarribar, A., Burgos-Panadero, R., López-Carrasco, A., Navarro, S., Samitier, J. & Noguera, R. Digital Image Analysis Applied to Tumor Cell Proliferation, Aggressiveness, and Migration-Related Protein Synthesis in Neuroblastoma 3D Models. *International journal of molecular sciences* (2020). **21**, 8676 https://doi.org:10.3390/ijms21228676

166 Kuzucu, M., Vera, G., Beaumont, M., Fischer, S., Wei, P., Shastri, V. P. & Forget, A. Extrusion-Based 3D Bioprinting of Gradients of Stiffness, Cell Density, and Immobilized Peptide Using Thermogelling Hydrogels. *ACS Biomaterials Science & Engineering* (2021). **7**, 2192-2197 https://doi.org:10.1021/acsbiomaterials.1c00183

167 Freeman, F. E. & Kelly, D. J. Tuning Alginate Bioink Stiffness and Composition for Controlled Growth Factor Delivery and to Spatially Direct MSC Fate within Bioprinted Tissues. *Scientific Reports* (2017). **7**, 17042 https://doi.org:10.1038/s41598-017-17286-1

168 Crapo, P. M., Gilbert, T. W. & Badylak, S. F. An overview of tissue and whole organ decellularization processes. *Biomaterials* (2011). **32**, 3233-3243 https://doi.org:10.1016/j.biomaterials.2011.01.057

169 Hoshiba, T. Decellularized Extracellular Matrix for Cancer Research. *Materials (Basel)* (2019). **12** https://doi.org:10.3390/ma12081311

170 Gilbert, T. W., Sellaro, T. L. & Badylak, S. F. Decellularization of tissues and organs. *Biomaterials* (2006). **27**, 3675-3683 https://doi.org:https://doi.org/10.1016/j.biomaterials.2006.02.014

171 Mendibil, U., Ruiz-Hernandez, R., Retegi-Carrion, S., Garcia-Urquia, N., Olalde-Graells, B. & Abarrategi, A. Tissue-Specific Decellularization Methods: Rationale and Strategies to Achieve Regenerative Compounds. *International journal of molecular sciences* (2020). **21** https://doi.org:10.3390/ijms21155447

172 Kort-Mascort, J., Bao, G., Elkashty, O., Flores-Torres, S., Munguia-Lopez, J. G., Jiang, T., Ehrlicher, A. J., Mongeau, L., Tran, S. D. & Kinsella, J. M. Decellularized Extracellular Matrix Composite Hydrogel Bioinks for the Development of 3D Bioprinted Head and Neck in Vitro Tumor Models. *ACS Biomaterials Science & Engineering* (2021). **7**, 5288-5300 https://doi.org:10.1021/acsbiomaterials.1c00812

173 Badylak, S. F., Freytes, D. O. & Gilbert, T. W. Reprint of: Extracellular matrix as a biological scaffold material: Structure and function. *Acta Biomaterialia* (2015). **23**, S17-S26 https://doi.org:https://doi.org/10.1016/j.actbio.2015.07.016

174 Freytes, D. O., Martin, J., Velankar, S. S., Lee, A. S. & Badylak, S. F. Preparation and rheological characterization of a gel form of the porcine urinary bladder matrix. *Biomaterials* (2008). **29**, 1630-1637 https://doi.org:https://doi.org/10.1016/j.biomaterials.2007.12.014

175 Kort-Mascort, J., Flores-Torres, S., Peza Chavez, O., Jang, J., Pardo, L. A., Tran, S. D. & Kinsella, J. Decellularized ECM hydrogels: Prior Use Considerations, Applications, and Opportunities in Tissue Engineering and Biofabrication. *Biomaterials Science* (2023). https://doi.org:10.1039/d2bm01273a

176 Na, G. C., Butz, L. J. & Carroll, R. J. Mechanism of in vitro collagen fibril assembly. Kinetic and morphological studies. *J Biol Chem* (1986). **261**, 12290-12299

177 Saldin, L. T., Cramer, M. C., Velankar, S. S., White, L. J. & Badylak, S. F. Extracellular matrix hydrogels from decellularized tissues: Structure and function. *Acta Biomaterialia* (2017). **49**, 1-15 https://doi.org:10.1016/j.actbio.2016.11.068

178 Chen, Y., Xu, L., Li, W., Chen, W., He, Q., Zhang, X., Tang, J., Wang, Y., Liu, B. & Liu, J. 3D bioprinted tumor model with extracellular matrix enhanced bioinks for nanoparticle evaluation. *Biofabrication* (2022). **14** https://doi.org:10.1088/1758-5090/ac48e4

179 Skardal, A., Devarasetty, M., Kang, H.-W., Mead, I., Bishop, C., Shupe, T., Lee, S. J., Jackson, J., Yoo, J., Soker, S. & Atala, A. A hydrogel bioink toolkit for mimicking native tissue biochemical and mechanical properties in bioprinted tissue constructs. *Acta Biomaterialia* (2015). **25**, 24-34 https://doi.org:https://doi.org/10.1016/j.actbio.2015.07.030

180 Jang, J., Kim, T. G., Kim, B. S., Kim, S.-W., Kwon, S.-M. & Cho, D.-W. Tailoring mechanical properties of decellularized extracellular matrix bioink by vitamin B2-induced photo-crosslinking. *Acta Biomaterialia* (2016). **33**, 88-95 https://doi.org:https://doi.org/10.1016/j.actbio.2016.01.013

181 Northcott, J. M., Dean, I. S., Mouw, J. K. & Weaver, V. M. Feeling Stress: The Mechanics of Cancer Progression and Aggression. *Frontiers in Cell and Developmental Biology* (2018). **6** https://doi.org:10.3389/fcell.2018.00017

182 Plodinec, M., Loparic, M., Monnier, C. A., Obermann, E. C., Zanetti-Dallenbach, R., Oertle, P., Hyotyla, J. T., Aebi, U., Bentires-Alj, M., Lim, R. Y. H. & Schoenenberger, C.-A. The nanomechanical signature of breast cancer. *Nature Nanotechnology* (2012). **7**, 757-765 https://doi.org:10.1038/nnano.2012.167

183 Masuzaki, R., Tateishi, R., Yoshida, H., Sato, T., Ohki, T., Goto, T., Yoshida, H., Sato, S., Sugioka, Y., Ikeda, H., Shiina, S., Kawabe, T. & Omata, M. Assessing liver tumor stiffness by transient elastography. *Hepatology International* (2007). **1**, 394-397 https://doi.org:10.1007/s12072-007-9012-7

184 Kawano, S., Kojima, M., Higuchi, Y., Sugimoto, M., Ikeda, K., Sakuyama, N., Takahashi, S., Hayashi, R., Ochiai, A. & Saito, N. Assessment of elasticity of colorectal

cancer tissue, clinical utility, pathological and phenotypical relevance. *Cancer Science* (2015). **106**, 1232-1239 https://doi.org:10.1111/cas.12720

185 Nia, H. T., Liu, H., Seano, G., Datta, M., Jones, D., Rahbari, N., Incio, J., Chauhan, V. P., Jung, K., Martin, J. D., Askoxylakis, V., Padera, T. P., Fukumura, D., Boucher, Y., Hornicek, F. J., Grodzinsky, A. J., Baish, J. W., Munn, L. L. & Jain, R. K. Solid stress and elastic energy as measures of tumour mechanopathology. *Nature Biomedical Engineering* (2017). **1**, 0004 https://doi.org:10.1038/s41551-016-0004

186 Pradhan, S. & Slater, J. H. Tunable hydrogels for controlling phenotypic cancer cell states to model breast cancer dormancy and reactivation. *Biomaterials* (2019). **215**, 119177 https://doi.org:10.1016/j.biomaterials.2019.04.022

187 Deng, Z., Wang, H., Liu, J., Deng, Y. & Zhang, N. Comprehensive understanding of anchorage-independent survival and its implication in cancer metastasis. *Cell Death & Disease* (2021). **12** https://doi.org:10.1038/s41419-021-03890-7

188 Huang, J., Zhang, L., Wan, D., Zhou, L., Zheng, S., Lin, S. & Qiao, Y. Extracellular matrix and its therapeutic potential for cancer treatment. *Signal Transduction and Targeted Therapy* (2021). **6** https://doi.org:10.1038/s41392-021-00544-0

189 Harisi, R. & Jeney, A. Extracellular matrix as target for antitumor therapy. *OncoTargets and therapy* (2015). **8**, 1387-1398 https://doi.org:10.2147/OTT.S48883

190 Huang, J., Zhang, L., Wan, D., Zhou, L., Zheng, S., Lin, S. & Qiao, Y. Extracellular matrix and its therapeutic potential for cancer treatment. *Signal Transduction and Targeted Therapy* (2021). **6**, 153 https://doi.org:10.1038/s41392-021-00544-0

191 Tian, M., Li, Y., Liu, W., Jin, L., Jiang, X., Wang, X., Ding, Z., Peng, Y., Zhou, J., Fan, J., Cao, Y., Wang, W. & Shi, Y. The nanomechanical signature of liver cancer tissues and its molecular origin. *Nanoscale* (2015). **7**, 12998-13010 https://doi.org:10.1039/c5nr02192h

192 Ciasca, G., Sassun, T. E., Minelli, E., Antonelli, M., Papi, M., Santoro, A., Giangaspero, F., Delfini, R. & De Spirito, M. Nano-mechanical signature of brain tumours. *Nanoscale* (2016). **8**, 19629-19643 https://doi.org:10.1039/c6nr06840e

193 Thompson, P. A., Rosner, G. L., Matthay, K. K., Moore, T. B., Bomgaars, L. R., Ellis, K. J., Renbarger, J. & Berg, S. L. Impact of body composition on pharmacokinetics of doxorubicin in children: a Glaser Pediatric Research Network study. *Cancer Chemotherapy and Pharmacology* (2008). **64**, 243 https://doi.org:10.1007/s00280-008-0854-z

194 Mentoor, I., Engelbrecht, A.-M., van Jaarsveld, P. J. & Nell, T. Chemoresistance: Intricate Interplay Between Breast Tumor Cells and Adipocytes in the Tumor Microenvironment. *Frontiers in Endocrinology* (2018). **9** https://doi.org:10.3389/fendo.2018.00758

195 Nieman, K. M., Romero, I. L., Van Houten, B. & Lengyel, E. Adipose tissue and adipocytes support tumorigenesis and metastasis. *Biochimica et Biophysica Acta (BBA) - Molecular and Cell Biology of Lipids* (2013). **1831**, 1533-1541 https://doi.org:https://doi.org/10.1016/j.bbalip.2013.02.010

196 Dirat, B., Bochet, L., Dabek, M., Daviaud, D., Dauvillier, S., Majed, B., Wang, Y. Y., Meulle, A., Salles, B., Le Gonidec, S., Garrido, I., Escourrou, G., Valet, P. & Muller, C. Cancer-Associated Adipocytes Exhibit an Activated Phenotype and Contribute to Breast Cancer Invasion. *Cancer Research* (2011). **71**, 2455-2465 https://doi.org:10.1158/0008-5472.Can-10-3323

197 Wu, Q., Li, B., Li, Z., Li, J., Sun, S. & Sun, S. Cancer-associated adipocytes: key players in breast cancer progression. *Journal of Hematology & Oncology* (2019). **12** https://doi.org:10.1186/s13045-019-0778-6

198 Wang, Y., Shi, W., Kuss, M., Mirza, S., Qi, D., Krasnoslobodtsev, A., Zeng, J., Band, H., Band, V. & Duan, B. 3D Bioprinting of Breast Cancer Models for Drug Resistance Study. *ACS Biomaterials Science & Engineering* (2018). **4**, 4401-4411 https://doi.org:10.1021/acsbiomaterials.8b01277

199 Jiang, T., Munguia-Lopez, J. G., Flores-Torres, S., Grant, J., Vijayakumar, S., Leon-Rodriguez, A. D. & Kinsella, J. M. Directing the Self-assembly of Tumour Spheroids by Bioprinting Cellular Heterogeneous Models within Alginate/Gelatin Hydrogels. *Scientific Reports* (2017). **7**, 4575 https://doi.org:10.1038/s41598-017-04691-9

200 Hanahan, D. & Lisa. Accessories to the Crime: Functions of Cells Recruited to the Tumor Microenvironment. *Cancer Cell* (2012). **21**, 309-322 https://doi.org:10.1016/j.ccr.2012.02.022

201 Pathria, P., Louis, T. L. & Varner, J. A. Targeting Tumor-Associated Macrophages in Cancer. *Trends Immunol* (2019). **40**, 310-327 https://doi.org:10.1016/j.it.2019.02.003

202 Sun, X.-x. & Yu, Q. Intra-tumor heterogeneity of cancer cells and its implications for cancer treatment. *Acta Pharmacologica Sinica* (2015). **36**, 1219-1227 https://doi.org:10.1038/aps.2015.92

203 Cairns, J. Mutation selection and the natural history of cancer. *Nature* (1975). **255**, 197-200 https://doi.org:10.1038/255197a0

204 Brock, A., Chang, H. & Huang, S. Non-genetic heterogeneity — a mutation-independent driving force for the somatic evolution of tumours. *Nature Reviews Genetics* (2009). **10**, 336-342 https://doi.org:10.1038/nrg2556

205 Komohara, Y. & Takeya, M. CAFs and TAMs: maestros of the tumour microenvironment. *The Journal of Pathology* (2017). **241**, 313-315 https://doi.org:https://doi.org/10.1002/path.4824

206 Larionova, I., Cherdyntseva, N., Liu, T., Patysheva, M., Rakina, M. & Kzhyshkowska, J. Interaction of tumor-associated macrophages and cancer chemotherapy. *Oncoimmunology* (2019). **8**, 1596004 https://doi.org:10.1080/2162402x.2019.1596004

207 Jena, B. C., Das, C. K., Bharadwaj, D. & Mandal, M. Cancer associated fibroblast mediated chemoresistance: A paradigm shift in understanding the mechanism of tumor progression. *Biochimica et Biophysica Acta (BBA) - Reviews on Cancer* (2020). **1874**, 188416 https://doi.org:https://doi.org/10.1016/j.bbcan.2020.188416

208 Qiu, G.-Z., Jin, M.-Z., Dai, J.-X., Sun, W., Feng, J.-H. & Jin, W.-L. Reprogramming of the Tumor in the Hypoxic Niche: The Emerging Concept and Associated Therapeutic

Strategies. *Trends in Pharmacological Sciences* (2017). **38**, 669-686 https://doi.org:10.1016/j.tips.2017.05.002

209 Emami Nejad, A., Najafgholian, S., Rostami, A., Sistani, A., Shojaeifar, S., Esparvarinha, M., Nedaeinia, R., Haghjooy Javanmard, S., Taherian, M., Ahmadlou, M., Salehi, R., Sadeghi, B. & Manian, M. The role of hypoxia in the tumor microenvironment and development of cancer stem cell: a novel approach to developing treatment. *Cancer Cell International* (2021). **21**, 62 https://doi.org:10.1186/s12935-020-01719-5

210 Conforti, L., Petrovic, M., Mohammad, D., Lee, S., Ma, Q., Barone, S. & Filipovich, A. H. Hypoxia Regulates Expression and Activity of Kv1.3 Channels in T Lymphocytes: A Possible Role in T Cell Proliferation. *The Journal of Immunology* (2003). **170**, 695-702 https://doi.org:10.4049/jimmunol.170.2.695

211 Lee, C. T., Mace, T. & Repasky, E. A. Hypoxia-driven immunosuppression: a new reason to use thermal therapy in the treatment of cancer? *Int J Hyperthermia* (2010). **26**, 232-246 https://doi.org:10.3109/02656731003601745

212 Stylianopoulos, T., Martin, J. D., Chauhan, V. P., Jain, S. R., Diop-Frimpong, B., Bardeesy, N., Smith, B. L., Ferrone, C. R., Hornicek, F. J., Boucher, Y., Munn, L. L. & Jain, R. K. Causes, consequences, and remedies for growth-induced solid stress in murine and human tumors. *Proceedings of the National Academy of Sciences* (2012). **109**, 15101-15108 https://doi.org:doi:10.1073/pnas.1213353109

213 Patel, A. P., Tirosh, I., Trombetta, J. J., Shalek, A. K., Gillespie, S. M., Wakimoto, H., Cahill, D. P., Nahed, B. V., Curry, W. T., Martuza, R. L., Louis, D. N., Rozenblatt-Rosen, O., Suvà, M. L., Regev, A. & Bernstein, B. E. Single-cell RNA-seq highlights intratumoral heterogeneity in primary glioblastoma. *Science* (2014). **344**, 1396-1401 https://doi.org:10.1126/science.1254257

214 Valastyan, S. & Weinberg, R. A. Tumor metastasis: molecular insights and evolving paradigms. *Cell* (2011). **147**, 275-292 https://doi.org:10.1016/j.cell.2011.09.024

215 Mohammadi, H. & Sahai, E. Mechanisms and impact of altered tumour mechanics. *Nat Cell Biol* (2018). **20**, 766-774 https://doi.org:10.1038/s41556-018-0131-2

216 Tang, X., Hou, Y., Yang, G., Wang, X., Tang, S., Du, Y. E., Yang, L., Yu, T., Zhang, H., Zhou, M., Wen, S., Xu, L. & Liu, M. Stromal miR-200s contribute to breast cancer cell invasion through CAF activation and ECM remodeling. *Cell Death Differ* (2016). **23**, 132-145 https://doi.org:10.1038/cdd.2015.78

217 DeNardo, D. G., Brennan, D. J., Rexhepaj, E., Ruffell, B., Shiao, S. L., Madden, S. F., Gallagher, W. M., Wadhwani, N., Keil, S. D., Junaid, S. A., Rugo, H. S., Hwang, E. S., Jirström, K., West, B. L. & Coussens, L. M. Leukocyte complexity predicts breast cancer survival and functionally regulates response to chemotherapy. *Cancer Discov* (2011). **1**, 54-67 https://doi.org:10.1158/2159-8274.Cd-10-0028

218 van der Woude, L. L., Gorris, M. A. J., Halilovic, A., Figdor, C. G. & de Vries, I. J. M. Migrating into the Tumor: a Roadmap for T Cells. *Trends in Cancer* (2017). **3**, 797-808 https://doi.org:https://doi.org/10.1016/j.trecan.2017.09.006

219 Jiang, Y., Li, Y. & Zhu, B. T-cell exhaustion in the tumor microenvironment. *Cell Death & Disease* (2015). **6**, e1792-e1792 https://doi.org:10.1038/cddis.2015.162

220 Han, Y., Liu, D. & Li, L. PD-1/PD-L1 pathway: current researches in cancer. *Am J Cancer Res* (2020). **10**, 727-742

221 Grywalska, E., Pasiarski, M., Góźdź, S. & Roliński, J. Immune-checkpoint inhibitors for combating T-cell dysfunction in cancer. *OncoTargets and therapy* (2018). **11**, 6505-6524 https://doi.org:10.2147/ott.S150817

222 Dai, H., Wang, Y., Lu, X. & Han, W. Chimeric Antigen Receptors Modified T-Cells for Cancer Therapy. *J Natl Cancer Inst* (2016). **108** https://doi.org:10.1093/jnci/djv439

223 Sterner, R. C. & Sterner, R. M. CAR-T cell therapy: current limitations and potential strategies. *Blood Cancer Journal* (2021). **11**, 69 https://doi.org:10.1038/s41408-021-00459-7

224 Drake, C. G., Jaffee, E. & Pardoll, D. M. in *Advances in Immunology* Mechanisms of Immune Evasion by Tumors Vol. 90 (Academic Press, 2006) 51-81 https://doi.org:https://doi.org/10.1016/S0065-2776(06)90002-9.

225 Nagaraj, S., Gupta, K., Pisarev, V., Kinarsky, L., Sherman, S., Kang, L., Herber, D. L., Schneck, J. & Gabrilovich, D. I. Altered recognition of antigen is a mechanism of CD8+ T cell tolerance in cancer. *Nature Medicine* (2007). **13**, 828-835 https://doi.org:10.1038/nm1609

226 Marincola, F. M., Jaffee, E. M., Hicklin, D. J. & Ferrone, S. in *Advances in Immunology* Escape of Human Solid Tumors from T–Cell Recognition: Molecular Mechanisms and Functional Significance Vol. 74 (Academic Press, 1999) (ed Frank J. Dixon) 181-273 https://doi.org:https://doi.org/10.1016/S0065-2776(08)60911-6.

227 Zong, J., Keskinov, A. A., Shurin, G. V. & Shurin, M. R. Tumor-derived factors modulating dendritic cell function. *Cancer Immunology, Immunotherapy* (2016). **65**, 821-833 https://doi.org:10.1007/s00262-016-1820-y

228 Bandola-Simon, J. & Roche, P. A. Dysfunction of antigen processing and presentation by dendritic cells in cancer. *Molecular immunology* (2019). **113**, 31-37 https://doi.org:10.1016/j.molimm.2018.03.025

229 Driessens, G., Kline, J. & Gajewski, T. F. Costimulatory and coinhibitory receptors in anti-tumor immunity. *Immunological reviews* (2009). **229**, 126-144 https://doi.org:10.1111/j.1600-065X.2009.00771.x

230 Yuen, G. J., Demissie, E. & Pillai, S. B Lymphocytes and Cancer: A Love–Hate Relationship. *Trends in Cancer* (2016). **2**, 747-757 https://doi.org:10.1016/j.trecan.2016.10.010

231 Salmon, H., Franciszkiewicz, K., Damotte, D., Dieu-Nosjean, M. C., Validire, P., Trautmann, A., Mami-Chouaib, F. & Donnadieu, E. Matrix architecture defines the preferential localization and migration of T cells into the stroma of human lung tumors. *J Clin Invest* (2012). **122**, 899-910 https://doi.org:10.1172/jci45817

232 Hartmann, N., Giese, N. A., Giese, T., Poschke, I., Offringa, R., Werner, J. & Ryschich, E. Prevailing role of contact guidance in intrastromal T-cell trapping in human pancreatic cancer. *Clin Cancer Res* (2014). **20**, 3422-3433 https://doi.org:10.1158/1078-0432.Ccr-13-2972

233 Clark, C. E., Hingorani, S. R., Mick, R., Combs, C., Tuveson, D. A. & Vonderheide, R. H. Dynamics of the immune reaction to pancreatic cancer from inception to invasion. *Cancer Res* (2007). **67**, 9518-9527 https://doi.org:10.1158/0008-5472.Can-07-0175

234 Bonaventura, P., Shekarian, T., Alcazer, V., Valladeau-Guilemond, J., Valsesia-Wittmann, S., Amigorena, S., Caux, C. & Depil, S. Cold Tumors: A Therapeutic Challenge for Immunotherapy. *Front Immunol* (2019). **10**, 168 https://doi.org:10.3389/fimmu.2019.00168

235 Talkenberger, K., Cavalcanti-Adam, E. A., Voss-Böhme, A. & Deutsch, A. Amoeboid-mesenchymal migration plasticity promotes invasion only in complex heterogeneous microenvironments. *Scientific Reports* (2017). **7**, 9237 https://doi.org:10.1038/s41598-017-09300-3

236 Krummel, M. F., Friedman, R. S. & Jacobelli, J. Modes and mechanisms of T cell motility: roles for confinement and Myosin-IIA. *Current Opinion in Cell Biology* (2014). **30**, 9-16 https://doi.org:https://doi.org/10.1016/j.ceb.2014.05.003

237 Hughes, P., Marshall, D., Reid, Y., Parkes, H. & Gelber, C. The costs of using unauthenticated, over-passaged cell lines: how much more data do we need? *BioTechniques* (2007). **43**, 575-586 https://doi.org:10.2144/000112598

238 Vlachogiannis, G., Hedayat, S., Vatsiou, A., Jamin, Y., Fernández-Mateos, J., Khan, K., Lampis, A., Eason, K., Huntingford, I., Burke, R., Rata, M., Koh, D. M., Tunariu, N., Collins, D., Hulkki-Wilson, S., Ragulan, C., Spiteri, I., Moorcraft, S. Y., Chau, I., Rao, S., Watkins, D., Fotiadis, N., Bali, M., Darvish-Damavandi, M., Lote, H., Eltahir, Z., Smyth, E. C., Begum, R., Clarke, P. A., Hahne, J. C., Dowsett, M., de Bono, J., Workman, P., Sadanandam, A., Fassan, M., Sansom, O. J., Eccles, S., Starling, N., Braconi, C., Sottoriva, A., Robinson, S. P., Cunningham, D. & Valeri, N. Patient-derived organoids model treatment response of metastatic gastrointestinal cancers. *Science* (2018). **359**, 920-926 https://doi.org:10.1126/science.aao2774

239 Pinto, M. L., Rios, E., Silva, A. C., Neves, S. C., Caires, H. R., Pinto, A. T., Durães, C., Carvalho, F. A., Cardoso, A. P., Santos, N. C., Barrias, C. C., Nascimento, D. S., Pinto-do-Ó, P., Barbosa, M. A., Carneiro, F. & Oliveira, M. J. Decellularized human colorectal

cancer matrices polarize macrophages towards an anti-inflammatory phenotype promoting cancer cell invasion via CCL18. *Biomaterials* (2017). **124**, 211-224 https://doi.org:10.1016/j.biomaterials.2017.02.004

240 Al-Ani, A., Toms, D., Kondro, D., Thundathil, J., Yu, Y. & Ungrin, M. Oxygenation in cell culture: Critical parameters for reproducibility are routinely not reported. *PLOS ONE* (2018). **13**, e0204269 https://doi.org:10.1371/journal.pone.0204269

241 Strese, S., Fryknäs, M., Larsson, R. & Gullbo, J. Effects of hypoxia on human cancer cell line chemosensitivity. *BMC Cancer* (2013). **13**, 331 https://doi.org:10.1186/1471-2407-13-331

242 Vaupel, P., Kallinowski, F. & Okunieff, P. Blood flow, oxygen and nutrient supply, and metabolic microenvironment of human tumors: a review. *Cancer Res* (1989). **49**, 6449-6465

243 Höckel, M. & Vaupel, P. Tumor hypoxia: definitions and current clinical, biologic, and molecular aspects. *J Natl Cancer Inst* (2001). **93**, 266-276 https://doi.org:10.1093/jnci/93.4.266

244 Vander Heiden, M. G. & DeBerardinis, R. J. Understanding the Intersections between Metabolism and Cancer Biology. *Cell* (2017). **168**, 657-669 https://doi.org:10.1016/j.cell.2016.12.039

245 Muz, B., De La Puente, P., Azab, F. & Azab, A. K. The role of hypoxia in cancer progression, angiogenesis, metastasis, and resistance to therapy. *Hypoxia* (2015). 83 https://doi.org:10.2147/hp.s93413

246 Heldin, C.-H., Rubin, K., Pietras, K. & Östman, A. High interstitial fluid pressure — an obstacle in cancer therapy. *Nature Reviews Cancer* (2004). **4**, 806-813 https://doi.org:10.1038/nrc1456

247 Yu, T., Liu, K., Wu, Y., Fan, J., Chen, J., Li, C., Zhu, G., Wang, Z. & Li, L. High interstitial fluid pressure promotes tumor cell proliferation and invasion in oral squamous cell carcinoma. *International Journal of Molecular Medicine* (2013). **32**, 1093-1100 https://doi.org:10.3892/ijmm.2013.1496

248 Ou, Z., Dou, X., Tang, N. & Liu, G. Pressure increases PD-L1 expression in A549 lung adenocarcinoma cells and causes resistance to anti-ROR1 CAR T cell-mediated cytotoxicity. *Scientific Reports* (2022). **12** https://doi.org:10.1038/s41598-022-10905-6

249 Munson, J. & Shieh, A. Interstitial fluid flow in cancer: implications for disease progression and treatment. *Cancer Management and Research* (2014). 317 https://doi.org:10.2147/cmar.s65444

250 Boucher, Y. & Jain, R. K. Microvascular pressure is the principal driving force for interstitial hypertension in solid tumors: implications for vascular collapse. *Cancer Res* (1992). **52**, 5110-5114

251 Ribatti, D., Annese, T., Ruggieri, S., Tamma, R. & Crivellato, E. Limitations of Anti-Angiogenic Treatment of Tumors. *Transl Oncol* (2019). **12**, 981-986 https://doi.org:10.1016/j.tranon.2019.04.022

252 Ackermann, T. & Tardito, S. Cell Culture Medium Formulation and Its Implications in Cancer Metabolism. *Trends in Cancer* (2019). **5**, 329-332 https://doi.org:10.1016/j.trecan.2019.05.004

253 Chow, M. T. & Luster, A. D. Chemokines in Cancer. *Cancer Immunology Research* (2014). **2**, 1125-1131 https://doi.org:10.1158/2326-6066.cir-14-0160

254 Witsch, E., Sela, M. & Yarden, Y. Roles for Growth Factors in Cancer Progression. *Physiology* (2010). **25**, 85-101 https://doi.org:10.1152/physiol.00045.2009

255 Jones, V. S., Huang, R.-Y., Chen, L.-P., Chen, Z.-S., Fu, L. & Huang, R.-P. Cytokines in cancer drug resistance: Cues to new therapeutic strategies. *Biochimica et Biophysica Acta (BBA) - Reviews on Cancer* (2016). **1865**, 255-265 https://doi.org:https://doi.org/10.1016/j.bbcan.2016.03.005

256 Tan, C., Hu, W., He, Y., Zhang, Y., Zhang, G., Xu, Y. & Tang, J. Cytokine-mediated therapeutic resistance in breast cancer. *Cytokine* (2018). **108**, 151-159 https://doi.org:https://doi.org/10.1016/j.cyto.2018.03.020

257 Rodier, F., Coppé, J.-P., Patil, C. K., Hoeijmakers, W. A. M., Muñoz, D. P., Raza, S. R., Freund, A., Campeau, E., Davalos, A. R. & Campisi, J. Persistent DNA damage

signalling triggers senescence-associated inflammatory cytokine secretion. *Nature Cell Biology* (2009). **11**, 973-979 https://doi.org:10.1038/ncb1909

258 Kumari, N., Dwarakanath, B. S., Das, A. & Bhatt, A. N. Role of interleukin-6 in cancer progression and therapeutic resistance. *Tumor Biology* (2016). **37**, 11553-11572 https://doi.org:10.1007/s13277-016-5098-7

259 Xu, J., Lamouille, S. & Derynck, R. TGF-β-induced epithelial to mesenchymal transition. *Cell Research* (2009). **19**, 156-172 https://doi.org:10.1038/cr.2009.5

260 Medici, D., Hay, E. D. & Goodenough, D. A. Cooperation between Snail and LEF-1 Transcription Factors Is Essential for TGF-β1-induced Epithelial-Mesenchymal Transition. *Molecular Biology of the Cell* (2006). **17**, 1871-1879 https://doi.org:10.1091/mbc.e05-08-0767

261 Russo, J. & Russo, I. H. The role of estrogen in the initiation of breast cancer. *J Steroid Biochem Mol Biol* (2006). **102**, 89-96 https://doi.org:10.1016/j.jsbmb.2006.09.004

262 Han, R., Gu, S., Zhang, Y., Luo, A., Jing, X., Zhao, L., Zhao, X. & Zhang, L. Estrogen promotes progression of hormone-dependent breast cancer through CCL2-CCR2 axis by upregulation of Twist via PI3K/AKT/NF-κB signaling. *Scientific Reports* (2018). **8**, 9575 https://doi.org:10.1038/s41598-018-27810-6

263 Trabert, B., Sherman, M. E., Kannan, N. & Stanczyk, F. Z. Progesterone and Breast Cancer. *Endocr Rev* (2020). **41**, 320-344 https://doi.org:10.1210/endrev/bnz001

264 Lumachi, F., Santeufemia, D. A. & Basso, S. M. Current medical treatment of estrogen receptor-positive breast cancer. *World J Biol Chem* (2015). **6**, 231-239 https://doi.org:10.4331/wjbc.v6.i3.231

265 Lumachi, F., Brunello, A., Maruzzo, M., Basso, U. & Basso, S. M. Treatment of estrogen receptor-positive breast cancer. *Curr Med Chem* (2013). **20**, 596-604 https://doi.org:10.2174/092986713804999303

266 Auchus, R. J. & Sharifi, N. Sex Hormones and Prostate Cancer. *Annual Review of Medicine* (2020). **71**, 33-45 https://doi.org:10.1146/annurev-med-051418-060357

267 Hogenson, T. L., Xie, H., Phillips, W. J., Toruner, M. D., Li, J. J., Horn, I. P., Kennedy, D. J., Almada, L. L., Marks, D. L., Carr, R. M., Toruner, M., Sigafoos, A. N., Koenig-Kappes, A. N., Olson, R. L. O., Tolosa, E. J., Zhang, C., Li, H., Doles, J. D., Bleeker, J., Barrett, M. T., Boyum, J. H., Kipp, B. R., Mahipal, A., Hubbard, J. M., Scheffler Hanson, T. J., Petersen, G. M., Dasari, S., Oberg, A. L., Truty, M. J., Graham, R. P., Levy, M. J., Zhu, M., Billadeau, D. D., Adjei, A. A., Dusetti, N., Iovanna, J. L., Bekaii-Saab, T. S., Ma, W. W. & Fernandez-Zapico, M. E. Culture media composition influences patient-derived organoids ability to predict therapeutic response in gastrointestinal cancers. *JCI Insight* (2022). https://doi.org:10.1172/jci.insight.158060

For Table of Contents Use Only

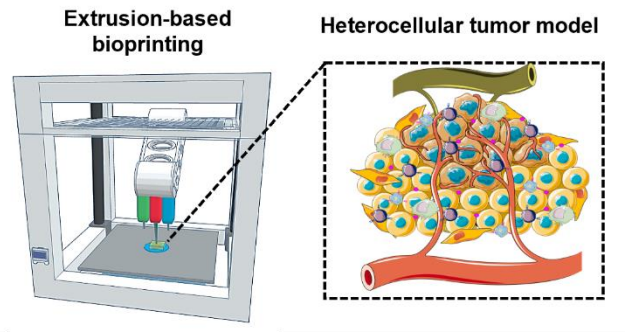

3. Body of the thesis

3.1. Chapter 1. Research Article No.1: Alginate-gelatin-Matrigel hydrogels enable the development and multigenerational passaging of patient-derived 3D bioprinted cancer spheroid models

After reviewing the literature relevant to this project, the upcoming chapter will present the experimental approach to complete aims 1 and 2.

Aim 1: Characterize the rheological performance of alginate-gelatin-Matrigel (AxGyMz) hydrogels, evaluate the effect of the matrix constituents on cell culture, and document the chemosensitivity of cancer spheroids.

Aim 2: Evaluate 3D cell culture passaging by chelating calcium ions from calcium-alginate and document post-printing cancer spheroid development.

As reviewed in chapter 1, the parenchymal element of a solid tumor is the main driver of neoplastic disease. In this chapter, I will cover the completion of aim 1 and aim 2. I demonstrated the use of extrusion-based bioprinting as a tool to recapitulate and study the parenchyma of a tumor within an alginate, gelatin, and Matrigel bioink. I highlight the use of chelating agents to remove calcium ions to dissolve calcium-alginate constructs and harvest cancer spheroids to further re-print these into new constructs. The material candidate originally selected to continue was comprised of 1% alginate (w/v) and 7% gelatin (w/v). Alginate is a highly studied bioinert polysaccharide extracted from seaweed that is popular in both the food and biomedical industries[173]. A single alginate polymeric chain contains successive β-d-mannuronic acid (M) and C5-epimer α-l-guluronic acid (G)[174]. One of the most attractive characteristics of alginate networks is their susceptibility to ionic crosslinking, by which the macroscopic network acquires specific mechanical characteristics[175]. For instance, ionic magnesium does not promote macroscopic gelation,

while calcium ions crosslink the polymeric networks by interacting with the carboxylic acids within alginate chains[136]. Ionic calcium is the preferred crosslinker of cell-laden alginate gels as it endows the final construct with the ability to resist dissolution in aqueous conditions over long periods of time[174]. Gelatin is a widely used linear biopolymer derived from collagen inverse hydrolyzation[176]. Extracted from highly collagenous sources such as pigskin, gelatin retains the biological properties of collagen as it provides cell adhesion sites vital for cell survival and development[177]. Gelatin materials naturally exhibit reversible physical gelation when dissolved in aqueous conditions and exposed at temperatures below 30°C[177]. In combination, alginate-gelatin materials composites are attractive biomaterials for cell and tissue engineering applications, including extrusion bioprinting[178]. As we will see in this chapter, the addition of Matrigel (5% v/v) further enhances the alginate-gelatin composite's bioactivity without compromising the composite's mechanical stability and promotes patient-derived cancer spheroid development.

Figure 1 presents the methodology followed in this investigation. Briefly, patient-derived esophagogastric adenocarcinoma cells derived from xenografts were encapsulated in bioinks. Cell-laden constructs were generated and incubated for up to 21 days to allow cancer cells to reorganize into tumor spheroids. Then, these structures were extracted by dissociating the alginate-based constructs using calcium-chelating agents. Tumor spheres were further dissociated into single cells and (re)encapsulated in fresh bioinks to bioprint the subsequent cell passage in 3D. Alternatively, tumor spheroids were challenged with the standard-of-care chemotherapeutics to investigate if these patient-derived tumor miniatures retained the chemosensitivity from the parental tumor. Moreover, aside from

the iterative bioprinting methodology developed in this investigation, I present the quantitative methods that enable the quantification of an *in vitro* tumor population. These methods proved crucial in understanding how cancer cells develop when encapsulated in the alginate, gelatin, Matrigel bioink.

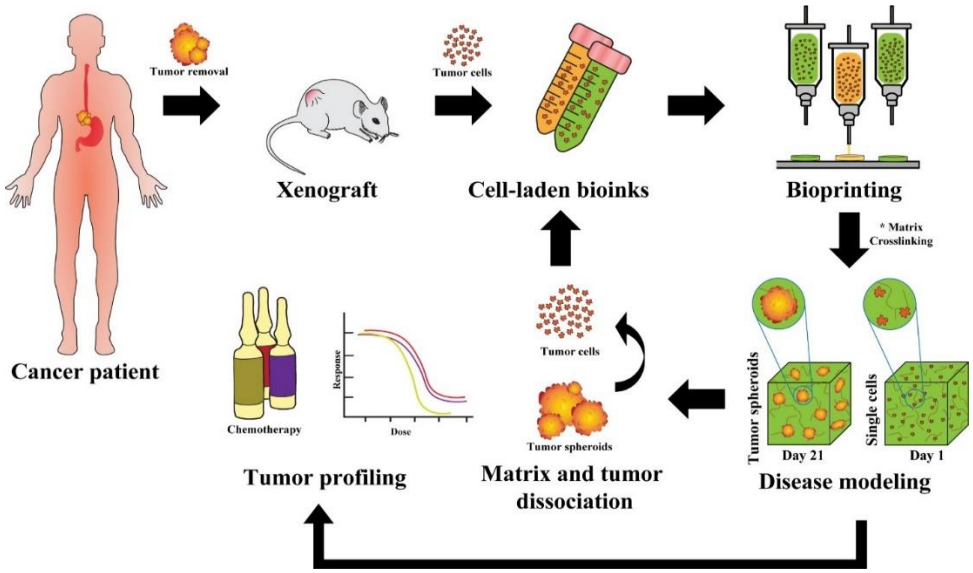

Figure 1. Graphical representation of the iterative bioprinting methodology developed in chapter 1. Patient-derived cancer cells from biopsy or xenografts are mixed with bioink materials, bioprinted, crosslinked, incubated, and challenged with chemotherapy drugs.

The following paper will demonstrate the concepts mentioned above rigorously and scientifically.

Article type: Research Article - DOI: 10.1088/1758-5090/abdb87

Alginate-gelatin-Matrigel hydrogels enable the development and multigenerational passaging of patient-derived 3D bioprinted cancer spheroid models

Salvador Flores-Torres [a], Omar Peza-Chavez [a], Hellen Kuasne [e], Jose G. Munguia-Lopez [a,b], Jacqueline Kort-Mascort [a], Lorenzo Ferri [d,g], Tao Jiang [c], Charles V. Rajadurai [e,f], Morag Park [e,f,g,h,i], Veena Sangwan [d], Joseph M. Kinsella [a,*]

[a] Department of Bioengineering, McGill University, Montreal, Quebec, Canada.

[b] Faculty of Dentistry, McGill University, Montreal, Quebec, Canada.

[c] Department of Intelligent Machinery and Instrument, College of Intelligence Science and Technology, National University of Defense Technology Changsha, Hunan, China.

[d] Department of Surgery, McGill University, Montreal, Quebec, Canada.

[e] Rosalind and Morris Goodman Cancer Centre, McGill University, Montreal, Quebec, Canada.

[f] Department of Biochemistry, McGill University, Montreal, Quebec, Canada.

[g] Department of Medicine, McGill University, Montreal, Quebec, Canada.

[h] Department of Oncology, McGill University, Montreal, Quebec, Canada

[i] Department of Pathology, McGill University, Montreal, Quebec, Canada.

* Corresponding author.

Keywords: bioprinting, cell reprinting, cancer spheroids, 3D cancer cell culture.

3.1.1. Abstract

Hydrogels consisting of controlled fractions of alginate, gelatin, and Matrigel enable the development of patient-derived bioprinted tissue models that support cancer spheroid growth and expansion. These engineered models can be dissociated to be then reintroduced to new hydrogel solutions and subsequently reprinted to generate multigenerational models. The process of harvesting cells from 3D bioprinted models is possible by chelating the ions that crosslink alginate, causing the gel to weaken. Inclusion of the gelatin and Matrigel fractions to the hydrogel increases the bioactivity by providing cell-matrix binding sites and promoting cross-talk between cancer cells and their microenvironment. Here we show that immortalized triple-negative breast cancer cells (MDA-MB-231) and patient-derived gastric adenocarcinoma cells can be reprinted for at least three 21-day culture cycles following bioprinting in the alginate/gelatin/Matrigel hydrogels. Our drug testing results suggest that our 3D bioprinted model can also be used to recapitulate *in vivo* patient drug response. Furthermore, our results show that iterative bioprinting techniques coupled with alginate biomaterials can be used to maintain and expand patient-derived cancer spheroid cultures for extended periods without compromising cell viability, altering division rates, or disrupting cancer spheroid formation.

3.1.2. Introduction

Bioprinting has enabled the accurate reproduction of tissue microenvironments capable of recapitulating complex cellular and tissue-level physiological and functional activity[1]. The ability to develop sophisticated samples using bioprinting lies in its ability to deposit multiple cell types within tunable biomaterials at specific initial locations that better represent tissue architecture and mimic the physiological cell-matrix and multidimensional cell-cell interactions required for function.[2-5] Extracellular matrix (ECM)-mimicking polymers are known to increase the clinical relevance of *in-vitro* environments by giving volumetric space that favors cell biochemical and mechanical stimuli.[6] Soft hydrogel materials have been extensively studied and used in 3D cultures. However, these materials often possess poor mechanical properties that are not suitable for extrusion bioprinting or by automated handling techniques. Setting 3D culture environments by hand often results in irreproducible samples due to the lack of control over essential parameters such as construct geometry, cell density, and cell location.[7]

For the appropriate physiological phenomena to be recapitulated, bioink materials should be extensively characterized to understand the biological response of cells to the biomaterial inputs.[8,9] The bioink material functions as structural support to organize cells and biological components into volumetrically controlled patterns. The ideal bioink is designed to (1) contain cells into the desired structure, (2) provide post-printing structural support, (3) sustain cell populations under culture conditions for extended periods, and (4) allow their intrinsic biological and biochemical functions to occur.[10]

Among the many biopolymers used for 3D cell cultures, alginate-gelatin hydrogels are attractive biomaterials due to their biocompatibility, degradation by ionic chelation, cell

encapsulation capabilities, and printability.[11,12] Alginate hydrogels display bioinert and non-cell adhesive characteristics, requiring chemical modification or blending with other bioactive materials to allow interactions with encapsulated cells.[13,14] Chemical modifications can be performed directly in alginate chains to enhance their bioactivity by promoting cell adhesion.[15] Bioactivity can also be enhanced by developing alginate composite materials by incorporating biomolecules such as gelatin and collagen, which increase cell-matrix adhesions without sacrificing alginate's contributions to the mechanical properties of the hydrogel.[12]

Gelatin is a denatured collagen-derived protein that provides bioactive amino acid residues for cellular adhesion.[16] Gelatin solutions containing more than 0.5% (w/w) in water, exhibit sol-gel transitions. In the sol form, the solution cannot support its weight, and it collapses under the force of gravity ("flows"). In the gel form, gelatin solutions can support their weight and possess the ability to be molded into various shapes.[17] The sol-gel transition occurs when gelatin undergoes gelation or melting because of temperature changes. For bioprinting applications, the stabilized gel-phase of gelatin allows the creation of reproducible cell-laden constructs, while the sol-phase allows the introduction of cells into the bioink.[18]

Harvesting cells from 3D constructs can be challenging if the matrix material is not biodegradable. Cell harvesting is of vital importance for researchers to study cells exposed to the biophysical or biochemical contributions afforded by the 3D matrix or chemo-physical stimuli such as the effects of antineoplastic drugs. Cell-compatible materials such as collagen, Matrigel®, gelatin, alginate, chitosan, and hyaluronic acid (HA), can be designed to degrade via enzymatic hydrolysis, ionic chelation, photolytic cleavage, or a

combination of these mechanisms to control degradation rates of individual components.[19] Calcium alginate hydrogels are vulnerable to chelating agents such as citrate, ethylenediaminetetraacetic acid (EDTA), phosphate, and lactate due to the process of decalcification.[20] The use of chelating agents has introduced novel alternatives to manipulate ECM environments in a time-dependent manner. Zhengjie et al. highlighted the use of sodium citrate to degrade their alginate-based bioprinted models. They reported that encapsulated human corneal epithelial cells showed higher proliferation rates as construct degradation happened.[21]

In this work, we feature the use of hydrogel bioinks comprised of alginate (A), gelatin (G) and Matrigel (M) (AxGyMz) to create cancer cell-laden environments by extrusion-based bioprinting (EBB). The bioink formulations were selected based on the biophysical conditions promote spheroid formation. Our bioinks allowed the growth of patient-derived gastric adenocarcinoma samples as well as the triple-negative breast cancer cell line MDA-MB-231. We take advantage of alginate's ionic properties to encapsulate cells and harvest cancer spheroids from bioprinted constructs. We used AxGyMz blends that promote cancer development and sustain 3D cell cultures for periods of up to three weeks. Cancer spheroids can be retrieved and further dissociated into single-cell suspensions to undergo several rounds of iterative bioprinting. This process allows for controlled cell expansion and multigenerational development of cancer models.

3.1.3. Materials and methods

Bioink manufacturing

The bioink was synthesized as reported previously.[22] Briefly, sodium alginate (Protanal LF 10/60 FT, FMC biopolymer) and type B gelatin from bovine skin (G9391, Sigma-

Aldrich) powders were sterilized via UV exposure for 6 h. Alginate (1 w/v%) and gelatin (7 w/v%) (A1G7) were dissolved in sterile calcium- and magnesium-free D-PBS (1x, Gibco) and mixed using a magnetic hotplate stirrer for 1 h at 55 °C and, then, for 2 h at room temperature. The mixed hydrogel precursors were centrifuged at 834 *g* for 10 minutes to eliminate gas bubbles and stored at 4 °C. Matrigel (M) was incorporated by heating A1G7 to 37 °C and pipetting 5% v/v of Matrigel to create A1G7M5. The blend was then mixed using a magnetic hotplate stirrer for 1h at 37 °C. A1G7 and A1G7M5 were both used within one week of preparation.

The crosslinking solution was prepared by dissolving $CaCl_2$ (Sigma-Aldrich) in sterile ultrapure water to a final concentration of 100 mM. The de-crosslinking solution was prepared by dissolving trisodium citrate (≥ 99.0%, Sigma-Aldrich) in ultrapure water at a final concentration of 55 mM. Both solutions were filter-sterilized (0.22 µm, Millipore) and stored at 4°C until use.

Rheological characterization

Rheological tests were conducted on an MCR302 rheometer (Anton Paar) with a □□25 mm parallel measuring tool (PP25). Amplitude sweeps of the material were performed to determine the shear strain γ_c used in other tests, which was taken as 1/10 of the ultimate linear strain of the material for safety reasons. The bioink was pre-heated in a water bath at 37 °C for 2 h to allow for the thermal stabilization of the material. The rheometer testing plate was pre-heated to 37 °C. The hydrogel precursors were loaded onto the plate of the rheometer, and the temperature was abruptly decreased from 37 °C to 25 °C at the start of the analysis to simulate when the bioink is taken from the water bath (37 °C) to room temperature. While the test was being performed, a sinusoidal strain of γ_c at 1 Hz was

applied for a period of 2 h. G' and G" were recorded once per minute during the gelation process.

Cell culture preparation

MDA-MB-231 breast cancer cells (unlabeled and nuclear-GFP labeled) were cultured in T-25 flasks (Corning) as a monolayer in the presence of 5% CO_2, 37 °C in DMEM medium (Gibco, pH 7.2) supplemented with 10% fetal bovine serum (FBS, Wisent Bioproducts), 100 U/mL penicillin, and 100 µg/mL streptomycin (Wisent Bioproducts). When cell monolayers reached 80% confluency, 2D cultures were washed twice with DPBS, incubated with trypsin-EDTA (0.25%-1X, Gibco) for 5 min and split into two T-25 flasks for passaging. The culture medium was replaced every three days, and cells were used within the 3-6 passages to start the 3D cultures. MDA-MB-231 cancer cells were validated via STR (**Supporting Table 1**).

Gastric cancer samples were obtained from consenting patients undergoing endoscopy or surgical resection at the McGill University Health Center, and tissue collected as per Institutional Review Board guidelines (Protocol # 2007-856). A small piece of tumor was subcutaneously implanted into immunocompromised NOD-Scid IL2Rgamma^{null} mice (Jackson Labs). All animal protocols were performed in accordance with the ethical treatment guidelines of the McGill University Animal Care Committee and the Canadian Council on Animal Care.

Once tumor volume reached 1000 mm^3, mice were sacrificed, and tumors dissociated into single-cell suspensions using a Tumor Dissociation Kit (Miltenyi Biotec) in combination with the gentleMACS™ Dissociator (Miltenyi Biotec). Mouse Cell Depletion Kit (Miltenyi

Biotec) was used to remove murine cells, and the remaining cells were mixed with hydrogel and grown in organoids medium.[23]

Model design and 3D bioprinting

Prior to 3D bioprinting, the bioinks were heated in a water bath at 37 °C for 30 min to induce their liquid phase. Cells in 2D culture were harvested using trypsin-EDTA and centrifuged at 130 *g* for 5 min. Then, 50 µL of DMEM containing $1x10^6$ cells was gently mixed with 1 mL of liquid AxGyMz by pipetting. Cells from xenografts were mixed, considering the same volumes and density. The cell-laden bioink was transferred into a sterile 3 cc cartridge, sealed, and centrifuged at 209 *g* for 3 min to eliminate gas bubbles, and moved to RT for 35 min to induce gelation. We designed the 3D construct models as disks with a diameter of 4 mm and 150 µm layer thickness; 3 layers per model. Lattices were bioprinted using a BioScaffolder 3.1 extrusion bioprinter (GeSiM, Germany). The models were printed with an extrusion pressure of 65 ± 5 kPa using 25-gauge conical nozzles. Extrusion time before the movement was set to 0.1 s, and the printing speed was 10 mm/s. Immediately after printing, each model was soaked into a 100 mM $CaCl_2$ solution for 1 min, rinsed twice with 1x D-PBS, placed into an agarose-coated (electrophoresis grade) 6-well plate, and incubated at 37 °C with 5% CO_2 in DMEM medium (Gibco, pH 7.2) supplemented with 10% fetal bovine serum (FBS, Wisent Bioproducts), 100 U/ mL penicillin, 100 µg/mL streptomycin (Wisent Bioproducts). Patient-derived cells were cultured using gastric organoid media.[23] Samples were transferred to new agarose-coated plates every 6 days, and the cell culture medium was replaced every 3 days. Iterative bioprinting (3D cell passaging) was performed after 21 days in culture. Sample reproducibility was evaluated by assessing the cell number within

19 bioprinted cell-laden samples that were randomly selected from 3 independent experiments. These were imaged immediately after crosslinking and viability was monitored using calcein dye via confocal microscopy.

Iterative bioprinting: 3D cell harvesting and passaging

After 21 days of culture, ten bioprinted disks were collected and placed into 15 mL conical tubes. Calcium-crosslinked A1G7 and A1G7M5 constructs were decalcified by adding 3 mL of trisodium citrate (55 mM, 37 °C) and gently pipetted for 3 min. Once digested, the solution containing cancer spheroids was centrifuged at 130 *g* for 5 min; the resultant pellet was resuspended in D-PBS and re-centrifuged. The supernatant was discarded, and trypsin-EDTA was added for 5 min to dissociate the spheroids. After trypsinization, DMEM supplemented with FBS was added to samples to inhibit trypsin activity. Finally, the single-cell suspension was centrifuged at 130 *g* for 5 min, resuspended in FBS-containing DMEM, and cells were counted using trypan blue and an automated cell counter (Countless II, Invitrogen). Finally, $1x10^6$ cells were then mixed with 1 ml of fresh AxGyMz bioink, and a new set of models were reprinted following previously described protocols. This iterative process was repeated for each bioprinted passage. Based on our experiments and our cell types, the yield after digesting ten disks was ~ $5x10^6$ cells, considering $1x10^6$ cells/ml as the previous initial concentration.

Fluorescent-based live/dead biochemical assays

Fluorescent-based viability assays (Live/Dead) were performed using ethidium homodimer (4 mM) (Biotium, cat# 40010) and calcein-AM (2 mM) (ATT Bioquest, cat# 22002).

Histological and immunostaining sample preparation

For histology, bioprinted samples were rinsed twice with DPBS and fixed with 4% paraformaldehyde (PFA) for 2 h at RT. 15-day-old samples were dehydrated using a serial ethanol gradient (25%, 50%, 70%, and 95%) by incubating the samples for 10 min per ethanol concentration. Next, ethanol (95%) washes were repeated 3 times followed by 3 xylene washes. Finally, the samples we immersed (twice) in paraffin wax for 1 h and 8 µm sections were obtained using a microtome. Eosin and hematoxylin staining (H&E, Leica ST Infinity H&E stain) were applied to each section using a Leica® TS5025 specimen stainer.

Confocal microscopy

Sample imaging was performed using a confocal spinning disk inverted microscope (Olympus IX83, Olympus Life Science) to analyze cell morphology and spheroid formation during the growth experiments. Four disks were randomly selected and were imaged inside sterile containers (ibidi, Cat. No 81156) at RT (25 °C). At each position, a Z-stack scan (500 µm) was implemented with 10 µm steps, at magnifications of 4x and 10x. As a comparative parameter, we measured the surface area of the spheroids using Image J. Image acquisition was performed using a Nikon A1 laser microscope, with a Z-stack scan of 25 µm steps and magnification of 4x (Plan Apo Lambda 4X). High magnification images were taken with a 20x water-immersion objective (Plan Fluor 20XC MI, Nikon), considering 1.5 µm steps. Images were reconstructed using NIS-Elements Imaging software from Nikon. Confocal images were projected to 2D using the maximum intensity projection; then, background noise was removed based on the “rolling ball” algorithm (50-500 pixels depending on spheroid size) using the Fiji software package.[24,25]

Image segmentation (ImageJ Fiji) was applied to obtain kinetic cell growth data from confocal images.

Drug sensitivity

Doxorubicin hydrochloride was dissolved in sterile ultrapure water (8.6mM) 5-Fluorouracil [0.01^{-1} μM to 10^{2} μM] and Docetaxel [10^{-4} μM to 10^{1} μM] were dissolved in DMSO (307.5 mM and 4.95 mM respectively). Testing doses were prepared using supplemented cell media. Cisplatin [10^{-3} μM to 10^{3} μM] was dissolved in sterile saline (0.9% w/w NaCl) solutions. 2D drug testing was conducted by plating a 96 well plate with 5,000 cells per well. Cell monolayers were starved using serum-free medium for 12h before treatment. MDA-MB-231 spheroids were grown over a period of 7 days within the A1G7 bioprinted disk models prior to drug administration. For doxorubicin administration, both the 2D and 3D samples were incubated for 24 h with [10^{-2} μM to 10 μM] doxorubicin. Wells were washed twice with DPBS before evaluating cell viability with a WST-1 Cell Proliferation Assay Kit (Cayman Chemical). Patient-derived xenograft gastric cancer cells were allowed to develop for 7 days in A1G7M5 bioprinted constructs before exposing them to antineoplastic drugs for 7 days as previously reported.[26] Negative controls were incubated with cell growth media containing the highest dose of DMSO or saline solution used for the highest dose of anticancer drug for each drug considered. All drugs were purchased from Cayman Chemical unless otherwise indicated. Growth rate (GR) inhibition and inhibition concentrations (IC) metrics for the MDA-MB-231 cell line were computed with the online GR calculator at http://www.grcalculator.org/ following the methods reported by Hafner M., et al.[27] for a viability/proliferation surrogate (WST-1 Cayman Chemical).

Statistical analysis

Iterative bioprinting methods were conducted at 4 different times for MDA-MB-231 and 3 different times for gastric cancer samples. All data points were performed in triplicate unless stated otherwise. Statistical analysis and plotting were conducted using GraphPad Prism 8 and MATLAB software. Data are presented as the Mean ± SD and Geometric mean. Comparisons were made using one-way ANOVA and Tukey's and Bonferroni's *post hoc* tests using $P < 0.05$ as a significance indicator, unless stated otherwise. Unpaired *t*-test considered $P < 0.05$ as a significance indicator.

3.1.4. Results

In this work, we characterized bioinks containing 1% alginate (w/v) and 7% gelatin (w/v) (A1G7) and 1% alginate (w/v), 7% gelatin (w/v), and 5% Matrigel (v/v) (A1G7M5). The rationale behind the bioink composition was based on our preliminary 3D culture experiments shown in **Supporting Figure 2.a and b**. Patient-derived gastric cancer cells (GP-118) developed into larger and more frequent spheroids when cultured in the A1G7M5 bioink compared to those GP-118 cells grown in A1G7. Spheroid genesis from GP-118 cells significantly benefited from the Matrigel fraction within the bioink (**Supporting Figure 2.c**). The opposite scenario presented for the MDA-MB-231 cell line. Spheroid development appeared to be inconsistent after day 7 in A1G7M5 bioprinted constructs. In contrast, when MDA-MB-231 were encapsulated in A1G7, some spheroid formations reached a sectional area of ~ 1.3 mm^2 by day 21. (**Supporting Figure 2.b** and **d**). Regardless of the material selection and cell growth kinetics, the vast majority of the encapsulated cells retained their viability as revealed by the dead cell counts in

Supporting Figure 2.e and **f**. In-dept analysis in spheroid growth kinetics will be provided in the following pages.

The gelation kinetics of A1G7 and A1G7M5 bioinks are shown in ***Figure 1*.a**. A vial inversion test revealed the temperature-dependent behavior of A1G7 bioink at 37°C and 25°C (***Figure 1*.b**). The gelatin component exists in a liquid state at 37°C for 30 min and exhibits elastic behavior at 25°C. While gelatin gels at temperatures below ~30°C, Matrigel transitions into an elastic material at temperatures above 4°C. When mixed, 5% Matrigel (v/v) and A1G7 (A1G7M5), the Matrigel component accelerates the gelation process, as shown in ***Figure 1*.a**. While the loss factor (tan(δ)) for A1G7 reaches the value of 1 at 27.67 ± 0.58 min, the addition of 5% (v/v) of Matrigel into the bioink accelerated the gelation by 2.0 ± 0.0 min in A1G7M5 (25.67 ± 0.58 min) ($P < 0.0132$) (**Supporting Figure 3**). The presence of Matrigel in A1G7M5 decreases its storage modulus by 19.7 ± 4.6 % (from 72.64 ± 1.6 Pa to 58.32 ± 3.48 Pa at t = 90 min), indicating that Matrigel is a rheological modifier that softens the bioink when incorporated into A1G7 gels. Experimentally, we found that A1G7 or A1G7M5 gels can be extruded from a cylindrical 3 cc cartridge after 35 min of incubation at room temperature. The difference between our gelation kinetic experiments and the experimental time can be explained by the difference in the thermal diffusion within the extrusion cartridge and the parallel plates of the rheometer.[28]

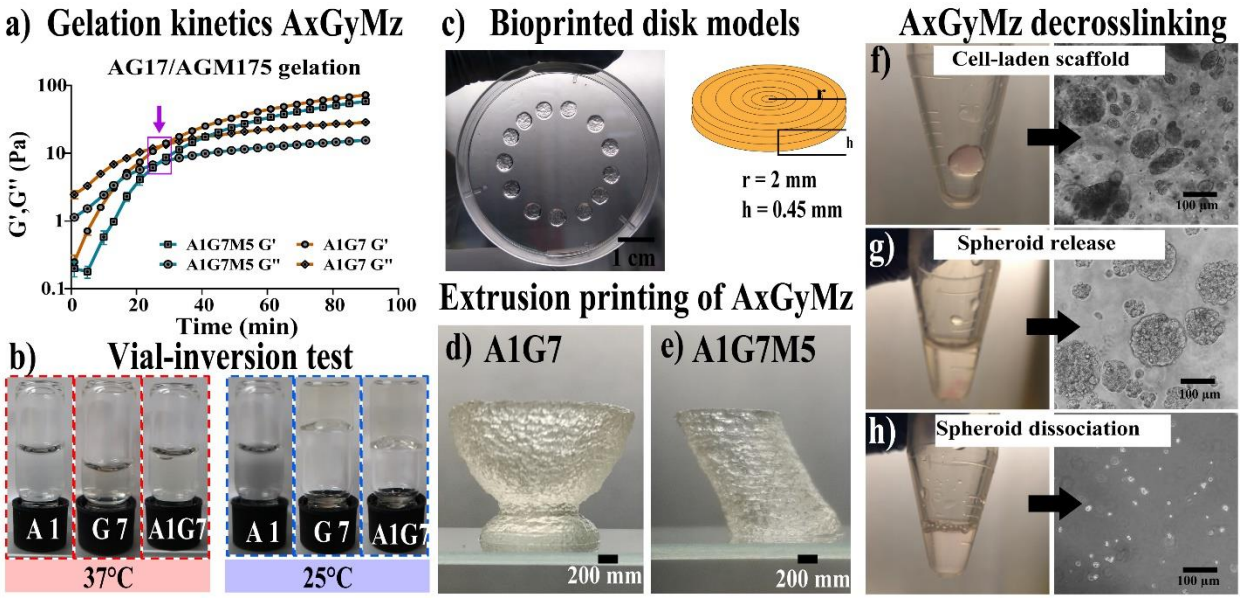

Figure 1. Bioink handling: bioink printability and cell-laden construct digestion. a) A1G7 and A1G7M5 gelation kinetics (triplicates). Gelation points indicated by a purple arrow. b) Vial inversion test of A1G7 and its constituents at 37 °C and 25 °C. c) Photograph of example bioprinted cell-laden disk and computer-aided design input model. d) and e) Non-crosslinked bioprinted wine cup and tilted tube demonstrating post-printing stability of A1G7 and A1G7M5 bioinks. f), g), and h) Alginate decalcification and cell harvesting. f) Spheroids inside AxGyMz bioprinted disk after 21 days of cell culture. g) Spheroid release by alginate de-crosslinking. Calcium ions are removed from the crosslinked chains by citrate cations, destabilizing the alginate constructs. h) spheroid dissociation into single cells by trypsinization.

Moreover, the gelation process increases the yield stress of the material, allowing the materials to be extruded as filaments when they exit the nozzle and deposit onto the printing platform. The filament formats of A1G7 and A1G7M5 allow the formation of 3D constructs with sufficient structural integrity to persist in shape following deposition

(**Figure 1.*c*, d**, and **e**). However, even though the gelation process gives the freshly extruded construct structural integrity, subsequent exposure to cell culture conditions requires crosslinking alginate chains with calcium ions to maintain the structure for prolonged incubation.[29]

The iterative bioprinting process starts by recovering spheroids from the bioprinted AxGyMz constructs by incubating them with trisodium citrate solution (55 mM) (**Figure 1.f** and **g**). Even though citrate has a weaker binding affinity for calcium ($K = 10^{3.5}\ M^{-1}$)[30], an aqueous trisodium citrate solution chelates calcium from alginate since the presence of sodium inhibits the electrostatic interaction between alginate and calcium ($K = 1.33 \times 10^{6}\ M^{-1}$).[31] The spheroids are then dissociated into single cells (***Figure 1*.h**) by trypsinization, and 1×10^{6} cells are isolated and transferred into liquid-phase A1G7 or A1G7M5 bioinks in order to iterate the cell population into subsequent passages within bioprinted models. Cell viability assessments via Trypan blue after spheroid harvesting revealed cell viability of 92.8 ± 2.6 % (n = 6).

We investigated 3D cell morphology of MDA-MB-231 breast cancer cells and cells from gastric patient (GP) xenografts cultured within the bioprinted AxGyMz models. Both MDA-MB-231 and GP-118 cells developed into spheroids (**Figure 2.b** and **d**). We followed both cell types using confocal microscopy using MDA-MB-231 with GFP-labeled nuclei and GP-118 stained with cell viability Live/Dead assay. By day 7, microscopy revealed cancer spheroids already present within AxGyMz constructs. By day 21 (**Figure 2.a** and **c**), the volumetric and orthogonal views for both cancers reveal solid structures of ~50,000 μm^3.

For the first round of bioprinted samples, “2D-3D” or R0 (**Figure 2.b** and **d** and **Supporting Figure 2.a** and **b**) refers to bioprinted samples during the first 21-day culture period prior to subsequent rounds of bioprinting. Once the 2D-3D samples were incubated for 21 days, the alginate matrices were digested, and spheroids were collected, dissociated into single cells using trypsin, and reprinted to create reprint number 1 (R1). This procedure was repeated for three generations of bioprinted cell passages. Cell density was adjusted to $1x10^6$ cell/mL before every iteration. Each iteration or bioprinted passage is referred to as reprint 1 (R1), reprint 2 (R2), and reprint 3 (R3) based upon the number of cycles.

Spheroid development during each reprinted sample was tracked by projecting the image z-stacks into 2D images of the maximum intensity projections. **Supporting Figure 4** illustrates each round of iterative bioprinting for both cell types acquired at time points (0, 7, 14, and 21 days). The spheroid frequency and area were calculated from maximum intensity projections of confocal microscopy acquisitions and condensed into histogram representations shown in **Figure 3**. For both cell types, histogram representations reveal a significant positive asymmetry (skewness).

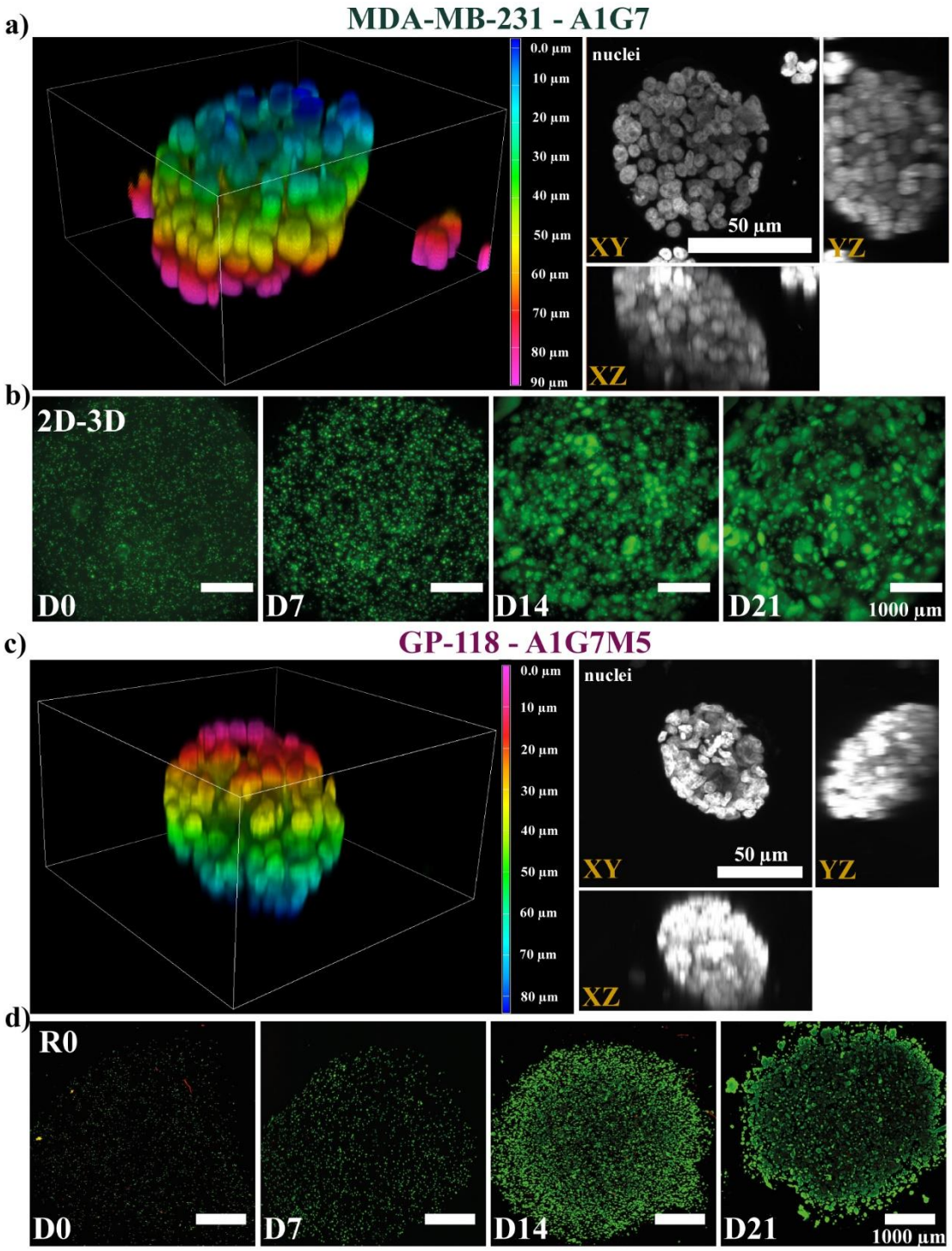

Figure 2. Spheroid imaging and morphological analysis. a) MDA-MB-231 spheroid 3D reconstruction and orthogonal views. Nuclei stained by Hoechst. b) Bioprinted MDA-MB-231 cells developed in bioprinted A1G7 constructs (nuclear GFP transfection). c) GP-118

spheroid 3D reconstruction and orthogonal views. Nuclei stained by Hoechst. d) Bioprinted GP-118 cells developed in bioprinted A1G7M5 constructs (Live/Dead assay: viable cells in green, dead cells in red). d) indicated days in culture following printing. All scale bars are 1000 μm.

The average projected area of MDA-MB-231 cells immediately after printing for each generation was 220 μm^2 as calculated in the condensed histogram RxD0 shown in **Figure 3.a**. Initially following the printing of GP-118 cells, their arithmetic mean cell area is 429 μm^2 as calculated in the histogram shown in **Figure 3.c**. At a 99% confidence interval, the average number of cells for Day 0 of our sample population is between 7404 and 8546 cells per model (**Supporting Figure 1**).

The condensed histogram analyses (**Figure 3.a** and **c)** revealed the presence of extreme outlying values of spheroid area sizes. To reduce the effect of outliers and extreme values without removing them in our following results, we used the geometric mean value (GM) of each data set, as it is a resilient metric to the presence of outliers in skewed distributions as the ones observed in **Figure 3.a** and **c**. The GM analyses yielded consistent growth trends for the 3 reprints for MDA-MB-231 and GP-118 spheroids (**Figure 3.b** and **d**). Using the GM values, we further computed the size doubling time using the exponential growth function $y(\mathrm{x}) = y(0) * e^{k*x}$. The average doubling rate of MDA-MB-231 cells in bioprinted A1G7 constructs was computed as 4 ± 0.5 days and 5.8 ± 1.2 days for GP-118 cells in bioprinted A1G7M5 constructs (**Figure 3.b** and **d**).

Moreover, to evaluate the feasibility of A1G7M5 as a matrix to grow patient-derived cells, we created models from tumor xenografts grown from samples derived from different patient sources **(Supporting Figure 5.b**, and **c)**. Membrane integrity assays (Live:

Dead) revealed patient-to-patient differences in measured growth by day 21 (**Supporting Figure 5.a**).Additional information on the growth of these samples as PDX format is provided in **Supporting Figure 5.d**.

To complement our growth rate studies, we confirmed cell proliferation for each passage by looking at the cellular proliferation marker Ki67. **Supporting Figure 7** shows hematoxylin and eosin (H&E) and immunohistochemistry of Ki67 for every 15th day of each MDA-MB-231 reprint.

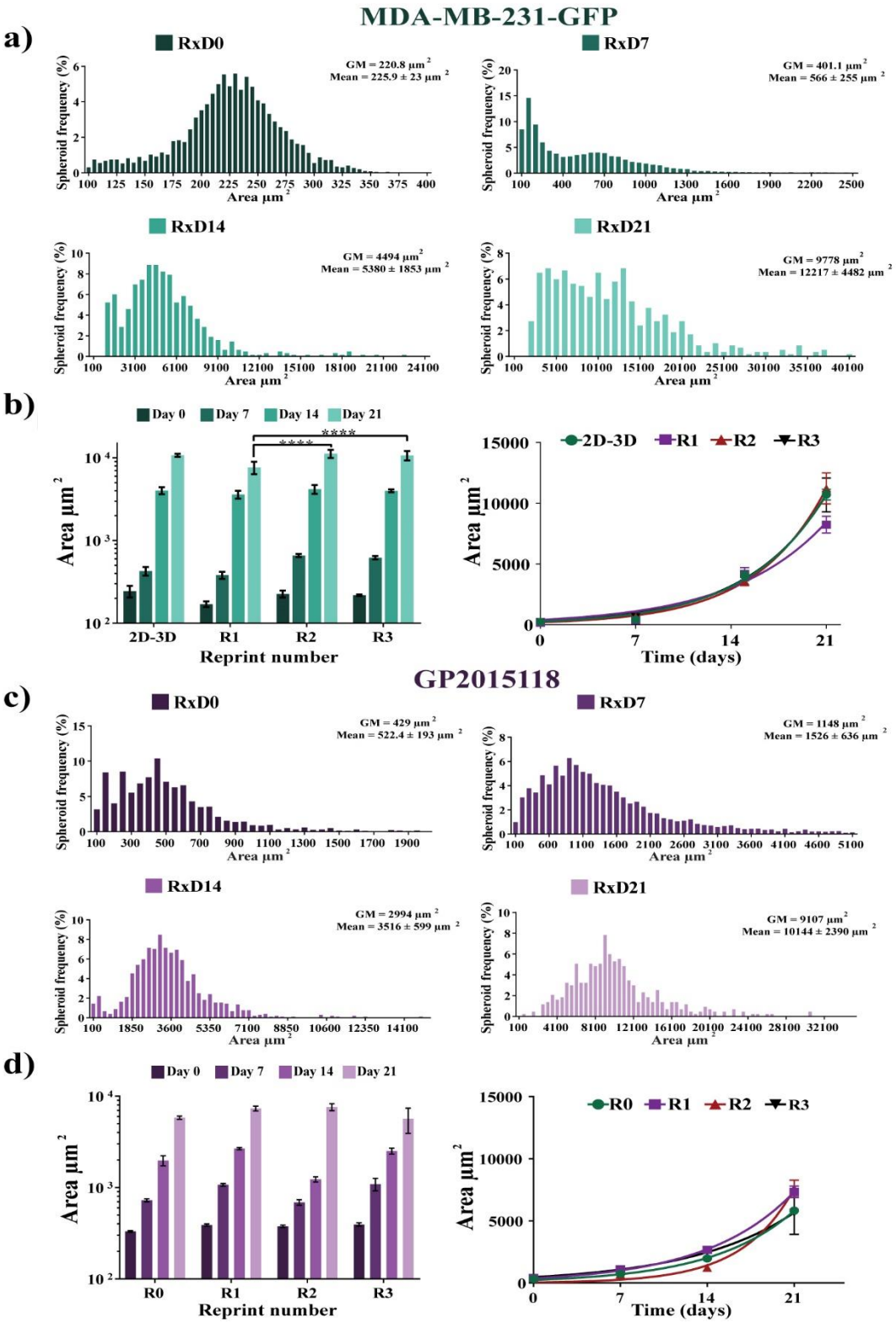

Figure 3. Iterative bioprinting of MDA-MB-231-GFP breast cancer cells and patient-derived GP-118 gastric cancer cells. a) Condensed histogram representations of the size

distribution of MDA-MB-231-GFP cells b) Geometric mean (GM) and exponential trend analysis of MDA-MB-231-GFP reprints. c) Condensed histogram representations of the size distribution of GP-118 spheroids. d) Geometric mean (GM) and exponential trend analysis of GP-118 reprints. Doubling time computed from $t = \ln(2)/K$.

By day 15, spheroids were not found to be cytostatic and continued to divide following each harvesting and successive passage. Our histology results showed tight cellular structures without a hollow core (**Supporting Figure** 7, H&E row).

Furthermore, we challenged our 3D systems with the standard of care antineoplastic drugs. Monolayer MDA-MB-231 and 7-day-old spheroid formats were exposed to doxorubicin. Doxorubicin internalization was confirmed by fluorescent microscopy ($470_{ex}/594_{em}$) (**Supporting Figure 6**). As shown in **Figure 4.a**, MDA-MB-231 monolayers (2D) exhibited an IC_{50}[32] of 1.21 μM and a GR50 of 1.27 μM after 24 h of continuous exposure, while 7-day-old spheroids grown in A1G7 were more resistant with an IC_{50} of 4.26 μM and GR50 of 3.24 μM.

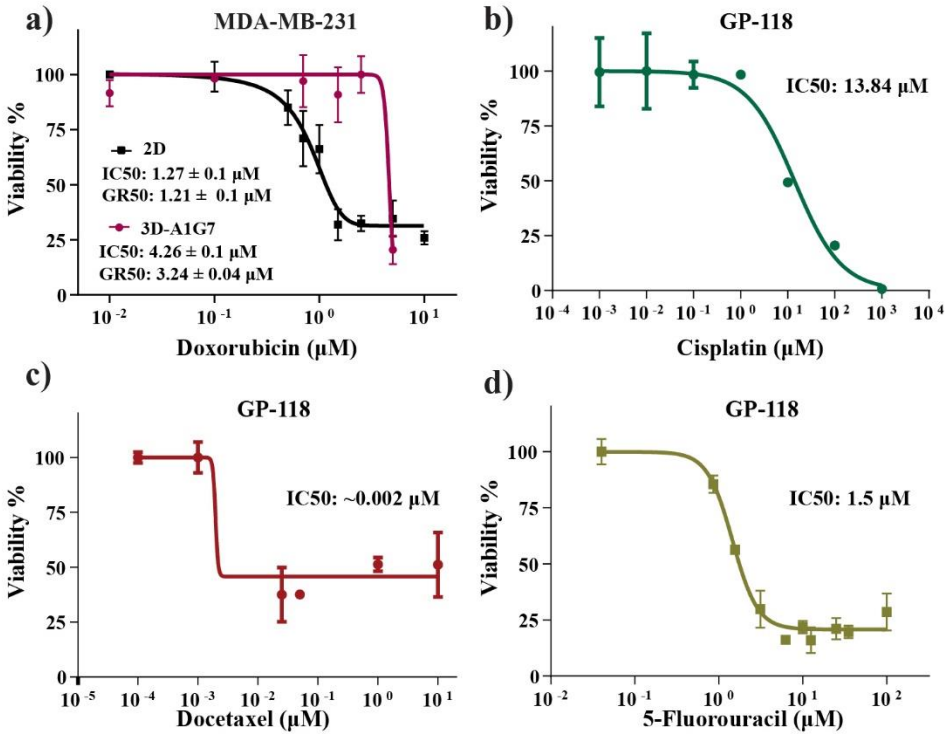

Figure 4. Dose-response of MDA-MB-231 against Doxorubicin, and dose-response of GP-118 against Docetaxel, Cisplatin, and 5-Fluorouracil. a) Doxorubicin dose-response comparison of MDA-MB-231 cells grown as a 2D monolayer (2D) and as 7-day old spheroids in A1G7 (3D-A1G7). b) Cisplatin, c) Docetaxel, and d) 5-Fluorouracul dose-response of 7-day old spheroid GP-118 in A1G7M5.

Next, we investigated the feasibility of using patient-derived cells developed in bioprinted A1G7M5 constructs to evaluate the efficacy of antineoplastic drugs. Spheroids were developed from the tumor of a 67-year old male with adenocarcinoma of the stomach (stage IV) who had demonstrated poor response to neoadjuvant standard of care chemotherapy (Docetaxel, 5-FU, and Cisplatin) (**Supporting figure 5.b**). After conducting the first reprint (R1), 7-day-old GP-118 spheroids from were challenged with the standard of care drugs Docetaxel, Cisplatin, and 5-Fluorouracil (5-FU). Even though

docetaxel generated an IC_{50} at ~ 2 nM, increasing doses did not further reduce cell viability below 40%. Similarly, Cisplatin dose-responses revealed a high IC_{50} at 13.8 μM **Figure 4.c**. The dose-response of GP-118 towards 5-FU treatment revealed an IC_{50} of 1.5 μM, which is within the standard sensitivity regime.[26]

3.1.5. Discussion

Iterative bioprinting is a novel integration of additive manufacturing and tissue engineering that offers a new method for cell expansion, spheroid growth, and bioink control. We demonstrated the use of extrusion-based bioprinting as a tool to engineer and study cancer spheroid models for several generations in 3D culture conditions using both immortalized cancer cells and patient-derived samples.

Due to alginate's unique molecular composition, alginate-based constructs allow spheroid, and single-cell, recovery by decalcifying the ionic crosslinkers from the alginate gels with chelating agents, as reported by *Li et al.*[32] The use of $CaCl_2$ as a crosslinker before culture and sodium citrate as a chelating solution for cell harvesting demonstrated a cell recovery efficiency of > 88.5%. Alginate has previously been used to create cell-laden constructs as demonstrated by *Wang et al.*, their 3D model allowed cells to be cultured for up to 28 days, and crosslinked alginate was the critical element required to maintain structural integrity during culture conditions.[33] By developing an iterative step-wise process of bioprinting, we demonstrated that we could collect cancer spheroids at specific times during culture and reincorporate the cells into fresh bioinks that can be reprinted to create multiple generational models.

While alginate has a critical role in enabling the spheroids to be recovered and reprinted by de-crosslinking the gels, gelatin drives the gelation of both types of bioink, and it

provides a sol-gel transition within a reasonable temperature range for cell incorporation. Even though A1G7M5 better promoted patient-derived cell growth, the rheological performance was affected by the Matrigel content. The storage modulus was reduced by 19.7 ± 4.6 %, while the gelation time was accelerated by 2 ± 0 min.

Both MDA-MB-231 and GP-118 cancer cells developed into solid spheroid structures by day 7 while encapsulated inside the AxGyMz bioinks. Spheroids continued to grow for the duration of the 21-day culture period. It is worth noting that biomaterial compositions clearly influenced different spheroid growth behavior as noted in **Supporting Figure 2.** GP-118 spheroid formation was favored by the Matrigel fraction while MDA-MB-231 cells exhibited a preferential reorganization into multicellular structures that were up to 1000 times (~1.3 mm^2) larger than the geometric mean value (~1300 μm^2) (day 21). This growth behavior can be attributed to the addition of basal membrane macromolecules such as laminin and collagen IV present in Matrigel[34]; these ECM components are drivers of progression of cancer lesions[35], cancer cell proliferation[36], and survival.[37] The additional ECM components are known to influence cell phenotype[38], functionality[39], and malignancy.[40-42] Moreover, phenotypic changes of breast cancer epithelial cells have been reported due to the presence Matrigel.[43,44]

The hydrogel-embedded tumor spheroid model serves as an *in-vitro* tool to recapitulate *in vivo* tumor architectures such as cell-extracellular matrix (ECM) and cell-cell interactions. Several studies have demonstrated that 3D cancer cell cultures display different drug sensitivities compared to their 2D monolayer formats, as 3D architectures recapitulate essential features of the *in vivo* tumor physiology.[45,46] Even though landmark discoveries have been made using traditional 2D cell culture settings and cell lines, it is

imperative to utilize 3D models comprised of ECM-mimicking biomaterials and physiologically relevant patient-derived cells.

Our drug sensitivity examinations using MDA-MB-231 monolayers and 7-day old spheroids revealed different dose-exposure responses for the antineoplastic drug doxorubicin. We found that spheroids grown in bioprinted samples for 7 days were less sensitive to equivalent doxorubicin doses that cause a significant reduction of cell viability in a cell monolayer. According to recent studies, MDA-MB-231 cells in spheroid format display less sensitivity towards antineoplastic agents. Less sensitivity to doxorubicin in 3D culture vs the 2D monolayer of MDA-MB-231 has been further demonstrated by Huang et al.[47]. Furthermore, 3D culture of MDA-MB-231 is generally less responsive to other commonly used anti-tumor drugs, such as: Epirubicin[48,49], Vinorelbine,[49] Paclitaxel[49,50], Docetaxel,[48] Carboplatin[47], and Cisplatin[48,50]. The fact that some cell monolayers are sensitive to anticancer drugs can be attributed to the flat morphology that promotes aberrant surface receptor organization relative to 3D culture systems that promote physiologically important cell-ECM interactions in addition to cell-cell interactions.[46,51] Antineoplastic drugs often target surface receptors; hence their absence or overexpression may directly impact drug efficacy when performing screening assays using cells or spheroids grown in the different conditions.[52] Moreover, cells cultured in 2D conditions are often forced to synchronize their division rates before drug testing, whereas 3D spheroids are known to possess different proliferative zones dependent upon nutrient and oxygen availability[53]. Taking into consideration that *in vivo* tumors are highly heterogeneous, *in-vitro* 3D tumor models are better suited than 2D monolayer cultures to recapitulate cell cycle-mediated antineoplastic resistance[54].

Furthermore, the bioactivity enhancement of the A1G7 bioink by incorporating 5% Matrigel into the hydrogel enabled us to use this platform to grow and evaluate drug responses of patient-derived spheroids. These samples were derived from a xenograft previously developed out of a human gastric adenocarcinoma, where the patient exhibited a poor response to neoadjuvant chemotherapy comprised of Docetaxel, 5-FU, and Cisplatin. Our data show that all doses used were unable to kill all tumor cells, recapitulating the resistance of the patient in our bioprinted model. Moreover, A1G7M5 bioink supported the development of different gastric patient tumor cells. These samples exhibited differences in growth *in-vitro*, which reflects the differences in growth rates found among patient populations.

After long term cell culture, encapsulated cells can experience steric effects that impede any further tumor growth with the fixed volume of the bioprinted models as they become space limited.[55] We were able to overcome these physical constraints by digesting the AxGyMz constructs, dissociating the spheroids into single-cell suspensions, and reprinting a portion of the collected cells into new 3D bioprinted passage models. We observed steric effects within the 3D constructs after 21 days of culture as cell proliferation was markedly limited due to the lack of free gel volume, and spheroids, or single cells, began to escape from the bioprinted matrix into the surrounding medium.

3.1.6. Conclusions

To the best of our knowledge, this is the first report to date where harvested cells are used for continuous passaging in 3D bioprintable alginate-gelatin systems. As shown by our results, MDA-MB-231 triple-negative breast cancer and patient-derived gastric cancer cells can proliferate and reorganize into cancer spheroids during three iterative rounds of

3D bioprinting, harvesting, dissociation, and subsequent rounds of bioprinting. In this investigation, we found that both cell line and patient-derived cells grown within A1G7(M5) bioink resulted in spheroid generation after 7 days of culture. Our iterative bioprinting methodology does not limit the ability of single cells to reorganize into spheroids following the initial bioprinting generation and after being reprinted for up to 3 rounds. We believe our iterative bioprinting work is a suitable technique that could be adapted to different cell types considering alginate-gelatin-Matrigel based bioinks.

3.1.7. Author contributions

SFT designed, planned, and executed bioprinting, imaging, cell culture, drug testing experiments, and genotyping experiments, acquired and processed data. OPC executed bioprinting, 3D cell culture, cell viability experiments, acquired and processed data. HK developed the GP-118 and other organoid lines from PDXs established in the lab of MP, and LF provided patient samples and clinical expertise for the study. JKM contributed to image analysis and statistical data results. JGML executed cell culture and assay experiments, acquired and processed data. TJ assisted in characterizing biomaterial printability. CVR and MP provided cell lines and expertise in 3D cell biology techniques. VS co-supervised this work, contributed to the experimental design and data processing. JMK supervised the research, designed, and planned experimental methods. SFT wrote the first draft of the manuscript. SFT, OPC, HK, JMK, VS, JGML, JKM, LF, and TJ each contributed to writing the article.

3.1.8. Acknowledgments:

JMK thanks the National Science and Engineering Research Council (NSERC RGPIN-06671-14), the Canadian Foundation for Innovation, the Townshend-Lamarre Family Foundation at the Goodman Cancer Research Centre at McGill University (with MP), and

McGill University for funding. This study was funded in part by a grant to VS from the Cancer Research Society and by the Canadian Institute of Health Research Foundation grant to MP. SFT thanks CONACYT-I2T2 for scholarship funding (754427), McGill Engineering Doctoral Award (90025) and FRQNT (291010) for the scholarships. JGML thanks CONACYT for scholarship funding (291168 and 291258) and FRQNT (258421). JKM thanks CONACYT-I2T2 for scholarship funding (751540), McGill Engineering Doctoral Award (90025), and FRQNT (288490) for the scholarships. OPC thanks MITACS for scholarship funding (58362). TJ thanks the China Scholarship Council (201403170354) and McGill Engineering Doctoral Award (90025) for the scholarship. The authors thank the Biobanking Technology Platform of the Research Institute of the McGill University Health Centre and staff for providing services and assistance with tissue collection.

3.1.9. References:

1 Duan, B., Hockaday, L. A., Kang, K. H. & Butcher, J. T. 3D bioprinting of heterogeneous aortic valve conduits with alginate/gelatin hydrogels. *Journal of biomedical materials research Part A* **101**, 1255-1264 (2013).

2 Lee, J., Cuddihy, M. J. & Kotov, N. A. Three-Dimensional Cell Culture Matrices: State of the Art. *Tissue Engineering Part B: Reviews* **14**, 61-86, doi:10.1089/teb.2007.0150 (2008).

3 Rocca, M., Fragasso, A., Liu, W., Heinrich, M. A. & Zhang, Y. S. Embedded Multimaterial Extrusion Bioprinting. *SLAS TECHNOLOGY: Translating Life Sciences Innovation* **23**, 154-163, doi:10.1177/2472630317742071 (2018).

4 Liu, W. *et al.* Rapid Continuous Multimaterial Extrusion Bioprinting. *Advanced Materials* **29**, 1604630, doi:10.1002/adma.201604630 (2017).

5 Rhee, S., Puetzer, J. L., Mason, B. N., Reinhart-King, C. A. & Bonassar, L. J. 3D Bioprinting of Spatially Heterogeneous Collagen Constructs for Cartilage Tissue Engineering. *ACS Biomaterials Science & Engineering* **2**, 1800-1805, doi:10.1021/acsbiomaterials.6b00288 (2016).

6 Liu, Z. & Vunjak-Novakovic, G. Modeling tumor microenvironments using custom-designed biomaterial scaffolds. *Current opinion in chemical engineering* **11**, 94-105 (2016).

7 El-Sherbiny, I. M. & Yacoub, M. H. Hydrogel scaffolds for tissue engineering: Progress and challenges. *Glob Cardiol Sci Pract* **2013**, 316-342, doi:10.5339/gcsp.2013.38 (2013).

8 Lv, H. *et al.* Mechanism of regulation of stem cell differentiation by matrix stiffness. *Stem Cell Research & Therapy* **6**, 103, doi:10.1186/s13287-015-0083-4 (2015).

9 Li, Z. *et al.* Tuning Alginate-Gelatin Bioink Properties by Varying Solvent and Their Impact on Stem Cell Behavior. *Scientific Reports* **8**, 8020, doi:10.1038/s41598-018-26407-3 (2018).

10 Hospodiuk, M., Dey, M., Sosnoski, D. & Ozbolat, I. T. The bioink: a comprehensive review on bioprintable materials. *Biotechnology advances* **35**, 217-239 (2017).

11 Gao, T. *et al.* Optimization of gelatin-alginate composite bioink printability using rheological parameters: a systematic approach. *Biofabrication* **10**, 034106-034106, doi:10.1088/1758-5090/aacdc7 (2018).

12 Sarker, B. *et al.* Alginate-based hydrogels with improved adhesive properties for cell encapsulation. *International journal of biological macromolecules* **78**, 72-78, doi:10.1016/j.ijbiomac.2015.03.061 (2015).

13 Zhao, Y. *et al.* Three-dimensional printing of Hela cells for cervical tumor model in vitro. *Biofabrication* **6**, 035001 (2014).

14 Jia, J. *et al.* Engineering alginate as bioink for bioprinting. *Acta biomaterialia* **10**, 4323-4331 (2014).

15 Andersen, T., Auk-Emblem, P. & Dornish, M. 3D Cell Culture in Alginate Hydrogels. *Microarrays (Basel)* **4**, 133-161, doi:10.3390/microarrays4020133 (2015).

16 Davidenko, N. *et al.* Evaluation of cell binding to collagen and gelatin: a study of the effect of 2D and 3D architecture and surface chemistry. *Journal of Materials Science: Materials in Medicine* **27**, 148 (2016).

17 Winter, J. & Shifler, D. The material properties of gelatin gels. (MARVALAUD INC WESTMINSTER MD, 1975).

18 Jiang, T. *et al.* Directing the self-assembly of tumour spheroids by bioprinting cellular heterogeneous models within alginate/gelatin hydrogels. *Scientific Reports* **7**, 4575 (2017).

19 Nicodemus, G. D. & Bryant, S. J. Cell encapsulation in biodegradable hydrogels for tissue engineering applications. *Tissue Eng Part B Rev* **14**, 149-165, doi:10.1089/ten.teb.2007.0332 (2008).

20 Smidsrød, O. & Skja˚k-Br1k, G. Alginate as immobilization matrix for cells. *Trends in Biotechnology* **8**, 71-78, doi:https://doi.org/10.1016/0167-7799(90)90139-O (1990).

21 Wu, Z. *et al.* Bioprinting three-dimensional cell-laden tissue constructs with controllable degradation. *Scientific Reports* **6**, 24474, doi:10.1038/srep24474 https://www.nature.com/articles/srep24474#supplementary-information (2016).

22 Jiang, T. *et al.* Bioprintable Alginate/Gelatin Hydrogel 3D In Vitro Model Systems Induce Cell Spheroid Formation. *JoVE*, e57826, doi:doi:10.3791/57826 (2018).

23 Sato, T. *et al.* Single Lgr5 stem cells build crypt-villus structures in vitro without a mesenchymal niche. *Nature* **459**, 262-265, doi:10.1038/nature07935 (2009).

24 Schindelin, J. *et al.* Fiji: an open-source platform for biological-image analysis. *Nature Methods* **9**, 676, doi:10.1038/nmeth.2019 https://www.nature.com/articles/nmeth.2019#supplementary-information (2012).

25 Sternberg, S. R. Biomedical image processing. *Computer* **16**, 22-34 (1983).

26 Yan, H. H. N. *et al.* A Comprehensive Human Gastric Cancer Organoid Biobank Captures Tumor Subtype Heterogeneity and Enables Therapeutic Screening. *Cell Stem Cell* **23**, 882-897.e811, doi:10.1016/j.stem.2018.09.016 (2018).

27 Hafner, M., Niepel, M., Chung, M. & Sorger, P. K. Growth rate inhibition metrics correct for confounders in measuring sensitivity to cancer drugs. *Nature methods* **13**, 521-527 (2016).

28 Jiang, T., Munguia-Lopez, J. G., Flores-Torres, S., Kort-Mascort, J. & Kinsella, J. M. Extrusion bioprinting of soft materials: An emerging technique for biological model fabrication. *Applied Physics Reviews* **6**, 011310, doi:10.1063/1.5059393 (2019).

29 Remuñán-López, C. & Bodmeier, R. Mechanical, water uptake and permeability properties of crosslinked chitosan glutamate and alginate films. *Journal of Controlled Release* **44**, 215-225, doi:https://doi.org/10.1016/S0168-3659(96)01525-8 (1997).

30 Keowmaneechai, E. & McClements, D. J. Influence of EDTA and Citrate on Physicochemical Properties of Whey Protein-Stabilized Oil-in-Water Emulsions Containing CaCl2. *Journal of Agricultural and Food Chemistry* **50**, 7145-7153, doi:10.1021/jf020489a (2002).

31 De, S. & Robinson, D. Polymer relationships during preparation of chitosan–alginate and poly-l-lysine–alginate nanospheres. *Journal of Controlled Release* **89**, 101-112, doi:https://doi.org/10.1016/S0168-3659(03)00098-1 (2003).

32 Li, X. *et al.* Culture of neural stem cells in calcium alginate beads. *Biotechnology progress* **22**, 1683-1689, doi:10.1021/bp060185z (2006).

33 Wang, X. *et al.* Tumor-like lung cancer model based on 3D bioprinting. *3 Biotech* **8**, 501-501, doi:10.1007/s13205-018-1519-1 (2018).

34 Hughes, C. S., Postovit, L. M. & Lajoie, G. A. Matrigel: A complex protein mixture required for optimal growth of cell culture. *PROTEOMICS* **10**, 1886-1890, doi:https://doi.org/10.1002/pmic.200900758 (2010).

35 Qiu, X., Tan, H., Fu, D., Zhu, Y. & Zhang, J. Laminin is over expressed in breast cancer and facilitate cancer cell metastasis. *Journal of Cancer Research and Therapeutics* **14**, 1170-1172, doi:10.4103/0973-1482.191035 (2018).

36 Öhlund, D., Franklin, O., Lundberg, E., Lundin, C. & Sund, M. Type IV collagen stimulates pancreatic cancer cell proliferation, migration, and inhibits apoptosis through an autocrine loop. *BMC Cancer* **13**, 154, doi:10.1186/1471-2407-13-154 (2013).

37 Burnier, J. V. *et al.* Type IV collagen-initiated signals provide survival and growth cues required for liver metastasis. *Oncogene* **30**, 3766-3783, doi:10.1038/onc.2011.89 (2011).

38 Timraz, S. B. H., Rezgui, R., Boularaoui, S. M. & Teo, J. C. M. Stiffness of Extracellular Matrix Components Modulates the Phenotype of Human Smooth Muscle Cells in Vitro and Allows for the Control of Properties of Engineered Tissues. *Procedia Engineering* **110**, 29-36, doi:https://doi.org/10.1016/j.proeng.2015.07.006 (2015).

39 Bruno, R. D. *et al.* Mammary extracellular matrix directs differentiation of testicular and embryonic stem cells to form functional mammary glands in vivo. *Scientific Reports* **7**, 40196, doi:10.1038/srep40196 (2017).

40 Henke, E., Nandigama, R. & Ergün, S. Extracellular Matrix in the Tumor Microenvironment and Its Impact on Cancer Therapy. *Frontiers in Molecular Biosciences* **6**, doi:10.3389/fmolb.2019.00160 (2020).

41 Walker, C., Mojares, E. & Del Río Hernández, A. Role of Extracellular Matrix in Development and Cancer Progression. *International journal of molecular sciences* **19**, 3028, doi:10.3390/ijms19103028 (2018).

42 Lu, P., Weaver, V. M. & Werb, Z. The extracellular matrix: A dynamic niche in cancer progression. *The Journal of Cell Biology* **196**, 395 (2012).

43 Cavo, M. *et al.* A new cell-laden 3D Alginate-Matrigel hydrogel resembles human breast cancer cell malignant morphology, spread and invasion capability observed "in vivo". *Scientific Reports* **8**, 5333, doi:10.1038/s41598-018-23250-4 (2018).

44 Chaudhuri, O. *et al.* Extracellular matrix stiffness and composition jointly regulate the induction of malignant phenotypes in mammary epithelium. *Nature Materials* **13**, 970-978, doi:10.1038/nmat4009 (2014).

45 Lv, D., Hu, Z., Lu, L., Lu, H. & Xu, X. Three-dimensional cell culture: A powerful tool in tumor research and drug discovery. *Oncology letters* **14**, 6999-7010, doi:10.3892/ol.2017.7134 (2017).

46 Weigelt, B., Ghajar, C. M. & Bissell, M. J. The need for complex 3D culture models to unravel novel pathways and identify accurate biomarkers in breast cancer. *Advanced Drug Delivery Reviews* **69-70**, 42-51, doi:https://doi.org/10.1016/j.addr.2014.01.001 (2014).

47 Huang, Z., Yu, P. & Tang, J. Characterization of Triple-Negative Breast Cancer MDA-MB-231 Cell Spheroid Model. *Onco Targets Ther* **13**, 5395-5405, doi:10.2147/OTT.S249756 (2020).

48 Dubois, C. *et al.* Development and cytotoxic response of two proliferative MDA-MB-231 and non-proliferative SUM1315 three-dimensional cell culture models of triple-negative basal-like breast cancer cell lines. *Oncotarget* **8**, 95316-95331, doi:10.18632/oncotarget.20517 (2017).

49 Lovitt, C. J., Shelper, T. B. & Avery, V. M. Evaluation of chemotherapeutics in a three-dimensional breast cancer model. *Journal of Cancer Research and Clinical Oncology* **141**, 951-959, doi:10.1007/s00432-015-1950-1 (2015).

50 Reynolds, D. S. *et al.* Breast Cancer Spheroids Reveal a Differential Cancer Stem Cell Response to Chemotherapeutic Treatment. *Scientific Reports* **7**, 10382, doi:10.1038/s41598-017-10863-4 (2017).

51 Langhans, S. A. Three-Dimensional in Vitro Cell Culture Models in Drug Discovery and Drug Repositioning. *Front Pharmacol* **9**, 6, doi:10.3389/fphar.2018.00006 (2018).

52 Large, D. E., Soucy, J. R., Hebert, J. & Auguste, D. T. Advances in Receptor-Mediated, Tumor-Targeted Drug Delivery. *Advanced Therapeutics* **2**, 1800091, doi:10.1002/adtp.201800091 (2019).

53 Hirschhaeuser, F. *et al.* Multicellular tumor spheroids: An underestimated tool is catching up again. *Journal of Biotechnology* **148**, 3-15, doi:https://doi.org/10.1016/j.jbiotec.2010.01.012 (2010).

54 Shah, M. A. & Schwartz, G. K. Cell cycle-mediated drug resistance: an emerging concept in cancer therapy. *Clinical cancer research : an official journal of the American Association for Cancer Research* **7**, 2168-2181 (2001).

55 Cidonio, G., Glinka, M., Dawson, J. I. & Oreffo, R. O. C. The cell in the ink: Improving biofabrication by printing stem cells for skeletal regenerative medicine. *Biomaterials* **209**, 10-24, doi:10.1016/j.biomaterials.2019.04.009 (2019).

3.1.10. SUPPORTING INFORMATION

Alginate-gelatin-Matrigel hydrogels enable the development and multigenerational passaging of patient-derived 3D bioprinted cancer spheroid models.

Authors

Salvador Flores-Torres [a], Omar Peza-Chavez [a], Hellen Kuasne [i], Jose G. Munguia-Lopez [a,b], Jacqueline Kort-Mascort [a], Lorenzo Ferri[d,g], Tao Jiang [c], Charles V. Rajadurai [e,i], Morag Park [e,f,g,h,i], Veena Sangwan [d], Joseph M. Kinsella [a,*]

[a] Department of Bioengineering, McGill University, Montreal, Quebec, Canada.

[b] Faculty of Dentistry, McGill University, Montreal, Quebec, Canada.

[c] Department of Intelligent Machinery and Instrument, College of Intelligence Science and Technology, National University of Defense Technology Changsha, Hunan, China.

[d] Department of Surgery, McGill University, Montreal, Quebec, Canada.

[e] Department of Biochemistry, McGill University, Montreal, Quebec, Canada.

[f] Department of Pathology, McGill University, Montreal, Quebec, Canada.

[g] Department of Medicine, McGill University, Montreal, Quebec, Canada.

[h] Department of Oncology, McGill University, Montreal, Quebec, Canada.

[i] Rosalind and Morris Goodman Cancer Centre, McGill University, Montreal, Quebec, Canada.

* Corresponding author.

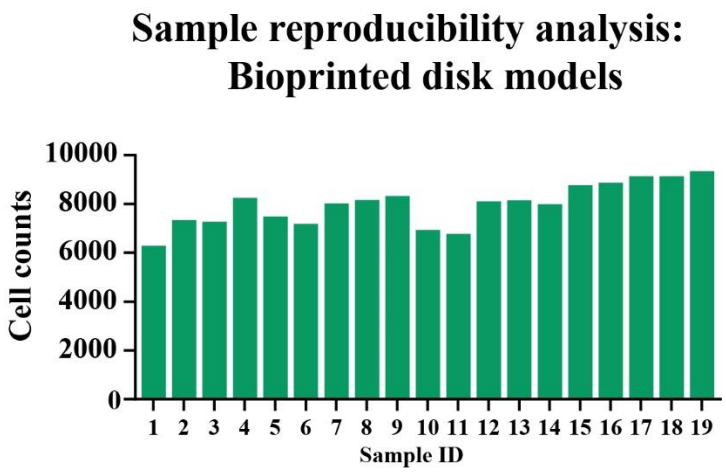

Supporting Figure 1. Sample reproducibility analysis. Cell counts per disk were determined from the maximum intensity projections from 19 samples from Day 0. Cell-laden disk samples were extruded using A1G7M5. At a 99% confidence interval, the average number of cells for Day 0 of our sample population is between 7404 and 8546 cells per model.

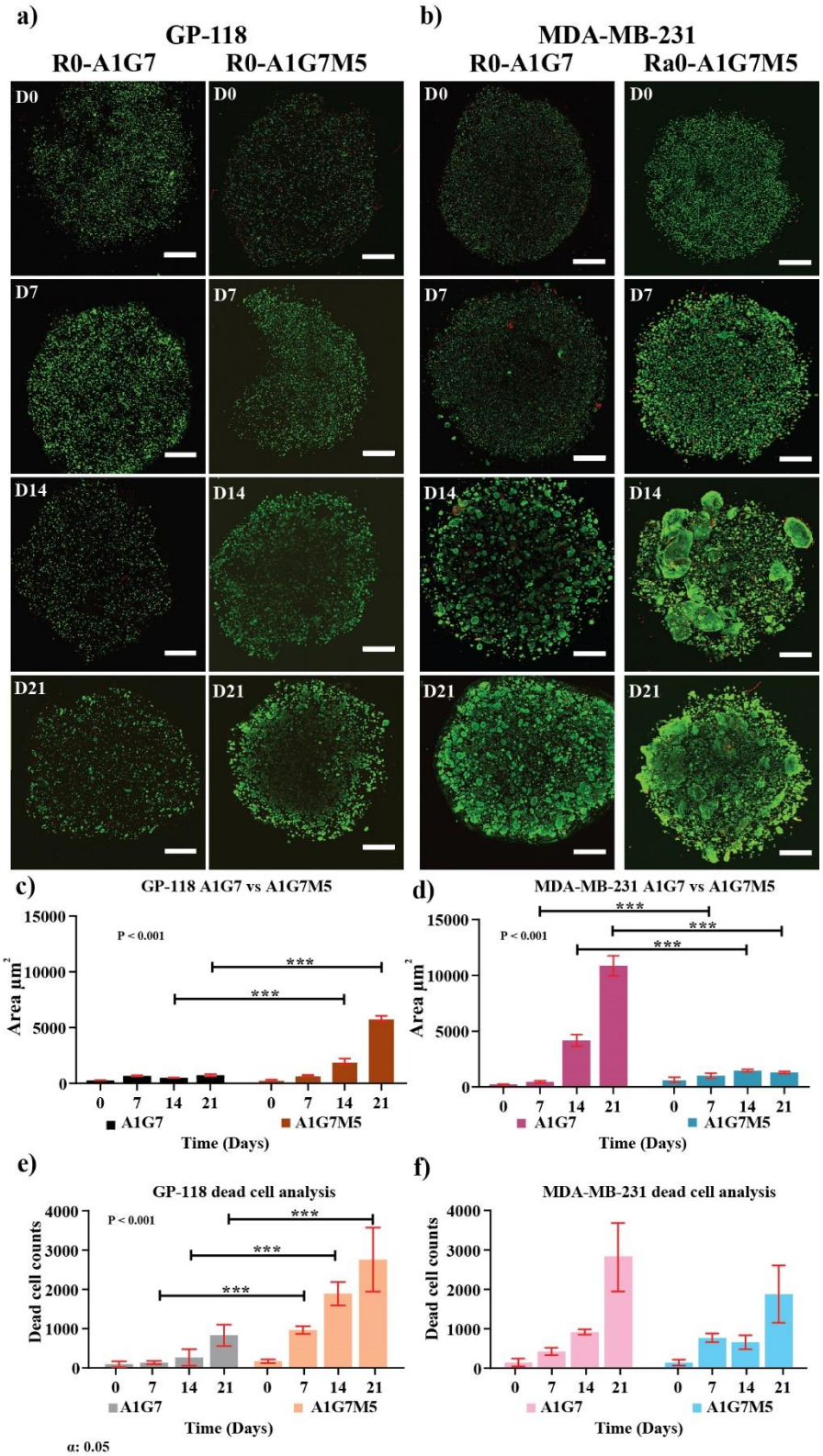
a)
GP-118
R0-A1G7
R0-A1G7M5
b)
MDA-MB-231
R0-A1G7
Ra0-A1G7M5
D0
D7
D14
D21
c)
GP-118 A1G7 vs A1G7M5
P < 0.001
Area µm²
Time (Days)
A1G7
A1G7M5
d)
MDA-MB-231 A1G7 vs A1G7M5
e)
GP-118 dead cell analysis
Dead cell counts
f)
MDA-MB-231 dead cell analysis
α: 0.05

Supporting Figure 2. Confocal Imaging of GP-118 and MDA-MB-21 cells in A1G7 and A1G7M5 bioprinted constructs. a) and b) Live/dead assay: maximum intensity projections of whole bioprinted disk models. Scale bar 1000 µm. c) and d) Surface area of spheroids vs time. Growth kinetics on A1G7 and A1G7M5: geometric mean representations. e) and f) Dead cell count analyses of MDA-MB-231 and GP-118 cells that developed within A1G7 and A1G7M5 scaffolds. For b) the arithmetic means for Day 14 and Day 21 are 3732 ± 25420 µm² and 9263.5 ± 58764.5 µm² respectively. α= 0.05.

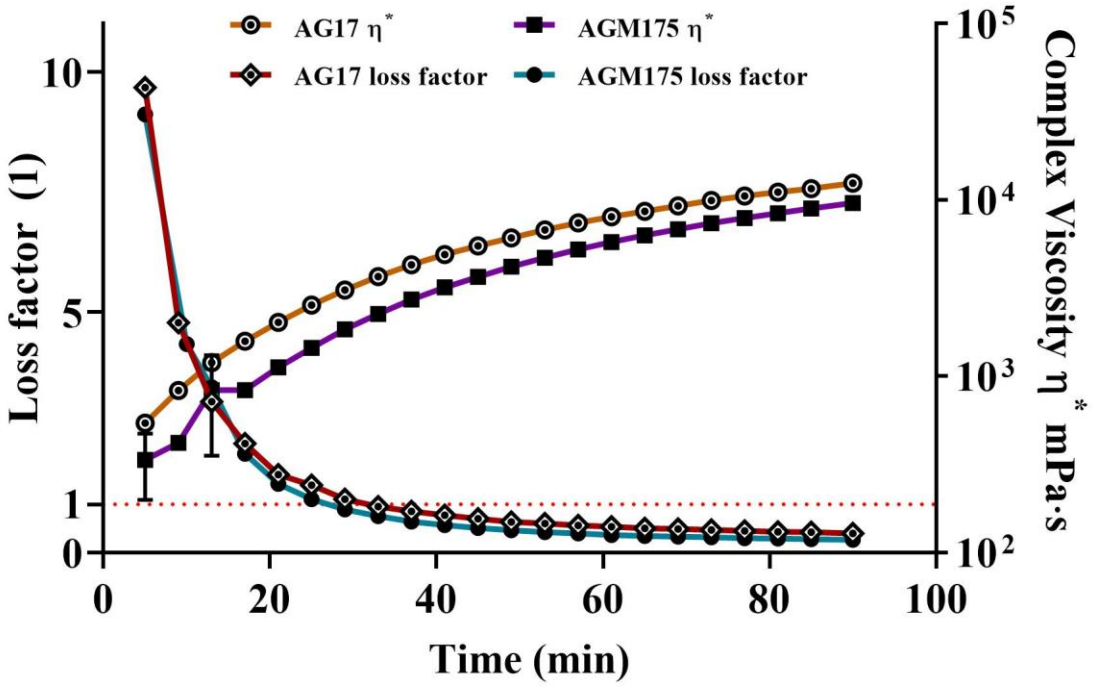

Supporting Figure 3. AxGyMz Gelation profile. Loss factor (1) and complex viscosity η^*.

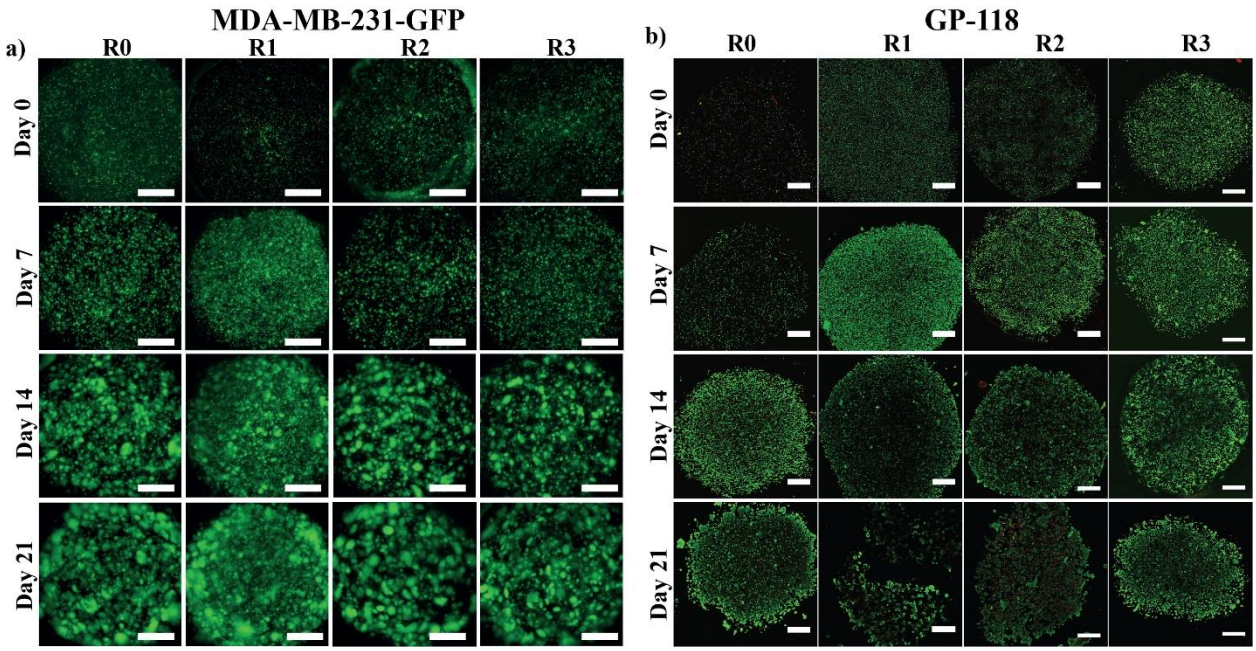

Supporting Figure 4. Iterative bioprinting results in cancer cells. Confocal Imaging. Maximum Z stack representation of whole bioprinted disks. a) MDA-MB-231-GFP cells were reprinted every 21 days in A1G7. b) GP-118 cancer cells were reprinted every 21 in A1G7M5. In green, living cells, in red, dead cells. Scale bar: 1000 μm.

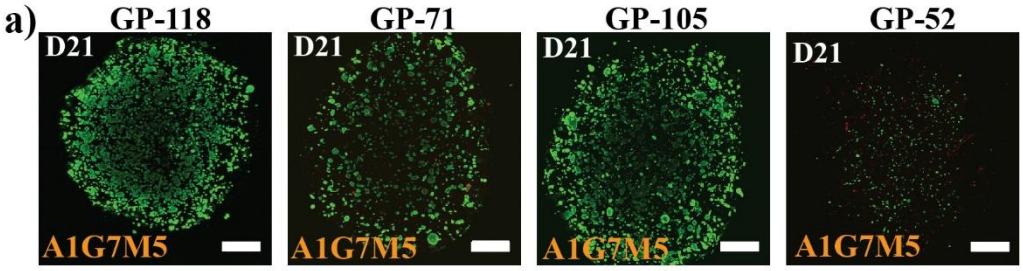

b)

Patient	Response	Tumor site	Treatment
GP-118	Poor	Proximal Stomach	DCF
GP-71	Poor	Esophagogastric junction	DCF
GP-105	Moderate	Distal third of the esophagus	DCF
GP-52	Poor	Esophagogastric junction	FLOT

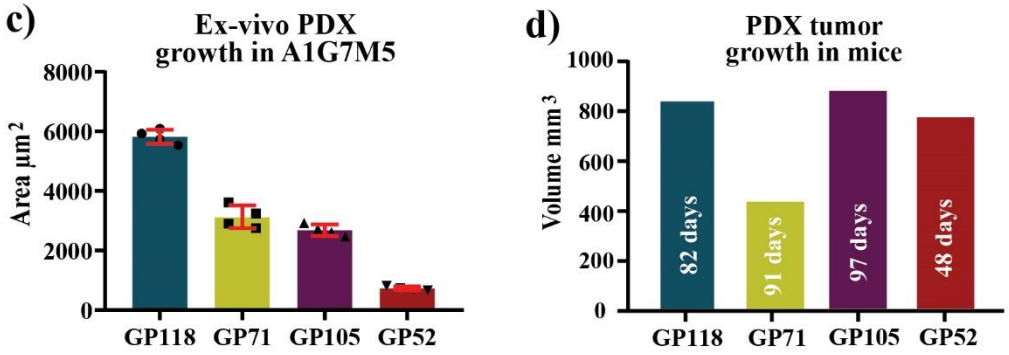

Supporting Figure 5. Comparison of patient-derived (xenograft) spheroids from different gastric cancer patients developed in bioprinted A1G7M5 constructs. a) Maximum intensity projections after 21 days of culture. Live/Dead assay. Living cells in green, dead cells in red. Scale bar 1000 µm. Growth (geometric mean) representations. b) Patient clinical history; patient's response, original tumor site, and treatment. c) PDX tumor growth in A1G7M5 constructs by day 21 of culture. d) PDX tumor growth in mice measured before extraction. Size comparison. At the time of printing (D0) single cell size was 430 microns in area.

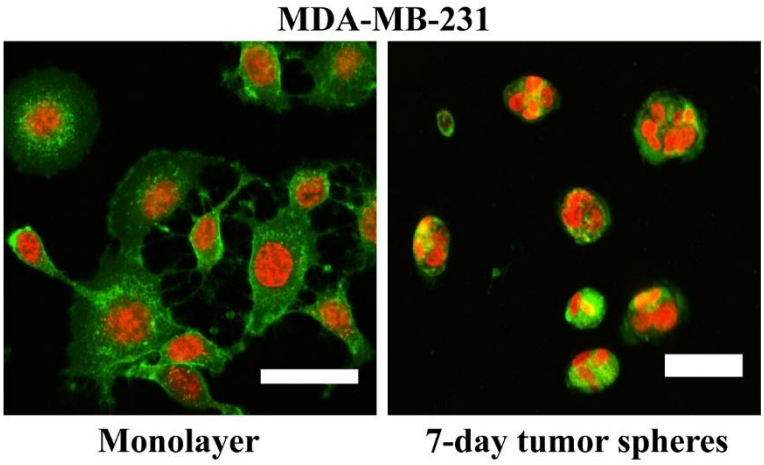

Supporting Figure 6. Doxorubicin imaging. MDA-MB-231 cells in silico and in A1G7 as spheroids exposed to 2.5 μM of Doxorubicin for 24h. CellMask™ Green Plasma Membrane Stain (ThermoFisher Scientific) was used to visualize the membrane (FITC). The fluorescent features of Doxorubicin were revealed by using an excitation wavelength of 470 nm and detecting the emitted light at 594 nm.

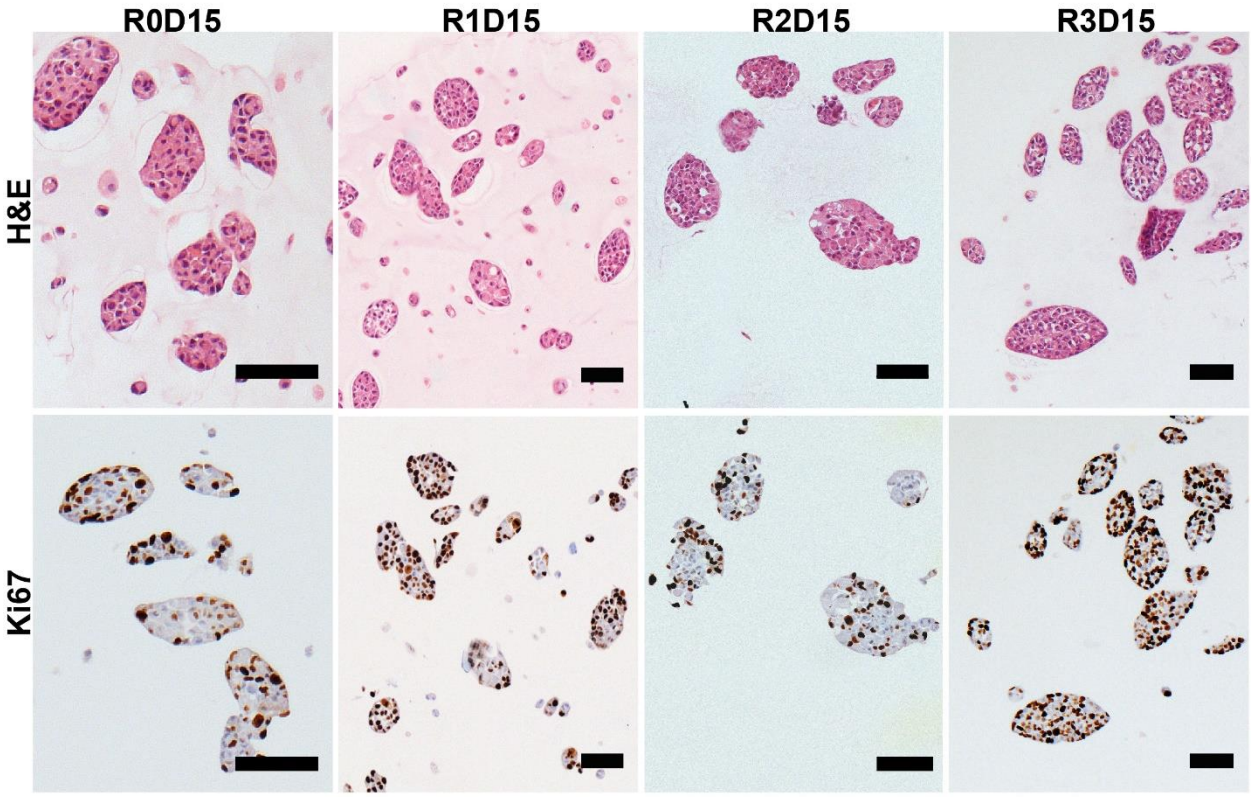

Supporting Figure 7. Immunohistochemical staining of 15-day-old MDA-MB-231 spheroids in A1G7. Top row, hematoxylin and eosin (H&E) staining the nuclei in blue-purple and extracellular matrix and cytoplasm in pink. Bottom row, Ki67 stained with the Ki67 antigen to assess cellular proliferation. Proliferative cells (interphase) are shown in brown. Scale bars = 100 μm.

Supporting Table 1 MDA-MB-231 short tandem repeat (STR) analysis and cell line validation.

MDA-MB-231	CSF1PO	D13S317	D16S539	D5S818	D7S820	THO1	TPOX	vWA
AddexBio	12,13	13	12	12	8,9	7,9.3	8,9	15,19
Before 3DBP	12,13	13	12	12	8,9	7,9.3	8,9	15,19
2D-3D D15	12,13	13	12	12	8,9	7,9.3	8,9	15,19
R1D15	12,13	13	12	12	8,9	7,9.3	8,9	15,19
R2D15	12,13	13	12	12	8,9	7,9.3	8,9	15,19
R3D15	12,13	13	12	12	8,9	7,9.3	8,9	15,19

3.2. Chapter 2: Introduction

In the following chapter, I will present the implementation of the bioprinted model and its quantitative methods developed in aims 1 and 2 to study the interactions between cancer cells and tumor-infiltrated lymphocytes (TILs). The upcoming chapter includes the second research article, which focuses on the completion of the third aim:

Aim 3: Evaluate tumor-infiltrated lymphocyte motility and activation in bioprinted co-culture constructs.

This aim will help me complete the evaluation of my initial hypothesis, which states that *extrusion bioprinting (EB) of alginate-gelatin-Matrigel-based biomaterial scaffolds will enable the study of tumor-infiltrating lymphocyte (TIL) directional motility and activation towards gastric cancer cells*. The available literature offers information on how immune cells and cancer cells interact in a liquid suspension setting. Here, however, I introduced an ECM analog that TILs need to navigate to reach the tumor zone. By using extrusion bioprinting, I will demonstrate how precise patterning of cell-laden biomaterials affords me the possibility of reconstructing heterogeneous cancer-immune cell models where complex phenomena can be studied.

Specifically, immune cell response to the presence of cancer cells is of particular importance. In this investigation, I wanted to characterize the functional activity of TILs when co-incubated with cancerous cells by evaluating the patterns of cytotoxic degranulation and protein secretion over a period of 15 days. My previously acquired knowledge f cancer cell growth patterns allowed me to draw important correlations and further hypothesize how the presence of TILs could hinder cancer cell proliferation. A

parameterized simulation was performed that evaluated the migration using experimental obtained data.

This initial demonstration will serve as the steppingstone into the future, where tissue-like biomaterials and selected cell types are used to recapitulate specific aspects of the native tumor microenvironment and the immune system's behavior is better estimated.

This upcoming chapter presents the results that correspond to the third aim of this work. Together with aim 1 and 2, aim 3 complements the cancer discovery platform by proving its usefulness in studying the immune response against cancer in an *in-vitro* model.

The manuscript in this chapter is ready to be submitted for publication.

3.3. Chapter 2. Bioprinted Multi-Component Hydrogel Co-Culture Tumor-Immune Model for Assessing and Simulating Tumor-Infiltrated Lymphocyte Migration and Functional Activation

Salvador Flores-Torres a, Nikolaos M. Dimitriou a, Lucas Antonio Pardo a, Jacqueline Kort-Mascort a, Sanjima Pal b, Omar Peza-Chavez a, Hellen Kuasne d, Julie Berube b, Nicholas Bertos c, Morag Park e,f,g,h Georgios D. Mitsis a, Lorenzo Ferri b,c, Veena Sangwan d,*, Joseph M. Kinsella a,*.

[a] Department of Bioengineering, McGill University, Montreal, Quebec, Canada.

[c] Department of Surgery, McGill University, Montreal, Quebec, Canada.

[e] Research Institute of the McGill University Health Centre (RI-MUHC)

[f] Rosalind and Morris Goodman Cancer Centre, McGill University, Montreal, Quebec, Canada.

[g] Department of Biochemistry, McGill University, Montreal, Quebec, Canada.

[h] Department of Medicine, McGill University, Montreal, Quebec, Canada.

[i] Department of Oncology, McGill University, Montreal, Quebec, Canada.

[j] Department of Pathology, McGill University, Montreal, Quebec, Canada.

* Corresponding author.

Corresponding author information:

Joseph M. Kinsella

Address line 1: 3480 University, Room 350, McConnell Engineering Building, Montreal, Quebec Address line 2: Canada, H3A 0E9

E-mail: joseph.kinsella@mcgill.ca

Field codes: Bioprinting, tumor immune microenvironment, tumor infiltrated lymphocytes, cell therapy, hydrogel

3.3.1. Abstract

The immune response against a tumor is characterized by the interplay among components of the immune system and neoplastic cells. Here, we bioprinted a model with two distinct regions containing gastric cancer patient-derived organoids (PDOs) and tumor-infiltrated lymphocytes (TILs). The initial cellular distribution allows for the longitudinal study of TIL migratory patterns concurrently with multiplexed cytokine analysis. The chemical properties of the bioink were designed to present physical barriers that immune T-cells must breech during infiltration and migration towards a tumor by using an alginate, gelatin, and basement membrane hydrogel. TIL activity, degranulation, and regulation of proteolytic activity reveal insights into the time-dependent biochemical dynamics. Regulation of the sFas and sFas-ligand present on PDOs and TILs, respectively, and the perforin and granzyme secretion confirms TIL activation when encountering PDOs. TIL migratory profiles were used to create a deterministic reaction-advection diffusion model. The simulation provides insights that decouple passive from active cell migration mechanisms used by TILs, and other adoptive cell therapeutics, as they infiltrate the tumor barrier, which is poorly understood at a mechanistic level. This study presents a pre-screening strategy for therapeutic immune cells where motility and activation within the extracellular matrix microenvironment are crucial indicators of cellular fitness.

3.3.2. Introduction

Circulating immune cells survey and promote cellular homeostasis by removing abnormal cells in a controlled manner [1] using both innate and adaptive mechanisms. During surveillance if the immune system recognizes potential threats, such as cancer, it mounts a response. [2] Antigens shed by abnormal cells are used to prime and activate T-cells. These T-cells then eradicate identified threats and mount a cyclic immune response in the tumor microenvironment. [3]

Tumors can evade destruction by using immunosuppressive strategies that favor cancer progression. [4] The activities of immune evasion mechanisms are often reflected in the geographic distribution of immune cells within and around a tumor. Generally, tumor phenotypes are categorized as immune-hot (recognized) or immune-cold (goes unrecognized). [5] Hot or inflamed tumors contain an abundant number of tumor-infiltrated lymphocytes (TILs) and are generally more responsive to immunotherapy and result in better patient outcomes.[6] The presence, type, functionality, and abundance of TILs at the margin and inside the tumor parenchyma have been directly correlated with disease progression and patient outcomes. [7-11] Conversely, cold tumors result from biomolecular and physical immunosuppressive adaptations that keep immune cells from infiltrating the tumor microenvironment. Immune-cold tumors prevent T-cells from penetrating, leading to their accumulation at the tumor margins. Moreover, immune-ignored tumors, a subvariant of cold tumors, are characterized by the absence of T-cells within and at the tumor margins.[12,13]

The ability of immune cells to migrate and infiltrate sites of malignant inflammation is among their essential roles when fighting a developing tumor.[14] T-cell motility has been

linked to improved patient outcomes by increasing immuno-surveillance and tumor recognition.[14] For T-cells to infiltrate solid tumors and migrate toward the parenchyma a chemokine gradient is regulated within the tumor-immune microenvironment (TIME).[15,16] Greater T-cell motility allows T-cells to scout, identify, swarm, and eradicate malignant neoplastic cells.[17]

Preclinical models of the TIME, including humanized immunodeficient mouse strains, undergo genetic modifications to study engrafted immune cells against engrafted tumors.[18] A popular humanized mouse model to study the interactions between human immune cells and human tumors is the human peripheral blood leucocyte (Hu-PBL) severe combined immunodeficiency disease (SCID) mouse.[19,20] This model supports the engraftment of an allogenic cell line, or human tumor tissue, and peripheral blood monocytes (PBMCs), or TILs, from the engrafted tumor tissue. The Hu-PBL-SCID model has proven useful in testing immunotherapy, such as the bispecific therapy targeting the immune checkpoint inhibitor PD-1/PD-L1 axis.

Patient-derived organoids (PDOs) cultured in soft tissue-like hydrogels have become an attractive alternative to small animal models when investigating immune response and activity in the TIME. Hydrogels can be precisely defined chemically to offer meticulous control over biomechanical signals that replicate the structural and mechanical properties of native tissue, including those akin to the TIME during cancer growth and progression.[21] By providing such precise control, hydrogels enable the creation of in vitro models that more accurately recreate the histopathology of the infiltrated immune cells in the tumor, thus significantly improving the usefulness of these models in cancer research. Numerous research groups have successfully shown that bioprinting is a

valuable tool for exerting precise spatial control over engineered cell-laden hydrogels. The outcome of this technique is the creation of highly intricate and physiologically realistic 3D models, which significantly advances the development of in vitro cancer-TIL models.[22-26]

Here, we use extrusion-based bioprinting (EBB) to model the TIME using patient-derived esophagogastric adenocarcinoma (EGA) cells and allogenic patient-derived tumor-infiltrated lymphocytes (TILs) acquired from a biopsy of a treatment-naïve EGA tumor. A mechanically defined alginate-gelatin-Matrigel hydrogel (AGM), previously used to create patient-derived models from a patient-derived EGA clinical case,[27] was used to provide a laminin-rich extracellular matrix providing a stromal-like physical barrier to infiltration to T-cells. Our previous work utilized the AGM biomaterial platform to promote ex vivo EGA organoid growth and challenged the model with standard-of-care antineoplastic therapeutics. This bioprintable model demonstrated the hydrogel's ability to promote EGA cell growth from the distal third of the esophagus to the stomach.

Here we leverage the chemical properties of the composite bioink composed of alginate, gelatin, and Matrigel that can be gently disassociated. The alginate is responsive to ionic crosslinking, imparting samples with structural integrity during culture.[28] Through the use of chelating agents such as citrate ions, we have been able to rapidly extract tumor-infiltrating lymphocytes (TILs) and cancer cells from the models to investigate viability and activation status at specified intervals. The analysis thoroughly examines the behavior of TILs and cancer cells, not only at a specific moment but also in a dynamic manner as they continually interact with one another over time.

The bioprinted model consists of a PDO core with a radially symmetric TIL containing region to evaluate TIL motility, PDO cytotoxicity, and associated cytokines. We developed a mathematical model that enables us to create a numerical representation of the co-evolution of TILs and cancer cells in co-culture. Specifically, our experimental data confirmed the algorithm's accuracy to represent motility patterns and division rates of TILs and cancer cells.

We monitored TIL functional activity by documenting degranulation events using an anti-CD107a antibody that binds to the lysosome-associated membrane protein (LAMP1), which is directly correlated to the cytotoxic activity of T-cells.[29] Using advanced multiplexed detection assays, we were able to uncover the patterns of granzyme and perforin secretion throughout 15 days of co-incubation. Granzymes are the main effector molecules utilized by T-cells to exert cytotoxicity against a target cell after perforin opens the cellular membrane of the target by inducing small pores.[30] Additionally, we observed that TILs migrated towards the cancer core of the model by day 7, corresponding to the peak in the degranulation and protein secretion. Also, an increasing concentration of soluble Fas (sFas) suggests TILs exert an immunoregulatory effect on cancer cells. EGA PDOs co-existing with TILs in the bioprinted constructs exhibited no proliferation compared to PDOs in control. Our experimental strategy offers a unique set of tools to study lymphocyte functional activity and motility in the presence of cancer cells within a controlled environment.

3.3.3. Materials and methods

Bioink manufacturing

Sodium alginate (Protanal 10/60) and type B gelatin from bovine skin (G9391, Sigma-Aldrich) powders were sterilized via UV exposure for 12 h. Alginate (4% w/v) and gelatin (10% w/v) were independently dissolved in calcium- and magnesium-free D-PBS (1x, Gibco) and mixed using a magnetic stirrer for 3 h at 37° C. Then, the alginate and gelatin gels were mixed alongside Matrigel (ThermoFisher) to create the final hydrogel precursor at a concentration of alginate 1%, gelatin 7% and Matrigel 5% (v/v) (A1G7M5).

The crosslinking solution was prepared by dissolving $CaCl_2$ (Sigma-Aldrich) in sterile ultrapure water to a final concentration of 100 mM. The calcium chelating solution was prepared by dissolving trisodium citrate (≥99.0%, Sigma-Aldrich) in ultrapure water at a final concentration of 55 mM. Both solutions were filter-sterilized (0.22 μm) and stored at 4 °C until use and used within one week of preparation.

Primary cell isolation and cell culture

Esophagogastric cancer samples were obtained from consenting patients undergoing endoscopy or surgical resection at the McGill University Health Center (MUHC). This study was approved by the MUHC Research Ethics Board (Protocol # 2007-856). A small piece of tumor was subcutaneously implanted into immunocompromised NOD-Scid IL2Rgammanull mice (Jackson Labs). All animal protocols were performed in accordance with the ethical treatment guidelines of the McGill University Animal Care Committee and the Canadian Council on Animal Care.

Once tumor volume reached 1000 mm3, mice were sacrificed, and tumors dissociated into single-cell suspensions using a Tumor Dissociation Kit (Miltenyi Biotec) in combination with the gentleMACS™ Dissociator (Miltenyi Biotec). Mouse Cell Depletion Kit (Miltenyi Biotec) was used to remove murine cells, and the remaining cells were mixed with hydrogel and grown in GEA medium as previously described.[31]

Tumor infiltrated lymphocytes were extracted from a patient with gastroesophageal adenocarcinoma following endoscopic biopsy. A board-certified pathologist defined the tumor or tumor adjacent normal tissue regions in the biopsy and transferred them in 10 cm plastic dishes on ice. Biopsy derived tissues were transferred to the lab while immersed in transport medium RPMI 1640, Gentamicin (50 ug/mL), Pen/Strep (100 U/mL), Fungizone (2.5 ug/mL). Upon arrival, tissue pieces were washed with sterile media (AD-DF+++ medium) to remove of excess blood. Necrotic parts of tumors (white and fluffy) were removed with razor blades and viable tissue pieces were moved to a new dish. Tissues were cut into small pieces (~1 mm3), and these were placed in 24 well plates with 500 µL of T-cell medium (STEMCELL Technologies, Cat. # 10981) containing interleukin-2 (IL-2) (STEMCELL Technologies, Cat. # 78063) at a concentration of 1 ng/mL and Pen/Strep (100 U/mL) (Sigma, Cat. # P4333). The tiny pieces of tissue were incubated and left undisturbed (5% CO2, 37 °C, 95% RH) except for medium changes every 5th day. Once TILs emerged from tissue to enter suspension, these were collected in 15 mL tubes, centrifuged at 500 rcf for 5 min, and recultivated. After 3 passages, TILs exhibited a consistent proliferation rate and these were slow-frozen (1°C/min) in a solution of 10% DMSO, 90% FBS and stored in liquid nitrogen.

Model design and bioprinting

We designed a three-dimensional (3D) multi-material environment that comprised of preprogramed concentric rings. The initial middle region of the model (2.4 mm internal diameter) contained EGA cancer cells surrounded by a TIL-laden region (4.4 mm external diameter). All 3D monoculture controls were bioprinted considering similar areas, geometry, and cell density. The visual graphics and printed model are presented in the result section as **Figure 1**.

Prior to 3D bioprinting, the bioinks were heated in a water bath at 37 °C for 30 min to induce their liquid phase. Freshly harvested (from PDX) cancer cells were centrifuged at 130 g for 5 min. Then, 50 µL of DMEM containing 3x106 cells were gently mixed with 1 mL of liquid A1G7M5 by pipetting. TILs were collected from suspension culture and centrifuged at 130 g for 5 min. Then, 50 µL of DMEM containing 15x106 cells were gently mixed with 1 mL of liquid A1G7M5. The cell-laden bioink was transferred into a sterile 3 cc cartridge, sealed, and centrifuged at 300 g for 3 min to eliminate gas bubbles, and introduced to ice for three minutes to induce rapid gelation.

The concentric models were printed with an extrusion pressure of 70 ± 5 kPa using 27-gauge conical nozzles. Extrusion time before the movement was set to 0.1 s, and the printing speed was 14 mm s−1. Once deposited, each model was soaked into a 100 mM CaCl2 solution for two min, rinsed twice with 1× D-PBS, placed into an agarose-coated (electrophoresis grade) twelve-well plate, and incubated at 37 °C with 5% CO2 in ½ TIL and ½ EGA medium. Samples were carefully transferred to new agarose-coated plates every sixth day, and the cell culture medium was replaced every third day.

Confocal microscopy

Sample imaging was performed using a Nikon A1 laser confocal microscope, with a Z-stack scan of 5 µm for 10X magnifications and 25 µm for 4X magnifications. Images were reconstructed using NIS-Elements Imaging software (Nikon) and ImageJ FIJI software. Orthogonal views from the regions of interest were used to quantify cell migration and behavior within the concentric co-culture environment. Anti-CD45 (FITC) and anti-CD236(APC) (Miltenyibiotech) were used to tag cells for microscopy sessions. Images were automatically stitched in the NIS-Elements Imaging software. Image segmentation (ImageJ Fiji) was applied to obtain kinetic cell growth data from confocal images. For every timepoint in the experimental series, four cell-laden constructs were randomly selected and removed from culture conditions and placed into a #1.5 polymer coverslip bottom µ-Dish (Ibidi Cat.No: 81150) and a microscopy incubator chamber (37°C, 5% CO2, and 95% relative humidity) was used throughout the acquisition time. Each sample was scanned through a 4X and 10X objective. The 4X objective was used to locate the sample, scan its overall architecture while the 10X objective was used to acquire the region of interest by stitching six consecutive images from a selected column or row across the center line.

The microscopy antibody panel was composed of anti-CD45 (FITC) and anti-CD326 (APC) (Miltenyibiotech). FACs buffer was prepared fresh in D-PBS (1X) adding FBS to a final concentration of 2% (v/v) and kept in ice during the binding process. FACs buffer was used to wash the samples twice. The antibody mix was prepared in 100 µL of FACs buffer and 2 µL of anti-CD45 and 2 µL of anti-CD326. Samples were mixed within their tube and incubated at 4C away from light for 10 min. 0.5 mL of FACs buffer was added to

each sample to wash the excess antibodies by removing and adding buffer four times. Green CMDFA and red CMPTX cell tracker dyes (Thermo Fisher Scientific. C2925 and C34552 respectively) were implemented following manufacturer's protocols and recommendations.

Fluorescent antibodies

Anti-CD45 (FITC), anti-CD8 (PEVio770), anti-CD4 (PE), anti-CD326(APC), anti-CD107a (Viogreen), and anti-GRZNB (FITC) and isotype antibodies (Miltenyi Biotech) were used to build a compensation matrix for each fluorophore within the panel. All flow cytometry experiments were conducted in a CytoFLEX flow cytometer. The machine was calibrated with quality control (QC) beads every time before an experimental readout.

Flow cytometry and cell membrane staining

FACs (2% FBS v/v) buffer was used in every step of the antibody binding process to wash, resuspend, and transport cells to the flow cytometer equipment.

Cells were recovered from suspension culture or extracted from bioprinted constructs by chelating calcium from alginate with trisodium citrate (55 mM). Centrifugation rounds were conducted at 300 g to pellet the cells. Trypsin was used in samples past day 1 where cancer cells were expected to be present in multicellular spheroid formats. Trypsin was neutralized with FACs buffer before centrifugation. All antibody staining protocols were conducted following the manufacturer's recommended protocol. Briefly, 2 µL of each antibody was added to 100 µL of FACs buffer containing cells in suspension. Samples were mixed within their tube and incubated at 4°C away from light for 10 min. 1 mL of

FACs buffer was added to each sample to wash the excess antibodies by centrifugation (twice).

Multiplex analysis of cytokines

In this study, we used Luminex xMAP technology for multiplexed quantification of 5 human cytokines, chemokines, and growth factors. The multiplexing analysis was performed using the Luminex™ 200 system (Luminex, Austin, TX, USA) by Eve Technologies Corp. (Calgary, Alberta). Five markers were simultaneously measured in the samples using Eve Technologies' Human CD8+ 5-Plex Discovery Assay® (MilliporeSigma, Burlington, Massachusetts, USA) according to the manufacturer's protocol. The 5-plex consisted of sFas, sFas Ligand, Granzyme A, Granzyme B, and Perforin. Assay sensitivities of these markers range from 0.6 – 87.7 pg/mL for the 5-plex. Individual analyte sensitivity values are available in the MilliporeSigma MILLIPLEX® MAP protocol. Cell culture medium was collected during the longitudinal studies.

Time lapse microscopy

Time lapse microscopy was performed in a Nikon A1 laser confocal microscope, with imaging intervals of 3 minutes and a 20X magnification in glycerol immersion; cells were kept under simulated cell culture conditions. Staining of cells was performed only on cancer cells with CellTracker™ Green CMFDA. A thin layer of collagen type I (100 µL) (CORNING, Cat. # 354249) was deposited on a #1.5 polymer coverslip bottom µ-Dish (Ibidi Cat.No: 81150) and allowed to dry for one hour inside the biosafety cabinet. Cancer cells were introduced on top of the collagen layer in a concentration of 2 $x10^5$ cells/mL in 150 µL of culture media. Cells were allowed to adhere to the collagen layer for 4 hours, after which the staining process started. The lyophilized stain was diluted in DMSO to a

concentration of 1mM for the stock solution. Immediately before the staining process, the stock solution was diluted in serum-free medium to a final concentration of 1 μM, and 150 μL were added to the chamber. Cells were incubated for 30 minutes, after which the staining solution was removed, and the tumor infiltrating lymphocytes were added in new growth medium at a concentration of $2x10^6$ cells/mL for immediate imaging in a 1:10 cell ratio. Statistical analyses

All experiments were conducted three different times considering biological replicates. All data points were performed in at least triplicates unless stated otherwise. Statistical analysis and plotting were conducted using GraphPad Prism 8, JMP®, Julia and MATLAB software. Data are presented as the mean value ± SD. Unless stated otherwise, comparisons were made using one-way ANOVA and the Brown-Forsythe and Welch ANOVA tests and Games-Howell for multiple comparisons tests using $P < 0.05$ as a significance indicator, unless stated otherwise. Unpaired t-test with Welch's correction considered $P < 0.05$ as a significance indicator.

Mathematical modeling

The mathematical model consists of two Partial Differential Equations (PDEs), each of which describes the spatiotemporal evolution of the cancer cell density U and TIL density T. The PDE system is presented in Equation. 1 and 2 and considers the initial conditions shown in Figure S1.

$$\frac{\partial U}{\partial t} = D_U \nabla^2 U + sU(1-U) - c_U UT \qquad (Equation.\,1)$$

$$\frac{\partial T}{\partial t} = D_U \nabla^2 T - C(x)\nabla \cdot T + KT\,\frac{U}{\Lambda + U} - c_T UT \qquad (Equation.\,2)$$

In this model, Equation. 1 is also known as the Fisher Kolmogorov Pishkunov Petrov (FKPP) equation[32,33] which is combined with a death term owing to the interaction between cancer cells and TILs. The temporal version of Equation. 2 of this model was presented in [34] to describe the dynamics of immune cells in the presence of cancer and therapy. In this study, we extended it to both spatial and temporal scales, similar to.[35] In both equations, the left-hand side represents the rate of change of the cancer cells (Equation. 1), and immune cells (Equation. 2). The terms $D_U \nabla^2 U$ and $D_U \nabla^2 T$ describe the random motion of cancer cells and TILs, respectively. The advection term $-C(x)\nabla\cdot T$ biases the movement of the TILs towards cancer cells under the assumption of a linear velocity field due to gradients of chemotactic signals spanning outward from the tumor. Therefore, C represents the velocity field of the TILs and is assumed to be a static parameter. The cancer cell density increases according to the logistic growth term $sU(1-U)$ and the TIL density according to the $KT\, U/(\Lambda+ U)$ term, which requires the presence of cancer cells to stimulate growth. The denominator of this term scales and saturates the response rate of the TILs based on the threshold constant Λ and the cancer cell density. The death terms $c_U UT$ and $c_T UT$ represent the interaction between cancer cells and TILs that results in the death of both populations with rates c_U and c_T, respectively. In addition, we neglected the natural decay of TILs, under the assumption that it has minimal contribution to the model solutions.

Numerical approximation

We approximated the model solution using the method of lines [36] which converts the system of PDEs into ODEs, and we integrated it in time using the trapezoid backward

difference, which is a second-order A-B-L-S-stable one-step explicit singly diagonal implicit Runge-Kutta (ESDIRK) method in Julia. [37,38]

Parameter estimation

We used the Improved Stochastic Ranking Evolution Strategy (ISRES) algorithm,[39] found in the NLopt package[40] in Julia software.[37] As in every evolutionary strategy algorithm, ISRES uses an array of candidate solutions that are updated based on mutation and selection rules. Mutation represents the step size between the parent solution and the offspring. In ISRES, mutation is controlled via a log-normal step size update and exponential smoothing. To avoid biases introduced by spherical symmetry assumptions,[41] the ISRES algorithm performs a differential variation step using a Nelder-Mead-like update method.[42] The selection rule is based on fitness ranking.

In this study, the fitness ranking was the sum of squared error (SSE) between the simulation and experimental data. The SSE is expressed as:

$$SSE = \sum_{i=1}^{N} \left(d_{i,k} - q_{i,k}\right)^2 \qquad (\boldsymbol{Equation\ 3})$$

where $d_{i,k}$ and $q_{i,k}$ are the cell counts of the experimental sample and simulation results, respectively, at the grid point i and dataset k. In this study, the number of candidate solutions in every step is 20 × (n + 1), where n is the number of model parameters. The performance of the model was evaluated using the normalized root mean squared error metric which is defined as:

$$NRMSE = \frac{1}{\max(u_e) - \min(u_e)} \sqrt{\frac{\sum_{i=1}^{N} \left(u_s^i - u_e^i\right)^2}{N}} \qquad (\boldsymbol{Equation\ 4})$$

where i is the spatial index of the cell density.

Uncertainty analysis

We quantified the uncertainty of the model parameters propagated as the output of the model using the Metropolis-Hastings (MH) Markov Chain Monte Carlo (MCMC) using the Turing package in Julia software. In this step, we assumed normally distributed prior distributions of the model parameters around the region of the optimal provided by the optimization algorithm which is defined as:

$$Priors \sim \mathcal{N}(\theta^*, 0.3\theta^*) \bigcap [\theta_{\boldsymbol{min}}, \theta_{\boldsymbol{max}}] \qquad (\boldsymbol{Equation\ 5})$$

At every step, the MH algorithm evaluates the likelihood of the experimental data with the resulting model output, which is:

$$D \sim MVN(, M, \sigma^2 I), \text{ where } \sigma \sim \text{InverseGamma } (6,1.4) \quad (\boldsymbol{Equation\ 6})$$

3.3.4. Results

In this work, we studied the behavior of T-cells within a compartmentalized co-culture environment containing gastric cancer cells. Despite using cells from different patients, we observed significant effects on cancer cell behavior when TILs were patterned adjacent to them. Interactions between allogenic T-cells and human tumors are have played important roles in the development of allogeneic and autologous adoptive T-cell (ATC) therapy.[43-46] In our model, we validated the functional activity and migration profile of TILs, degranulation, and cytokine release using non-destructive methods during several weeks in culture. Our results suggest that TILs exert an immunoregulatory effect on cancer cells. Although cancer cells continued to be present by day 15 of co-culture, as indicated by our flow cytometry results, control samples reveal striking differences in cell and PDO growth behavior when TILs are present in the surrounding stroma.

Biomaterial attributes

The alginate network within the biomaterial is susceptible to ionic crosslinking, providing samples with post-printing structural stability during culture and handling. By utilizing chelation agents such as citrate ions, we were able to quickly extract TILs and cancer cells and study their viability and activation status at different timepoints. Moreover, the alginate fraction of the composite defines the post-crosslinked gel mechanics in a directly proportional manner.[48] The gelatin fraction of the composite drives the reversible thermal sol-gel transitions of the bioink and enables the introduction of cells when in its liquid phase and extrusion upon gelation.[48] Also, the inclusion of gelatin increases bioactivity of the microenvironment, providing cells with anchoring sites.[49] Matrigel, a gelatinous protein mixture derived from Engelbreth-Holm-Swarm (EHS) mouse sarcoma

tumor, contains various ECM proteins including laminin collagen IV, entactin, and proteoglycans, that resemble the basement membrane and are known to interact with cells and influence their behavior.[27,50-52] Together, alginate 1% (w/v), gelatin 7% (w/v), and Matrigel 5% (v/v) constitute a viscoelastic, bioprintable and biocompatible material that enables cell recovery without influencing cell viability.

TIL cell culture and suspension killing assays.

We evaluated the cytotoxicity of patient-derived TILs in suspension against patient-derived gastric PDOs developed within the A1G7M5 hydrogel. First, TILs were cultured in suspension monoculture to increase the population numbers (**Figure S2.a**). The gastric cancer cells were grown as PDOs within an alginate-gelatin-Matrigel bioprinted model and harvested after maturing in culture for 7 days (**Figure S2.b**).[27] We co-incubated TILs and 7-day-old cancer organoids (**Figure S2.c**) with ~50k cancer cells and used cancer cell:TIL ratios to 1:0, 1:1, 1:5, 1:10, and 1:15. In **Figure S2.d** fluorescent microscopy at 24 h and 96 h timepoints where TILs (red, CMTPX) were found in close proximity to PDOs (green, CMFDA). Using flow cytometry following the gating strategy presented in **Figure S3**, we found that cancer cell viability is inversely proportional to the number of TILs in the co-culture. Significant differences in cancer cell viability relative to the control samples (PDO:TIL) are noted when cell ratios of 1:5, 1:10, and 1:15 are used (see **Figure S2.e**). TIL viability status remained above 95% (<5% PI+ cells) under these conditions, as shown in **Figure S2.f**.

Flow cytometry was used to characterize the CD8-to-CD4 ratio of TILs. As shown in **Figure S4.a**, ~93% of TILs in cell culture were CD8+, no cells expressed CD4, and ~ 3% were double positive (CD8+CD4+). We conducted time-lapse microscopy of gastric

cancer cells attached to a thin collagen layer in co-culture with TILs (1:10 ratio). Our qualitative results revealed that TILs swarm cancer cells within the first hours of co-culture (**Figure S4.b**). Changes to cell morphology of the gastric cancer cells suggest that cell integrity and viability were affected by the cytotoxic action of TILs.

Bioprinted model design

Our bioprinted co-culture model was designed considering the distribution of cells in a gastric tumor sampled from a patient biopsy. A representative immunohistochemistry image from a formalin-fixed patient sample showing the cellular distribution of esophago-gastric adenocarcinomas (**Figure S5**) was used to inform our *in vitro* bioprinted model. The microenvironmental cell distribution of a gastric tumor often contains tumor-infiltrated lymphocytes and T-cells in the stromal regions away from the tumor parenchyma. We designed our co-culture model considering the tumor core (PDO region) with an adjacent stromal compartment where T-cells are deposited (TIL region). **Figure 1.a** illustrates the details of our bioprinted model. The model has an external radius (R) of 2.2 mm and an internal radius (r) of 1.2 mm to maintain a cancer cell to TIL ratio > 1:5 and <1:15 (~72,000 TILs and ~6120 cancer cells) (**Figure 1.a**). Following deposition, regions of interest (ROIs) representing the interface between PDO and TIL regions were selected for microscopic analysis (**Figure 1.b**).

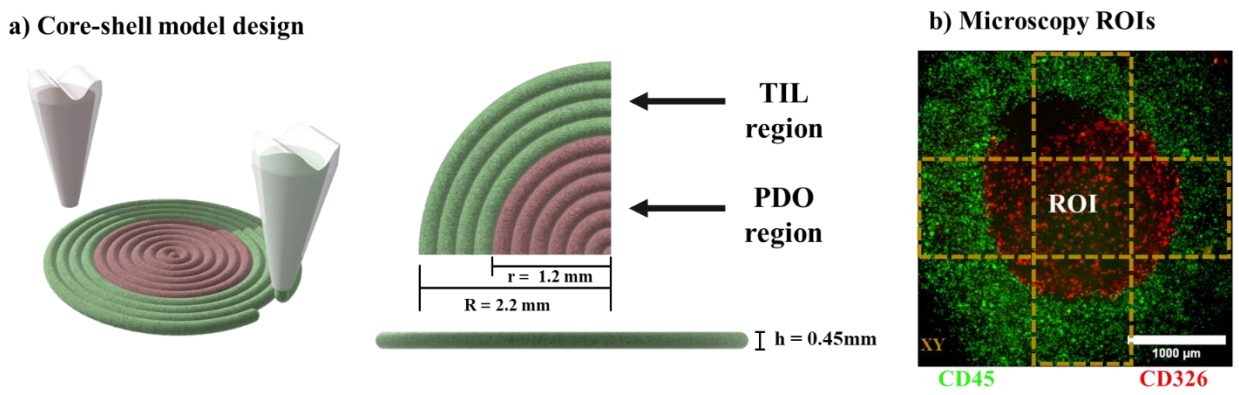

Figure 1. Bioprinted co-culture model. a) Model design and geometry. b) confocal microscopy of the bioprinted model showing the maximum intensity projection. Regions of interest (ROIs) are marked by golden lines. TILs are shown in green (CD45/FITC) and PDOs in red (CD326/APC) XY view.

The bioink was extruded at 70 ± 5 kPa, at a height of 200 µm, and its best printability was exhibited at speeds between 14 mm/s and 16 mm/s. At this pressure, strand thickness was found to be approximately 400 microns when extruded with a G27 conical nozzle. Additional layers to the model shown in **Figure 1.a** resulted in defect accumulation, material dragging, and undesired initial conditions.

The model in **Figure 1.** was bioprinted using $15x10^6$ TILs /mL and $3x10^6$ cancer cells/mL (~72,000 TILs and ~6120 cancer cells). Both cell types were individually loaded into cartridges and patterned into the proposed geometry from **Figure 1**.

Co-culture of EGA-PDOs and TILs

The experimental samples were imaged at several points during culture using confocal microscopy. **Figure 2.a** illustrates the progression of the co-culture throughout 15 days of incubation. Our results indicate that TILs migrate towards the cancer core, as seen in the TIL migratory and infiltration profiles obtained from intensity values of the

microscopy images (**Figure 2.b**). TILs in co-culture clustered into large structures once they reached the tumor core by day 7 (**Figure 2.c**) compared to TILs in monoculture **(Figure 2.d**). By day 15, significantly larger TIL aggregates were found in the center (CI 95% [656, 883] μm²) of the co-culture models compared to the outer regions (CI 95% [348, 412] μm²) (**Figure S6.a**, **b**, and **c**).

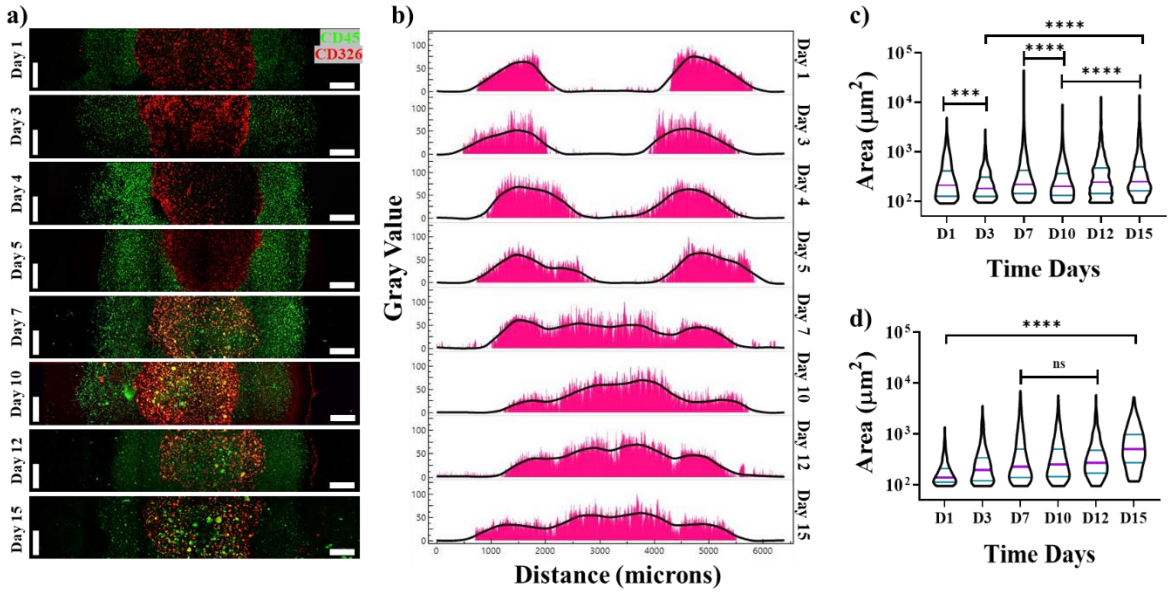

Figure 2. Bioprinted co-culture model during 15 days of growth. a) Maximum intensity projections (XY). TILs in green (CD45) and gastric cancer cells in red (CD326). Images from representative samples. b) Normalized TIL migratory profile. Normalized gray value in the Y axis. Distance in microns in the X axis. c) Co-culture TIL aggregate size in bioprinted models. d) 3D monoculture TIL aggregate size in bioprinted controls. α = 0.05. n = 7. Scalebar = 500 μm

TIL degranulation and cytokine secretion patterns

Furthermore, we evaluated TIL degranulation by immunolabeling membrane-bound CD107a in the CD8+ T-cell subset present in the TIL population at different time points.

Following the gating strategy presented in **Figure S3**, flow cytometry revealed that degranulation profiles of the TIL population within the model peaked at ~30% by day 7 and dropped to their baseline levels (~10%) by day 15 (**Figure 3.a**). These results correlate with the TIL presence in the cancer core. Moreover, we further investigated TIL degranulation phenomena by conducting a longitudinal cytokine analysis of the cell-culture media, monitoring proteolytic enzymes and perforin. We detected the presence of granzyme A, granzyme B, and perforin (**Figure 3.b**), which showed a similar temporal profile to TIL degranulation, as illustrated in **Figure 3.a**. On day 7, we observed a 4.3-fold increase in the concentration of granzyme A compared to the 3D TIL monoculture control (from 3,574 pg/ml to approximately 15,400 pg/ml). This fold increase is consistent with the pattern of degranulation shown in **Figure 3.a**, which exhibits a similar trend with a fold increase of 4.22 on day 7, considering the baseline levels depicted in **Figure S7.b** and **.e**. Moreover, granzyme A expression was significantly different by day 3 ($P<0.0013$). ANOVA analysis between control (**Figure S7.e**) and experimental measurements of granzyme B concentration revealed significant differences by days 3, 7, and 10. Despite a calculated 22-fold change, the detected concentration of granzyme B on day 7 was only 474 pg/ml (normalized to the control), as shown in **Figure S7.d**.

In addition to the granzymes, we also detected perforin in the co-culture, which exhibited a similar increasing trend over time with TIL degranulation, as demonstrated in **Figure 3.**. Perforin release experienced a 7.9-fold-increase by day 7 (15,500 pg/ml) (control sample contained 1960 pg/ml). Perforin is responsible for piercing the membrane of the target cell, and granzymes are the main effector molecules that are released from the inside of a T-cell or TIL. The use of anti-CD107a antibodies to identify degranulation

events allows the correlation of the secretion of proteolytic enzymes and perforin to the cytolytic potential and cytokine production of CD8+ T-cells. A direct correlation exists between the level of cell-surface CD107a expression after stimulation on CD8+ T-cells and their ability to kill target cells.[53] This study further shows a correlation between TIL motility towards the cancer core and TIL degranulation. The number of degranulating TILs (CD107a+) increases by the 3rd day in co-culture conditions, peaks by day 7, and goes back to baseline levels by the 15th day. Considering TIL motility, immune cells appear in greater numbers within the PDO region by day 7 and most of this region is populated by TILs by day 15. Chemoattractant molecules that serve as T-cell recruitment agents are secreted alongside proteolytic enzymes secreted during degranulation and infiltration processes.[54,55] Proteolytic enzymes, such as extracellular granzyme B, facilitate lymphocyte transmigration through the epithelium by cleaving ECM.[56]

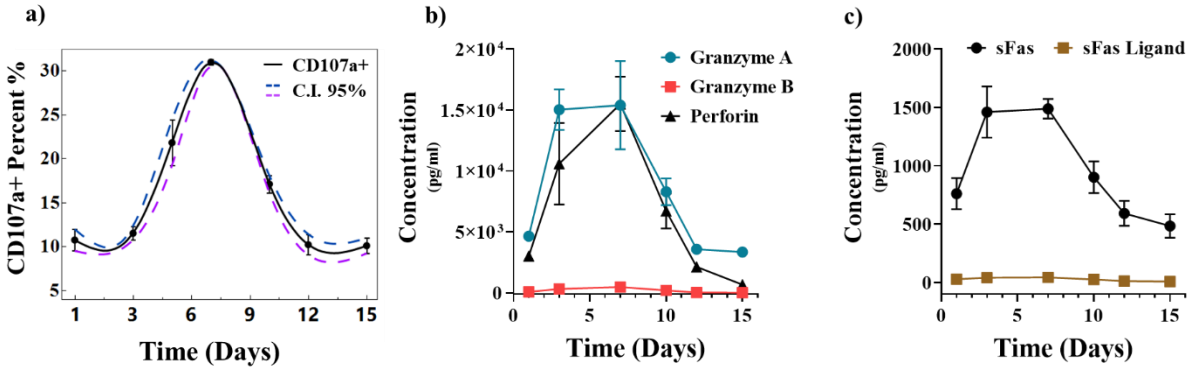

Figure 3. Longitudinal TIL activation profile in co-culture alongside cancer cells. a) TIL degranulation profile over time in co-culture conditions. Acquisitions via flow cytometry. b) Proteolytic enzymes and perforin found in co-culture medium via cytokine analysis. Granzyme A, granzyme B, and perforin (pg/ml). c) Soluble Fas and Fas ligand observed in co-culture medium (pg/ml) over time.

Finally, we evaluated soluble (s) Fas and Fas ligand (FasL) concentration during co-culture. The soluble version of Fas is the result of the natural shedding of these proteins thus, their detection in cell culture medium is possible.[57] As shown in **Figure 3.c**, sFas shedding displayed a 3.9-fold increase by day 7 following a similar trend to the degranulating molecules. sFasL however remained at basal levels displaying no significant differences as per statistical comparison of the mean values between groups (P= 0.918). Collectively, these results, including the migration of TILs, their degranulation profile, the detection of granule contents, and soluble Fas and FasL in bioprinted monocultures demonstrate that the presence of cancer cells is responsible for TIL activation in the co-culture. In solid tumors, cancer cells can develop different mechanisms to avoid Fas-mediated apoptosis. Such mechanisms include the downregulation of membrane-bound Fas receptors and the production of soluble Fas ligands (sFasL).[58-60] In our co-culture experiments, we observed an upregulation of sFas and no significant change in the concentration of sFasL. This pattern of sFas could be related to the pre-disposition of T-cells to regulate their removal to prevent uncontrolled expansion and TCR-mediated activity that could be detrimental to the host.[61] Nevertheless, the presence of FasL presenting cells, such as T-helper cells, is necessary to terminate an immune response or recruit new effector cells if needed.[62,63] Previous studies have shown that the Fas axis can either hinder the immune response by "countering" effector cells when cancer cells upregulate FasL or, it can serve as an additional pathway to induce apoptosis on the target cell.[64,65] Although we did not see an upregulation of sFasL in the co-culture over time, we initially hypothesized that cancer cells could upregulate this ligand as a way to develop a barrier for T-cells to tolerate malignancy as seen in human tumors and stroma.[66,67] Our results show that sFasL

secretion did not increase significantly compared to the control conditions. This suggests that TILs have an immunoregulatory effect on cancer cells.

TIL motility analysis

To quantify the macroscopic characteristics of TIL migration and their interaction with cancer cells, we implemented a mathematical model using **Equations 1** and **2**. We solved the forward problem using the initial and longitudinal conditions of the TIL population obtained from experimentation. To estimate the model parameters, we utilized the ISRES algorithm, which is a global optimization method to find the parameter set that minimizes the sum squared errors between experimental and simulation data. The ISRES algorithm was set to perform 10000 evaluations. To examine the uncertainty of the model parameters, we then performed Bayesian inference using the Metropolis-Hastings Markov Chain Monte Carlo (MH-MCMC) algorithm. The initial distribution of tumor cell density was assumed to be a square function because the tumor was printed in a discoid shape. To estimate the model parameters, we utilized the algorithm to find the optimal set of parameters that minimizes the Euclidean distance between experimental and simulation data points. The ISRES algorithm found the parameter values for which the resulting TIL distributions were close to the experimentally observed values. Further uncertainty quantification analysis was performed using 10 independent chains, each of them performed for 1000 MC steps (**Figure S8**). The results indicated some level of uncertainty, especially in the parameter of the cancer cells, since we used only the experimental data of TILs to calibrate the model, and cancer cells did not exhibit proliferation. The results of the parameter uncertainty analysis are presented in **Table 1** as the mean and standard deviation. To assess the propagation of the uncertainty of the

model parameters in the output, we performed 300 simulations with the parameter values drawn from their corresponding posterior distributions. The results presented in **Figure 4** show the uncertainty in the model output, which remains within acceptable levels and increases with time. The resulting normalized root mean squared error (NRMSE) between experimental data and the parametrized model was found to be 15.5 ± 8.0%, suggesting a good performance in describing the observed data.

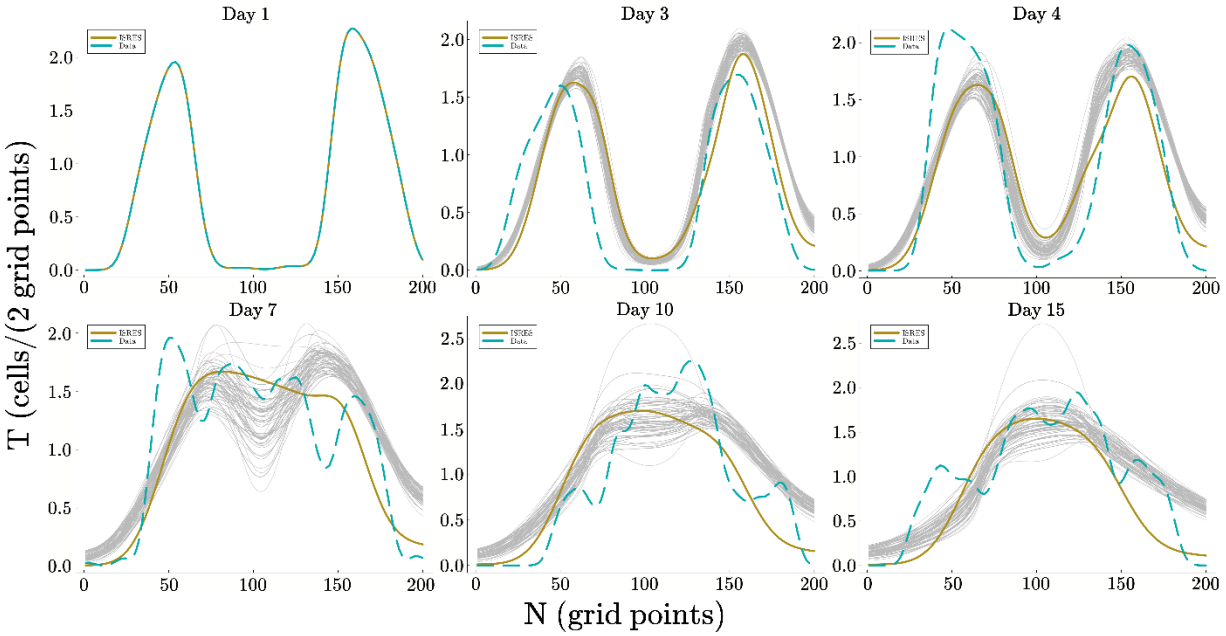

Figure 4. Propagation of the parameter uncertainty to model the TIL migratory profile. The grey lines represent 500 simulations with the parameter values drawn from their corresponding posteriors. The gold line corresponds to the results obtained from the likelihood optimization problem. The dashed cyan line corresponds to the experimental data. The distance between two consecutive grid points is 0.03 mm.

Our mathematical model resolved both active (C) and random (D_T) movement components of the TIL population in mm²/day (**Table 1**). The active movement speed was determined to be 0.13 ± 0.02 mm/day, while the passive or random movement

component appeared as 0.021 ± 0.005 mm^2/day, a complete order of magnitude below the biased movement. These velocity profiles describe active TIL migration events from the outer regions to the central region of the bioprinted construct. The model offers a TIL (K) population increment rate of 0.05 ± 0.02 day^{-1} given the presence of cancer cells. Moreover, cancer cell directed motion D_U was computed as 0.009 ± 0.004 mm^2/day, a value that fits the non-migratory behavior of cancer cells.

The estimated parameters indicate that the preferential directional movement of the TILs towards the cancer region of the bioprinted construct is considerably more pronounced than their random movement. T-cell motility *in vitro* is often described as both random and informed or directional motion.[68,69] This is observed from the values of D_T and C, which correspond to the diffusion and advection coefficients, respectively (**Table 1**).

Table 1 Parameter uncertainty analysis. Average values of the inferred model parameters and their corresponding standard deviation. The prior distributions used for the MH-MCMC were determined by truncating the results obtained from the optimization problem in a normal distribution with the average optimal value and standard deviation of 0.3× optimal value, and the bounds used to constrain the optimization.

Parameters	Units	Prior	Inferred (Mean ± SD)
σ	[cells/(0.06mm)]	InverseGamma (6,1.4)	0.38 ± 0.04
D_T	[mm²/day]	$N(0.013,0.00039) \cap [0,2]$	0.021 ± 0.005
C	[mm/day]	$N(0.013,0.00039) \cap [0,2]$	0.13 ± 0.02
K	[day⁻¹]	$N(1.3,0.4) \cap [0,2]$	0.05 ± 0.02
Λ	[cells/(0.06mm)]	$N(0.7,0.2) \cap [0,5]$	0.7 ± 0.3
C_T	[0.06 mm day⁻¹cells⁻¹]	$N(0.05,0.002) \cap [0,0.2]$	0.05 ± 0.02
D_U	[mm²/day]	$N(0.011,0.003) \cap [0,0.2]$	0.009 ± 0.004
S	[day⁻¹]	$N(0.003,0.0009) \cap [0,0.2]$	0.0028 ± 0.0009
C_U	[0.06 mm day⁻¹cells⁻¹]	$N(0.9,0.3) \cap [0,1.2]$	0.7 ± 0.2

EGA-PDO development

Through our investigation of PDO monoculture growth, we discovered that the presence of TILs (as seen through confocal microscopy with CD326-labeled EGA cells in **Figure 5.a** and **b**) resulted in less growth compared to the 3D monoculture control conditions. In the 3D bioprinted monoculture constructs, cancer cells in the control group proliferate as revealed by the increasing cell counts over time (**Figure 5.c**). In contrast, in co-culture conditions (**Figure 5.d**), PDO surface area does not increase, nor follow a defined growth pattern, as compared to the control, where PDOs developed without the presence of TILs. This phenomenon is reflected in our mathematical computation as a cancer cell proliferation rate S of 0.0028 ± 0.0009 day⁻¹ (**Table 1**). T-test evaluations between

matching day sets of control and co-culture (**Table S1**) indicate that cancer cell growth is non-statistically different during the first 3 days while it statistically differs by day 7 and after (**Figure 5.c** and **.d**).

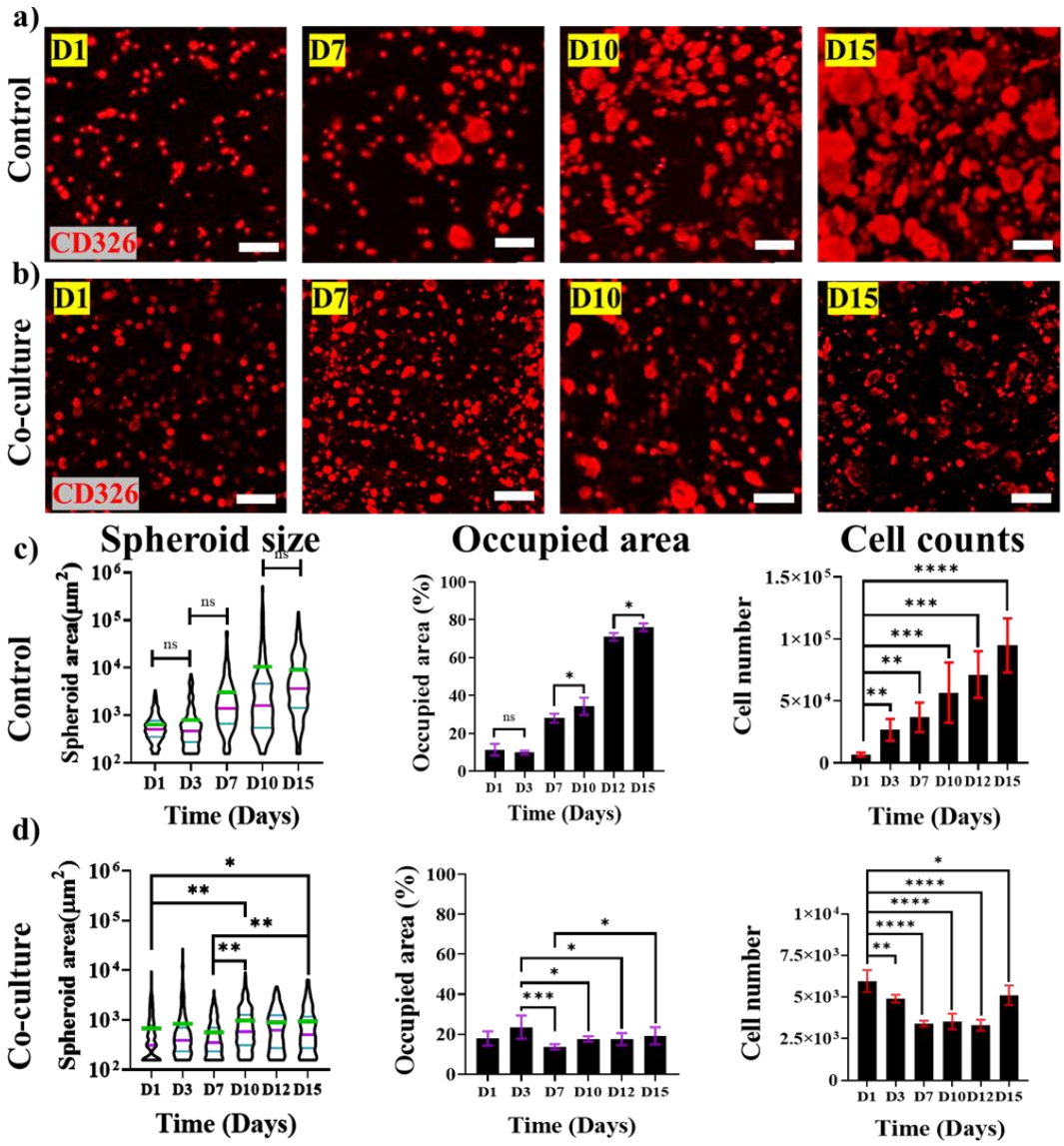

Figure 5. Growth patterns of PDO (CD326+) in co-culture and control samples. Maximum intensity projections of confocal microscopy images. a) PDO (CD326, red) in control 3D monoculture gels. b) EGA cells in co-culture conditions. c) PDO spheroid size, occupied area, and average cell numbers per sample through time (flow cytometry) of the

control 3D monoculture gels. The graphs in c) show only non-significant differences between groups, while the omitted comparisons are significantly different ($P<0.0001$). d) PDO spheroid size, occupied area, and average cell numbers per sample through time (flow cytometry) during co-culture conditions. Data from occupied areas are normalized (0-100%) to represent the available and maximum space that cells could occupy as they divide. The graph shows only the groups with statistically significant differences as indicated by Tukey's post hoc test. In violin plots, the median is shown in magenta lines, the mean value is represented by the green lines, and the quartile range is indicated by cyan lines. Non-significant comparisons are not shown. $\alpha = 0.05$. $n = 7$. Scalebars = 200 μm. Significance indicators: * for $p<0.05$, ** for $p<0.01$, *** for $p<0.001$, and **** for $p<0.0001$.

Total cancer cell counts via flow cytometry were measured from co-culture samples, and the results revealed that the population of cancer cells did not increase significantly from its baseline number of ~6,000. Under co-culture conditions, cancer cells do not proliferate into PDOs; rather, they do not appear to divide beyond their initial seeding number and exhibit a slight decrease in number (from ~6,000 cells to ~5,100 cells) throughout the 15 days of co-incubation with TILs (**Figure 5.d**). The growth trend of cancer cells in co-culture in terms of occupied area does not follow an increasing exponential pattern as compared to the control (**Figure S9.a**). In addition, the results of our algorithm in **Table 1** provide a computed rate of cancer cell death (C_U) as 0.7 ± 0.02 (0.06 mm $day^{-1}cells^{-1}$), while the proliferation of cancer cells (S) remains small and almost negligible (0.0028 ± 0.0009 day^{-1}), which also depends on the presence of TILs.

Furthermore, the number of cancer cells present in the core within the first 24 h is theoretically estimated to be 6,120 cells in 2mm^3 (2μL) of patterned bioink in the central region of the construct. Flow cytometry analysis of the total cell counts in control samples indicated 5,957 ± 658 cancer cells in the central region on day 1. By day 15, cancer cells co-cultured with TILs did not significantly increase in number (5,100 ± 595), while those in control conditions (where TILs are absent) followed an exponential growth trend, exhibiting a doubling time of 4.4 to 6.2 days (R^2 = 0.9) (**Figure S9.b**) as the total cell numbers increased from an average of 6,598 ± 1,540 cells at day 1 to 105,133 ± 10,215 cells by day 15 (**Figure 5.c**).

These results suggest that in our model, TILs affect the growth and proliferation of cancer cells. We hypothesize that this is the result of an immunoregulatory effect exerted by T-cells in the stroma since T-cell degranulation releases cytotoxic enzymes against target cells or released as the result of TIL stimulation.

Microscopy (**Figure 5.a** and **.b** and **Table S1**) and flow cytometry (**Figure 5.c** and **.d**) results indicate that cancer cells do not increase in numbers during the 15 days of co-incubation with TILs. Together, these results support the hypothesis that cancer cells in 3D co-culture do not proliferate when co-incubated with TILs. One of the challenges that effector cells face when reaching a tumor site is the presence of an immunosuppressive stroma that hinders infiltration and the cytotoxic effect of T-cells through cytokine stimulation and protein binding. Some of these immune evasion mechanisms that tumor cells employ to avoid eradication include the overexpression of membrane proteins such as the programmed death ligand-1 (PDL-1) protein, Fas ligands (FasL) to bind to Fas and induce T-cell apoptosis, and CTLA4 binding site that promotes T-cell anergy.[44]

Malignant tumors remodel their adjacent microenvironment as they progress, introducing heterogeneity that can create physical barriers, hindering the effectiveness of the mounted immune response.[70,71] Using bioprinting techniques, we incorporate these physical barriers in the form of fibrous ECM-rich regions of our bioink. The composition of biomolecules, the mechanical properties, and the heterogeneous cellular populations of tumors have critical roles in tumor progression and prognosis. For instance, solid tumors with dense, fibrous ECM networks can influence the fate of tumor-infiltrating T-cells and their migration patterns.[72,73] A common characteristic of immune evading tumors is its immunosuppressive stroma,[74,75] which is characterized by immune cells that promote tumorigenesis.[75] Future versions of this model could incorporate those cells found in the immunosuppressive or immune-promoting TME. Specifically, the inclusion exhausted T-cells,[76] M2 macrophages,[77] B-cells,[78,79] and N2 neutrophils,[80] which have lesser understood mechanistic roles in cancer progression, cancer immune evasion, immunosuppression, and microenvironmental remodeling.[75] The mechanical properties of human tumors include their solid stress, interstitial fluid pressure, ECM stiffness, and distinctive microarchitectures[81] can be defined by the material formulation used to build the tumor and stromal compartments. Different weight fractions of alginate, gelatin, and extracellular matrix polymers have been proven useful to modulate the stiffness and bioactivity of bioprinted cell-laden constructs.[27,48]

Implementing a mathematical model enables us to optimize the experimental design. For instance, the model suggests a small T-cell (K) population increment rate of 0.05 ± 0.02 day^{-1} given the presence of cancer cells. This parameter K provides an estimate of the recruitment rate of new TILs by an active immune system, as would occur physiologically.

Parametrizing these settings describes an immune response by introducing a finite number of cells either by perfusion, medium changes, or material aggregation. Also, mathematical modeling offers a way to keep track of and further control changes in the system that occur during culture. Changes in the migration velocity, infiltration patterns, and cell population densities are not only identified but could be predicted. For example, additional predictions of the cancer density profiles suggested that the tumor area does not shrink in space, however, it becomes less dense, suggesting that TILs would act both on the tumor periphery and also within its volume (**Figure S10**). As more patient-derived samples become available for analysis, future simulations will possess greater significance and we expect our model to reduce the NRMSE metric and become an even more robust descriptor of the experimental phenomena.

Overall, our bioprinted model provides a window to study immune cell motility and activation in the presence of cancer cells. We demonstrated that TILs not only actively move towards the cancer compartment of the model, but these also increase their degranulation signature as they populate the cancer core. Moreover, our data suggests a direct correlation between T-cell activity and motility.

3.3.5. Conclusions

We present an engineered co-culture model to study TIL infiltration, motility, and cytotoxicity in a solid esophagogastric adenocarcinoma tumor model grown in a mechanically defined alginate-gelatin-basement membrane hydrogel. Our model introduces a three-dimensional model format to evaluate TIL infiltration, motility, and cytotoxicity, which are often conducted in suspension cultures without the physical barrier formed by the extracellular matrix *in vivo*. Our approach involves using EGA cells

and tumor-infiltrating lymphocytes that are obtained directly from the patient. This makes our model useful for precision therapy and enhances its potential for clinical translation. The formulation of the bioink (alginate-gelatin-Matrigel) provides a matrix that can undergo co-culture for long periods while also enabling cells and PDOs to be isolated via a gentle dissociation process for downstream processing. Overall, our bioprinted PDO:TIL co-culture model integrated with a descriptive and predictive algorithm provides access to non-destructive longitudinal experimental measurements to better achieve mechanistic insight into the migration and cytotoxic outcomes of immune cell therapies in patient-derived models that may reduce or replace small animal pre-clinical models.

3.3.6. Acknowledgements:

We thank those patients who consented to participate in this study. We thank the BioBank Technology Platforms of the Research Institute of the McGill University Health Centre and staff for providing services and assistance with tissue procurement. Grant support for this project was provided by the Cancer Research Society (CRS) to V.S. and L.F. JMK thanks the Natural Sciences and Engineering Research Council of Canada (RGPIN-2020-05692) for funding. SFT thanks the FRQNT (291010) and the McGill Engineering Doctoral Award (90025) for scholarship funding. JKM thanks the FRQNT (288490) and the McGill Engineering Doctoral Award (90025) for scholarship funding. **Author contributions:** SFT, JMK, and VS conceived the original ideas, designed the research study, and interpreted the results. SFT maintained cells in culture conditions, prepared biomaterials, conducted bioprinting, acquired data in all experiments, conducted statistical analyses, interpreted results, and wrote the first draft of this manuscript. NMD designed and implemented mathematical model, conducted calibration analyses, and

formulated analysis reports. LAP maintained cells in culture conditions, acquired the biological replicates for this investigation, and verified all the analyses. JKM reviewed the results, helped in preparing the figures, and interpreted the results. SP stablished the T-cell lines prior to experimentation and helped in the selection of the antibody panels. OPC reconstructed 3D images and performed initial analyses. HK stablished the PDX lines in MP laboratory. JB isolated T-cells from primary tissue. NB provided his expertise throughout this project and provided the histological data. MP provided PDX-derived cells and expertise in 3D cell biology techniques. GM provided his expertise in mathematical modeling and algorithm design. LF provided his clinical expertise and insights to this project. All authors discussed the conclusions and commented on the manuscript.

Competing interests: The authors declare that they have no competing interests.

3.3.7. References:

1 Chaplin, D. D. Overview of the immune response. *Journal of Allergy and Clinical Immunology* 125, S3-S23 (**2010**). https://doi.org:10.1016/j.jaci.2009.12.980

2 Gonzalez, H., Hagerling, C. & Werb, Z. Roles of The Immune System in Cancer: From Tumor Initiation to Metastatic Progression. *Genes Dev* 32, 1267-1284 (**2018**). https://doi.org:10.1101/gad.314617.118

3 Chen, D. S. & Mellman, I. Oncology Meets Immunology: The Cancer-Immunity Cycle. *Immunity* 39, 1-10 (**2013**). https://doi.org:10.1016/j.immuni.2013.07.012

4 Beatty, G. L. & Gladney, W. L. Immune Escape Mechanisms as a Guide for Cancer Immunotherapy. *Clinical Cancer Research* 21, 687-692 (**2015**). https://doi.org:10.1158/1078-0432.ccr-14-1860

5 van der Woude, L. L., Gorris, M. A. J., Halilovic, A., Figdor, C. G. & de Vries, I. J. M. Migrating into the Tumor: a Roadmap for T Cells. *Trends in Cancer* 3, 797-808 (**2017**). https://doi.org:https://doi.org/10.1016/j.trecan.2017.09.006

6 Binnewies, M., Roberts, E. W., Kersten, K., Chan, V., Fearon, D. F., Merad, M., Coussens, L. M., Gabrilovich, D. I., Ostrand-Rosenberg, S., Hedrick, C. C., Vonderheide, R. H., Pittet, M. J., Jain, R. K., Zou, W., Howcroft, T. K., Woodhouse, E. C., Weinberg, R. A. & Krummel, M. F. Understanding the Tumor Immune Microenvironment (TIME) for Effective Therapy. *Nature Medicine* 24, 541-550 (**2018**). https://doi.org:10.1038/s41591-018-0014-x

7 Li, F., Li, C., Cai, X., Xie, Z., Zhou, L., Cheng, B., Zhong, R., Xiong, S., Li, J., Chen, Z., Yu, Z., He, J. & Liang, W. The Association Between CD8+ Tumor-Infiltrating Lymphocytes and the Clinical Outcome of Cancer Immunotherapy: A Systematic Review and Meta-Analysis. *eClinicalMedicine* 41, 101134 (**2021**). https://doi.org:10.1016/j.eclinm.2021.101134

8 Miyashita, M., Sasano, H., Tamaki, K., Hirakawa, H., Takahashi, Y., Nakagawa, S., Watanabe, G., Tada, H., Suzuki, A., Ohuchi, N. & Ishida, T. Prognostic Significance

of Tumor-Infiltrating CD8+ and FOXP3+ Lymphocytes in Residual Tumors and Alterations in These Parameters after Neoadjuvant Chemotherapy in Triple-Negative Breast Cancer: a Retrospective Multicenter Study. *Breast Cancer Research* 17 (**2015**). https://doi.org:10.1186/s13058-015-0632-x

9 Pagès, F., Galon, J., Dieu-Nosjean, M. C., Tartour, E., Sautès-Fridman, C. & Fridman, W. H. Immune Infiltration in Human Tumors: A Prognostic Factor that Should not be Ignored. *Oncogene* 29, 1093-1102 (**2010**). https://doi.org:10.1038/onc.2009.416

10 Oble, D. A., Loewe, R., Yu, P. & Mihm, M. C., Jr. Focus on TILs: Prognostic Significance of Tumor Infiltrating Lymphocytes in Human Melanoma. *Cancer Immunity* 9 (**2009**). https://doi.org:10.1158/1424-9634.Dcl-3.9.1

11 Mlecnik, B., Bindea, G., Pagès, F. & Galon, J. Tumor Immunosurveillance in Human Cancers. *Cancer and Metastasis Reviews* 30, 5-12 (**2011**). https://doi.org:10.1007/s10555-011-9270-7

12 Bonaventura, P., Shekarian, T., Alcazer, V., Valladeau-Guilemond, J., Valsesia-Wittmann, S., Amigorena, S., Caux, C. & Depil, S. Cold Tumors: A Therapeutic Challenge for Immunotherapy. *Front Immunol* 10, 168 (**2019**). https://doi.org:10.3389/fimmu.2019.00168

13 Liu, Y. T. & Sun, Z. J. Turning Cold Tumors into Hot Tumors by Improving T-cell Infiltration. *Theranostics* 11, 5365-5386 (**2021**). https://doi.org:10.7150/thno.58390

14 Kim, R., Emi, M. & Tanabe, K. Cancer Immunoediting from Immune Surveillance to Immune Escape. *Immunology* 121, 1-14 (**2007**). https://doi.org:10.1111/j.1365-2567.2007.02587.x

15 Kohli, K., Pillarisetty, V. G. & Kim, T. S. Key Chemokines Direct Migration of Immune Cells in Solid Tumors. *Cancer Gene Therapy* 29, 10-21 (**2022**). https://doi.org:10.1038/s41417-021-00303-x

16 Franciszkiewicz, K., Boissonnas, A., Boutet, M., Combadière, C. & Mami-Chouaib, F. Role of Chemokines and Chemokine Receptors in Shaping the Effector Phase of the Antitumor Immune Response. *Cancer Research* 72, 6325-6332 (**2012**). https://doi.org:10.1158/0008-5472.Can-12-2027

17 Kuczek, D. E., Larsen, A. M. H., Thorseth, M. L., Carretta, M., Kalvisa, A., Siersbæk, M. S., Simões, A. M. C., Roslind, A., Engelholm, L. H., Noessner, E., Donia, M., Svane, I. M., Straten, P. T., Grøntved, L. & Madsen, D. H. Collagen Density Regulates the Activity of Tumor-Infiltrating T cells. *J Immunother Cancer* 7, 68 (**2019**). https://doi.org:10.1186/s40425-019-0556-6

18 Chuprin, J., Buettner, H., Seedhom, M. O., Greiner, D. L., Keck, J. G., Ishikawa, F., Shultz, L. D. & Brehm, M. A. Humanized Mouse Models for Immuno-Oncology Research. *Nature Reviews Clinical Oncology* (**2023**). https://doi.org:10.1038/s41571-022-00721-2

19 Pearson, T., Greiner, D. L. & Shultz, L. D. Creation of "Humanized" Mice to Study Human Immunity. *Curr Protoc Immunol* Chapter 15, 15.21.11-15.21.21 (**2008**). https://doi.org:10.1002/0471142735.im1521s81

20 Morton, J. J., Alzofon, N. & Jimeno, A. The Humanized Mouse: Emerging Translational Potential. *Mol Carcinog* 59, 830-838 (**2020**). https://doi.org:10.1002/mc.23195

21 Baruffaldi, D., Palmara, G., Pirri, C. & Frascella, F. 3D Cell Culture: Recent Development in Materials with Tunable Stiffness. *ACS Applied Bio Materials* 4, 2233-2250 (**2021**). https://doi.org:10.1021/acsabm.0c01472

22 Dey, M., Kim, M. H., Dogan, M., Nagamine, M., Kozhaya, L., Celik, N., Unutmaz, D. & Ozbolat, I. T. Chemotherapeutics and CAR-T Cell-Based Immunotherapeutics Screening on a 3D Bioprinted Vascularized Breast Tumor Model. *Adv Funct Mater* 32, 2203966 (**2022**). https://doi.org:https://doi.org/10.1002/adfm.202203966

23 Dey, M., Kim, M. H., Nagamine, M., Karhan, E., Kozhaya, L., Dogan, M., Unutmaz, D. & Ozbolat, I. T. Biofabrication of 3D Breast Cancer Models for Dissecting the Cytotoxic Response of Human T cells Expressing Egineered MAIT Cell Receptors. *Biofabrication* 14, 044105 (**2022**). https://doi.org:10.1088/1758-5090/ac925a

24 Grolman, J. M., Zhang, D., Smith, A. M., Moore, J. S. & Kilian, K. A. Rapid 3D Extrusion of Synthetic Tumor Microenvironments. *Advanced Materials* 27, 5512-5517 (**2015**). https://doi.org:10.1002/adma.201501729

25 Heinrich, M. A., Bansal, R., Lammers, T., Zhang, Y. S., Michel Schiffelers, R. & Prakash, J. 3D-Bioprinted Mini-Brain: A Glioblastoma Model to Study Cellular Interactions and Therapeutics. *Advanced Materials* 31, 1806590 (**2019**). https://doi.org:10.1002/adma.201806590

26 Morley, C. D., Flores, C. T., Drake, J. A., Moore, G. L., Mitchell, D. A. & Angelini, T. E. Spatiotemporal T cell Dynamics in a 3D Bioprinted Immunotherapy Model. *Bioprinting* 28, e00231 (**2022**). https://doi.org:https://doi.org/10.1016/j.bprint.2022.e00231

27 Flores-Torres, S., Peza-Chavez, O., Kuasne, H., Munguia-Lopez, J. G., Kort-Mascort, J., Ferri, L., Jiang, T., Rajadurai, C. V., Park, M., Sangwan, V. & Kinsella, J. M. Alginate–gelatin–Matrigel hydrogels Enable the Development and Multigenerational Passaging of Patient-Derived 3D Bioprinted Cancer Spheroid Models. *Biofabrication* 13, 025001 (**2021**). https://doi.org:10.1088/1758-5090/abdb87

28 Andersen, T., Auk-Emblem, P. & Dornish, M. 3D Cell Culture in Alginate Hydrogels. *Microarrays (Basel)* 4, 133-161 (**2015**). https://doi.org:10.3390/microarrays4020133

29 Aktas, E., Kucuksezer, U. C., Bilgic, S., Erten, G. & Deniz, G. Relationship Between CD107a Expression and Cytotoxic Activity. *Cell Immunol* 254, 149-154 (**2009**). https://doi.org:10.1016/j.cellimm.2008.08.007

30 Weigelin, B., den Boer, A. T., Wagena, E., Broen, K., Dolstra, H., de Boer, R. J., Figdor, C. G., Textor, J. & Friedl, P. Cytotoxic T cells are Able to Efficiently Eliminate Cancer Cells by Additive Cytotoxicity. *Nature Communications* 12, 5217 (**2021**). https://doi.org:10.1038/s41467-021-25282-3

31 Sato, T., Vries, R. G., Snippert, H. J., van de Wetering, M., Barker, N., Stange, D. E., van Es, J. H., Abo, A., Kujala, P., Peters, P. J. & Clevers, H. Single Lgr5 Stem Cells Build Crypt-Villus Structures In Vitro Without a Mesenchymal Niche. *Nature* 459, 262-265 (**2009**). https://doi.org:10.1038/nature07935

32 Murray, J. D. *Mathematical Biology II: Spatial Models and Biomedical Applications*. Vol. 3 (Springer New York, **2001**).

33 Murray, J. D. *Mathematical biology: I. An introduction*. (Springer, **2002**).

34 De Pillis, L. G. & Radunskaya, A. A Mathematical Tumor Model with Immune Resistance and Drug Therapy: An Optimal Control Approach. *Journal of Theoretical Medicine* 3, 318436 (**2001**). https://doi.org:10.1080/10273660108833067

35 Matzavinos, A., Chaplain, M. A. & Kuznetsov, V. A. Mathematical Modelling of the Spatio-Temporal Response of Cytotoxic T-lymphocytes to a Solid Tumour. *Math Med Biol* 21, 1-34 (**2004**). https://doi.org:10.1093/imammb/21.1.1

36 Lee, H. J. & Schiesser, W. E. *Ordinary and Partial Differential Equation Routines in C, C++, Fortran, Java, Maple, and MATLAB*. (Chapman and Hall/CRC, **2003**).

37 Bezanson, J., Karpinski, S., Shah, V. B. & Edelman, A. Julia: A fast dynamic language for technical computing. *arXiv preprint arXiv:1209.5145* (**2012**).

38 Rackauckas, C. & Nie, Q. DifferentialEquations.jl – A Performant and Feature-Rich Ecosystem for Solving Differential Equations in Julia. *Journal of Open Research Software* 5, 15 (**2017**). https://doi.org:10.5334/jors.151

39 Runarsson, T. P. & Xin, Y. Search Biases in Constrained Evolutionary Optimization. *IEEE Transactions on Systems, Man, and Cybernetics, Part C (Applications and Reviews)* 35, 233-243 (**2005**). https://doi.org:10.1109/TSMCC.2004.841906

40 Johnson, S. G. The NLopt Nonlinear-Optimization Package (**2014**).

41 Salomon, R. Some Comments on Evolutionary Algorithm Theory. *Evolutionary Computation* 4, 405-415 (**1996**).

42 Nelder, J. A. & Mead, R. A simplex Method for Function Minimization. *The Computer Journal* 7, 308-313 (**1965**).

43 Gomez, G. G., Read, S. B., Gerschenson, L. E., Santoli, D., Zweifach, A. & Kruse, C. A. Interactions of the Allogeneic Effector Leukemic T cell line, TALL-104, with Human Malignant Brain Tumors. *Neuro Oncol* 6, 83-95 (**2004**). https://doi.org:10.1215/s1152851703000140

44 Waldman, A. D., Fritz, J. M. & Lenardo, M. J. A Guide to Cancer Immunotherapy: from T cell Basic Science to Clinical Practice. *Nature Reviews Immunology* 20, 651-668 (**2020**). https://doi.org:10.1038/s41577-020-0306-5

45 Benjamin, R., Graham, C., Yallop, D., Jozwik, A., Mirci-Danicar, O. C., Lucchini, G., Pinner, D., Jain, N., Kantarjian, H., Boissel, N., Maus, M. V., Frigault, M. J., Baruchel, A., Mohty, M., Gianella-Borradori, A., Binlich, F., Balandraud, S., Vitry, F., Thomas, E., Philippe, A., Fouliard, S., Dupouy, S., Marchiq, I., Almena-Carrasco, M., Ferry, N., Arnould, S., Konto, C., Veys, P. & Qasim, W. Genome-Edited, Donor-Derived Allogeneic Anti-CD19 Chimeric Antigen Receptor T cells in Paediatric and Adult B-cell Acute Lymphoblastic Leukaemia: Results of Two Phase 1 Studies. *Lancet* 396, 1885-1894 (**2020**). https://doi.org:10.1016/s0140-6736(20)32334-5

46 Hu, Y., Zhou, Y., Zhang, M., Zhao, H., Wei, G., Ge, W., Cui, Q., Mu, Q., Chen, G., Han, L., Guo, T., Cui, J., Jiang, X., Zheng, X., Yu, S., Li, X., Zhang, X., Chen, M., Li,

X., Gao, M., Wang, K., Zu, C., Zhang, H., He, X., Wang, Y., Wang, D., Ren, J. & Huang, H. Genetically modified CD7-targeting allogeneic CAR-T Cell Therapy with Enhanced Efficacy for Relapsed/Refractory CD7-Positive Hematological Malignancies: a Phase I Clinical Study. *Cell Research* 32, 995-1007 (**2022**). https://doi.org:10.1038/s41422-022-00721-y

47 Schloßmacher, U., Schröder, H. C., Wang, X., Feng, Q., Diehl-Seifert, B., Neumann, S., Trautwein, A. & Müller, W. E. G. Alginate/Silica Composite Hydrogel as A Potential Morphogenetically Active Scaffold for Three-Dimensional Tissue Engineering. *RSC Advances* 3, 11185 (**2013**). https://doi.org:10.1039/c3ra23341c

48 Jiang, T., Munguia-Lopez, J. G., Gu, K., Bavoux, M. M., Flores-Torres, S., Kort-Mascort, J., Grant, J., Vijayakumar, S., De Leon-Rodriguez, A., Ehrlicher, A. J. & Kinsella, J. M. Engineering Bioprintable Alginate/Gelatin Composite Hydrogels with Tunable Mechanical and Cell Adhesive Properties to Modulate Tumor Spheroid Growth Kinetics. *Biofabrication* 12, 015024 (**2019**). https://doi.org:10.1088/1758-5090/ab3a5c

49 Davidenko, N., Schuster, C. F., Bax, D. V., Farndale, R. W., Hamaia, S., Best, S. M. & Cameron, R. E. Evaluation of Cell Binding to Collagen and Gelatin: a Study of the Effect of 2D and 3D Architecture and Surface Chemistry. *J Mater Sci Mater Med* 27, 148 (**2016**). https://doi.org:10.1007/s10856-016-5763-9

50 Debnath, J. & Brugge, J. S. Modelling Glandular Epithelial Cancers in Three-Dimensional Cultures. *Nature Reviews Cancer* 5, 675-688 (**2005**). https://doi.org:10.1038/nrc1695

51 Hughes, C. S., Postovit, L. M. & Lajoie, G. A. Matrigel: a complex protein mixture required for optimal growth of cell culture. *Proteomics* 10, 1886-1890 (**2010**). https://doi.org:10.1002/pmic.200900758

52 Kleinman, H. K. & Martin, G. R. Matrigel: Basement Membrane Matrix with Biological Activity. *Seminars in Cancer Biology* 15, 378-386 (**2005**). https://doi.org:https://doi.org/10.1016/j.semcancer.2005.05.004

53 Rubio, V., Stuge, T. B., Singh, N., Betts, M. R., Weber, J. S., Roederer, M. & Lee, P. P. Ex vivo Identification, Isolation and analysis of Tumor-Cytolytic T cells. *Nature medicine* 9, 1377-1382 (**2003**).

54 Galeano Niño, J. L., Pageon, S. V., Tay, S. S., Colakoglu, F., Kempe, D., Hywood, J., Mazalo, J. K., Cremasco, J., Govendir, M. A., Dagley, L. F., Hsu, K., Rizzetto, S., Zieba, J., Rice, G., Prior, V., O'Neill, G. M., Williams, R. J., Nisbet, D. R., Kramer, B., Webb, A. I., Luciani, F., Read, M. N. & Biro, M. Cytotoxic T Cells Swarm by Homotypic Chemokine Signalling. *eLife* 9, e56554 (**2020**). https://doi.org:10.7554/eLife.56554

55 Taub, D. D., Anver, M., Oppenheim, J. J., Longo, D. L. & Murphy, W. J. T lymphocyte recruitment by interleukin-8 (IL-8). IL-8-Induced Degranulation of Neutrophils Releases Potent Chemoattractants for Human T Lymphocytes Both in vitro and in vivo. *Journal of Clinical Investigation* 97, 1931-1941 (**1996**). https://doi.org:10.1172/jci118625

56 Monica, Marcia, Jain, R., Philip, Koskinen, A., Regner, M., Kleifeld, O., Ho, B., Olson, M., Stephen, Mrass, P., Weninger, W. & Phillip. Granzyme B Promotes Cytotoxic Lymphocyte Transmigration via Basement Membrane Remodeling. *Immunity* 41, 960-972 (**2014**). https://doi.org:10.1016/j.immuni.2014.11.012

57 Tanaka, M., Itai, T., Adachi, M. & Nagata, S. Downregulation of Fas Ligand by Shedding. *Nature Medicine* 4, 31-36 (**1998**). https://doi.org:10.1038/nm0198-031

58 Igney, F. H., Behrens, C. K. & Krammer, P. H. Tumor Counterattack--Concept and Reality. *Eur J Immunol* 30, 725-731 (**2000**). https://doi.org:10.1002/1521-4141(200003)30:3<725::Aid-immu725>3.0.Co;2-d

59 Chappell, D. B. & Restifo, N. P. T Cell-Tumor Cell: a Fatal Interaction? *Cancer Immunol Immunother* 47, 65-71 (**1998**). https://doi.org:10.1007/s002620050505

60 O'Connell, J., O'Sullivan, G. C., Collins, J. K. & Shanahan, F. The Fas Counterattack: Fas-Mediated T cell Killing by Colon Cancer Cells Expressing Fas Ligand. *J Exp Med* 184, 1075-1082 (**1996**). https://doi.org:10.1084/jem.184.3.1075

61 Green, D. R., Droin, N. & Pinkoski, M. Activation-Induced Cell Death in T cells. *Immunol Rev* 193, 70-81 (**2003**).

62 Strasser, A., Jost, P. J. & Nagata, S. The Many Roles of FAS Receptor Signaling in the Immune System. *Immunity* 30, 180-192 (**2009**). https://doi.org:10.1016/j.immuni.2009.01.001

63 Tateyama, M., Oyaizu, N., McCloskey, T. W., Than, S. & Pahwa, S. CD4 T Lymphocytes are Primed to Express Fas Ligand by CD4 Cross-Linking and to Contribute to CD8 T-cell Apoptosis via Fas/FasL Death Signaling Pathway. *Blood* 96, 195-202 (**2000**).

64 Hahne, M., Rimoldi, D., Schröter, M., Romero, P., Schreier, M., French, L. E., Schneider, P., Bornand, T., Fontana, A., Lienard, D., Cerottini, J. & Tschopp, J. Melanoma Cell Expression of Fas(Apo-1/CD95) Ligand: Implications for Tumor Immune Escape. *Science* 274, 1363-1366 (**1996**). https://doi.org:10.1126/science.274.5291.1363

65 Volpedo, G., Pacheco-Fernández, T., de Carvalho Clímaco, M. & Satoskar, A. R. in *Immunotherapy in Resistant Cancer: From the Lab Bench Work to Its Clinical Perspectives* Vol. 2 (eds Jorge Morales-Montor & Mariana Segovia-Mendoza) 47-68 (Academic Press, **2021**).

66 Motz, G. T., Santoro, S. P., Wang, L. P., Garrabrant, T., Lastra, R. R., Hagemann, I. S., Lal, P., Feldman, M. D., Benencia, F. & Coukos, G. Tumor Endothelium FasL

Establishes a Selective Immune Barrier Promoting Tolerance in Tumors. *Nat Med* 20, 607-615 (**2014**). https://doi.org:10.1038/nm.3541

67 Lakins, M. A., Ghorani, E., Munir, H., Martins, C. P. & Shields, J. D. Cancer-Associated Fibroblasts Induce Antigen-Specific Deletion of CD8 (+) T Cells to Protect Tumour Cells. *Nat Commun* 9, 948 (**2018**). https://doi.org:10.1038/s41467-018-03347-0

68 Krummel, M. F., Friedman, R. S. & Jacobelli, J. Modes and Mechanisms of T Cell Motility: Roles for Confinement and Myosin-IIA. *Curr Opin Cell Biol* 30, 9-16 (**2014**). https://doi.org:10.1016/j.ceb.2014.05.003

69 Vroomans, R. M. A., Marée, A. F. M., De Boer, R. J. & Beltman, J. B. Chemotactic Migration of T Cells towards Dendritic Cells Promotes the Detection of Rare Antigens. *PLoS Computational Biology* 8, e1002763 (**2012**). https://doi.org:10.1371/journal.pcbi.1002763

70 Jurj, A., Ionescu, C., Berindan-Neagoe, I. & Braicu, C. The extracellular Matrix Alteration, Implication in Modulation of Drug Resistance Mechanism: Friends or Foes? *Journal of Experimental & Clinical Cancer Research* 41, 276 (**2022**). https://doi.org:10.1186/s13046-022-02484-1

71 Khalaf, K., Hana, D., Chou, J. T., Singh, C., Mackiewicz, A. & Kaczmarek, M. Aspects of the Tumor Microenvironment Involved in Immune Resistance and Drug Resistance. *Front Immunol* 12, 656364 (**2021**). https://doi.org:10.3389/fimmu.2021.656364

72 Salmon, H., Franciszkiewicz, K., Damotte, D., Dieu-Nosjean, M.-C., Validire, P., Trautmann, A., Mami-Chouaib, F. & Donnadieu, E. Matrix Architecture Defines the Preferential Localization and Migration of T cells into the Stroma of Human Lung Tumors. *The Journal of clinical investigation* 122, 899-910 (**2012**). https://doi.org:10.1172/JCI45817

73 Hartmann, N., Giese, N. A., Giese, T., Poschke, I., Offringa, R., Werner, J. & Ryschich, E. Prevailing Role of Contact Guidance in Intrastromal T-cell Trapping in Human Pancreatic Cancer. *Clinical Cancer Research* 20, 3422-3433 (**2014**). https://doi.org:10.1158/1078-0432.Ccr-13-2972

74 Drake, C. G., Jaffee, E. & Pardoll, D. M. in *Advances in Immunology* Vol. 90 51-81 (Academic Press, **2006**).

75 Valkenburg, K. C., de Groot, A. E. & Pienta, K. J. Targeting the Tumour Stroma to Improve Cancer Therapy. *Nat Rev Clin Oncol* 15, 366-381 (**2018**). https://doi.org:10.1038/s41571-018-0007-1

76 Jiang, Y., Li, Y. & Zhu, B. T-cell Exhaustion in the Tumor Microenvironment. *Cell Death & Disease* 6, e1792-e1792 (**2015**). https://doi.org:10.1038/cddis.2015.162

77 Yunna, C., Mengru, H., Lei, W. & Weidong, C. Macrophage M1/M2 Polarization. *European Journal of Pharmacology* 877, 173090 (**2020**). https://doi.org:https://doi.org/10.1016/j.ejphar.2020.173090

78 DeNardo, D. G., Andreu, P. & Coussens, L. M. Interactions between Lymphocytes and Myeloid Cells Regulate Pro- Versus Anti-Tumor Immunity. *Cancer and Metastasis Reviews* 29, 309-316 (**2010**). https://doi.org:10.1007/s10555-010-9223-6

79 Fridman, W. H., Petitprez, F., Meylan, M., Chen, T. W.-W., Sun, C.-M., Roumenina, L. T. & Sautès-Fridman, C. B cells and Cancer: To B or not to B? *Journal of Experimental Medicine* 218 (**2020**). https://doi.org:10.1084/jem.20200851

80 Fridlender, Z. G. & Albelda, S. M. Tumor-Associated Neutrophils: Friend or Foe? *Carcinogenesis* 33, 949-955 (**2012**). https://doi.org:10.1093/carcin/bgs123

81 Nia, H. T., Munn, L. L. & Jain, R. K. Physical Traits of Cancer. *Science* 370, eaaz0868 (**2020**). https://doi.org:doi:10.1126/science.aaz0868

3.4. Supporting Information

Bioprinted Multi-Component Hydrogel Co-Culture Tumor-Immune Model for Assessing and Simulating Tumor-Infiltrated Lymphocyte Migration and Functional Activation

Authors

Salvador Flores-Torres [a], Nikolaos M. Dimitriou [a], Lucas Antonio Pardo [a], Jacqueline Kort-Mascort [a], Sanjima Pal [b], Omar Peza-Chavez [a], Hellen Kuasne [d], Julie Berube [b], Nicholas Bertos [c], Morag Park [e,f,g,h] Georgios D. Mitsis [a], Lorenzo Ferri [b,c], Veena Sangwan [d,], Joseph M. Kinsella [a,*].*

[a] Department of Bioengineering, McGill University, Montreal, Quebec, Canada.

[b] Department of Surgery, McGill University, Montreal, Quebec, Canada.

[c] Research Institute of the McGill University Health Centre (RI-MUHC).

[d] Rosalind and Morris Goodman Cancer Institute, McGill University, Montreal, Quebec, Canada.

[e] Department of Biochemistry, McGill University, Montreal, Quebec, Canada.

[f] Department of Medicine, McGill University, Montreal, Quebec, Canada.

[g] Department of Oncology, McGill University, Montreal, Quebec, Canada.

[h] Department of Pathology, McGill University, Montreal, Quebec, Canada.

* Corresponding author.

Corresponding author information:

Joseph M. Kinsella

Address line 1: 386 Macdonald Engineering 817 Sherbrooke Street West Montreal, Quebec, **Address line 2:** Canada, H3A 0C3

E-mail: joseph.kinsella@mcgill.ca

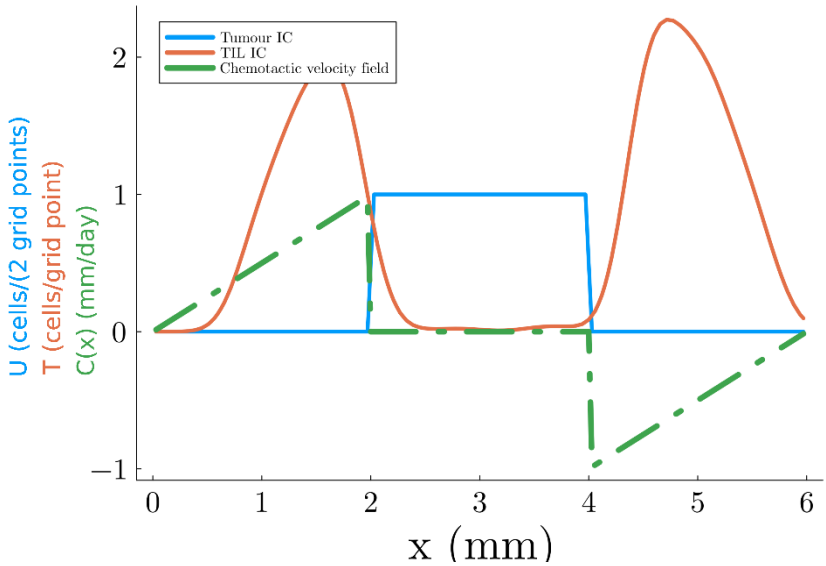

Figure S1. Initial conditions for the model. For tumour and TIL profiles, the cell density is shown as cells per grid point. The velocity field takes the form of a linear gradient that appears at the tumour borders and decreases outwards. The negative velocity field denotes cell movement towards the left side and vice versa. The velocity field disappears in the tumour core since it has a uniform cell distribution.

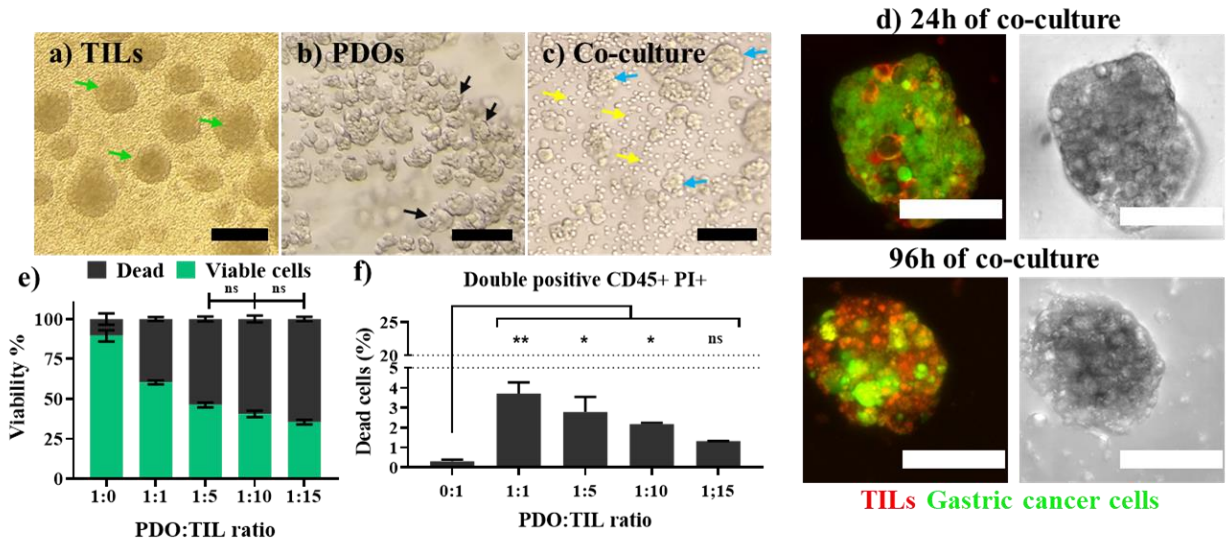

Figure S2. T-cell (TILs) suspension killing assays. Heterologous conditions. a) TILs in regular suspension culture b) 7-day-old cancer spheroids in suspension culture of gastric cancer cells extracted from A1G7M5 hydrogel. c) Co-culture at time 0h. Yellow arrows indicate TILs and cyan arrows indicate cancer cell spheroids. d) Maximum intensity images of day 1 and day 4 of co-culture conditions. TILs in red (CMTPX) and cancer cells in green (CMFDA). Scale bars for a), b), and c): 100 microns. Scale bars for d): 25 microns. e) Cancer cell viability 4 days in co-culture with T-cells. Cancer cell : TIL ratio indicates the number of TILs per cancer cell in culture. i.e., 1:1 ratio represents 50k cancer cells and 50k T-cells. No statistical differences ($P < 0.05$) were found in cancer cell viability when exposed to 5 ,10, and 15 times the number of TILs. f) TIL viability from every experimental co-culture condition.

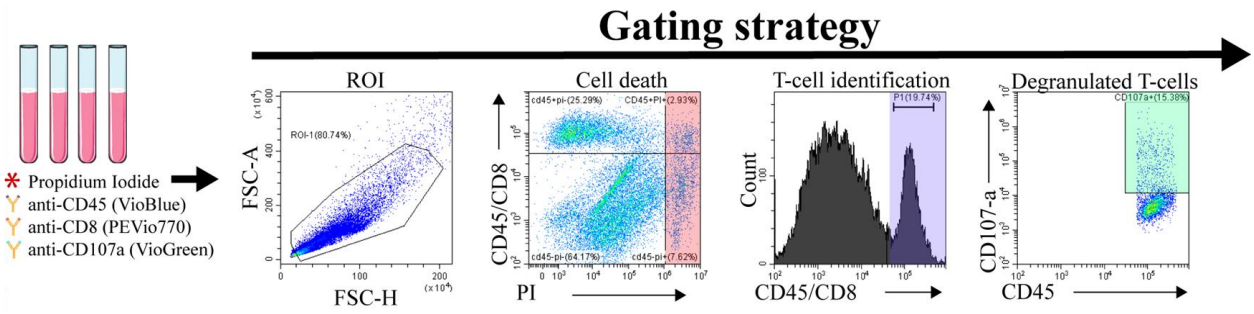

Figure S3. Flow cytometry gating strategy to identify TILs with anti-CD45 and anti-CD8. Propidium iodide (1X) is used to identify dead cells. Degranulation status is detected with an anti-CD107a antibody.

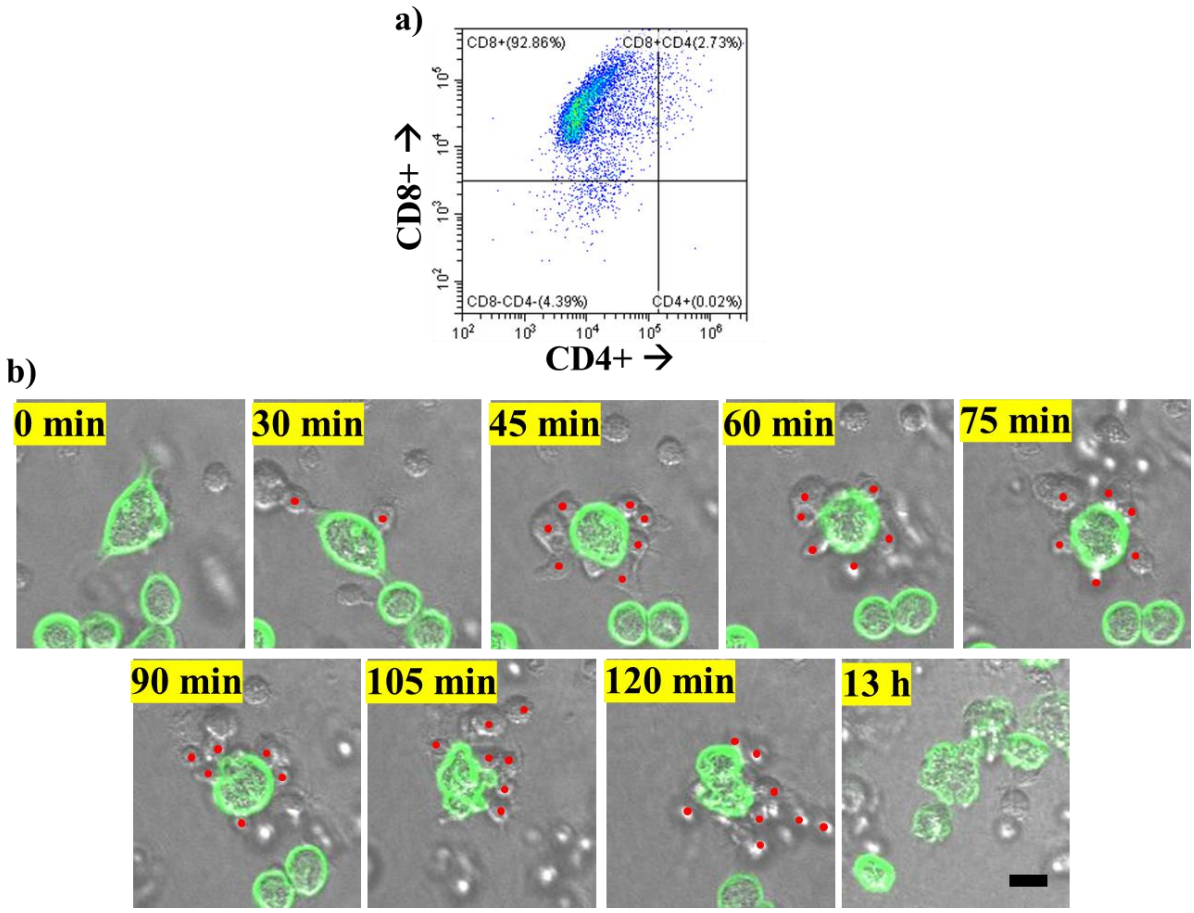

Figure S4. Membrane characterization of the TILs used in this investigation. a) CD4/CD8 ratio via flow cytometry. b) Time-lapse snap shots of TILs swarming a gastric

cancer cell during the first 13 hours of co-incubation. In green, cancer cells (live cell CMFDA viability dye, only outline is indicated). Swarming TILs are indicated with red dots around the cell. Scale bar 15 um.

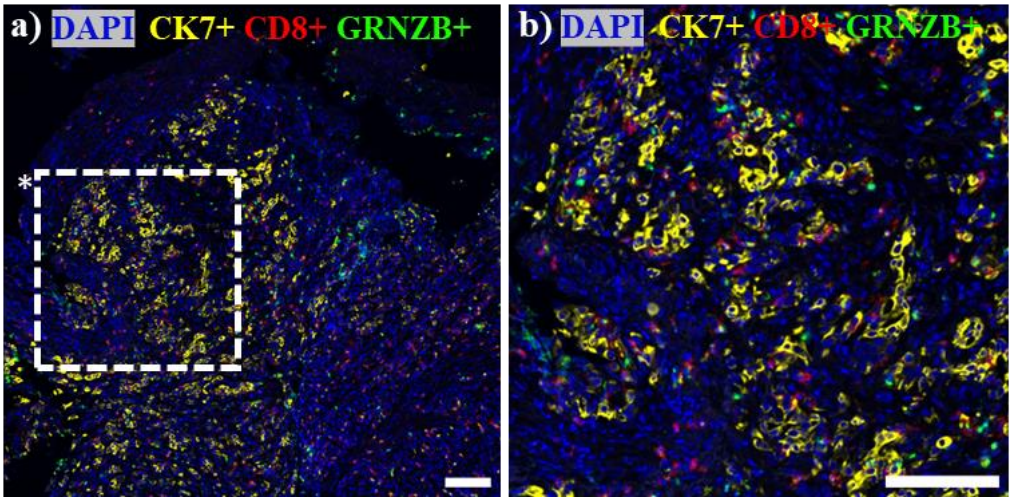

Figure S5. Immunofluorescence staining of TILs, stromal cells, and cancer cells in human solid tumor tissue. a) Esophago-gastric adenocarcinoma tumor cellular distribution. b) Close-up view of a selected region in panel a, indicated by a white dotted square, showing a dense tumor region. Nuclei in blue, cancer cells in yellow, cytotoxic CD8+ T cells in red, granzyme positive T cells in green. Scale bars represent 100um.

a)

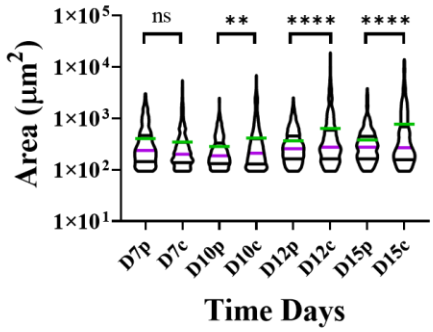

b)

Games-Howell's multiple comparisons test	Significant?	Summary	P Value
D7 periphery Vs D7 Core	No	ns	0.1249
D10 periphery Vs D10 Core	Yes	**	0.0016
D12 periphery Vs D12 Core	Yes	****	<0.0001
D15 periphery Vs D15 Core	Yes	****	<0.0001
D7 core Vs D10 core	No	ns	0.4213
D7 core Vs D12 core	Yes	****	<0.0001
D7 core Vs D15 core	Yes	****	<0.0001
D10 core Vs D12 core	Yes	***	0.0005
D10 core Vs D15 core	Yes	****	<0.0001
D12 core Vs D15 core	No	ns	0.5458

c)

	Day	CI 95% [LL, UP] µm·µm
Core	7	321, 370
	10	335, 470
	12	551, 715
	15	656, 883
	Day	CI 95% [LL, UP] µm·µm
Periphery	7	370, 433
	10	257, 309
	12	341, 388
	15	348, 412

Figure S6. TIL single cell and clump size comparison. "P" indicates peripheral TILs and "c" refers to those TILs present in the inner core. a) Area comparison between peripheral TILs (p) and TILs found in the core (c) alongside cancer cells. The median is shown in magenta lines, the mean value is represented by the green lines, and the quartile range is indicated by black lines. b) Multiple comparisons test Games-Howell's. Statistical significance summary. TILs found in the core region are significantly bigger than those TILs that remained in the peripheral zones of the bioprinted constructs. c) Confidence intervals of area values of TIL sectional areas over time. The table contains data from those TILs found in the core and the periphery of the co-culture modes. $\alpha = 0.05$.

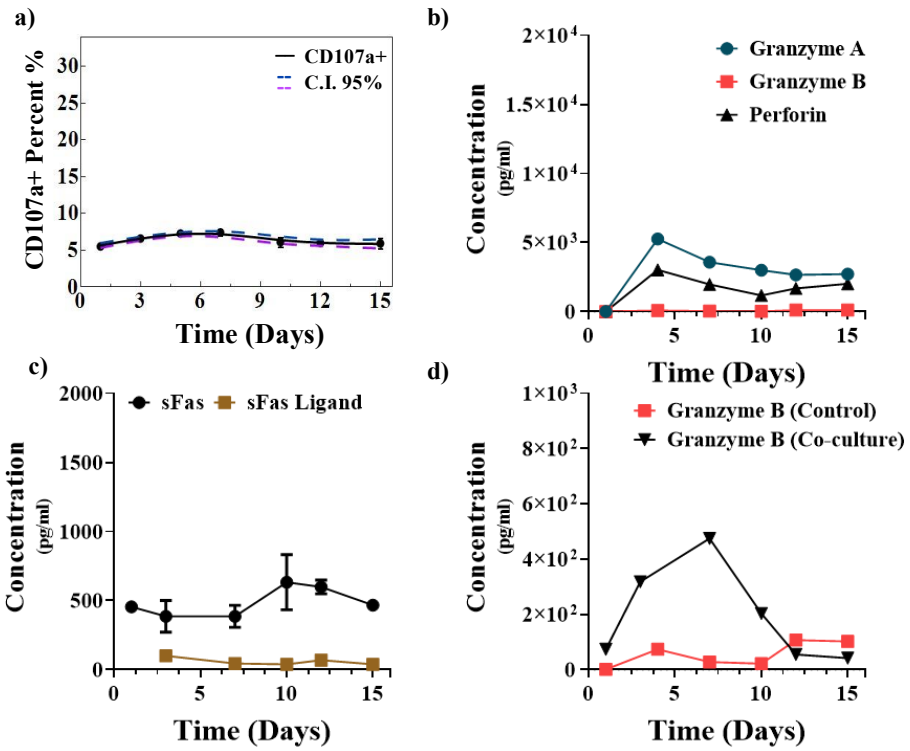

e)

Degranulation (CD107a+)			
Games-Howell's multiple comparisons test	Significant?	Summary	Adjusted P Value
Control Day 1 vs. Samples Day 1	Yes	***	0.0009
Control Day 3 vs. Samples Day 3	Yes	****	<0.0001
Control Day 5 vs. Samples Day 5	Yes	***	0.0005
Control Day 7 vs. Samples Day 7	Yes	****	<0.0001
Control Day 10 vs. Samples Day 10	Yes	****	<0.0001
Control Day 12 vs. Samples Day 12	Yes	*	0.0123
Control Day 15 vs. Samples Day 15	Yes	***	0.0003

Granzyme A			
Games-Howell's multiple comparisons test	Significant?	Summary	Adjusted P Value
Control Day 1 vs. Samples Day 1	Yes	***	0.0008
Control Day 3 vs. Samples Day 3	Yes	**	0.0013
Control Day 7 vs. Samples Day 7	Yes	**	0.0073
Control Day 10 vs. Samples Day 10	Yes	**	0.0023
Control Day 12 vs. Samples Day 12	No	ns	0.06
Control Day 15 vs. Samples Day 15	Yes	*	0.0155

Granzyme B			
Unpaired t with Welch's correction	Significant?	Summary	Adjusted P Value
Control Day 1 vs. Samples Day 1	No	ns	0.0736
Control Day 3 vs. Samples Day 3	Yes	**	0.0052
Control Day 7 vs. Samples Day 7	Yes	****	<0.0001
Control Day 10 vs. Samples Day 10	Yes	**	0.0043
Control Day 12 vs. Samples Day 12	No	ns	0.9167
Control Day 15 vs. Samples Day 15	No	ns	0.8601

Perforin			
Games-Howell's multiple comparisons test	Significant?	Summary	Adjusted P Value
Control Day 1 vs. Samples Day 1	Yes	*	0.0452
Control Day 3 vs. Samples Day 3	Yes	*	0.0191
Control Day 7 vs. Samples Day 7	Yes	**	0.001
Control Day 10 vs. Samples Day 10	Yes	**	0.0044
Control Day 12 vs. Samples Day 12	No	ns	0.2285
Control Day 15 vs. Samples Day 15	No	ns	0.3096

sFas			
Tukey's multiple comparisons test	Significant?	Summary	Adjusted P Value
Control Day 1 vs. Samples Day 1	No	ns	0.2721
Control Day 3 vs. Samples Day 3	Yes	****	<0.0001
Control Day 7 vs. Samples Day 7	Yes	****	<0.0001
Control Day 10 vs. Samples Day 10	No	ns	0.4382
Control Day 12 vs. Samples Day 12	No	ns	>0.9999
Control Day 15 vs. Samples Day 15	No	ns	>0.9999

sFasL			
Tukey's multiple comparisons test	Significant?	Summary	Adjusted P Value
Control Day 3 vs. Samples Day 3	Yes	****	<0.0001
Control Day 7 vs. Samples Day 7	No	ns	0.9189
Control Day 10 vs. Samples Day 10	No	ns	0.0824
Control Day 12 vs. Samples Day 12	No	ns	0.2551
Control Day 15 vs. Samples Day 15	No	ns	0.1673

Figure S7. Encapsulated TIL monoculture degranulation profile and soluble Fas and FasL shedding. a) 3D monoculture degranulation trend over time via flow cytometry. b) Proteolytic enzymes detected in medium over time. c) 3D monoculture soluble Fas and Fas ligand concentration in medium. Soluble Fas ligand was below detection range in day 1. d) Additional representation of granzyme B data from control samples and co-culture

samples. e) Comparisons were conducted using both Games-Howell's and Tukey's post-hoc tests. Tukey's test was used for parameters with equal variances, while Games-Howell's test was used for parameters with unequal variances. analysis results comparing results from controls and experimental samples. α = 0.05.

Figure S8. Joint (lower triangle) and marginal (top and right sides) posterior distributions of the model parameters obtained from Bayesian inference using MH-MCMC. The propagation of the parameter uncertainty is presented in Figure 4 of the main manuscript.

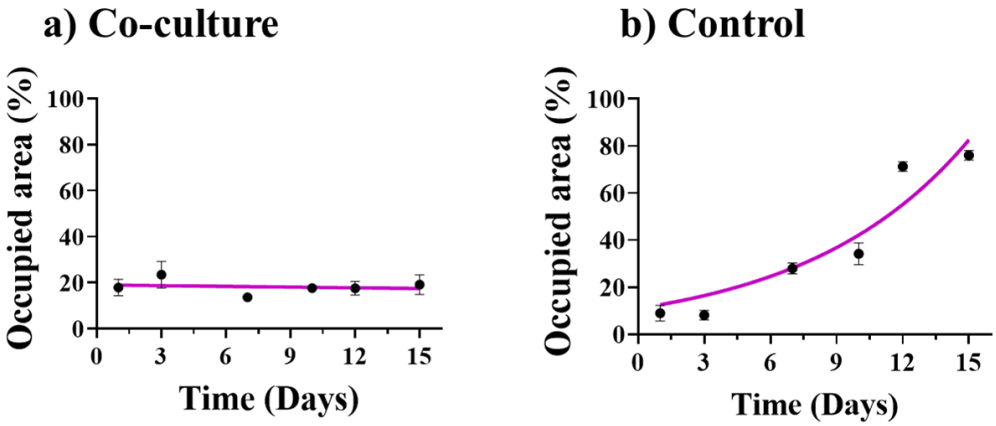

Y0	16.1 – 22.0
K	-0.02 – 0.01
Tau	-
Doubling time	-

Y0	7.8 - 14.6
K	0.11 – 0.15
Tau	6.3 – 8.9
Doubling time	4.4 – 6.2

Figure S9. Cancer cell growth trends. Microscopy data from main Figure 5.c and .d. Occupied areas are normalized (0-100%) to represent the available and maximum space that cells could occupy as they divide. a) Growth trend of cancer cells in co-culture with TILs. b) Growth trend of cancer cells in 3D monoculture conditions. Doubling time computed at 4.4 to 6.2 days ($R^2 = 0.9$).

Unpaired t test with Welch's correction	D1	D3	D7	D10	D15
P value	0.6074	0.8118	<0.0001	0.0217	<0.0001
P value summary	ns	ns	****	*	****
Significantly different (P < 0.05)?	No	No	Yes	Yes	Yes
One- or two-tailed P value?	Two-tailed	Two-tailed	Two-tailed	Two-tailed	Two-tailed
Welch-corrected t, df	t=0.5140, df=782.2	t=0.2382, df=486.3	t=8.627, df=483.3	t=2.325, df=129.1	t=8.422, df=278.5

Table S1. Unpaired t test with Welch's correction. Control and co-culture cancer spheroid growth metrics; comparisons by day. Variances of each group were compared through F-tests which revealed statistically significant differences (P < 0.0001 for F-test results). Data from confocal microscopy.

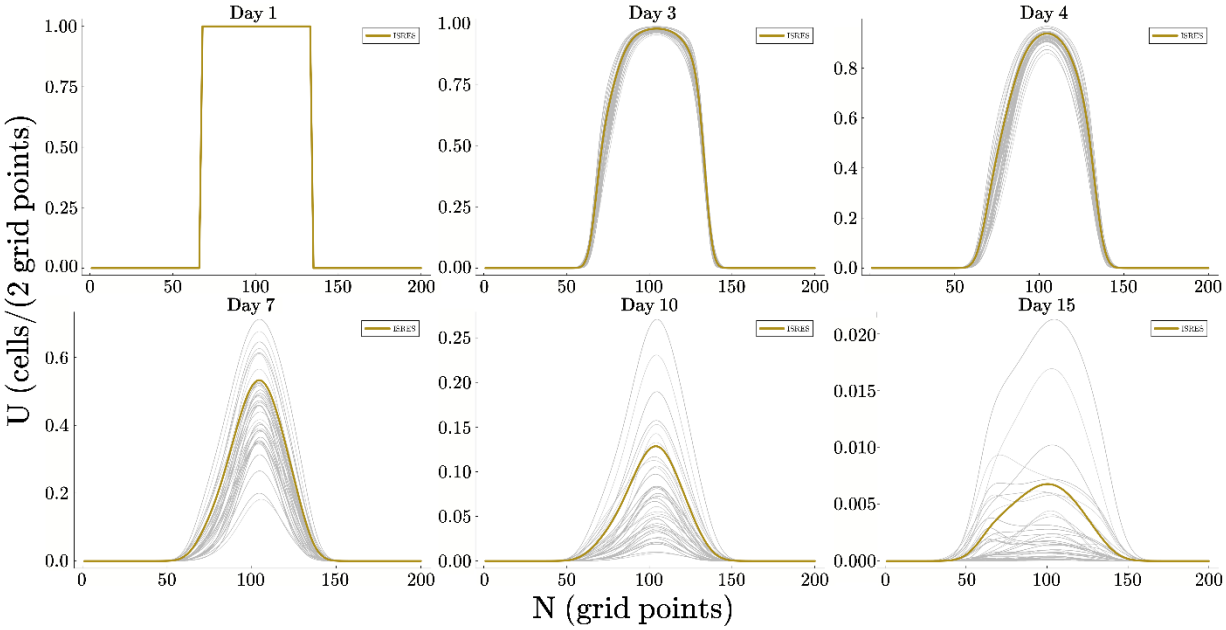

Figure S10. Predicted tumour density profiles during their interaction with TILs. The grey lines represent 500 simulations with the parameter values drawn from their corresponding posteriors. The gold line corresponds to the results obtained from the likelihood optimization problem. We observe that the spatial profile of the simulated tumour does not shrink in space, however it becomes less dense, suggesting that TILs infiltrated within the tumour volume. The distance between two consecutive grid points is 0.03mm.

4. Discussion

Cancer is a life-threatening disease, and current treatment options have life-altering side effects. We now recognize cancer not only as the uncontrolled proliferation of cancerous cells but also, understand the critical pro-tumoral roles of the adjacent stroma and the difficulty of recapitulating these in current pre-clinical cancer models. In 2022, the Food and Drug Administration (FDA) passed the FDA Modernization Act 2.0 to reduce and replace animal testing with *in-vitro* mimics of disease by permitting alternate preclinical models to assess the efficacy and safety of emerging anticancer treatments. With this bill in place, it is predicted that miniature disease models will be included as part of pre-clinical testing pipelines. As a result, it is expected that the rate at which novel antineoplastic drug candidates are found, evaluated, and introduced into clinical trials will be improved. Currently, the vast majority of therapeutical strategies against cancer, either chemical or cellular, tend to fail in clinical trials due to the poor predictive capabilities of pre-clinical cancer models[64-66]. The predictive power of a pre-clinical model is strongly dependent on the ability of the *in-vitro* system to recapitulate human neoplastic phenomena. Small animal models and simple cell culture systems fail to recapitulate the important features of disease[64-66,179]. This is reflected in the clinical translation of anticancer drugs, which is estimated to be 3.4% for clinical trials and has been slowly improving given the availability of new technology[180]. There is an unmet need for an *in-vitro* platform that provides the testing grounds to interrogate cancer biology in a controlled, relevant, and reproducible way.

The outcome of this work is an *in-vitro* platform for investigating the interactions between the parenchymal component of a tumor and the immune components that

infiltrate the tumor (TILs). I hypothesized that extrusion bioprinting (EB) of alginate-gelatin-Matrigel-based biomaterial scaffolds will enable the study of tumor-infiltrating lymphocyte (TIL) directional motility and activation towards gastric cancer cells. I had the opportunity to work with patient-derived tissues previously collected, expanded, and stored by the BioBank Technology Platforms of the Research Institute of the McGill University Health Centre. As I discussed in chapter 1, patient-derived biological material can retain and display key features of the tissue of origin, including chemosensitivity patterns, when the appropriate conditions are met *in-vitro*. I approached this hypothesis with three successive aims where a bioprintable material was proposed, developed, and used in experimentation. The first aim focused on investigating alginate, gelatin, and Matrigel as the constituents of a composite bioprintable material that would promote cancer cell proliferation and reorganization over time with the intent of conducting drug testing experiments. The second aim focused on chelating calcium ions from calcium-alginate to dissolve the cell-laden constructs, harvest the cells, and conduct subsequent bioprinting to iterate and expand the cellular population in 3D. The final aim focused on incorporating TILs in co-culture with EGA (esophagogastric adenocarcinoma) cells and documenting the co-evolution of the system using sophisticated equipment and analytical tools such as flow cytometry and confocal microscopy coupled with fluorescent antibodies.

To accomplish these aims and fulfill the main goal of this work, I developed and implemented a bioprintable platform to recapitulate the interactions between tumor parenchyma and the cells from the immune system within a controlled environment. In the first aim, I focused on testing bioprintable composite materials to find a suitable

formulation that could host patient-derived EGA cells. Throughout the material selection phase, the first biomaterial candidate was composed of alginate 1% (w/v) and gelatin 7% (w/v) (A1G7). The rheological performance of this material allowed me to encapsulate cells during the liquid phase at 37°C and use it as a cell-laden volumetric construct once extrusion bioprinting took place. The addition of Matrigel slightly changed the gelation time of the A1G7 biomaterial by speeding up its gelation kinetics by 2 minutes. This particular change did not affect the subsequent extrusion process. As reported in chapter 2 (supporting figure 2), the growth patterns of EGA cells and breast cancer cell line MDA-MB-231 depended upon the biomaterial formulation used to set the 3D cell culture environments. In A1G7, breast cancer cells (MDA-MB-231) exhibited preferential reorganization patterns to form cancer spheroids following an exponential trend. In contrast, EGA cells experienced higher cell death, and the growth trend did not follow the expected exponential growth seen in cancer cells in 3D cultures[181]. The growth of EGA cells was achieved by enhancing the original A1G7 bioink with Matrigel. Incorporating Matrigel at 5% v/v (M5) similarly induced EGA cell reorganization as that of breast cancer cells in A1G7. On the other hand, MDA-MB-231 cells encapsulated in A1G7M5 formed large and irregular multicellular arrangements seen throughout development. These differences can be attributed to the biomolecular contributions of Matrigel in the A1G7M5 bioink. Comprised of laminin (60%), collagen IV (30%), and entactin (8%), Matrigel is a commercial protein mixture of solubilized basement membrane matrix extracted from Engelbreth-Holm-Swarm (EHS) mouse sarcoma tumors[182]. The irregular breast cancer multicellular formations observed in A1G7M5 could be related to the fact that laminin and collagen stimulate cancer invasion *in-vivo*[183,184]. In human breast cancers, overexpression of laminin has been correlated with regional invasion, and metastasis[183], and collagen IV

has been recently investigated as a potential biomarker for metastatic breast cancer[184]. Even though EGA cells and breast cancer cells behaved differently in the proposed materials, the main purpose of this investigation was to test whether patient-derived cancer cells retained parental chemosensitivity; thus, the materials that favored consistent sphere formation were selected to conduct the studies. The phenomena mentioned above were reported in **Supporting figure 2** presented in chapter 1.

Furthermore, to test if *in-vitro* EGA tumor spheres retained the parental tumor characteristics, I challenged these multicellular cancer spheroids with the standard-of-care chemotherapeutic regime for EGA malignancies. These samples were derived from a xenograft previously developed out of a human esophagogastric adenocarcinoma from a patient who exhibited a poor response to neoadjuvant chemotherapy (Docetaxel, Cisplatin, and 5-Fluorouracil). In addition to patient-derived cancer cells, the commercially available and widely studied breast cancer cell line MDA-MB-231 was considered to provide a reproducible and validation metric to the scientific community. As revealed by our drug sensitivity experiments in 3D bioprinted constructs, 7-day-old MDA-MB-231 were less sensitive to the same doses of Doxorubicin, which caused a significant reduction of viability in a cell monolayer format. Due to the lack of an ECM environment, it is generally expected that cell monolayers exhibit higher sensitivity toward antineoplastic drugs. The reduced sensitivity of 3D cancer spheres may not only be the result of the 3D distribution of cells instead, but resistance may also be the result of the activation of cellular mechanisms when these are in 3D configurations[185]. Also, cell-cycle mediated chemoresistance is known to occur in 3D cancer spheroids[186].

Furthermore, data obtained from challenging EGA tumors in bioprinted samples revealed that high doses of the standard-of-care drugs could not eradicate the spheroid population, reflecting the chemoresistant nature of the parental tumor in our bioprinted model and thus, fulfilling aim 1 of this investigation. Additionally, I explored different patient-derived organoid lines by bioprinting cell-laden constructs and following cell development through time. As I demonstrated in the supporting section of the first research manuscript, cancer samples from patients with gastroesophageal malignancies exhibited different proliferative behaviors. The most interesting part of this observation was that the original cancer sites in patients varied from the distal third of the esophagus to the proximal stomach. These observations provide evidence for the platform's biocompatibility to recapitulate EGA *in-vitro* cancers.

In the second aim, besides characterizing cancer cell growth and response to therapy, an additional goal of this investigation was to engineer a testing platform in the form of a biomaterial that could be integrated within current analytical methods such as microscopy, histology, and flow cytometry. I strategized around calcium-alginate's susceptibility to chelating ions to harvest multicellular EGA tumor formations. Using citrate ions, I was able to induce calcium chelation from alginate chains, recover cancer cells from 3D constructs, dissociate these from tumor spheres into single cells, reintroduce them into fresh bioink material, and bioprint the population to reset the cell numbers in the system. I proved that it is possible to expand patient-derived EGA cells as well as cancer cell lines for up to three consecutive rounds of bioprinting without altering their growth behavior. Overall, MDA-MB-231 breast cancer cells and patient-derived EGA cell samples maintained their multiplication trends after being reprinted three times over

84 days as seen in their exponential growth trends shown in Chapter 2, Figure 3. This is an important finding because the methods alongside the biomaterial combination could serve as an alternative growth platform for EGA cell expansion and controlled experimentation.

Within the bioprinted constructs initially developed to host cancer cells, I demonstrated the use of extrusion-based bioprinting to exert geometrical control over the 3D cell culture environment and study cancer spheroid models for several generations in 3D culture conditions using both immortalized and patient-derived EGA cells. Even though the proposed composite biomaterial can be used in simple casts, these would lack the geometrical control and would translate into 3D constructs with significant differences in the number of encapsulated cells. Manual manipulation of the cell-laden hydrogels would result in non-reproducible experiments and misleading results when conducting drug testing, growth kinetic analyses, and 3D passaging. Extrusion bioprinters facilitate sample reproducibility and fine-tuning of experimental specimens for fundamental biological discovery and drug testing applications[187]. As I discussed in the review paper indexed in this thesis, bioprinting is an enabling technology that can elevate *in-vitro* model complexity without losing control over essential variables. Initial and precise cell deposition is among the variables that bioprinting can exert control, and it is, perhaps, the most crucial consideration when recapitulating the TME *in-vitro* with the intent of documenting cell-to-cell interactions and progressive maturation.

In the second and final research article included in this work, I demonstrated that extrusion bioprinting is a tool that can enable the creation of tumoral scenarios where different cells are distributed in a physiologically relevant arrangement. To complete the

third aim, I investigated the co-evolution of cancer cells and TILs within a bioprinted concentric co-culture model. I was able to evaluate the activation status of the T-cells in order to describe their degranulation patterns. Here, I initially addressed the traditional approach to evaluate T-cell cytotoxicity against cancer cells. First, I conducted flow cytometry experiments to document the type of TILs present in the population. Data revealed that TILs mainly were comprised of CD8+ T-cells (~93%) with only a few CD4+ T-cells (<3%). Then, I conducted time-lapse microscopy to qualitatively assess whether TILs could interact with the EGA cells used in aims 1 and 2. Preparing 2D EGA cell monolayers and deploying TILs in the cell medium allowed for detailed 24 h time-lapse observation. Results from this setup revealed that cancer cell integrity and viability were affected after TILs swarmed cancer. I considered these experiments as the preliminary ground to conduct more complex iterations of the TIL-cancer cell co-culture experiments.

The next iteration of the co-culture experiment involved the creation of multicellular cancer spheres and exposing these to varying concentrations of TILs in suspension conditions and document cancer cell viability. I utilized the methods developed in aim 1 and 2 of this work to prepare EGA multicellular spheroids, extract them from A1G7M5 biomaterial constructs, and co-incubate both TILs and spheroids in a suspension setting. The most potent cytotoxicity effects of TILs were seen in those samples with TIL-to-cancer cell ratios above 5 to 1 and under 15 to 1. Considering these results, I pre-program sample geometries to yield a TIL-to-cancer cell ratio above within the effective cytotoxic range. For the next set of experiments, the interactions between cancer cells and TILs were studied in bioprinted constructs designed to host cancer cells and TILs in adjacent volumetric zones within the same bioprinted construct. Here again, I demonstrated that

bioprinting facilitated the creation of *in-vitro* models in a controlled and reproducible way. I designed the co-culture platform after having the opportunity to observe multiple patient histological evaluations of EGA tumors. The TME cell distribution of an EGA often contains TILs and non-infiltrated T-cells in the stromal regions away from tumor structures. I designed a three-dimensional co-culture model considering a centric tumor element with a radially symmetric adjacent stromal compartment where TILs were deposited. These allowed me to set the initial conditions of the model where TILs and EGA cells were physically separated in a defined volumetric space. Without these conditions, creating numerous samples for experimental purposes would have been nearly impossible.

To complement my experimental results, I implemented an algorithm that considers data from microscopy, and in return, it offers numerical descriptions of T-cell motility, killing rates, and proliferation in the presence of cancer cells. Due to the physical constraints of the bioprinted constructs and the observational limits, there was an opportunity to use a mathematical model to describe some aspects of the co-evolution of the platform. Although not all of the variables rendered precise insights, this simple strategy enabled the detailed understanding of how fast TILs invade the cancer core despite not capturing it using continuous time-lapse microscopy.

The bioprinted co-culture platform provided a window of opportunity for detailed observations of the co-evolution of cancer cells and TILs. My experiments revealed that TILs actively move towards the inner cancer compartment and degranulate and secrete proteins such as granzymes and perforin throughout 15 days of co-incubation. The data suggest a direct correlation between TILs' functional activity and motility. The activation

status of TILs was measured using an antibody that binds the lysosomal-associated membrane protein 1 (LAMP-1 or CD107a) fluorescent antibody optimized for flow cytometry. Targeting this structure was particularly interesting because of the mechanism behind T-cell cytotoxicity via proteolytic enzymes. Briefly, the proteolytic enzymes and perforin are stored in the cytoplasm of activated effector cells as specialized organelles known as lytic granules[188]. During the degranulation process, these lytic granules merge with the membrane of the activated effector cell, and its contents are released during the immunological interaction between the target and effector cells[188,189]. The efficacy of activated effector T-cells to destroy target cells is directly correlated with the degree of cell-surface CD107a expression upon stimulation[190]. My findings show that, under co-culture circumstances, the quantity of CD107a+ TILs start to rise on the 3rd day, peaks on the 7th day (4.22-fold from baseline controls) and returns to baseline levels on the 15th day. TIL motility profiles show that by day 7, immune cells are more prevalent within the cancer core, and by day 15, TILs occupy most of the tumor core. The fact that several chemoattractant chemicals that function as agents for T-cell recruitment are produced together with proteolytic enzymes throughout the degranulation process can be used to explain this correlation[191,192].

I conducted cytokine analysis of the cell-culture medium to document the time course of the perforin and proteolytic enzymes in co-culture media. Utilizing advanced multiplexed detection assays, I was able to capture the secretion of crucial proteins involved in the interaction between an effector cell and its target. Granzyme A, granzyme B, and perforin were detected throughout time, and they all had a pattern comparable to that of the fraction of CD107a+ positive TILs seen by flow cytometry. More specifically, compared to

control samples, by day 7, the amount of granzyme A in the co-culture increased by 4.3 times, while the release of granzyme B was less prominent. In these experiments, granzyme A was found in more significant quantities than granzyme B, suggesting that affected cells could be caspase-independent programmed cell dead similar to apoptosis but dependent on different mediators[193]. Moreover, perforin release showed a 7.9-fold change by day 7 (compared to the baseline controls). Together, these results indicate that TILs degranulated and secreted proteolytic enzymes as they migrated towards the cancer core. Cytokines sFas and sFasL were also included in the analysis. It is important to note that because these proteins naturally shed, the soluble form of the Fas membranal proteins may be found in cell culture medium[194]. The results revealed an overexpression of sFas in our co-culture trials but no appreciable change in the concentration of sFasL. This pattern of sFas may be linked to T-cells' propensity to prevent their own unwanted proliferation and TCR-mediated activity that may be harmful to the host[195]. To complete this natural process, however, FasL presenting cells, such as T-helper cells, are required. This is done so that an immune response may be stopped or, if necessary, more effector cells can be recruited[196,197]. It has been established that the Fas axis (Fas-FasL) and its ligand play dual roles in cancer. While the Fas axis serves as an additional pathway to induce target cell apoptosis, tumors have the ability to upregulate FasL expression and inhibit the effector cells[198,199].

Advanced immuno-oncological in vitro models may soon be a reality by taking into account the cells present in immune-excluded and immune-ignored tumors and the inhibitory signal molecules that encourage T-cell anergy and immune evasion. This work is evidence that relevant cell populations of the TIME can be amplified from a tumor

biopsy and incorporated within a co-culture system by encapsulating cells in ECM-mimicking bioinks.

I identify this work as part of a future T-cell pre-screening strategy where simulated tumoral microenvironments provide the testing grounds to improve our current T-cell selection and amplification strategies. In other words, this platform could serve as a tool to evaluate the functional activity and fitness of T-cell populations in terms of motility and performance within co-culture environments before and after the immunoenhancement procedures conducted for cell therapies.

Although my work ends here, I believe the future of this project could lead to the development of accurate prediction strategies for the fate of T-cells once these (re)enter the body and encounter the target tumor site. Currently, the main challenge for an effector cell is the immunosuppressed stroma, where pro-tumoral immune cells reside and contribute to cancer progression. Understanding and predicting how effector T-cells behave when encountering an immunosuppressed stroma is one of the main purposes of future research, and this bioprinted platform could be an essential tool in doing so. Another big step towards more effective immunotherapies could be the result of understanding how effector T-cells can breach an immunosuppressive environment[200]. This particular question could be addressed in the future by conducting modifications to the presented model in a way that it could host cancer cells alongside other types of stromal cells known to be involved in challenging the immune response.

Conclusion and summary

In conclusion, I fulfilled the main objective of this project by completing the three sub-aims presented at the beginning of this thesis. I developed a bioprintable biomaterial platform that harnesses its constituents' biomolecular and physical attributes to exhibit the required biophysical properties to promote gastroesophageal cancer cell growth. I tested specific ratios of biomaterials to induce cancer cell spheroid formation to create homogeneous organoid populations for subsequent tumor profiling experiments. The developed platform was able to host cancer organoids that exhibited the chemosensitivity of the parental tumor. Moreover, the unique chemistry of the platform's constituents allowed me to recollect cancer organoids and expand these by implementing an iterative methodology aided by extrusion bioprinting methods. The resulting technology proved to effectively expand cancer cells without hindering their proliferative pattern and tumorigenic potential. The developed biomaterial platform was implemented to study the interactions between gastroesophageal cancer cells and those immune cells found in cancerous tissue within a volumetric arrangement of adjacent regions. This configuration allowed me to look at the preferential T-cell motility towards cancer cells and the patterns of protein secretions involved in the anticancer immune response. The resulting platform proves that appropriate biomaterials and biofabrication techniques can elucidate physiologically relevant phenomena in an *in-vitro* setting. This model and its future formats possess the versatility and compatibility with enough analytical techniques to revolutionize current anticancer strategies and complement or, outperform current preclinical small animal models.

Master reference list

1 Sung, H., Ferlay, J., Siegel, R. L., Laversanne, M., Soerjomataram, I., Jemal, A. & Bray, F. Global Cancer Statistics 2020: GLOBOCAN Estimates of Incidence and Mortality Worldwide for 36 Cancers in 185 Countries. *CA: A Cancer Journal for Clinicians* (2021). **71**, 209-249 https://doi.org:10.3322/caac.21660

2 Sarfati, D. & Gurney, J. Preventing cancer: the only way forward. *Lancet* (2022). **400**, 540-541 https://doi.org:10.1016/s0140-6736(22)01430-1

3 Lewandowska, A., Rudzki, M., Rudzki, S., Lewandowski, T. & Laskowska, B. Environmental risk factors for cancer – review paper. *Annals of Agricultural and Environmental Medicine* (2019). **26**, 1-7 https://doi.org:10.26444/aaem/94299

4 Delpisheh, A., Veisani, Y., Sayehmiri, K. & Rahimi, E. Esophageal carcinoma: long-term survival in consecutive series of patients through a retrospective cohort study. *Gastroenterol Hepatol Bed Bench* (2014). **7**, 101-107

5 Tustumi, F., Kimura, C. M., Takeda, F. R., Uema, R. H., Salum, R. A., Ribeiro-Junior, U. & Cecconello, I. PROGNOSTIC FACTORS AND SURVIVAL ANALYSIS IN ESOPHAGEAL CARCINOMA. *Arq Bras Cir Dig* (2016). **29**, 138-141 https://doi.org:10.1590/0102-6720201600030003

6 Rawla, P. & Barsouk, A. Epidemiology of gastric cancer: global trends, risk factors and prevention. *Prz Gastroenterol* (2019). **14**, 26-38 https://doi.org:10.5114/pg.2018.80001

7 Ferri, L. E., Ades, S., Alcindor, T., Chasen, M., Marcus, V., Hickeson, M., Artho, G. & Thirlwell, M. P. Perioperative docetaxel, cisplatin, and 5-fluorouracil (DCF) for locally advanced esophageal and gastric adenocarcinoma: a multicenter phase II trial. *Ann Oncol* (2012). **23**, 1512-1517 https://doi.org:10.1093/annonc/mdr465

8 Al-Batran, S. E., Homann, N., Pauligk, C., Goetze, T. O., Meiler, J., Kasper, S., Kopp, H. G., Mayer, F., Haag, G. M., Luley, K., Lindig, U., Schmiegel, W., Pohl, M., Stoehlmacher, J., Folprecht, G., Probst, S., Prasnikar, N., Fischbach, W., Mahlberg, R., Trojan, J., Koenigsmann, M., Martens, U. M., Thuss-Patience, P., Egger, M., Block, A., Heinemann, V., Illerhaus, G., Moehler, M., Schenk, M., Kullmann, F., Behringer, D. M., Heike, M., Pink, D., Teschendorf, C., Lohr, C., Bernhard, H., Schuch, G., Rethwisch, V., von Weikersthal, L. F., Hartmann, J. T., Kneba, M., Daum, S., Schulmann, K., Weniger, J., Belle, S., Gaiser, T., Oduncu, F. S., Guntner, M., Hozaeel, W., Reichart, A., Jager, E., Kraus, T., Monig, S., Bechstein, W. O.,

Schuler, M., Schmalenberg, H., Hofheinz, R. D. & Investigators, F. A. Perioperative chemotherapy with fluorouracil plus leucovorin, oxaliplatin, and docetaxel versus fluorouracil or capecitabine plus cisplatin and epirubicin for locally advanced, resectable gastric or gastro-oesophageal junction adenocarcinoma (FLOT4): a randomised, phase 2/3 trial. *Lancet* (2019). **393**, 1948-1957 https://doi.org:10.1016/S0140-6736(18)32557-1

9 Brenner, D. R., Weir, H. K., Demers, A. A., Ellison, L. F., Louzado, C., Shaw, A., Turner, D., Woods, R. R., Smith, L. M. & Canadian Cancer Statistics Advisory, C. Projected estimates of cancer in Canada in 2020. *CMAJ* (2020). **192**, E199-E205 https://doi.org:10.1503/cmaj.191292

10 Yoon, H. H., Shi, Q., Sukov, W. R., Lewis, M. A., Sattler, C. A., Wiktor, A. E., Wu, T. T., Diasio, R. B., Jenkins, R. B. & Sinicrope, F. A. Adverse prognostic impact of intratumor heterogeneous HER2 gene amplification in patients with esophageal adenocarcinoma. *J Clin Oncol* (2012). **30**, 3932-3938 https://doi.org:10.1200/JCO.2012.43.1890

11 Kwak, E. L., Ahronian, L. G., Siravegna, G., Mussolin, B., Borger, D. R., Godfrey, J. T., Jessop, N. A., Clark, J. W., Blaszkowsky, L. S., Ryan, D. P., Lennerz, J. K., Iafrate, A. J., Bardelli, A., Hong, T. S. & Corcoran, R. B. Molecular Heterogeneity and Receptor Coamplification Drive Resistance to Targeted Therapy in MET-Amplified Esophagogastric Cancer. *Cancer Discov* (2015). **5**, 1271-1281 https://doi.org:10.1158/2159-8290.CD-15-0748

12 Lin, D., Khan, U., Goetze, T. O., Reizine, N., Goodman, K. A., Shah, M. A., Catenacci, D. V., Al-Batran, S.-E. & Posey, J. A. Gastroesophageal Junction Adenocarcinoma: Is There an Optimal Management? *American Society of Clinical Oncology Educational Book* (2019). e88-e95 https://doi.org:10.1200/edbk_236827

13 Jiang, T., Munguia-Lopez, J. G., Gu, K., Bavoux, M. M., Flores-Torres, S., Kort-Mascort, J., Grant, J., Vijayakumar, S., De Leon-Rodriguez, A., Ehrlicher, A. J. & Kinsella, J. M. Engineering bioprintable alginate/gelatin composite hydrogels with tunable mechanical and cell adhesive properties to modulate tumor spheroid growth kinetics. *Biofabrication* (2019). **12**, 015024 https://doi.org:10.1088/1758-5090/ab3a5c

14 Pietras, K. & Östman, A. Hallmarks of cancer: Interactions with the tumor stroma. *Experimental Cell Research* (2010). **316**, 1324-1331 https://doi.org:https://doi.org/10.1016/j.yexcr.2010.02.045

15 Hanahan, D. & Weinberg, R. A. The Hallmarks of Cancer. *Cell* (2000). **100**, 57-70 https://doi.org:10.1016/s0092-8674(00)81683-9

16 Hanahan, D. & Robert. Hallmarks of Cancer: The Next Generation. *Cell* (2011). **144**, 646-674 https://doi.org:10.1016/j.cell.2011.02.013

17 Hanahan, D. Hallmarks of Cancer: New Dimensions. *Cancer Discovery* (2022). **12**, 31-46 https://doi.org:10.1158/2159-8290.Cd-21-1059

18 Chen, D. S. & Mellman, I. Oncology meets immunology: the cancer-immunity cycle. *Immunity* (2013). **39**, 1-10 https://doi.org:10.1016/j.immuni.2013.07.012

19 Gonzalez, H., Hagerling, C. & Werb, Z. Roles of the immune system in cancer: from tumor initiation to metastatic progression. *Genes & development* (2018). **32**, 1267-1284 https://doi.org:10.1101/gad.314617.118

20 Li, F., Li, C., Cai, X., Xie, Z., Zhou, L., Cheng, B., Zhong, R., Xiong, S., Li, J., Chen, Z., Yu, Z., He, J. & Liang, W. The association between CD8+ tumor-infiltrating lymphocytes and the clinical outcome of cancer immunotherapy: A systematic review and meta-analysis. *eClinicalMedicine* (2021). **41**, 101134 https://doi.org:10.1016/j.eclinm.2021.101134

21 Miyashita, M., Sasano, H., Tamaki, K., Hirakawa, H., Takahashi, Y., Nakagawa, S., Watanabe, G., Tada, H., Suzuki, A., Ohuchi, N. & Ishida, T. Prognostic significance of tumor-infiltrating CD8+ and FOXP3+ lymphocytes in residual tumors and alterations in these parameters after neoadjuvant chemotherapy in triple-negative breast cancer: a retrospective multicenter study. *Breast Cancer Research* (2015). **17** https://doi.org:10.1186/s13058-015-0632-x

22 Pagès, F., Galon, J., Dieu-Nosjean, M. C., Tartour, E., Sautès-Fridman, C. & Fridman, W. H. Immune infiltration in human tumors: a prognostic factor that should not be ignored. *Oncogene* (2010). **29**, 1093-1102 https://doi.org:10.1038/onc.2009.416

23 Oble, D. A., Loewe, R., Yu, P. & Mihm, M. C., Jr. Focus on TILs: Prognostic significance of tumor infiltrating lymphocytes in human melanoma. *Cancer Immunity* (2009). **9** https://doi.org:10.1158/1424-9634.Dcl-3.9.1

24 Mlecnik, B., Bindea, G., Pagès, F. & Galon, J. Tumor immunosurveillance in human cancers. *Cancer and Metastasis Reviews* (2011). **30**, 5-12 https://doi.org:10.1007/s10555-011-9270-7

25 Gao, G., Wang, Z., Qu, X. & Zhang, Z. Prognostic value of tumor-infiltrating lymphocytes in patients with triple-negative breast cancer: a systematic review and meta-analysis. *BMC Cancer* (2020). **20** https://doi.org:10.1186/s12885-020-6668-z

26 Loi, S., Drubay, D., Adams, S., Pruneri, G., Francis, P. A., Lacroix-Triki, M., Joensuu, H., Dieci, M. V., Badve, S., Demaria, S., Gray, R., Munzone, E., Lemonnier, J., Sotiriou, C., Piccart, M. J., Kellokumpu-Lehtinen, P.-L., Vingiani, A., Gray, K., Andre, F., Denkert, C., Salgado, R. & Michiels, S. Tumor-Infiltrating Lymphocytes and Prognosis: A Pooled Individual Patient Analysis of Early-Stage Triple-Negative Breast Cancers. *Journal of clinical oncology* (2019). **37**, 559-569 https://doi.org:10.1200/JCO.18.01010

27 Stanton, S. E. & Disis, M. L. Clinical significance of tumor-infiltrating lymphocytes in breast cancer. *Journal for ImmunoTherapy of Cancer* (2016). **4**, 59 https://doi.org:10.1186/s40425-016-0165-6

28 Ferris, R. L. & Galon, J. Additional Support for the Introduction of Immune Cell Quantification in Colorectal Cancer Classification. *JNCI: Journal of the National Cancer Institute* (2016). **108** https://doi.org:10.1093/jnci/djw033

29 Mei, Z., Liu, Y., Liu, C., Cui, A., Liang, Z., Wang, G., Peng, H., Cui, L. & Li, C. Tumour-infiltrating inflammation and prognosis in colorectal cancer: systematic review and meta-analysis. *Br J Cancer* (2014). **110**, 1595-1605 https://doi.org:10.1038/bjc.2014.46

30 Galon, J., Costes, A., Sanchez-Cabo, F., Kirilovsky, A., Mlecnik, B., Lagorce-Pagès, C., Tosolini, M., Camus, M., Berger, A., Wind, P., Zinzindohoué, F., Bruneval, P., Cugnenc, P. H., Trajanoski, Z., Fridman, W. H. & Pagès, F. Type, density, and location of immune cells within human colorectal tumors predict clinical outcome. *Science* (2006). **313**, 1960-1964 https://doi.org:10.1126/science.1129139

31 Kang, B. W., Kim, J. G., Lee, I. H., Bae, H. I. & Seo, A. N. Clinical significance of tumor-infiltrating lymphocytes for gastric cancer in the era of immunology. *World J Gastrointest Oncol* (2017). **9**, 293-299 https://doi.org:10.4251/wjgo.v9.i7.293

32 Lee, J. S., Won, H. S., Sun, S., Hong, J. H. & Ko, Y. H. Prognostic role of tumor-infiltrating lymphocytes in gastric cancer: A systematic review and meta-analysis. *Medicine (Baltimore)* (2018). **97**, e11769 https://doi.org:10.1097/md.0000000000011769

33 Hiraoka, K., Miyamoto, M., Cho, Y., Suzuoki, M., Oshikiri, T., Nakakubo, Y., Itoh, T., Ohbuchi, T., Kondo, S. & Katoh, H. Concurrent infiltration by CD8+ T cells and CD4+ T cells is a favourable prognostic factor in non-small-cell lung carcinoma. *Br J Cancer* (2006). **94**, 275-280 https://doi.org:10.1038/sj.bjc.6602934

34 Al-Shibli, K. I., Donnem, T., Al-Saad, S., Persson, M., Bremnes, R. M. & Busund, L. T. Prognostic effect of epithelial and stromal lymphocyte infiltration in non-small cell lung cancer. *Clin Cancer Res* (2008). **14**, 5220-5227 https://doi.org:10.1158/1078-0432.Ccr-08-0133

35 Spector, M. E., Bellile, E., Amlani, L., Zarins, K., Smith, J., Brenner, J. C., Rozek, L., Nguyen, A., Thomas, D., McHugh, J. B., Taylor, J. M. G., Wolf, G. T., Head, f. t. U. o. M. & Program, N. S. Prognostic Value of Tumor-Infiltrating Lymphocytes in Head and Neck Squamous Cell Carcinoma. *JAMA Otolaryngology–Head & Neck Surgery* (2019). **145**, 1012-1019 https://doi.org:10.1001/jamaoto.2019.2427

36 Kärjä, V., Aaltomaa, S., Lipponen, P., Isotalo, T., Talja, M. & Mokka, R. Tumour-infiltrating lymphocytes: A prognostic factor of PSA-free survival in patients with local prostate carcinoma treated by radical prostatectomy. *Anticancer Res* (2005). **25**, 4435-4438

37 Wang, J., Li, Z., Gao, A., Wen, Q. & Sun, Y. The prognostic landscape of tumor-infiltrating immune cells in cervical cancer. *Biomed Pharmacother* (2019). **120**, 109444 https://doi.org:10.1016/j.biopha.2019.109444

38 Hwang, W. T., Adams, S. F., Tahirovic, E., Hagemann, I. S. & Coukos, G. Prognostic significance of tumor-infiltrating T cells in ovarian cancer: a meta-analysis. *Gynecol Oncol* (2012). **124**, 192-198 https://doi.org:10.1016/j.ygyno.2011.09.039

39 Fu, Q., Chen, N., Ge, C., Li, R., Li, Z., Zeng, B., Li, C., Wang, Y., Xue, Y., Song, X., Li, H. & Li, G. Prognostic value of tumor-infiltrating lymphocytes in melanoma: a systematic review and meta-analysis. *Oncoimmunology* (2019). **8**, 1593806 https://doi.org:10.1080/2162402x.2019.1593806

40 Gooden, M. J., de Bock, G. H., Leffers, N., Daemen, T. & Nijman, H. W. The prognostic influence of tumour-infiltrating lymphocytes in cancer: a systematic review with meta-analysis. *Br J Cancer* (2011). **105**, 93-103 https://doi.org:10.1038/bjc.2011.189

41 Crespo, J., Sun, H., Welling, T. H., Tian, Z. & Zou, W. T cell anergy, exhaustion, senescence, and stemness in the tumor microenvironment. *Curr Opin Immunol* (2013). **25**, 214-221 https://doi.org:10.1016/j.coi.2012.12.003

42 Gonzalez, H., Hagerling, C. & Werb, Z. Roles of the immune system in cancer: from tumor initiation to metastatic progression. *Genes & development* (2018). **32**, 1267-1284 https://doi.org:10.1101/gad.314617.118

43 Clark, C. E., Hingorani, S. R., Mick, R., Combs, C., Tuveson, D. A. & Vonderheide, R. H. Dynamics of the Immune Reaction to Pancreatic Cancer from Inception to Invasion. *Cancer Research* (2007). **67**, 9518-9527 https://doi.org:10.1158/0008-5472.Can-07-0175

44 Drake, C. G., Jaffee, E. & Pardoll, D. M. in *Advances in Immunology* Mechanisms of Immune Evasion by Tumors Vol. 90 (Academic Press, 2006) 51-81 https://doi.org:https://doi.org/10.1016/S0065-2776(06)90002-9.

45 Nagaraj, S., Gupta, K., Pisarev, V., Kinarsky, L., Sherman, S., Kang, L., Herber, D. L., Schneck, J. & Gabrilovich, D. I. Altered recognition of antigen is a mechanism of CD8+ T cell tolerance in cancer. *Nature Medicine* (2007). **13**, 828-835 https://doi.org:10.1038/nm1609

46 Rabinovich, G. A., Gabrilovich, D. & Sotomayor, E. M. Immunosuppressive strategies that are mediated by tumor cells. *Annu Rev Immunol* (2007). **25**, 267-296 https://doi.org:10.1146/annurev.immunol.25.022106.141609

47 Zong, J., Keskinov, A. A., Shurin, G. V. & Shurin, M. R. Tumor-derived factors modulating dendritic cell function. *Cancer Immunology, Immunotherapy* (2016). **65**, 821-833 https://doi.org:10.1007/s00262-016-1820-y

48 Bandola-Simon, J. & Roche, P. A. Dysfunction of antigen processing and presentation by dendritic cells in cancer. *Molecular immunology* (2019). **113**, 31-37 https://doi.org:10.1016/j.molimm.2018.03.025

49 Driessens, G., Kline, J. & Gajewski, T. F. Costimulatory and coinhibitory receptors in anti-tumor immunity. *Immunological reviews* (2009). **229**, 126-144 https://doi.org:10.1111/j.1600-065X.2009.00771.x

50 Valkenburg, K. C., de Groot, A. E. & Pienta, K. J. Targeting the tumour stroma to improve cancer therapy. *Nat Rev Clin Oncol* (2018). **15**, 366-381 https://doi.org:10.1038/s41571-018-0007-1

51 Waldman, A. D., Fritz, J. M. & Lenardo, M. J. A guide to cancer immunotherapy: from T cell basic science to clinical practice. *Nature Reviews Immunology* (2020). **20**, 651-668 https://doi.org:10.1038/s41577-020-0306-5

52 Floris, M., Olla, S., Schlessinger, D. & Cucca, F. Genetic-Driven Druggable Target Identification and Validation. *Trends Genet* (2018). **34**, 558-570 https://doi.org:10.1016/j.tig.2018.04.004

53 King, E. A., Davis, J. W. & Degner, J. F. Are drug targets with genetic support twice as likely to be approved? Revised estimates of the impact of genetic support for drug mechanisms on the probability of drug approval. *PLoS genetics* (2019). **15**, e1008489

54 Nagaraja, A. K., Kikuchi, O. & Bass, A. J. Genomics and Targeted Therapies in Gastroesophageal Adenocarcinoma. *Cancer Discov* (2019). **9**, 1656-1672 https://doi.org:10.1158/2159-8290.CD-19-0487

55 First Tissue-Agnostic Drug Approval Issued. *Cancer Discov* (2017). **7**, 656 https://doi.org:10.1158/2159-8290.CD-NB2017-078

56 Vrána, D., Matzenauer, M., Neoral, Č., Aujeský, R., Vrba, R., Melichar, B., Rušarová, N., Bartoušková, M. & Jankowski, J. From Tumor Immunology to Immunotherapy in Gastric and Esophageal Cancer. *Int J Mol Sci* (2018). **20** https://doi.org:10.3390/ijms20010013

57 Lee J, Bass AJ & JA., A. Gastric Adenocarcinoma: An Update on Genomics, Immune System Modulations, and Targeted Therapy. *Am Soc Clin Oncol Educ Book* (2016). **35**, 104-111 https://doi.org:doi: 10.14694/EDBK_159091

58 Mergener, S. & Peña-Llopis, S. A new perspective on immune evasion: escaping immune surveillance by inactivating tumor suppressors. *Signal Transduction and Targeted Therapy* (2022). **7** https://doi.org:10.1038/s41392-022-00875-6

59 Olson, B., Li, Y., Lin, Y., Liu, E. T. & Patnaik, A. Mouse Models for Cancer Immunotherapy Research. *Cancer Discovery* (2018). **8**, 1358-1365 https://doi.org:10.1158/2159-8290.Cd-18-0044

60 Chuprin, J., Buettner, H., Seedhom, M. O., Greiner, D. L., Keck, J. G., Ishikawa, F., Shultz, L. D. & Brehm, M. A. Humanized mouse models for immuno-oncology research. *Nature Reviews Clinical Oncology* (2023). https://doi.org:10.1038/s41571-022-00721-2

61 Pearson, T., Greiner, D. L. & Shultz, L. D. Creation of "humanized" mice to study human immunity. *Curr Protoc Immunol* (2008). **Chapter 15**, 15.21.11-15.21.21 https://doi.org:10.1002/0471142735.im1521s81

62 Morton, J. J., Alzofon, N. & Jimeno, A. The humanized mouse: Emerging translational potential. *Mol Carcinog* (2020). **59**, 830-838 https://doi.org:10.1002/mc.23195

63 Schroeder, M. A. & DiPersio, J. F. Mouse models of graft-versus-host disease: advances and limitations. *Dis Model Mech* (2011). **4**, 318-333 https://doi.org:10.1242/dmm.006668

64 Mak Isabella Wy, I. W. Lost in translation: animal models and clinical trials in cancer treatment. *American Journal of Translational Research* (2014). **6**, 114-118

65 Akhtar, A. The Flaws and Human Harms of Animal Experimentation. *Cambridge Quarterly of Healthcare Ethics* (2015). **24**, 407-419 https://doi.org:10.1017/s0963180115000079

66 Van Norman, G. A. Limitations of Animal Studies for Predicting Toxicity in Clinical Trials: Is it Time to Rethink Our Current Approach? *JACC: Basic to Translational Science* (2019). **4**, 845-854 https://doi.org:https://doi.org/10.1016/j.jacbts.2019.10.008

67 Aparicio, S., Hidalgo, M. & Kung, A. L. Examining the utility of patient-derived xenograft mouse models. *Nature Reviews Cancer* (2015). **15**, 311-316 https://doi.org:10.1038/nrc3944

68 Hao, M., Cao, Z., Wang, Z., Xin, J., Kong, B., Xu, J., Zhang, L. & Chen, P. Patient-Derived Organoid Model in the Prediction of Chemotherapeutic Drug Response in Colorectal Cancer. *ACS Biomaterials Science & Engineering* (2022). **8**, 3515-3525 https://doi.org:10.1021/acsbiomaterials.2c00354

69 Driehuis, E., van Hoeck, A., Moore, K., Kolders, S., Francies, H. E., Gulersonmez, M. C., Stigter, E. C. A., Burgering, B., Geurts, V., Gracanin, A., Bounova, G., Morsink, F. H., Vries, R., Boj, S., van Es, J., Offerhaus, G. J. A., Kranenburg, O., Garnett, M. J., Wessels, L., Cuppen, E., Brosens, L. A. A. & Clevers, H. Pancreatic cancer organoids recapitulate disease and allow personalized drug screening. *Proc Natl Acad Sci U S A* (2019). **116**, 26580-26590 https://doi.org:10.1073/pnas.1911273116

70 Nagle, P. W., Plukker, J. T. M., Muijs, C. T., van Luijk, P. & Coppes, R. P. Patient-derived tumor organoids for prediction of cancer treatment response. *Seminars in Cancer Biology* (2018). **53**, 258-264 https://doi.org:https://doi.org/10.1016/j.semcancer.2018.06.005

71 Saengwimol, D., Rojanaporn, D., Chaitankar, V., Chittavanich, P., Aroonroch, R., Boontawon, T., Thammachote, W., Jinawath, N., Hongeng, S. & Kaewkhaw, R. A three-dimensional organoid model recapitulates tumorigenic aspects and drug responses of advanced human retinoblastoma. *Scientific Reports* (2018). **8**, 15664 https://doi.org:10.1038/s41598-018-34037-y

72 Shi, R., Radulovich, N., Ng, C., Liu, N., Notsuda, H., Cabanero, M., Martins-Filho, S. N., Raghavan, V., Li, Q., Mer, A. S., Rosen, J. C., Li, M., Wang, Y.-H., Tamblyn, L., Pham, N.-A., Haibe-Kains, B., Liu, G., Moghal, N. & Tsao, M.-S. Organoid Cultures as Preclinical Models of Non–Small Cell Lung Cancer. *Clinical Cancer Research* (2020). **26**, 1162-1174 https://doi.org:10.1158/1078-0432.Ccr-19-1376

73 Romero-Calvo, I., Weber, C. R., Ray, M., Brown, M., Kirby, K., Nandi, R. K., Long, T. M., Sparrow, S. M., Ugolkov, A., Qiang, W., Zhang, Y., Brunetti, T., Kindler, H., Segal, J. P., Rzhetsky, A., Mazar, A. P., Buschmann, M. M., Weichselbaum, R., Roggin, K. & White, K. P. Human Organoids Share Structural and Genetic Features with Primary Pancreatic Adenocarcinoma Tumors. *Molecular Cancer Research* (2019). **17**, 70-83 https://doi.org:10.1158/1541-7786.Mcr-18-0531

74 Weeber, F., van de Wetering, M., Hoogstraat, M., Dijkstra, K. K., Krijgsman, O., Kuilman, T., Gadellaa-van Hooijdonk, C. G., van der Velden, D. L., Peeper, D. S., Cuppen, E. P., Vries, R. G., Clevers, H. & Voest, E. E. Preserved genetic diversity in organoids cultured from biopsies of human colorectal cancer metastases. *Proc*

Natl Acad Sci U S A (2015). **112**, 13308-13311 https://doi.org:10.1073/pnas.1516689112

75 Luckett, K. A. & Ganesh, K. Engineering the Immune Microenvironment into Organoid Models. *Annual Review of Cancer Biology* (2023). **7** https://doi.org:10.1146/annurev-cancerbio-061421-040659

76 Kapałczyńska, M., Kolenda, T., Przybyła, W., Zajączkowska, M., Teresiak, A., Filas, V., Ibbs, M., Bliźniak, R., Łuczewski, Ł. & Lamperska, K. 2D and 3D cell cultures - a comparison of different types of cancer cell cultures. *Arch Med Sci* (2018). **14**, 910-919 https://doi.org:10.5114/aoms.2016.63743

77 Mak, I. W., Evaniew, N. & Ghert, M. Lost in translation: animal models and clinical trials in cancer treatment. *Am J Transl Res* (2014). **6**, 114-118

78 Nunes, A. S., Barros, A. S., Costa, E. C., Moreira, A. F. & Correia, I. J. 3D tumor spheroids as in vitro models to mimic in vivo human solid tumors resistance to therapeutic drugs. *Biotechnol Bioeng* (2019). **116**, 206-226 https://doi.org:10.1002/bit.26845

79 Kim, J., Koo, B.-K. & Knoblich, J. A. Human organoids: model systems for human biology and medicine. *Nature Reviews Molecular Cell Biology* (2020). **21**, 571-584 https://doi.org:10.1038/s41580-020-0259-3

80 Tuveson, D. & Clevers, H. Cancer modeling meets human organoid technology. *Science* (2019). **364**, 952-955 https://doi.org:doi:10.1126/science.aaw6985

81 Ivascu, A. & Kubbies, M. Rapid Generation of Single-Tumor Spheroids for High-Throughput Cell Function and Toxicity Analysis. *Journal of Biomolecular Screening* (2006). **11**, 922-932 https://doi.org:10.1177/1087057106292763

82 Timmins, N. E. & Nielsen, L. K. Generation of Multicellular Tumor Spheroids by the Hanging-Drop Method (Humana Press, 2007) 141-151 https://doi.org:10.1007/978-1-59745-443-8_8.

83 Ingram, M., Techy, G. B., Saroufeem, R., Yazan, O., Narayan, K. S., Goodwin, T. J. & Spaulding, G. F. Three-dimensional growth patterns of various human tumor cell lines in simulated microgravity of a NASA bioreactor. *In Vitro Cellular & Developmental Biology - Animal* (1997). **33**, 459-466 https://doi.org:10.1007/s11626-997-0064-8

84 Distefano, T., Chen, H. Y., Panebianco, C., Kaya, K. D., Brooks, M. J., Gieser, L., Morgan, N. Y., Pohida, T. & Swaroop, A. Accelerated and Improved Differentiation of Retinal Organoids from Pluripotent Stem Cells in Rotating-Wall Vessel Bioreactors. *Stem Cell Reports* (2018). **10**, 300-313 https://doi.org:10.1016/j.stemcr.2017.11.001

85 Souza, G. R., Molina, J. R., Raphael, R. M., Ozawa, M. G., Stark, D. J., Levin, C. S., Bronk, L. F., Ananta, J. S., Mandelin, J., Georgescu, M.-M., Bankson, J. A., Gelovani, J. G., Killian, T. C., Arap, W. & Pasqualini, R. Three-dimensional tissue culture based on magnetic cell levitation. *Nature Nanotechnology* (2010). **5**, 291-296 https://doi.org:10.1038/nnano.2010.23

86 Li, X., Valadez, A. V., Zuo, P. & Nie, Z. Microfluidic 3D cell culture: potential application for tissue-based bioassays. *Bioanalysis* (2012). **4**, 1509-1525 https://doi.org:10.4155/bio.12.133

87 Van Duinen, V., Trietsch, S. J., Joore, J., Vulto, P. & Hankemeier, T. Microfluidic 3D cell culture: from tools to tissue models. *Current Opinion in Biotechnology* (2015). **35**, 118-126 https://doi.org:10.1016/j.copbio.2015.05.002

88 Tibbitt, M. W. & Anseth, K. S. Hydrogels as extracellular matrix mimics for 3D cell culture. *Biotechnology and Bioengineering* (2009). **103**, 655-663 https://doi.org:10.1002/bit.22361

89 Deo, K. A., Singh, K. A., Peak, C. W., Alge, D. L. & Gaharwar, A. K. Bioprinting 101: Design, Fabrication, and Evaluation of Cell-Laden 3D Bioprinted Scaffolds. *Tissue Engineering Part A* (2020). **26**, 318-338 https://doi.org:10.1089/ten.tea.2019.0298

90 Knowlton, S., Onal, S., Yu, C. H., Zhao, J. J. & Tasoglu, S. Bioprinting for cancer research. *Trends in Biotechnology* (2015). **33**, 504-513 https://doi.org:10.1016/j.tibtech.2015.06.007

91 Zhuang, P., Chiang, Y. H., Fernanda, M. S. & He, M. Using Spheroids as Building Blocks Towards 3D Bioprinting of Tumor Microenvironment. *International journal of bioprinting* (2021). **7**, 444 https://doi.org:10.18063/ijb.v7i4.444

92 Caliari, S. R. & Burdick, J. A. A practical guide to hydrogels for cell culture. *Nature Methods* (2016). **13**, 405-414 https://doi.org:10.1038/nmeth.3839

93 Reid, J. A., Palmer, X.-L., Mollica, P. A., Northam, N., Sachs, P. C. & Bruno, R. D. A 3D bioprinter platform for mechanistic analysis of tumoroids and chimeric mammary organoids. *Scientific Reports* (2019). **9** https://doi.org:10.1038/s41598-019-43922-z

94 Langer, E. M., Allen-Petersen, B. L., King, S. M., Kendsersky, N. D., Turnidge, M. A., Kuziel, G. M., Riggers, R., Samatham, R., Amery, T. S., Jacques, S. L., Sheppard, B. C., Korkola, J. E., Muschler, J. L., Thibault, G., Chang, Y. H., Gray, J. W., Presnell, S. C., Nguyen, D. G. & Sears, R. C. Modeling Tumor Phenotypes In Vitro with Three-Dimensional Bioprinting. *Cell Reports* (2019). **26**, 608-623.e606 https://doi.org:10.1016/j.celrep.2018.12.090

95 Zhao, Y., Yao, R., Ouyang, L., Ding, H., Zhang, T., Zhang, K., Cheng, S. & Sun, W. Three-dimensional printing of Hela cells for cervical tumor model in vitro. *Biofabrication* (2014). **6**, 035001 https://doi.org:10.1088/1758-5082/6/3/035001

96 Swaminathan, S., Hamid, Q., Sun, W. & Clyne, A. M. Bioprinting of 3D breast epithelial spheroids for human cancer models. *Biofabrication* (2019). **11**, 025003 https://doi.org:10.1088/1758-5090/aafc49

97 Datta, P., Dey, M., Ataie, Z., Unutmaz, D. & Ozbolat, I. T. 3D bioprinting for reconstituting the cancer microenvironment. *npj Precision Oncology* (2020). **4** https://doi.org:10.1038/s41698-020-0121-2

98 Ma, X., Yu, C., Wang, P., Xu, W., Wan, X., Lai, C. S. E., Liu, J., Koroleva-Maharajh, A. & Chen, S. Rapid 3D bioprinting of decellularized extracellular matrix with regionally varied mechanical properties and biomimetic microarchitecture. *Biomaterials* (2018). **185**, 310-321 https://doi.org:10.1016/j.biomaterials.2018.09.026

99 Tang, M., Xie, Q., Gimple, R. C., Zhong, Z., Tam, T., Tian, J., Kidwell, R. L., Wu, Q., Prager, B. C., Qiu, Z., Yu, A., Zhu, Z., Mesci, P., Jing, H., Schimelman, J., Wang, P., Lee, D., Lorenzini, M. H., Dixit, D., Zhao, L., Bhargava, S., Miller, T. E., Wan, X., Tang, J., Sun, B., Cravatt, B. F., Muotri, A. R., Chen, S. & Rich, J. N. Three-dimensional bioprinted glioblastoma microenvironments model cellular dependencies and immune interactions. *Cell Research* (2020). **30**, 833-853 https://doi.org:10.1038/s41422-020-0338-1

100 Hakobyan, D., Médina, C., Dusserre, N., Stachowicz, M.-L., Handschin, C., Fricain, J.-C., Guillermet-Guibert, J. & Oliveira, H. Laser-assisted 3D bioprinting of exocrine pancreas spheroid models for cancer initiation study. *Biofabrication* (2020). **12**, 035001 https://doi.org:10.1088/1758-5090/ab7cb8

101 Mondal, A., Gebeyehu, A., Miranda, M., Bahadur, D., Patel, N., Ramakrishnan, S., Rishi, A. K. & Singh, M. Characterization and printability of Sodium alginate - Gelatin hydrogel for bioprinting NSCLC co-culture. *Scientific Reports* (2019). **9** https://doi.org:10.1038/s41598-019-55034-9

102 Xiang, Y., Miller, K., Guan, J., Kiratitanaporn, W., Tang, M. & Chen, S. 3D bioprinting of complex tissues in vitro: state-of-the-art and future perspectives. *Archives of Toxicology* (2022). https://doi.org:10.1007/s00204-021-03212-y

103 Shukla, P., Yeleswarapu, S., Heinrich, M. A., Prakash, J. & Pati, F. Mimicking tumor microenvironment by 3D bioprinting: 3D cancer modeling. *Biofabrication* (2022). **14**, 032002 https://doi.org:10.1088/1758-5090/ac6d11

104 Jiang, T., Munguia-Lopez, J. G., Flores-Torres, S., Kort-Mascort, J. & Kinsella, J. M. Extrusion bioprinting of soft materials: An emerging technique for biological model fabrication. *Applied Physics Reviews* (2019). **6**, 011310 https://doi.org:10.1063/1.5059393

105 Kim, Y., Castro, K., Bhattacharjee, N. & Folch, A. Digital Manufacturing of Selective Porous Barriers in Microchannels Using Multi-Material Stereolithography. *Micromachines* (2018). **9**, 125 https://doi.org:10.3390/mi9030125

106 Arcaute, K., Mann, B. & Wicker, R. Stereolithography of spatially controlled multi-material bioactive poly(ethylene glycol) scaffolds. *Acta Biomaterialia* (2010). **6**, 1047-1054 https://doi.org:10.1016/j.actbio.2009.08.017

107 Grigoryan, B., Sazer, D. W., Avila, A., Albritton, J. L., Padhye, A., Ta, A. H., Greenfield, P. T., Gibbons, D. L. & Miller, J. S. Development, characterization, and applications of multi-material stereolithography bioprinting. *Scientific Reports* (2021). **11** https://doi.org:10.1038/s41598-021-82102-w

108 Guillemot, F., Souquet, A., Catros, S. & Guillotin, B. Laser-assisted cell printing: principle, physical parameters versus cell fate and perspectives in tissue

engineering. *Nanomedicine (Lond)* (2010). **5**, 507-515 https://doi.org:10.2217/nnm.10.14

109 Guillotin, B., Souquet, A., Catros, S., Duocastella, M., Pippenger, B., Bellance, S., Bareille, R., Rémy, M., Bordenave, L., Amédée, J. & Guillemot, F. Laser assisted bioprinting of engineered tissue with high cell density and microscale organization. *Biomaterials* (2010). **31**, 7250-7256 https://doi.org:https://doi.org/10.1016/j.biomaterials.2010.05.055

110 Murphy, S. V. & Atala, A. 3D bioprinting of tissues and organs. *Nature Biotechnology* (2014). **32**, 773-785 https://doi.org:10.1038/nbt.2958

111 Tumbleston, J. R., Shirvanyants, D., Ermoshkin, N., Janusziewicz, R., Johnson, A. R., Kelly, D., Chen, K., Pinschmidt, R., Rolland, J. P., Ermoshkin, A., Samulski, E. T. & DeSimone, J. M. Continuous liquid interface production of 3D objects. *Science* (2015). **347**, 1349-1352 https://doi.org:doi:10.1126/science.aaa2397

112 Sun, C., Fang, N., Wu, D. M. & Zhang, X. Projection micro-stereolithography using digital micro-mirror dynamic mask. *Sensors and Actuators A: Physical* (2005). **121**, 113-120 https://doi.org:https://doi.org/10.1016/j.sna.2004.12.011

113 Shusteff, M., Browar, A. E. M., Kelly, B. E., Henriksson, J., Weisgraber, T. H., Panas, R. M., Fang, N. X. & Spadaccini, C. M. One-step volumetric additive manufacturing of complex polymer structures. *Science Advances* (2017). **3**, eaao5496 https://doi.org:10.1126/sciadv.aao5496

114 Bernal, P. N., Delrot, P., Loterie, D., Li, Y., Malda, J., Moser, C. & Levato, R. Volumetric Bioprinting of Complex Living-Tissue Constructs within Seconds. *Adv Mater* (2019). **31**, e1904209 https://doi.org:10.1002/adma.201904209

115 Kelly, B. E., Bhattacharya, I., Heidari, H., Shusteff, M., Spadaccini, C. M. & Taylor, H. K. Volumetric additive manufacturing via tomographic reconstruction. *Science* (2019). **363**, 1075 https://doi.org:10.1126/science.aau7114

116 Cook, C. C., Fong, E. J., Schwartz, J. J., Porcincula, D. H., Kaczmarek, A. C., Oakdale, J. S., Moran, B. D., Champley, K. M., Rackson, C. M., Muralidharan, A., McLeod, R. R. & Shusteff, M. Highly Tunable Thiol-Ene Photoresins for Volumetric Additive Manufacturing. *Adv Mater* (2020). **32**, e2003376 https://doi.org:10.1002/adma.202003376

117 Bernal, P. N., Bouwmeester, M., Madrid-Wolff, J., Falandt, M., Florczak, S., Rodriguez, N. G., Li, Y., Grossbacher, G., Samsom, R. A., van Wolferen, M., van der Laan, L. J. W., Delrot, P., Loterie, D., Malda, J., Moser, C., Spee, B. & Levato, R. Volumetric Bioprinting of Organoids and Optically Tuned Hydrogels to Build Liver-Like Metabolic Biofactories. *Adv Mater* (2022). **34**, e2110054 https://doi.org:10.1002/adma.202110054

118 Augustine, R., Kalva, S. N., Ahmad, R., Zahid, A. A., Hasan, S., Nayeem, A., McClements, L. & Hasan, A. 3D Bioprinted cancer models: Revolutionizing personalized cancer therapy. *Translational Oncology* (2021). **14**, 101015 https://doi.org:10.1016/j.tranon.2021.101015

119 Pepper, M. E., Seshadri, V., Burg, T. C., Burg, K. J. L. & Groff, R. E. Characterizing the effects of cell settling on bioprinter output. *Biofabrication* (2012). **4**, 011001 https://doi.org:10.1088/1758-5082/4/1/011001

120 Ayan, B., Celik, N., Zhang, Z., Zhou, K., Kim, M. H., Banerjee, D., Wu, Y., Costanzo, F. & Ozbolat, I. T. Aspiration-assisted freeform bioprinting of pre-fabricated tissue spheroids in a yield-stress gel. *Communications Physics* (2020). **3** https://doi.org:10.1038/s42005-020-00449-4

121 Ayan, B., Celik, N., Zhang, Z., Zhou, K., Kim, M. H., Banerjee, D., Wu, Y., Costanzo, F. & Ozbolat, I. T. Aspiration-assisted freeform bioprinting of pre-fabricated tissue spheroids in a yield-stress gel. *Communications Physics* (2020). **3**, 183 https://doi.org:10.1038/s42005-020-00449-4

122 Ayan, B., Wu, Y., Karuppagounder, V., Kamal, F. & Ozbolat, I. T. Aspiration-assisted bioprinting of the osteochondral interface. *Scientific Reports* (2020). **10**, 13148 https://doi.org:10.1038/s41598-020-69960-6

123 Ayan, B., Heo, D. N., Zhang, Z., Dey, M., Povilianskas, A., Drapaca, C. & Ozbolat, I. T. Aspiration-assisted bioprinting for precise positioning of biologics. *Science Advances* (2020). **6**, eaaw5111 https://doi.org:doi:10.1126/sciadv.aaw5111

124 Shiwarski, D. J., Hudson, A. R., Tashman, J. W. & Feinberg, A. W. Emergence of FRESH 3D printing as a platform for advanced tissue biofabrication. *APL Bioengineering* (2021). **5**, 010904 https://doi.org:10.1063/5.0032777

125 Hinton, T. J., Jallerat, Q., Palchesko, R. N., Park, J. H., Grodzicki, M. S., Shue, H.-J., Ramadan, M. H., Hudson, A. R. & Feinberg, A. W. Three-dimensional printing

of complex biological structures by freeform reversible embedding of suspended hydrogels. *Science Advances* (2015). **1**, e1500758 https://doi.org:doi:10.1126/sciadv.1500758

126 Jeon, O., Lee, Y. B., Jeong, H., Lee, S. J., Wells, D. & Alsberg, E. Individual cell-only bioink and photocurable supporting medium for 3D printing and generation of engineered tissues with complex geometries. *Mater Horiz* (2019). **6**, 1625-1631 https://doi.org:10.1039/c9mh00375d

127 Bhattacharjee, T., Gil, C. J., Marshall, S. L., Urueña, J. M., O'Bryan, C. S., Carstens, M., Keselowsky, B., Palmer, G. D., Ghivizzani, S., Gibbs, C. P., Sawyer, W. G. & Angelini, T. E. Liquid-like Solids Support Cells in 3D. *ACS Biomaterials Science & Engineering* (2016). **2**, 1787-1795 https://doi.org:10.1021/acsbiomaterials.6b00218

128 Schwab, A., Levato, R., D'Este, M., Piluso, S., Eglin, D. & Malda, J. Printability and Shape Fidelity of Bioinks in 3D Bioprinting. *Chemical Reviews* (2020). **120**, 11028-11055 https://doi.org:10.1021/acs.chemrev.0c00084

129 Nair, K., Gandhi, M., Khalil, S., Yan, K. C., Marcolongo, M., Barbee, K. & Sun, W. Characterization of cell viability during bioprinting processes. *Biotechnology Journal* (2009). **4**, 1168-1177 https://doi.org:10.1002/biot.200900004

130 He, Y., Yang, F., Zhao, H., Gao, Q., Xia, B. & Fu, J. Research on the printability of hydrogels in 3D bioprinting. *Scientific Reports* (2016). **6**, 29977 https://doi.org:10.1038/srep29977

131 Modeling Process-Induced Cell Damage in the Biodispensing Process. *Tissue Engineering Part C: Methods* (2010). **16**, 533-542 https://doi.org:10.1089/ten.tec.2009.0178

132 Wyss, H. M. Rheology of soft materials. *Fluids, colloids and soft materials: An introduction to soft matter physics* (2016). 149-164 https://doi.org:10.1002/9781119220510.ch9

133 Levato, R., Jungst, T., Scheuring, R. G., Blunk, T., Groll, J. & Malda, J. From Shape to Function: The Next Step in Bioprinting. *Advanced Materials* (2020). **32**, 1906423 https://doi.org:https://doi.org/10.1002/adma.201906423

134 Jiang, T., Munguia-Lopez, J. G., Flores-Torres, S., Grant, J., Vijayakumar, S., Leon-Rodriguez, A. D. & Kinsella, J. M. Directing the Self-assembly of Tumour

Spheroids by Bioprinting Cellular Heterogeneous Models within Alginate/Gelatin Hydrogels. *Scientific Reports* (2017). **7**, 4575 https://doi.org:10.1038/s41598-017-04691-9

135 GhavamiNejad, A., Ashammakhi, N., Wu, X. Y. & Khademhosseini, A. Crosslinking Strategies for 3D Bioprinting of Polymeric Hydrogels. *Small* (2020). **16**, 2002931 https://doi.org:https://doi.org/10.1002/smll.202002931

136 Genes, N. G., Rowley, J. A., Mooney, D. J. & Bonassar, L. J. Effect of substrate mechanics on chondrocyte adhesion to modified alginate surfaces. *Arch Biochem Biophys* (2004). **422**, 161-167 https://doi.org:10.1016/j.abb.2003.11.023

137 Van Den Bulcke, A. I., Bogdanov, B., De Rooze, N., Schacht, E. H., Cornelissen, M. & Berghmans, H. Structural and rheological properties of methacrylamide modified gelatin hydrogels. *Biomacromolecules* (2000). **1**, 31-38 https://doi.org:10.1021/bm990017d

138 Yang, X., Lu, Z., Wu, H., Li, W., Zheng, L. & Zhao, J. Collagen-alginate as bioink for three-dimensional (3D) cell printing based cartilage tissue engineering. *Materials Science and Engineering: C* (2018). **83**, 195-201 https://doi.org:https://doi.org/10.1016/j.msec.2017.09.002

139 Jia, J., Richards, D. J., Pollard, S., Tan, Y., Rodriguez, J., Visconti, R. P., Trusk, T. C., Yost, M. J., Yao, H., Markwald, R. R. & Mei, Y. Engineering alginate as bioink for bioprinting. *Acta Biomaterialia* (2014). **10**, 4323-4331 https://doi.org:10.1016/j.actbio.2014.06.034

140 Sandvig, I., Karstensen, K., Rokstad, A. M., Aachmann, F. L., Formo, K., Sandvig, A., Skjåk-Bræk, G. & Strand, B. L. RGD-peptide modified alginate by a chemoenzymatic strategy for tissue engineering applications. *Journal of Biomedical Materials Research Part A* (2015). **103**, 896-906 https://doi.org:https://doi.org/10.1002/jbm.a.35230

141 Paxton, N., Smolan, W., Böck, T., Melchels, F., Groll, J. & Jungst, T. Proposal to assess printability of bioinks for extrusion-based bioprinting and evaluation of rheological properties governing bioprintability. *Biofabrication* (2017). **9**, 044107 https://doi.org:10.1088/1758-5090/aa8dd8

142 Amorim, P. A., d'Ávila, M. A., Anand, R., Moldenaers, P., Van Puyvelde, P. & Bloemen, V. Insights on shear rheology of inks for extrusion-based 3D bioprinting.

Bioprinting (2021). **22**, e00129 https://doi.org:https://doi.org/10.1016/j.bprint.2021.e00129

143 Ding, H. & Chang, R. Printability Study of Bioprinted Tubular Structures Using Liquid Hydrogel Precursors in a Support Bath. *Applied Sciences* (2018). **8**, 403 https://doi.org:10.3390/app8030403

144 Garcia-Cruz, M. R., Postma, A., Frith, J. E. & Meagher, L. Printability and bio-functionality of a shear thinning methacrylated xanthan–gelatin composite bioink. *Biofabrication* (2021). **13**, 035023 https://doi.org:10.1088/1758-5090/abec2d

145 Hockaday, L. A., Kang, K. H., Colangelo, N. W., Cheung, P. Y. C., Duan, B., Malone, E., Wu, J., Girardi, L. N., Bonassar, L. J., Lipson, H., Chu, C. C. & Butcher, J. T. Rapid 3D printing of anatomically accurate and mechanically heterogeneous aortic valve hydrogel scaffolds. *Biofabrication* (2012). **4**, 035005 https://doi.org:10.1088/1758-5082/4/3/035005

146 Shao, L., Gao, Q., Xie, C., Fu, J., Xiang, M. & He, Y. Synchronous 3D Bioprinting of Large-Scale Cell-Laden Constructs with Nutrient Networks. *Advanced Healthcare Materials* (2020). **9**, 1901142 https://doi.org:https://doi.org/10.1002/adhm.201901142

147 Malda, J., Visser, J., Melchels, F. P., Jüngst, T., Hennink, W. E., Dhert, W. J. A., Groll, J. & Hutmacher, D. W. 25th Anniversary Article: Engineering Hydrogels for Biofabrication. *Advanced Materials* (2013). **25**, 5011-5028 https://doi.org:https://doi.org/10.1002/adma.201302042

148 Matamoros, M., Gómez-Blanco, J. C., Sánchez, Á. J., Mancha, E., Marcos, A. C., Carrasco-Amador, J. P. & Pagador, J. B. Temperature and Humidity PID Controller for a Bioprinter Atmospheric Enclosure System. *Micromachines* (2020). **11**, 999 https://doi.org:10.3390/mi11110999

149 Ahn, G., Min, K.-H., Kim, C., Lee, J.-S., Kang, D., Won, J.-Y., Cho, D.-W., Kim, J.-Y., Jin, S., Yun, W.-S. & Shim, J.-H. Precise stacking of decellularized extracellular matrix based 3D cell-laden constructs by a 3D cell printing system equipped with heating modules. *Scientific Reports* (2017). **7**, 8624-8624 https://doi.org:10.1038/s41598-017-09201-5

150 Mancha Sánchez, E., Gómez-Blanco, J. C., López Nieto, E., Casado, J. G., Macías-García, A., Díaz Díez, M. A., Carrasco-Amador, J. P., Torrejón Martín, D., Sánchez-

Margallo, F. M. & Pagador, J. B. Hydrogels for Bioprinting: A Systematic Review of Hydrogels Synthesis, Bioprinting Parameters, and Bioprinted Structures Behavior. *Frontiers in Bioengineering and Biotechnology* (2020). **8** https://doi.org:10.3389/fbioe.2020.00776

151 Liu, W., Heinrich, M. A., Zhou, Y., Akpek, A., Hu, N., Liu, X., Guan, X., Zhong, Z., Jin, X., Khademhosseini, A. & Zhang, Y. S. Extrusion Bioprinting of Shear-Thinning Gelatin Methacryloyl Bioinks. *Adv Healthc Mater* (2017). **6** https://doi.org:10.1002/adhm.201601451

152 Gao, T., Gillispie, G. J., Copus, J. S., Pr, A. K., Seol, Y. J., Atala, A., Yoo, J. J. & Lee, S. J. Optimization of gelatin-alginate composite bioink printability using rheological parameters: a systematic approach. *Biofabrication* (2018). **10**, 034106 https://doi.org:10.1088/1758-5090/aacdc7

153 Bom, S., Ribeiro, R., Ribeiro, H. M., Santos, C. & Marto, J. On the progress of hydrogel-based 3D printing: Correlating rheological properties with printing behaviour. *International Journal of Pharmaceutics* (2022). **615**, 121506 https://doi.org:https://doi.org/10.1016/j.ijpharm.2022.121506

154 Mouser, V. H. M., Melchels, F. P. W., Visser, J., Dhert, W. J. A., Gawlitta, D. & Malda, J. Yield stress determines bioprintability of hydrogels based on gelatin-methacryloyl and gellan gum for cartilage bioprinting. *Biofabrication* (2016). **8**, 035003 https://doi.org:10.1088/1758-5090/8/3/035003

155 Wilkes, G. L. An overview of the basic rheological behavior of polymer fluids with an emphasis on polymer melts. *Journal of Chemical Education* (1981). **58**, 880 https://doi.org:10.1021/ed058p880

156 Xin, S., Wyman, O. M. & Alge, D. L. Assembly of PEG Microgels into Porous Cell-Instructive 3D Scaffolds via Thiol-Ene Click Chemistry. *Advanced Healthcare Materials* (2018). **7**, 1800160 https://doi.org:https://doi.org/10.1002/adhm.201800160

157 Bian, L. Functional hydrogel bioink, a key challenge of 3D cellular bioprinting. *APL Bioengineering* (2020). **4**, 030401-030401 https://doi.org:10.1063/5.0018548

158 Bryant, S. J. & Vernerey, F. J. Programmable Hydrogels for Cell Encapsulation and Neo-Tissue Growth to Enable Personalized Tissue Engineering. *Advanced*

Healthcare Materials (2018). **7**, 1700605 https://doi.org:https://doi.org/10.1002/adhm.201700605

159 García-Lizarribar, A., Fernández-Garibay, X., Velasco-Mallorquí, F., Castaño, A. G., Samitier, J. & Ramon-Azcon, J. Composite Biomaterials as Long-Lasting Scaffolds for 3D Bioprinting of Highly Aligned Muscle Tissue. *Macromolecular Bioscience* (2018). **18**, 1800167 https://doi.org:https://doi.org/10.1002/mabi.201800167

160 Xu, H., Casillas, J., Krishnamoorthy, S. & Xu, C. Effects of Irgacure 2959 and lithium phenyl-2,4,6-trimethylbenzoylphosphinate on cell viability, physical properties, and microstructure in 3D bioprinting of vascular-like constructs. *Biomedical Materials* (2020). **15**, 055021 https://doi.org:10.1088/1748-605x/ab954e

161 Blaeser, A., Duarte Campos, D. F., Puster, U., Richtering, W., Stevens, M. M. & Fischer, H. Controlling Shear Stress in 3D Bioprinting is a Key Factor to Balance Printing Resolution and Stem Cell Integrity. *Advanced Healthcare Materials* (2016). **5**, 326-333 https://doi.org:https://doi.org/10.1002/adhm.201500677

162 Gillispie, G., Prim, P., Copus, J., Fisher, J., Mikos, A. G., Yoo, J. J., Atala, A. & Lee, S. J. Assessment methodologies for extrusion-based bioink printability. *Biofabrication* (2020). **12**, 022003 https://doi.org:10.1088/1758-5090/ab6f0d

163 Yu, K., Zhang, X., Sun, Y., Gao, Q., Fu, J., Cai, X. & He, Y. Printability during projection-based 3D bioprinting. *Bioact Mater* (2022). **11**, 254-267 https://doi.org:10.1016/j.bioactmat.2021.09.021

164 Ribeiro, A., Blokzijl, M. M., Levato, R., Visser, C. W., Castilho, M., Hennink, W. E., Vermonden, T. & Malda, J. Assessing bioink shape fidelity to aid material development in 3D bioprinting. *Biofabrication* (2017). **10**, 014102 https://doi.org:10.1088/1758-5090/aa90e2

165 Therriault, D., White, S. R. & Lewis, J. A. Rheological Behavior of Fugitive Organic Inks for Direct-Write Assembly. *Applied Rheology* (2007). **17**, 10112-10111-10112-10118 https://doi.org:10.1515/arh-2007-0001

166 Naghieh, S. & Chen, D. Printability – a Key Issue in Extrusion-based Bioprinting. *Journal of Pharmaceutical Analysis* (2021). https://doi.org:10.1016/j.jpha.2021.02.001

167 Ouyang, L., Yao, R., Zhao, Y. & Sun, W. Effect of bioink properties on printability and cell viability for 3D bioplotting of embryonic stem cells. *Biofabrication* (2016). **8**, 035020 https://doi.org:10.1088/1758-5090/8/3/035020

168 Lin, Z. N., Jiang, T., Kinsella, J. M., Shang, J. Z. & Luo, Z. R. Assessing roughness of extrusion printed soft materials using a semi-quantitative method. *Materials Letters* (2021). **303**, 4 https://doi.org:10.1016/j.matlet.2021.130480

169 Blaeser, A., Duarte Campos, D. F., Puster, U., Richtering, W., Stevens, M. M. & Fischer, H. Controlling Shear Stress in 3D Bioprinting is a Key Factor to Balance Printing Resolution and Stem Cell Integrity. *Adv Healthc Mater* (2016). **5**, 326-333 https://doi.org:10.1002/adhm.201500677

170 Nair, K., Gandhi, M., Khalil, S., Yan, K. C., Marcolongo, M., Barbee, K. & Sun, W. Characterization of cell viability during bioprinting processes. *Biotechnol J* (2009). **4**, 1168-1177 https://doi.org:10.1002/biot.200900004

171 Distler, T., Solisito, A. A., Schneidereit, D., Friedrich, O., Detsch, R. & Boccaccini, A. R. 3D printed oxidized alginate-gelatin bioink provides guidance for C2C12 muscle precursor cell orientation and differentiation via shear stress during bioprinting. *Biofabrication* (2020). **12**, 045005 https://doi.org:10.1088/1758-5090/ab98e4

172 Lin, S., Li, B., Yang, L., Zhai, Y., Wang, X. & Wang, C. New method for reducing viscosity and shear stress in hydrogel 3D printing via multidimension vibration. *Comput Methods Biomech Biomed Engin* (2022). 1-16 https://doi.org:10.1080/10255842.2022.2039129

173 Gheorghita Puscaselu, R., Lobiuc, A., Dimian, M. & Covasa, M. Alginate: From Food Industry to Biomedical Applications and Management of Metabolic Disorders. *Polymers* (2020). **12** https://doi.org:10.3390/polym12102417

174 Andersen, T., Auk-Emblem, P. & Dornish, M. 3D Cell Culture in Alginate Hydrogels. *Microarrays (Basel)* (2015). **4**, 133-161 https://doi.org:10.3390/microarrays4020133

175 Hu, C., Lu, W., Mata, A., Nishinari, K. & Fang, Y. Ions-induced gelation of alginate: Mechanisms and applications. *International Journal of Biological Macromolecules* (2021). **177**, 578-588 https://doi.org:https://doi.org/10.1016/j.ijbiomac.2021.02.086

176 Liu, D., Nikoo, M., Boran, G., Zhou, P. & Regenstein, J. M. Collagen and Gelatin. *Annual Review of Food Science and Technology* (2015). **6**, 527-557 https://doi.org:10.1146/annurev-food-031414-111800

177 Bello, A. B., Kim, D., Kim, D., Park, H. & Lee, S. H. Engineering and Functionalization of Gelatin Biomaterials: From Cell Culture to Medical Applications. *Tissue Eng Part B Rev* (2020). **26**, 164-180 https://doi.org:10.1089/ten.TEB.2019.0256

178 Rastogi, P. & Kandasubramanian, B. Review of alginate-based hydrogel bioprinting for application in tissue engineering. *Biofabrication* (2019). **11**, 042001 https://doi.org:10.1088/1758-5090/ab331e

179 Jensen, C. & Teng, Y. Is It Time to Start Transitioning From 2D to 3D Cell Culture? *Frontiers in Molecular Biosciences* (2020). **7** https://doi.org:10.3389/fmolb.2020.00033

180 Wong, C. H., Siah, K. W. & Lo, A. W. Estimation of clinical trial success rates and related parameters. *Biostatistics* (2019). **20**, 273-286 https://doi.org:10.1093/biostatistics/kxx069

181 Johnson, P. A., Menegatti, S., Chambers, A. C., Alibhai, D., Collard, T. J., Williams, A. C., Bayley, H. & Perriman, A. W. A rapid high throughput bioprinted colorectal cancer spheroid platform for in vitro drug- and radiation-response. *Biofabrication* (2022). **15**, 014103 https://doi.org:10.1088/1758-5090/ac999f

182 Hughes, C. S., Postovit, L. M. & Lajoie, G. A. Matrigel: a complex protein mixture required for optimal growth of cell culture. *Proteomics* (2010). **10**, 1886-1890 https://doi.org:10.1002/pmic.200900758

183 Qiu, X., Tan, H., Fu, D., Zhu, Y. & Zhang, J. Laminin is over expressed in breast cancer and facilitate cancer cell metastasis. *J Cancer Res Ther* (2018). **14**, S1170-s1172 https://doi.org:10.4103/0973-1482.191035

184 Lindgren, M., Jansson, M., Tavelin, B., Dirix, L., Vermeulen, P. & Nyström, H. Type IV collagen as a potential biomarker of metastatic breast cancer. *Clinical & Experimental Metastasis* (2021). **38**, 175-185 https://doi.org:10.1007/s10585-021-10082-2

185 Filipiak-Duliban, A., Brodaczewska, K., Kajdasz, A. & Kieda, C. Spheroid Culture Differentially Affects Cancer Cell Sensitivity to Drugs in Melanoma and RCC

Models. *International journal of molecular sciences* (2022). **23** https://doi.org:10.3390/ijms23031166

186 Beaumont, K. A., Hill, D. S., Daignault, S. M., Lui, G. Y. L., Sharp, D. M., Gabrielli, B., Weninger, W. & Haass, N. K. Cell Cycle Phase-Specific Drug Resistance as an Escape Mechanism of Melanoma Cells. *Journal of Investigative Dermatology* (2016). **136**, 1479-1489 https://doi.org:https://doi.org/10.1016/j.jid.2016.02.805

187 Neufeld, L., Yeini, E., Pozzi, S. & Satchi-Fainaro, R. 3D bioprinted cancer models: from basic biology to drug development. *Nature Reviews Cancer* (2022). **22**, 679-692 https://doi.org:10.1038/s41568-022-00514-w

188 Griffiths, G. M. & Argon, Y. Structure and Biogenesis of Lytic Granules (Springer Berlin Heidelberg, 1995) 39-58 https://doi.org:10.1007/978-3-642-79414-8_3.

189 Betts, M. R. & Koup, R. A. in *Methods in Cell Biology* Detection of T-Cell Degranulation: CD107a and b Vol. 75 (Academic Press, 2004) 497-512 https://doi.org:https://doi.org/10.1016/S0091-679X(04)75020-7.

190 Rubio, V., Stuge, T. B., Singh, N., Betts, M. R., Weber, J. S., Roederer, M. & Lee, P. P. Ex vivo identification, isolation and analysis of tumor-cytolytic T cells. *Nature Medicine* (2003). **9**, 1377-1382

191 Galeano Niño, J. L., Pageon, S. V., Tay, S. S., Colakoglu, F., Kempe, D., Hywood, J., Mazalo, J. K., Cremasco, J., Govendir, M. A., Dagley, L. F., Hsu, K., Rizzetto, S., Zieba, J., Rice, G., Prior, V., O'Neill, G. M., Williams, R. J., Nisbet, D. R., Kramer, B., Webb, A. I., Luciani, F., Read, M. N. & Biro, M. Cytotoxic T cells swarm by homotypic chemokine signalling. *eLife* (2020). **9**, e56554 https://doi.org:10.7554/eLife.56554

192 Taub, D. D., Anver, M., Oppenheim, J. J., Longo, D. L. & Murphy, W. J. T lymphocyte recruitment by interleukin-8 (IL-8). IL-8-induced degranulation of neutrophils releases potent chemoattractants for human T lymphocytes both in vitro and in vivo. *Journal of Clinical Investigation* (1996). **97**, 1931-1941 https://doi.org:10.1172/jci118625

193 Martinvalet, D., Zhu, P. & Lieberman, J. Granzyme A Induces Caspase-Independent Mitochondrial Damage, a Required First Step for Apoptosis. *Immunity* (2005). **22**, 355-370 https://doi.org:10.1016/j.immuni.2005.02.004

194 Tanaka, M., Itai, T., Adachi, M. & Nagata, S. Downregulation of Fas ligand by shedding. *Nature Medicine* (1998). **4**, 31-36 https://doi.org:10.1038/nm0198-031

195 Green, D. R., Droin, N. & Pinkoski, M. Activation-induced cell death in T cells. *Immunological reviews* (2003). **193**, 70-81

196 Strasser, A., Jost, P. J. & Nagata, S. The Many Roles of FAS Receptor Signaling in the Immune System. *Immunity* (2009). **30**, 180-192 https://doi.org:10.1016/j.immuni.2009.01.001

197 Tateyama, M., Oyaizu, N., McCloskey, T. W., Than, S. & Pahwa, S. CD4 T lymphocytes are primed to express Fas ligand by CD4 cross-linking and to contribute to CD8 T-cell apoptosis via Fas/FasL death signaling pathway. *Blood* (2000). **96**, 195-202

198 Hahne, M., Rimoldi, D., Schröter, M., Romero, P., Schreier, M., French, L. E., Schneider, P., Bornand, T., Fontana, A., Lienard, D., Cerottini, J. & Tschopp, J. Melanoma cell expression of Fas(Apo-1/CD95) ligand: implications for tumor immune escape. *Science* (1996). **274**, 1363-1366 https://doi.org:10.1126/science.274.5291.1363

199 Volpedo, G., Pacheco-Fernández, T., de Carvalho Clímaco, M. & Satoskar, A. R. in *Immunotherapy in Resistant Cancer: From the Lab Bench Work to Its Clinical Perspectives* Chapter 4 - The Fas/FasL pathway as a target for enhancing anticancer adoptive cell therapy Vol. 2 (Academic Press, 2021) (eds Jorge Morales-Montor & Mariana Segovia-Mendoza) 47-68 https://doi.org:https://doi.org/10.1016/B978-0-12-822028-3.00013-3.

200 Li, J., Li, W., Huang, K., Zhang, Y., Kupfer, G. & Zhao, Q. Chimeric antigen receptor T cell (CAR-T) immunotherapy for solid tumors: lessons learned and strategies for moving forward. *J Hematol Oncol* (2018). **11**, 22 https://doi.org:10.1186/s13045-018-0568-6

Copyright permissions

Review article

ACS Publications
Most Trusted. Most Cited. Most Read.

Constructing 3D In Vitro Models of Heterocellular Solid Tumors and Stromal Tissues Using Extrusion-Based Bioprinting

Author: Salvador Flores-Torres, Tao Jiang, Jacqueline Kort-Mascort, et al

Publication: ACS Biomaterials Science & Engineering

Publisher: American Chemical Society

Date: Jan 1, 2023

Copyright © 2023, American Chemical Society

PERMISSION/LICENSE IS GRANTED FOR YOUR ORDER AT NO CHARGE

This type of permission/license, instead of the standard Terms and Conditions, is sent to you because no fee is being charged for your order. Please note the following:

- Permission is granted for your request in both print and electronic formats, and translations.
- If figures and/or tables were requested, they may be adapted or used in part.
- Please print this page for your records and send a copy of it to your publisher/graduate school.
- Appropriate credit for the requested material should be given as follows: "Reprinted (adapted) with permission from {COMPLETE REFERENCE CITATION}. Copyright {YEAR} American Chemical Society." Insert appropriate information in place of the capitalized words.
- One-time permission is granted only for the use specified in your RightsLink request. No additional uses are granted (such as derivative works or other editions). For any uses, please submit a new request.

If credit is given to another source for the material you requested from RightsLink, permission must be obtained from that source.

BACK CLOSE WINDOW

Review article: Figure 4.A.1

License Details

This Agreement between Mr. Salvador Flores-Torres ("You") and Elsevier ("Elsevier") consists of your license details and the terms and conditions provided by Elsevier and Copyright Clearance Center.

Print Copy

License Number	5478991026382
License date	Jan 30, 2023
Licensed Content Publisher	Elsevier
Licensed Content Publication	Acta Biomaterialia
Licensed Content Title	3D bioprinted drug-resistant breast cancer spheroids for quantitative in situ evaluation of drug resistance
Licensed Content Author	Sera Hong,Joon Myong Song
Licensed Content Date	Jan 15, 2022
Licensed Content Volume	138
Licensed Content Issue	n/a
Licensed Content Pages	12
Type of Use	reuse in a thesis/dissertation
Portion	figures/tables/illustrations
Number of figures/tables/illustrations	1
Format	electronic
Are you the author of this Elsevier article?	No
Will you be translating?	No
Title	Development of an in-vitro Bioprinted Esophago-Gastric Cancer Platform for Therapy Evaluation and Immuno-Oncology Discovery
Institution name	McGill University
Expected presentation date	Jan 2023
Portions	Figure 4. Panel B
Requestor Location	Mr. Salvador Flores-Torres Department of Bioengineering 3480 University Street McConnell Engineering Building Montreal, QC H3A 0E9 Canada Attn: Mr. Salvador Flores-Torres
Publisher Tax ID	GB 494 6272 12
Total	**0.00 CAD**

Research article No.1 and Review article: Figure 4.A2

This is a License Agreement between Salvador Flores Torres ("User") and Copyright Clearance Center, Inc. ("CCC") on behalf of the Rightsholder identified in the order details below. The license consists of the order details, the Marketplace Order General Terms and Conditions below, and any Rightsholder Terms and Conditions which are included below.

All payments must be made in full to CCC in accordance with the Marketplace Order General Terms and Conditions below.

Order Date	03-Feb-2023	Type of Use	Republish in a thesis/dissertation
Order License ID	1319464-1	Publisher	IOP Publishing
ISSN	1758-5090	Portion	Chapter/article

LICENSED CONTENT

Publication Title	Biofabrication	Country	United Kingdom of Great Britain and Northern Ireland
Author/Editor	Institute of Physics (Great Britain)	Rightsholder	IOP Publishing, Ltd
Date	01/01/2009	Publication Type	e-Journal
Language	English	URL	http://iopscience.iop.org/1758-5090

REQUEST DETAILS

Portion Type	Chapter/article	Rights Requested	Main product and any product related to main product
Page Range(s)	1-13	Distribution	Worldwide
Total Number of Pages	13	Translation	Original language of publication
Format (select all that apply)	Electronic	Copies for the Disabled?	No
Who Will Republish the Content?	Academic institution	Minor Editing Privileges?	Yes
Duration of Use	Life of current and all future editions	Incidental Promotional Use?	No
Lifetime Unit Quantity	More than 2,000,000	Currency	CAD

NEW WORK DETAILS

Title	Development of an in-vitro Bioprinted Esophago-Gastric Cancer Platform for Therapy Evaluation and Immuno-Oncology Discovery	Institution Name	McGill University
		Expected Presentation Date	2023-02-10
Instructor Name	Joseph Matthew Kinsella		

ADDITIONAL DETAILS

Order Reference Number	N/A	The Requesting Person/Organization to Appear on the License	Salvador Flores Torres

REQUESTED CONTENT DETAILS

Title, Description or Numeric Reference of the Portion(s)	All content.including supporting information	Title of the Article/Chapter the Portion Is From	NA
Editor of Portion(s)	NA	Author of Portion(s)	Institute of Physics (Great Britain)
Volume of Serial or Monograph	NA	Issue, if Republishing an Article From a Serial	N/A
Page or Page Range of Portion	NA	Publication Date of Portion	2009-01-01

Review article: Figure 4.A3

License Details

This Agreement between Mr. Salvador Flores-Torres ("You") and Elsevier ("Elsevier") consists of your license details and the terms and conditions provided by Elsevier and Copyright Clearance Center.

Print Copy

License Number	5479081126703
License date	Jan 30, 2023
Licensed Content Publisher	Elsevier
Licensed Content Publication	Colloids and Surfaces B: Biointerfaces
Licensed Content Title	Bioprinting of glioma stem cells improves their endotheliogenic potential
Licensed Content Author	Xuanzhi Wang,Xinda Li,Xingliang Dai,Xinzhi Zhang,Jing Zhang,Tao Xu,Qing Lan
Licensed Content Date	Nov 1, 2018
Licensed Content Volume	171
Licensed Content Issue	n/a
Licensed Content Pages	9
Type of Use	reuse in a thesis/dissertation
Portion	figures/tables/illustrations
Number of figures/tables/illustrations	1
Format	electronic
Are you the author of this Elsevier article?	No
Will you be translating?	No
Title	Development of an in-vitro Bioprinted Esophago-Gastric Cancer Platform for Therapy Evaluation and Immuno-Oncology Discovery
Institution name	McGill University
Expected presentation date	Jan 2023
Portions	Figure 2 panels G and H
Requestor Location	Mr. Salvador Flores-Torres Department of Bioengineering 3480 University Street McConnell Engineering Building Montreal, QC H3A 0E9 Canada Attn: Mr. Salvador Flores-Torres
Publisher Tax ID	GB 494 6272 12
Total	**0.00 CAD**

Review article: Figure 4.B

Requesting permission to reuse content from an IEEE publication

Generation of 3-D glioblastoma-vascular niche using 3-D bioprinting

Conference Proceedings:
2015 41st Annual Northeast Biomedical Engineering Conference (NEBEC)

Author: Vivian K. Lee

Publisher: IEEE

Date: April 2015

Copyright © 2015, IEEE

Thesis / Dissertation Reuse

The IEEE does not require individuals working on a thesis to obtain a formal reuse license, however, you may print out this statement to be used as a permission grant:

Requirements to be followed when using any portion (e.g., figure, graph, table, or textual material) of an IEEE copyrighted paper in a thesis:

1) In the case of textual material (e.g., using short quotes or referring to the work within these papers) users must give full credit to the original source (author, paper, publication) followed by the IEEE copyright line © 2011 IEEE.
2) In the case of illustrations or tabular material, we require that the copyright line © [Year of original publication] IEEE appear prominently with each reprinted figure and/or table.
3) If a substantial portion of the original paper is to be used, and if you are not the senior author, also obtain the senior author's approval.

Requirements to be followed when using an entire IEEE copyrighted paper in a thesis:

1) The following IEEE copyright/ credit notice should be placed prominently in the references: © [year of original publication] IEEE. Reprinted, with permission, from [author names, paper title, IEEE publication title, and month/year of publication]
2) Only the accepted version of an IEEE copyrighted paper can be used when posting the paper or your thesis on-line.
3) In placing the thesis on the author's university website, please display the following message in a prominent place on the website: In reference to IEEE copyrighted material which is used with permission in this thesis, the IEEE does not endorse any of [university/educational entity's name goes here]'s products or services. Internal or personal use of this material is permitted. If interested in reprinting/republishing IEEE copyrighted material for advertising or promotional purposes or for creating new collective works for resale or redistribution, please go to http://www.ieee.org/publications_standards/publications/rights/rights_link.html to learn how to obtain a License from RightsLink.

If applicable, University Microfilms and/or ProQuest Library, or the Archives of Canada may supply single copies of the dissertation.

BACK CLOSE WINDOW

Review article: Figure 4.C

License Details

This Agreement between Mr. Salvador Flores-Torres ("You") and Elsevier ("Elsevier") consists of your license details and the terms and conditions provided by Elsevier and Copyright Clearance Center.

Print Copy

License Number	5479000575352
License date	Jan 30, 2023
Licensed Content Publisher	Elsevier
Licensed Content Publication	Methods
Licensed Content Title	Investigating lymphangiogenesis in a sacrificially bioprinted volumetric model of breast tumor tissue
Licensed Content Author	Tingting Liu,Qiong Liu,Ingrid Anaya,Di Huang,Weijia Kong,Luis S. Mille,Yu Shrike Zhang
Licensed Content Date	Jun 1, 2021
Licensed Content Volume	190
Licensed Content Issue	n/a
Licensed Content Pages	8
Type of Use	reuse in a thesis/dissertation
Portion	figures/tables/illustrations
Number of figures/tables/illustrations	1
Format	electronic
Are you the author of this Elsevier article?	No
Will you be translating?	No
Title	Development of an in-vitro Bioprinted Esophago-Gastric Cancer Platform for Therapy Evaluation and Immuno-Oncology Discovery
Institution name	McGill University
Expected presentation date	Jan 2023
Portions	Figure 4 panels C and D
Requestor Location	Mr. Salvador Flores-Torres Department of Bioengineering 3480 University Street McConnell Engineering Building Montreal, QC H3A 0E9 Canada Attn: Mr. Salvador Flores-Torres
Publisher Tax ID	GB 494 6272 12
Total	**0.00 CAD**

Review article: Figure 4.D

License Details

This Agreement between Mr. Salvador Flores-Torres ("You") and John Wiley and Sons ("John Wiley and Sons") consists of your license details and the terms and conditions provided by John Wiley and Sons and Copyright Clearance Center.

Print Copy

License Number	5479000727843
License date	Jan 30, 2023
Licensed Content Publisher	John Wiley and Sons
Licensed Content Publication	Advanced Materials
Licensed Content Title	Rapid 3D Extrusion of Synthetic Tumor Microenvironments
Licensed Content Author	Joshua M. Grolman, Douglas Zhang, Andrew M. Smith, et al
Licensed Content Date	Aug 18, 2015
Licensed Content Volume	27
Licensed Content Issue	37
Licensed Content Pages	6
Type of Use	Dissertation/Thesis
Requestor type	University/Academic
Format	Electronic
Portion	Figure/table
Number of figures/tables	1
Will you be translating?	No
Title	Development of an in-vitro Bioprinted Esophago-Gastric Cancer Platform for Therapy Evaluation and Immuno-Oncology Discovery
Institution name	McGill University
Expected presentation date	Jan 2023
Portions	Figure 3 panel (a)
Requestor Location	Mr. Salvador Flores-Torres Department of Bioengineering 3480 University Street McConnell Engineering Building Montreal, QC H3A 0E9 Canada Attn: Mr. Salvador Flores-Torres
Publisher Tax ID	EU826007151
Total	**0.00 CAD**

Review article: Figure 4.E1

Decellularized Extracellular Matrix Composite Hydrogel Bioinks for the Development of 3D Bioprinted Head and Neck in Vitro Tumor Models

ACS Publications
Most Trusted. Most Cited. Most Read.

Author: Jacqueline Kort-Mascort, Guangyu Bao, Osama Elkashty, et al

Publication: ACS Biomaterials Science & Engineering

Publisher: American Chemical Society

Date: Nov 1, 2021

PERMISSION/LICENSE IS GRANTED FOR YOUR ORDER AT NO CHARGE

This type of permission/license, instead of the standard Terms and Conditions, is sent to you because no fee is being charged for your order. Please note the following:

- Permission is granted for your request in both print and electronic formats, and translations.
- If figures and/or tables were requested, they may be adapted or used in part.
- Please print this page for your records and send a copy of it to your publisher/graduate school.
- Appropriate credit for the requested material should be given as follows: "Reprinted (adapted) with permission from {COMPLETE REFERENCE CITATION}. Copyright {YEAR} American Chemical Society." Insert appropriate information in place of the capitalized words.
- One-time permission is granted only for the use specified in your RightsLink request. No additional uses are granted (such as derivative works or other editions). For any uses, please submit a new request.

If credit is given to another source for the material you requested from RightsLink, permission must be obtained from that source.

BACK CLOSE WINDOW

Review article: Figure 4.E2

This is a License Agreement between Salvador Flores-Torres ("User") and Copyright Clearance Center, Inc. ("CCC") on behalf of the Rightsholder identified in the order details below. The license consists of the order details, the Marketplace Order General Terms and Conditions below, and any Rightsholder Terms and Conditions which are included below.

All payments must be made in full to CCC in accordance with the Marketplace Order General Terms and Conditions below.

Order Date	30-Jan-2023	Type of Use	Republish in a thesis/dissertation
Order License ID	1317708-1	Publisher	IOP Publishing
ISSN	1758-5090	Portion	Image/photo/illustration

LICENSED CONTENT

Publication Title	Biofabrication	Country	United Kingdom of Great Britain and Northern Ireland
Author/Editor	Institute of Physics (Great Britain)	Rightsholder	IOP Publishing, Ltd
Date	01/01/2009	Publication Type	e-Journal
Language	English	URL	http://iopscience.iop.org/1758-5090

REQUEST DETAILS

Portion Type	Image/photo/illustration	Distribution	Worldwide
Number of Images / Photos / Illustrations	1	Translation	Original language of publication
Format (select all that apply)	Electronic	Copies for the Disabled?	No
Who Will Republish the Content?	Academic institution	Minor Editing Privileges?	Yes
Duration of Use	Life of current and all future editions	Incidental Promotional Use?	No
Lifetime Unit Quantity	More than 2,000,000	Currency	CAD
Rights Requested	Main product		

NEW WORK DETAILS

Title	Development of an in-vitro Bioprinted Esophago-Gastric Cancer Platform for Therapy Evaluation and Immuno-Oncology Discovery	Institution Name	McGill University
		Expected Presentation Date	2023-01-31
Instructor Name	Joseph Matthew Kinsella		

ADDITIONAL DETAILS

Order Reference Number	N/A	The Requesting Person/Organization to Appear on the License	Salvador Flores-Torres

REUSE CONTENT DETAILS

Title, Description or Numeric Reference of the Portion(s)	Figure 11 panels c and d	Title of the Article/Chapter the Portion Is From	NA
Editor of Portion(s)	NA	Author of Portion(s)	Institute of Physics (Great Britain)
Volume of Serial or Monograph	NA	Issue, if Republishing an Article From a Serial	N/A
Page or Page Range of Portion	16	Publication Date of Portion	2009-01-01

IOP Publishing, Ltd Terms and Conditions

Review article: Figure 4.F1

ACS Publications
Most Trusted. Most Cited. Most Read.

3D Bioprinting of Breast Cancer Models for Drug Resistance Study

Author: Ying Wang, Wen Shi, Mitchell Kuss, et al

Publication: ACS Biomaterials Science & Engineering

Publisher: American Chemical Society

Date: Dec 1, 2018

PERMISSION/LICENSE IS GRANTED FOR YOUR ORDER AT NO CHARGE

This type of permission/license, instead of the standard Terms and Conditions, is sent to you because no fee is being charged for your order. Please note the following:

- Permission is granted for your request in both print and electronic formats, and translations.
- If figures and/or tables were requested, they may be adapted or used in part.
- Please print this page for your records and send a copy of it to your publisher/graduate school.
- Appropriate credit for the requested material should be given as follows: "Reprinted (adapted) with permission from {COMPLETE REFERENCE CITATION}. Copyright {YEAR} American Chemical Society." Insert appropriate information in place of the capitalized words.
- One-time permission is granted only for the use specified in your RightsLink request. No additional uses are granted (such as derivative works or other editions). For any uses, please submit a new request.

If credit is given to another source for the material you requested from RightsLink, permission must be obtained from that source.

BACK CLOSE WINDOW

Review article: Figure 4.F2

Modeling Tumor Phenotypes In Vitro with Three-Dimensional Bioprinting

Author:
Ellen M. Langer,Brittany L. Allen-Petersen,Shelby M. King,Nicholas D. Kendsersky,Megan A. Turnidge,Genevra M. Kuziel,Rachelle Riggers,Ravi Samatham,Taylor S. Amery,Steven L. Jacques,Brett C. Sheppard,James E. Korkola,John L. Muschler et al.

Publication: CELL REPORTS

Publisher: Elsevier

Date: 15 January 2019